UNIVERSITÉ DE STRASBOURG

ÉCOLE DOCTORALE DES SCIENCE CHIMIQUES

UPR3572

THÈSE présentée par :

Shi GUO

soutenue le : **27 Novembre 2020**

pour obtenir le grade de : **Docteur de l'université de Strasbourg**

Discipline/ Spécialité : Chimie Organique

Photothérapies combinées à base de matériaux 2D multifonctionnels pour le traitement du cancer et de maladies auto-immunes

THÈSE dirigée par :

M. BIANCO Alberto	Directeur de recherche, CNRS

RAPPORTEURS :

M. DORIS Eric	Directeur de recherche, CEA Université de Strasbourg
M. EIGLER Siegfried	Professeur, Freie Universität Berlin

AUTRES MEMBRES DU JURY :

Mme. MENARD-MOYON Cécilia	Chargé de recherches, CNRS
M. CIESIELSKI Artur	Ingénieur de Recherche, CNRS
Mme. HERRANZ Maria Angeles	Professeur, Universidad Complutense de Madrid

Acknowledgments

The three years past so fast that I barely noticed it is time to finish my study in Strasbourg. The time I spent was in here was fantastic and I met many really nice people here. The experiment here would be a precious treasure for my whole life.

I would like to thank my supervisor, Dr. Alberto Bianco, for giving me the position to do my PhD in his group that bring me from Shanghai to Strasbourg. I really appreciate all the creative suggestions and kind help from him not only in the lab, but also about my daily life here. It is my honor to have pursued my PhD under his supervision. His door was and is always opened for me when I met with problems. His passion and devotion to work is the thing that I should always learn from.

I also want to thank Dr. Cécilia Ménard-Moyon, for all the friendly suggestions and help I received. She has inspired me with many brilliant ideas and suggestions on my project with many exciting works coming out. Her kindness and patience during the discussion, the correction of papers and the guidance on my experiments gave me great support in the past three years.

I'm grateful to Dr. Artur Ciesielski, Prof. Maria Angeles Herranz, Dr. Éric Doris, Prof. Dr. Siegfried Eigler and Dr. Cécilia Ménard-Moyon for accepting to be member of my defense commission and reading the manuscript.

I would like to thank the Unit Director Dr. Hélène Dumortier and the past Unit Director, Dr. Sylviane Muller.

I wish to thank Dr. Jean-Daniel Fauny and Mrs. Hayet Dali for the training on biology experiments and work of macrophage activation.

I want to thank all the members of I^2CT Unit that I spent time with in the last three years. It's a warm place and people here are really nice.

I would like to thank Chloé for sharing the three PhD years with me and for her kind help for the translations, the experiment advice and all the university work that I went to you for help. I am really happy for you passing the defense and wish you and your family all the best in the future. A special thank is for Rym who was really nice to me and always encouraged me when the experiments were not working well. I would like to thank Lucas, Kim and Hazel for the nice moments in the lab and the kind help during the PhD, especially answering the French phone calls that I still do not understand. It is really happy to work with you. I would like to thank Baojin for the discussions we had in the lab, which were very interesting, and the kind concern when I work late in the lab. I wish to thank Zhengmei for helping me with the macrophage experiments. The results are really nice. I also want to thank Shiyuan and Tengfei for their hotpot and nice dishes and the happy moment we spent together.

I also wish to thank the friends that I used to work together with. I especially want to thank Giacomo who gave me many supports and advices during the past three years, as well as the help of cell experiments and the confocal images. I also want to thank Dingkun, a friend working in the same lab already in China for four years and two years in Strasbourg, and Christina and Matteo for all happy moments we had. I would also like to thank Dinesh for the advice on my experiments.

A special thank also goes to Prof. Yuta Nishina from Okayama University in Japan for providing me the GO samples and the valuable comments on the project. I would like to thank R. Khan and S. Obata in Prof. Nishina's group for cyclic voltammetry and AFM analyses.

Another thank is for Dr. Jésus Raya for all the MAS NMR samples.

A special thanks it's for Cathy Royer and Valérie Demais of the "Plateforme Imagerie in vitro" at the Center of Neurochemistry for the great effort on TEM.

I also would like to acknowledge Prof. Philippe Mésini for the help of ATR FT-IR.

I want to acknowledge Fanny Richard, Matilde Eredia, and Ye Wang in the group of Prof. Paolo Samorì who helped me with the XPS experiments.

I would like to thank the China Scholarship Council for supporting my PhD internship in France.

I wish to thank all my friends in France and in China. Thank you for your patience and understanding. It is a pity that I could not attend many of your wedding ceremonies.

Many thanks to my family, my parents, grandparents and all of you. Thank you for always being with me, trusting me, encouraging me and supporting me. I am sorry that I did not spend much time with you.

My biggest thank is to my girlfriend Xiaoqiao Qin. Thank you for keeping company with me for the whole three years. Thank you for your understanding, your patience and all the phone calls at midnight.

Abstract

Doctoral Thesis

By Shi Guo

2D materials including graphene oxide (GO) and MoS_2 have been raising a great interest due to their unique chemical and physical properties that make these materials with great potential applications in different fields. To achieve a better performance, especially for biomedical purposes, the surface modification allows to tune the intrinsic properties and to attach various functional groups onto the nanomaterials. In comparison with non-covalent methods, the covalent functionalization enables to prepare more stable conjugates. When conjugated with photosensitizers, the functionalized materials can act as a good platform for photodynamic therapy (PDT). Moreover, GO possesses high converting efficiency, making it a good photothermal material for photothermal therapy (PTT).

The main purpose of my thesis was to explore the possible therapeutic effect of GO conjugates functionalized with folic acid (FA) as a targeting agent towards the folate receptor on cancer cells or activated macrophages and a photosensitizer, chlorin e6 (Ce6), in the treatment of cancer cells and RA combining PTT and PDT. For this purpose, we investigated new methods for the double functionalization of GO by targeting the epoxide rings and hydroxyl groups on GO surface. The epoxide rings were first derived through a nucleophilic addition with amines or thiols. To obtain a higher reactivity of hydroxyl groups, the OH moieties on GO were modified by carboxylation or Michael addition of benzoquinone followed by the conjugation of the second functional groups.

While exploring the covalent double functionalization targeting different groups on GO, a FA/Ce6 double-functionalized GO was prepared by derivatizing the epoxides with two PEG chains. GO-FA/Ce6 exhibited high killing efficiency on breast cancer cells, MCF-7, after PTT or PDT alone. By combining the photothermal and photodynamic treatment, a higher therapeutic effect was achieved, leading to satisfactory antitumor efficacy. Furthermore, GO-FA/Ce6 was explored in the phototherapy against RA. Some preliminary experiments were performed on murine macrophage RAW 264.7 cells, obtaining a good therapeutic efficiency of PTT.

Finally, the chemical modification and the liquid phase exfoliation of MoS_2 assisted by benzoquinone were studied. The 2D MoS_2 nanosheets were derivatized by benzoquinone through Michael addition and the quinone-modified MoS_2 nanosheets were subsequently functionalized with 3-(pentafluorothio)-DL-phenylalanine. The benzoquinone-assisted liquid phase exfoliation was also investigated. The prepared 2D MoS_2 was well-dispersed in water at high concentration.

Index

Acknowledgments I

Abstract III

Index V

Acronyms and Abbreviations IX

Résumé de Thèse XIII

Chapter 1 Introduction 1

1.1 2D materials 1

1.1.1 Graphene oxide 1

1.1.2 Functionalization of graphene oxide 3

1.1.3 Application of GO in the treatment of diseases 6

1.1.4 Molybdenum disulfide 10

1.1.5 Synthesis of MoS_2 12

1.1.6 Functionalization of MoS_2 13

1.2 Photothermal therapy and photodynamic therapy 15

1.2.1 Introduction to PTT 15

1.2.2 Introduction to PDT 18

1.2.3 Synergistic therapy combining PTT and PDT 19

1.3 Autoimmune diseases and their treatment using nanomaterial 20

1.3.1 Introduction of autoimmune disease and macrophages 20

1.3.2 RA therapy targeting FR β 21

1.4 Objectives of this thesis 23

1.5 References 24

Chapter 2 The covalent double functional on GO 35

2.1 Introduction 35

2.2 Objectives of this chapter 35

2.3 Combination of epoxide opening and carboxylation 36

2.3.1 Carboxylation of GO with high amount of sodium hydroxide 36

2.3.2 Double functionalization of GO combining opening of epoxides and carboxylation with high amount of sodium hydroxide 40

2.3.3 Double functionalization of GO combining opening of epoxides and carboxylation with a reduced amount of sodium hydroxide 44

2.3.4 Conclusion 49

2.4 Combining the opening of epoxides and benzoquinone-mediated Michael addition reaction ..50

2.4.1 Double functionalization through epoxide ring opening reaction and Michael addition of benzoquinone 50

2.4.2 Double functionalization of GO with Boc-PEG_{10}-NH_2 and 3-(pentafluorothio)-DL-phenylalanine 55

2.4.3 Double functionalization with Boc-aminoethanethiol and 3-(pentafluorothio)-DL-phenylalanine 57

2.4.4 Conclusion 63

2.5 Material and methods 63

2.6 References 71

Chapter 3 The PTT and PDT of FA/Ce6 double functional GO on cancer cells and macrophages 77

3.1 Introduction 77

3.2 Objectives of this chapter 77

3.3 Preparation of FA/Ce6 double-functionalized GO 78

3.3.1 Synthesis of FA-PEG_{10}-NH_2 79

3.3.2 Synthesis and characterization of GO-FA/Ce6 80

3.3.3 Evaluation of the photothermal property of GO-FA/Ce6 and ROS generation 82

3.3.4 Conclusion 83

3.4 PTT and PDT of GO-FA/Ce6 on cancer cells 83

3.4.1 Cytotoxicity and uptake of GO-FA/Ce6 on Hela cells 84

3.4.2 PTT and PDT effects of GO-FA/Ce6 on HeLa cells 85

3.4.3 Cellular uptake and cytotoxicity of GO-FA/Ce6 on MCF-7 88

3.4.4 PTT and PDT effects of GO-FA/Ce6 on MCF-7 cells 90
3.5 PTT and PDT of GO-FA/Ce6 on macrophages 94
3.5.1 Cytotoxicity of GO-FA/Ce6 on RAW 264.7 cells 94
3.5.2 PTT and PDT effects of GO-FA/Ce6 on RAW 264.7 cell 95
3.6 Conclusions 96
3.7 Material and methods 97
3.7 References 103
Chapter 4 Benzoquinone-assisted covalent functionalization and liquid phase exfoliation of MoS_2 105
4.1 Introduction 105
4.2 Objectives of this chapter 105
4.3 Covalent functionalization of MoS_2 using benzoquinone 106
4.3.1 Liquid-phase exfoliation and characterization of MoS_2 106
4.3.2 Functionalization of MoS_2 with benzoquinone and 3-(pentafluorothio)-DL-phenylalanine 107
4.3.3 Functionalization of MoS_2 with Boc-PEG_{10}-NH_2 113
4.3.4 Conclusion 116
4.4 Benzoquinone-assisted liquid phase exfoliation of MoS_2 116
4.4.1 Exfoliation and characterization of MoS_2 nanosheets assisted by benzoquinone 116
4.4.2 Conclusion 119
4.5 Material and methods 119
4.6 References 122
Chapter 5 Conclusions and perspectives 125
5.1 Conclusions 125
5.2 Perspectives 126
List of publications and communications 129

Acronyms and Abbreviations

a.u.	Arbitrary units
ACPA	Anti-citrullinated protein antibodies
AFM	Atomic force microscopy
ATR FT-IR	Attenuated total reflection FT-IR
Boc	Di-tert-butyloxycarbonil group
BocNH-PEG_{10}-NH_2	*O*-(2-aminoethyl)-*O′*-[2-(Boc-amino)ethyl]decaethylene glycol
Boc-TEG-NH_2	2,2′-(ethylenedioxy)diethylamine
BSA	Bovine serum albumin
CAT	Catalase
CCK-8	Cell counting kit-8
Ce6	Chlorin e6
CSA	Chemical Shift Anisotropy
CVD	Chemical vapor deposition
DA	2,3-dimethylmaleic anhydride
DHR123	Dihydrorhodamine 123
Dox	Doxorubicin
DMF	N,N-dimethylformide
DMARDs	Disease-modifying anti-rheumatic drugs
DMSO	Dimethyl sulfoxide
DNA	Deoxyribonucleic acid
DSM	Dynamic structural model
EDC	N-(3-Dimethylaminopropyl)-N′-ethylcarbodiimide hydrochloride
EPR	Enhanced permeability and retention
EtOH	Ethanol
FA	Folic acid
FETs	Field effect transistors
Fmlp	N-formyl-methionyl-leucyl-phenylalanine
FR	folate receptor
FT-IR	Fourier transform IR
GCs	Glucocorticoids

GO	Graphene oxide
Hb	Hemoglobin
HPLC	High-performance liquid chromatography
IL	Interleukin
LPS	Lipopolysaccharides
m/z	Mass to charge ratio
MeOH	Methanol
MI	Myocardial infarction
MIC	Minimal inhibitory concentration
MMP	Matrix metalloproteinase
MRSA,	Methicillin-resistant Staphylococcus aureus
MS	Mass spectroscopy
MTT	3-(4,5-dimethylthiazol-2-yl)-2,5-diphenyltetrazolium bromide
MTS	3-(4,5-dimethylthiazol-2-yl)-5-(3-carboxymethoxyphenyl)-2-(4-sulfophenyl)-2H-tetrazolium
MTX	Methotrexate
NSAIDs	Nonsteroidal anti-inflammatory drugs (),
NHS	N-Hydroxysuccinimide
NIR	Near-infrared region
NMP	1-methyl-2-pyrrolidone
PAH	Polyallylamine hydrochloride
PEI	polyethyleneimine
PEG	Polyethylene glycol
PDT	Photodynamic therapy
PS	Photosensitizer
PTT	Photothermal therapy
$^1O_2$	Singlet oxygen
$O_2^{\cdot -}$	Superoxide anion radical
·OH	Hydroxyl radicals
OD	Oxidative Debris
RA	Rheumatoid arthritis
RF	Rheumatoid factor

RNA	Ribonucleic acid
ROS	Reactive oxygen species
S. aureus	Staphylococcus aureus
$SOCl_2$	Thionyl chloride
solid-state NMR	solid-state nuclear magnetic resonance
TEA	Triethylamine
diamino-TEG	2,2'-(ethylenedioxy)bis(ethylamine)
TEM	Transmission electron microscopy
TGA	Thermogravimetric analysis
TLC	Thin layer chromatography
TMDs	Inorganic transition-metal dichalchogenides
TNF-α	Tumor necrosis factor-α
Tris	Tris(hydroxymethyl)aminomethane
UV-Vis	Ultraviolet-visible spectroscopy
XPS	X-ray photoelectron spectroscopy

Résumé de Thèse

Chapitre 1. Introduction

L'oxyde de graphène (GO), la forme oxydée du graphène, est constituée d'un réseau hexagonal de carbone avec de nombreux groupes fonctionnels contenant de l'oxygène.[1] Sa bonne dispersabilité dans l'eau, sa rapide biodégradabilité et sa faible toxicité font du GO une plateforme idéale pour la nanomédecine, en particulier pour la thérapie du cancer.[2] Plusieurs méthodes ont été développées pour fonctionnaliser de façon covalente le GO en exploitant les fonctions oxygénées à sa surface.[3] Par rapport à la mono-fonctionnalisation, la double fonctionnalisation covalente permet de mieux contrôler l'attachement spécifique de molécules ou de nanoparticules distinctes *via* différentes réactions. Cependant, seules quelques stratégies pour la double fonctionnalisation covalente du GO ont été décrites et ces méthodes sont limitées par des conditions de réaction spécifiques et une faible efficacité.[4] Par conséquent, il est important de développer de nouvelles méthodes de double fonctionnalisation covalente du GO dans des conditions douces pour obtenir des taux de fonctionnalisation élevés.

Comme les matériaux à base de graphène, les dichalchogénures inorganiques de métaux de transition (TMD) ont récemment reçu une attention croissante en raison de leurs applications potentielles en optoélectronique, catalyse, électrochimie et médecine. Le disulfure de molybdène est un TMD prototypique et agit comme un excellent système modèle pour explorer la chimie des TMD 2D. L'exfoliation liquide est la voie "top-down" la plus efficace pour obtenir une monocouche ou quelques couches de MoS_2 à grande échelle.[5] Les propriétés intrinsèques des nanofeuillets de MoS_2 exfoliés peuvent être affinées par la modification de la surface avec de petites molécules permettant d'étendre leurs applications. Récemment, une méthode covalente douce a été décrite, en utilisant des dérivés de maléimide par addition de Michael.[6]

L'application des matériaux 2D dans le traitement des maladies a suscité un vif intérêt ces dernières années. En plus de l'administration de médicaments et la biodétection, le GO et les TMD ont montré leur grand potentiel en photothérapie en tant que vecteur de photosensibilisateurs (PS) et comme matériau photothermique. La photothérapie est un traitement thérapeutique non invasif avec des effets secondaires et une résistance aux médicaments négligeables ainsi qu'une faible toxicité systémique. La thérapie photothermique (PTT) et la thérapie photodynamique (PDT) sont deux types de photothérapies couramment utilisées pour le traitement du cancer et des maladies inflammatoires. La

PTT utilise des molécules ou des matériaux aux propriétés optiques uniques pour générer de la chaleur grâce à la conversion de l'énergie lumineuse absorbée, entraînant une augmentation locale de la température et la mort subséquente des cellules. Cependant, une forte intensité d'irradiation est requise car la mort irréversible des cellules dépend d'un accroissement de température suffisant.[7] La lumière intense peut induire des effets secondaires sur les tissus sains. La PDT utilise des agents photosensibilisateurs (PS) pour produire des espèces réactives de l'oxygène (ROS) sous irradiation lumineuse pour tuer les cellules. Mais, les PS traditionnels ne s'accumulent pas suffisamment dans la tumeur à cause de leur faible poids moléculaire, contrairement aux nanomatériaux en raison de l'effet EPR (perméabilité et rétention accrue).[10] De plus, la PDT consomme de l'oxygène produisant ainsi de l'hypoxie dans les cellules, ce qui empêche tout traitement ultérieur. Par conséquent, la combinaison de la PDT et de la PTT est nécessaire pour obtenir une plus grande efficacité thérapeutique. En introduisant la PTT, l'hyperthermie localisée peut favoriser la circulation sanguine conduisant à une teneur en oxygène accrue qui augmente simultanément l'effet de la PDT[8] avec une densité d'irradiation plus faible que la PTT.

La polyarthrite rhumatoïde (PR) est une maladie auto-immune inflammatoire chronique affectant plusieurs organes. Les macrophages sont l'une des principales cellules qui déclenchent la PR en libérant continuellement certaines molécules pro-inflammatoires. Le récepteur folate β (FRβ) est sélectivement surexprimé sur les macrophages dans la synoviale de la PR et a été utilisé comme cible pour le traitement de cette maladie, par exemple pour la biodétection et l'administration de médicaments.[9,10] Des études récentes ont montré le grand potentiel de la photothérapie dans le traitement de la polyarthrite rhumatoïde. Mais l'effet synergique de la PTT et de la PDT a été moins exploré. Lu *et al.* ont décrit le traitement combiné PTT/PDT avec des nanoparticules de $Cu_{7.2}S_4$ pour le traitement de la PR. En tant que méthode thérapeutique non invasive, il est intéressant d'appliquer la PTT et la PDT combinées pour le traitement de la PR.

L'objectif de ma thèse est centré sur les applications biomédicales des matériaux 2D, notamment l'oxyde de graphène et le MoS_2. Je me suis concentré sur la préparation de ces matériaux dans l'eau et sur les applications possibles comme systèmes d'administration de médicaments. La première partie de mon travail a consisté à explorer la double fonctionnalisation covalente du GO. Trois stratégies différentes ont été étudiées et un conjugué à base de GO fonctionnalisé avec l'acide folique et la chlorine e6 a été préparé. Dans la deuxième partie du travail, nous nous sommes concentrés sur l'application du GO doublement fonctionnalisé dans le traitement du cancer et de la PR en combinant la PTT et la PDT. La troisième partie concerne la fonctionnalisation covalente du MoS_2 par le biais de

la bénzoquinone. Nous avons en outre étudié la possibilité d'une exfoliation en phase liquide du MoS_2 à l'aide de la bénzoquinone.

Chapitre 2. Double fonctionnalisation de l'oxyde de graphène

La réaction de carboxylation du GO est une méthode largement utilisée pour introduire des acides carboxyliques supplémentaires à sa surface. Ces groupements peuvent être ensuite modifiés par des réactions d'amidation ou d'estérification. Cependant, les protocoles prévoient l'utilisation d'une base forte qui provoque souvent une désoxygénation, entraînant une réduction partielle du GO,[11] modifiant ainsi ses propriétés et influençant l'efficacité de la fonctionnalisation. Pour clarifier l'impact d'une solution alcaline forte sur le GO, nous avons préparé du GO carboxylé en utilisant différentes molarités de NaOH (Schéma 1) et caractérisé le GO préparé par différentes méthodes. L'augmentation significative des groupes carboxyliques sur le GO n'a été observée que dans des conditions basiques fortes (3 M NaOH dans l'eau) par spectroscopie photoélectronique aux rayons X (XPS), mais une réduction partielle concomitante du GO s'est également produite.

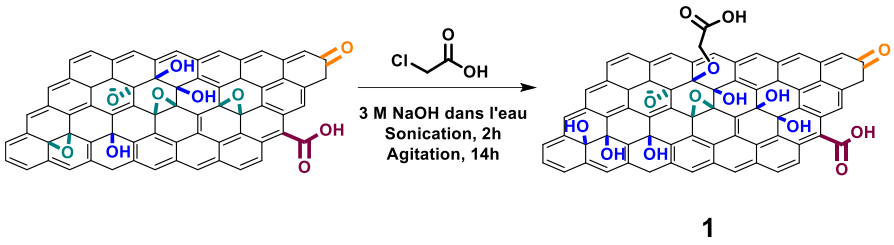

Schéma 1. Réaction de carboxylation du GO.

Pour mieux comprendre l'effet de la réduction partielle sur la fonctionnalisation du GO, nous avons combiné la réaction d'ouverture du cycle époxyde et la carboxylation du GO suivie d'une amidation en utilisant le dérivé *O*-(2-aminoéthyl)-*O′*-[2-(Boc-amino)éthyl]decaéthylene glycol (Boc-PEG_{10}-NH_2) pour réaliser d'abord la mono-fonctionnalisation puis la double fonctionnalisation en différentes étapes (Schéma 2). Les fonctionnalités sur le GO ont été caractérisées par le test de Kaiser et par analyse thermogravimétrique (ATG). Bien que le GO ait été doublement fonctionnalisé avec succès, la réduction partielle du GO a entraîné une efficacité moindre de la fonctionnalisation totale, limitant ainsi dans une certaine mesure cette méthode pour une application ultérieure.

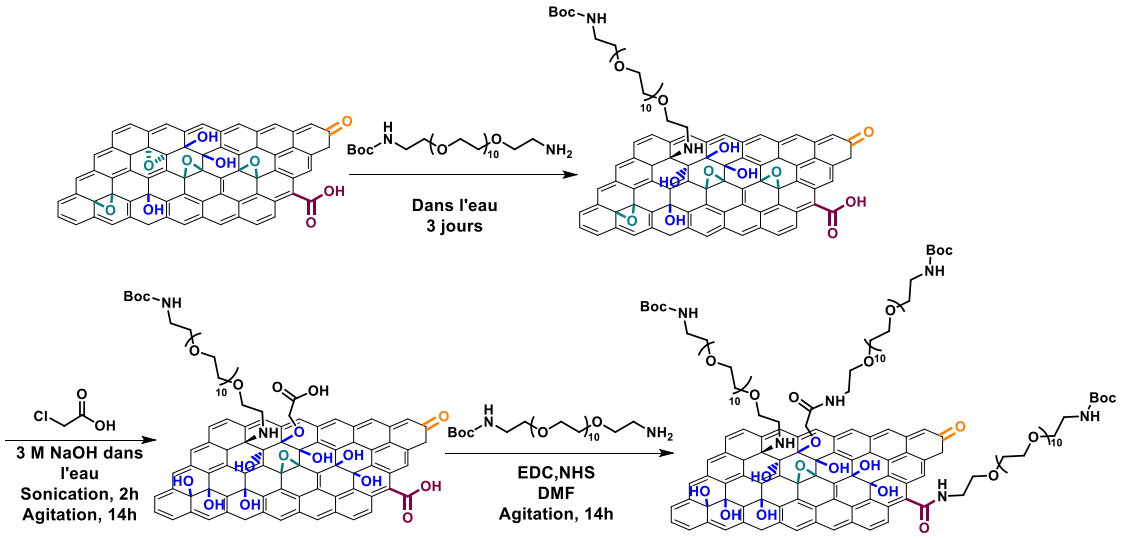

Schéma 2. Double fonctionnalisation du GO combinant la réaction d'ouverture du cycle époxyde et les réactions de carboxylation et d'amidation.

Afin de limiter la réduction significative du GO lors de la carboxylation, nous avons répété cette réaction en utilisant une quantité moindre d'hydroxyde de sodium. La carboxylation du GO a été effectuée dans une solution d'hydroxyde de sodium à pH 9 et pH 13. Les deux échantillons ont été caractérisés par XPS. Cependant, sur la base des spectres C1s, nous n'avons pas pu observer une augmentation évidente de la quantité de groupements carboxyliques dans les deux cas, indiquant une efficacité plus faible de la carboxylation. Pour confirmer si plus de groupements carboxyliques étaient liés par covalence sur la surface du GO, les échantillons de GO carboxylés préparés à pH 9 et pH 13 ont été dérivatisés avec de la *N*-Boc-2,2'-(éthylènedioxy) diéthylamine (BocNH-TEG-NH_2). Les deux GO à double fonctionnalité ne présentaient pas une quantité plus élevée d'amines par rapport aux précurseurs en raison de la faible efficacité de l'étape de carboxylation.

Au total, nos résultats démontrent que la carboxylation n'est pas une approche efficace pour la fonctionnalisation du GO en raison de la réduction partielle du GO et qu'elle peut difficilement être étendue pour atteindre une double fonctionnalisation efficace du GO pour d'autres modifications. Ce travail montre qu'il est très important de considérer les réactions secondaires qui peuvent ne pas être mentionnées dans la littérature. Le contrôle de la fonctionnalisation du GO est crucial, notamment à des fins biologiques.

Étant donné que le GO n'est pas stable à des températures élevées et des conditions de base fortes, il est important de développer une méthode de fonctionnalisation dans des conditions douces. Ici, nous avons développé une méthode facile et efficace pour doublement fonctionnaliser le GO par la

formation de liaisons covalentes *via* la combinaison de la réaction d'ouverture du cycle époxyde et une addition de Michael des groupes hydroxyles sur la bénzoquinone (Schéma 3).[12] La première étape a consisté à introduire du Boc-aminoéthanethiol par attaque nucléophile du thiol sur l'époxyde conduisant à l'ouverture du cycle et à la formation de liaisons thioéthers et de nouveaux groupes hydroxyles. Ensuite, les groupements hydroxyle du GO mono-fonctionnalisé ont été dérivés avec la bénzoquinone. La fraction hydroquinone est auto-oxydée par la bénzoquinone libre présente en excès pour préparer le GO fonctionnalisé avec la bénzoquinone permettant d'envisager une fonctionnalisation ultérieure avec des dérivés d'amine. Enfin, la 3-(pentafluorothio)-phénylalanine a été ajoutée au dérivé GO-bénzoquinone par une addition de Michael entre l'amine et la fraction bénzoquinone. Le groupe pentafluorothio facilite la caractérisation par XPS et FT-IR et la fonction COOH présente l'avantage de pouvoir être fonctionnalisée par amidation ou estérification.

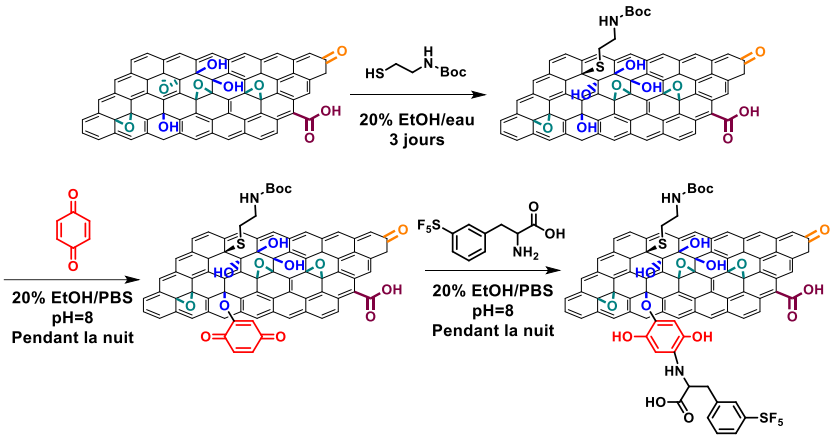

Schéma 3. Double fonctionnalisation du GO par la méthode impliquant la bénzoquinone.

L'analyse XPS a révélé que le GO a été dérivé avec succès avec deux groupes fonctionnels. Une augmentation des teneurs en azote et en soufre a été observée après l'introduction du Boc-aminoéthanethiol. De plus, l'élément fluor a été détecté par XPS (1,6%) après le greffage de la 3-(pentafluorothio)-phénylalanine, tandis que le pic était négligeable dans les conjugués précurseurs de GO. La déconvolution du pic haute résolution S2p du GO de départ n'a montré qu'un seul pic à 168,4 eV, qui a été attribué à la liaison S-O provenant de groupes organosulfates introduits sur la surface GO lors de sa synthèse impliquant des conditions acides fortes (par exemple, H_2SO_4) (figure 1d).[13] Après la fonctionnalisation avec le Boc-aminoéthanethiol, un nouveau pic est apparu à 164,0 eV, attribué à la nouvelle liaison S-C, confirmant ainsi l'ouverture des époxydes (figure 1e).[14] Après la conjugaison de la 3-(pentafluorothio)-phénylalanine, le pic S2p a clairement montré la présence du nouveau pic correspondant à la liaison S-F à 173,0 eV (figure 1f), indiquant une double fonctionnalisation réussie

du GO. La double fonctionnalisation a été confirmée par spectroscopie ATR FT-IR, TGA, voltampérométrie cyclique et microscopie à force atomique.

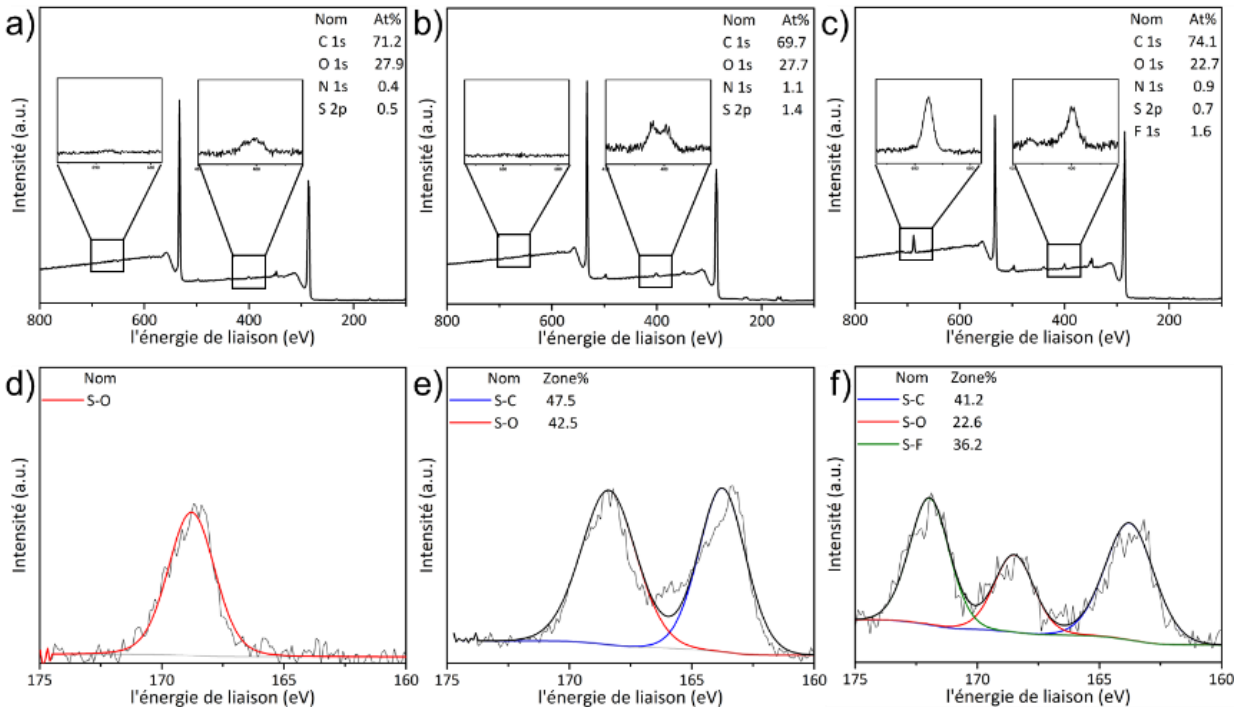

Figure 1. Spectres XPS (a, b, c) avec zoom sur les pics F1s (encart de gauche) et N1s (encart de droite) et spectres S2p (d, e, f) haute résolution du GO (colonne de gauche), du GO mono-fonctionnalisé (colonne du milieu) et du GO doublement fonctionnalité (colonne de droite).

En résumé, nous avons développé une méthode simple et directe pour la double fonctionnalisation du GO dans des conditions douces par dérivation successive des époxydes et des groupes hydroxyles sans chauffage ou sans ajout de catalyseurs métalliques. Notre stratégie est particulièrement appropriée pour la conjugaison de diverses biomolécules afin d'obtenir un GO multifonctionnel pour des applications en thérapie, en biocapture et en bioimagerie.

Chapitre 3. Thérapies photothermiques et photodynamiques combinées pour le traitement des cellules cancéreuses et de la PR

En plus d'exploiter à la fois les époxydes et les hydroxyles sur le plan basal du GO, une méthode simple a également été étudiée pour réaliser la multifonctionnalisation du GO par une réaction d'ouverture des époxydes en une seule étape (Schéma 4). L'acide folique (AF) a pu servir de groupe cible aux FRβ

surexprimés sur les macrophages activés. Le chlore e6 (Ce6) est un photosensibilisateur largement utilisé en PDT, qui pourrait produire une apoptose et une nécrose des cellules cancéreuses induisant des ROS lors de l'irradiation laser.[15] Le GO doublement fonctionnalisés avec le AF et la Ce6 (GO-AF/Ce6) a été en mesure de cibler les macrophages activés grâce à l'affinité du AF envers FRβ et il pourrait en outre être utilisé pour combiner la thérapie PTT et PDT sous irradiation avec différentes longueurs d'onde.

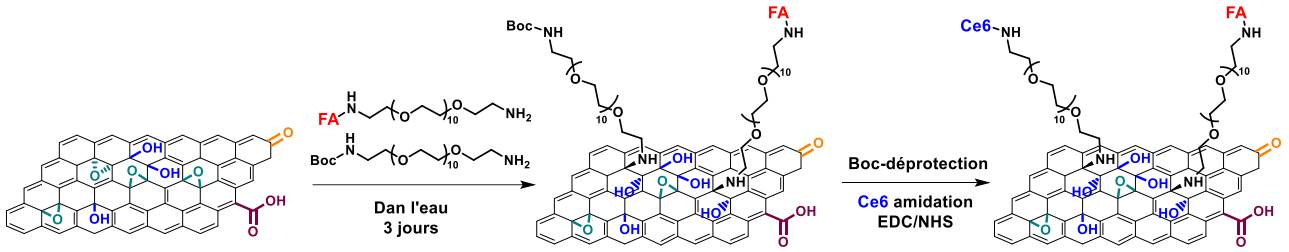

Schéma 4. Préparation du conjugué GO-AF/Ce6.

Le GO-AF/Ce6 a été caractérisé par différentes méthodes, y compris UV, immunocoloration et fluorimétrie (figure 2). Les spectres UV ont montré deux pics d'absorbance spécifique du AF et de la Ce6 centrés à 280 nm et 420 nm, respectivement. La conjugaison du FA sur le GO a ensuite été confirmée par immunocoloration. Les échantillons de GO fonctionnalisés avec et sans AF ont été incubés avec un anticorps anti-AF suivi par un anticorps secondaire (portant des nanoparticules d'or) qui reconnaît l'anticorps anti-FA. Les nanoparticules d'or ont un bon contraste en TEM. Le GO fonctionnalisé avec le AF a montré un nombre plus élevé de nanoparticules d'or par rapport au GO sans AF, indiquant que le AF a été lié avec succès au GO. La Ce6 sur le GO a été confirmée par spectroscopie de fluorescence. Comparé à une simple physisorption, le GO-AF/Ce6 présente une émission de fluorescence plus forte, indiquant que davantage de Ce6 a été ajouté au GO par amidation.

L'effet photothermique et photodynamique a ensuite été évalué. Après 10 min d'irradiation, la température a augmenté de 5°C dans une dispersion aqueuse de 25 µg mL^{-1} de GO-AF/Ce6, alors qu'aucun accroissement significatif n'a été observé après irradiation d'eau pure. La génération de ROS a été testée par dosage de dihydrorhodamine 123 et le GO doublement fonctionnalisé a montré une capacité de génération de ROS similaire à la Ce6 seule. Le GO/AF a été en outre utilisé pour des expériences cellulaires.

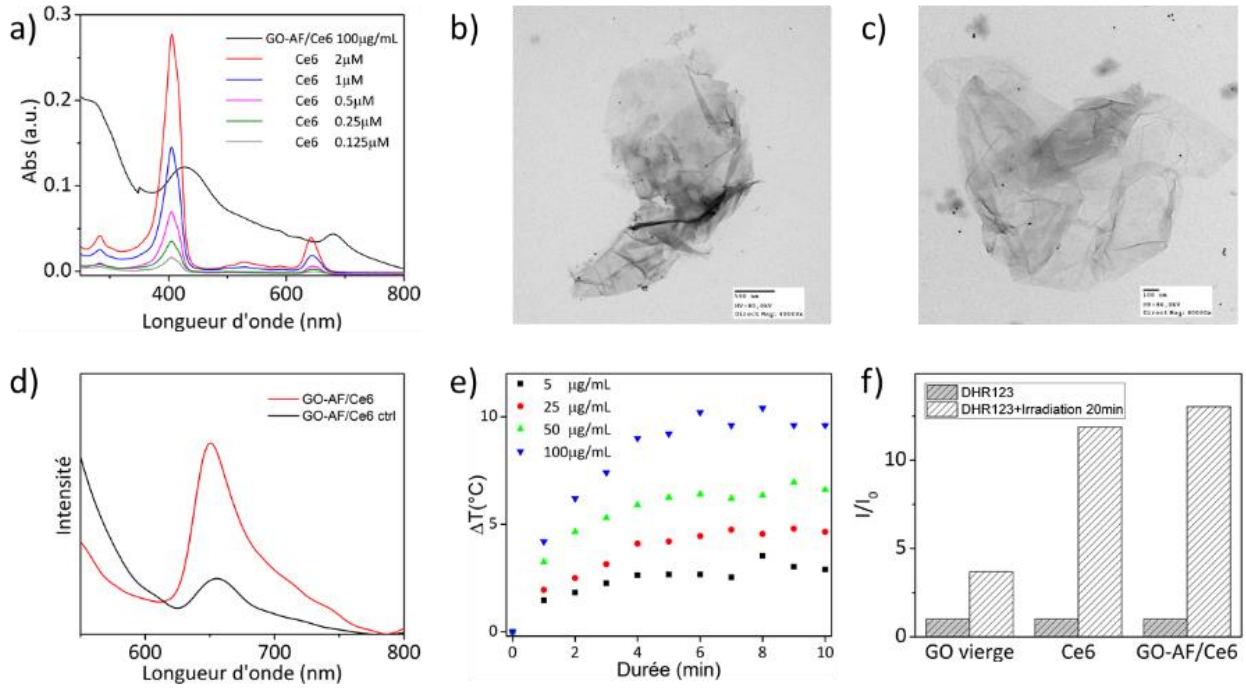

Figure 2. a) Spectres UV de GO-AF/Ce6, b, c) Images TEM d'immunocoloration du GO avec AF et du GO sans AF, d) Emission de fluorescence du GO-AF/Ce6 et du contrôle, e) Effet PTT du GO-AF/Ce6 dans l'eau et f) Génération de ROS du GO, de la Ce6 et du GO-AF/Ce6.

La photothérapie, y compris la thérapie photodynamique et photothermique, se développe rapidement pour le diagnostic et le traitement du cancer comme alternative à la radiothérapie et à la chimiothérapie. Ces traitements ont comme avantages une invasion minimale, une sélectivité élevée et moins toxique, avec des effets secondaires et une résistance aux médicaments négligeables. Grâce à la présence du AF sur le GO, le GO-AF/Ce6 a été utilisé comme vecteur de la Ce6 ciblant les cellules HeLa, accélérant l'accumulation de la Ce6 à l'intérieur des cellules. La PTT a pu réduire l'effet d'hypoxie en favorisant la circulation sanguine vers le site tumoral. Ainsi, un effet synergique de la PTT et de la PDT pourrait être obtenu grâce à un seul et unique conjugué.

La cytotoxicité du GO doublement fonctionnalisé sans irradiation a d'abord été évaluée et a montré une bonne viabilité cellulaire supérieure à 85% à une concentration de 25 $\mu g \cdot mL^{-1}$ après 24 h d'incubation. Tout en étudiant l'absorption cellulaire du GO, les images de microscopie confocale ont révélé que le GO doublement fonctionnalisé a commencé à pénétrer la cellule HeLa en 4 h d'incubation et a montré une fluorescence plus forte de Ce6 après 8 h. Cependant, la fluorescence s'est atténuée après 24 h d'incubation, ce qui indique que moins de Ce6 s'est accumulé dans les cellules, ce qui à son tour réduirait l'efficacité de la photothérapie. Après un traitement par irradiation lumineuse à 660 nm

(200 mW·cm^{-2}, 10 min) pour induire la PDT en 8 h d'incubation, le GO doublement fonctionnalisé a montré une viabilité cellulaire d'environ 53%. Pour la PTT (808 nm, 2 W·cm^{-2}, 10 min), une viabilité cellulaire similaire a été obtenue (autour de 49%). Pour améliorer l'effet thérapeutique, l'incubation du matériel a été raccourcie. Nous avons donc évalué l'efficacité de la PTT et de la PDT après 4 h et 8 h d'incubation. Cependant, une augmentation inattendue de la viabilité cellulaire a été observée probablement en raison de l'augmentation du métabolisme causée par la photothérapie.

En vue de ces résultats, nous avons donc décidé d'utiliser une autre ligné cellulaire. Les cellules cancéreuses du sein, MCF-7, ont été utilisées pour évaluer les propriétés antitumorales de GO-FA/Ce6. Après un traitement par irradiation lumineuse à 660 nm pour induire la PDT après 8 h d'incubation, le GO doublement fonctionnalisé a montré une viabilité cellulaire d'environ 68%. Pour la PTT, une viabilité cellulaire similaire a été obtenue (autour de 51%). En outre, la PDT suivie de la PTT a montré une efficacité de destruction plus élevée pour les cellules, montrant une viabilité cellulaire finale de 23% après irradiation (Figure 3).

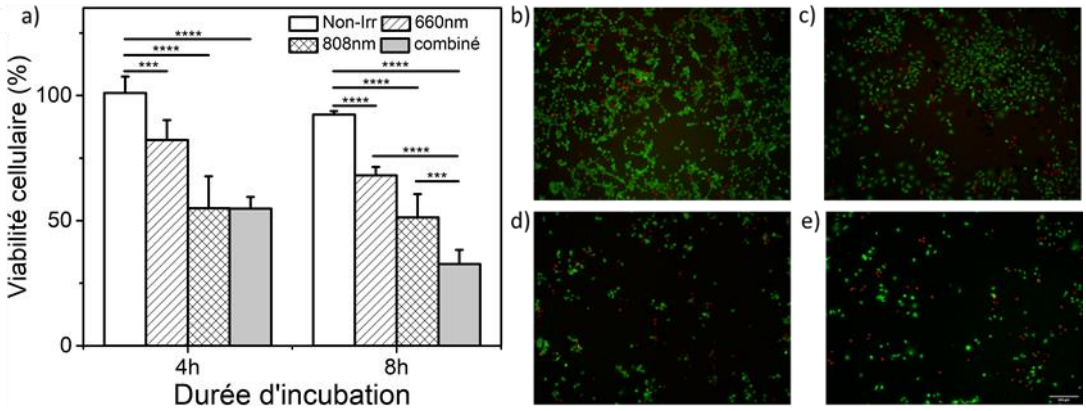

Figure 3. a) Viabilité cellulaire de MCF-7 traitées avec le GO doublement fonctionnalisé après irradiation. b, c, d, e) Images de microscopie à fluorescence de cellules MCF-7 traitées avec le même GO : b) sans irradiation, c) après irradiation à 660 nm, d) après irradiation à 808 nm, e) après une irradiation à 808 nm suivie d'une irradiation à 660 nm. Les cellules MCF-7 ont été marquées avec le kit Dead/Live (cellules vivantes: vert; cellules mortes: rouge).

Enfin, le GO-AF/Ce6 a été testé sur des macrophages, cellules impliquées dans la PR. Les macrophages RAW 264.7 ont montré une bonne tolérance au conjugué GO-AF/Ce6, même à la plus haute de concentration de 50 µg·mL^{-1} après 24 h d'incubation. Ces cellules se sont montrées plus sensibles au traitement PTT, leur viabilité cellulaire diminuant significativement à 25%. Cependant, les macrophages ont montré une résistance contre les ROS générés pendant la PDT avec une viabilité

cellulaire diminuée à 72% après irradiation. Les expériences pour vérifier les effets synergiques combinés de PDT et PTT sont en cours.

Chapitre 4. Fonctionnalisation covalente et exfoliation du MoS_2 à l'aide de la bénzoquinone

Dans cette partie, nous avons étudié la fonctionnalisation et l'exfoliation en phase liquide de MoS_2 à l'aide de bénzoquinone. Des colloïdes à faible couche de MoS_2 ont d'abord été préparés à l'aide du cholate de sodium dans une mélange d'éthanol/eau dans d'un bain à sonication. Après centrifugation et lavage, le matériau préparé a ensuite été mis à réagir avec un excès de bénzoquinone. La Boc-PEG_{10}-NH_2 et la 3-(pentafluorothio)-phénylalanine ont été choisies comme deux fonctionnalités à greffer sur le MoS_2 (Schéma 5). Le succès de la conjugaison du PEG sur le MoS_2 a été confirmé par ATG avec une perte de poids plus importante. Le MoS_2 dérivé avec la 3-(pentafluorothio)-phénylalanine a été caractérisé par XPS et une augmentation de la composition en élément fluor a été observée (Figure 4).

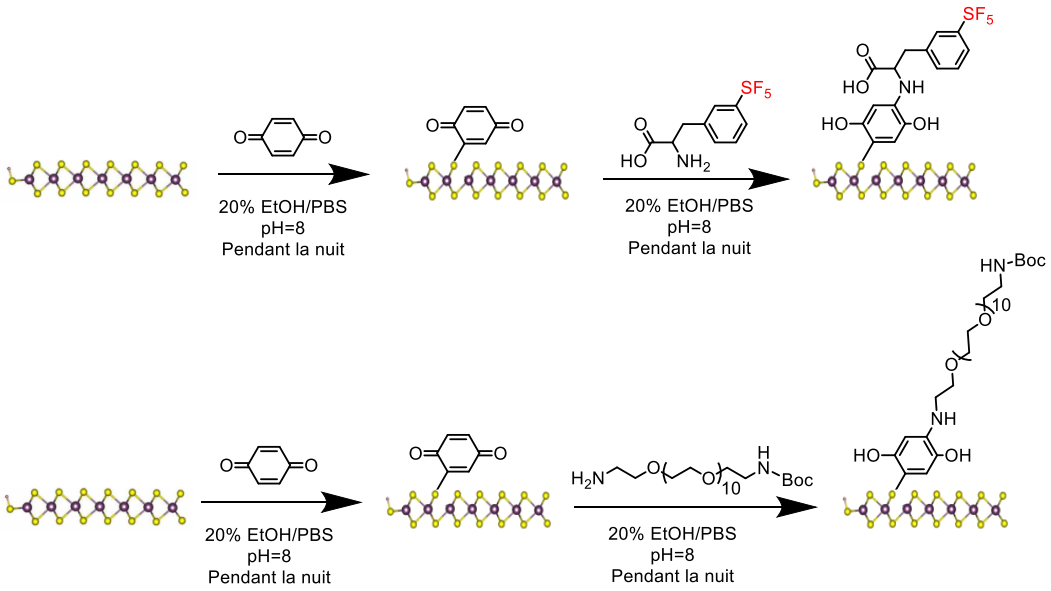

Schéma 5. Fonctionnalisation du MoS_2 par la méthode impliquant la bénzoquinone.

Comme le MoS_2 fonctionnalisé avec la bénzoquinone présente une meilleure dispersabilité dans l'eau que le MoS_2 comportant quelques feuillets, nous avons conçu une expérience afin d'exfolier le MoS_2 en utilisant la bénzoquinone à la place du cholate de sodium. La dérivation du MoS_2 avec la bénzoquinone peut être réalisée en même temps. Une expérience préliminaire a été réalisée et le matériau préparé a été caractérisé par TEM. Les images TEM ont montré que du MoS_2 constitué de quelques feuillets a été obtenu avec une taille latérale d'environ 100 nm et une bonne dispersabilité

dans l'eau. Une caractérisation plus détaillée du matériau préparé doit être effectuée, ainsi qu'une étude de sa réactivité.

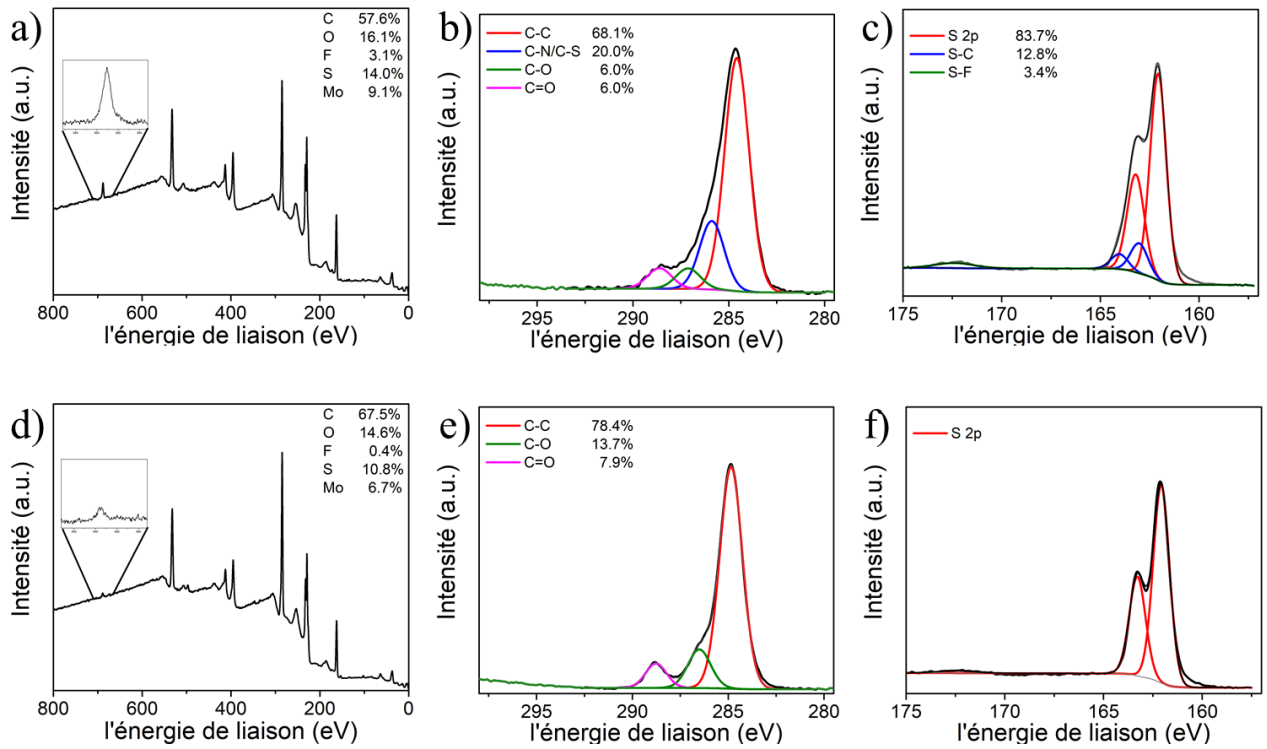

Figure 4. Spectres XPS (a, d) avec zoom sur les pics F1s (encart de gauche), spectres C1s (b, e) et spectres S2p (c, f) haute résolution du MoS_2 dérivé avec la 3-(pentafluorothio)-phénylalanine (première ligne), et de l'échantillon contrôle préparé en mélangeant MoS_2 avec la 3-(pentafluorothio)-phénylalanine (deuxième ligne).

Chapitre 5. Conclusions et perspectives

Au cours de ma thèse, j'ai exploré la double fonctionnalisation covalente du GO et son application dans le traitement des cellules cancéreuses et de la PR par le biais d'un traitement combiné PTT et PDT. Différentes stratégies de double fonctionnalisation ont été explorées. Le GO peut être doublement fonctionnalisé par une procédure par étapes *via* la combinaison d'une réaction de carboxylation en utilisant l'acide chloroacétique, suivie d'une amidation et d'une réaction d'ouverture des époxydes. Mais l'application d'un excès de NaOH entraîne la désoxygénation du GO, réduisant l'efficacité de fonctionnalisation. Une méthode à base de bénzoquinone a ensuite été développée. Lorsqu'elle est combinée avec une réaction d'ouverture des époxydes, une double fonctionnalisation flexible du GO peut être obtenue dans des conditions douces. En parallèle, du GO doublement fonctionnalisé avec l'acide folique et la chlorine 6 été préparé par une réaction d'ouverture des époxydes en une seule étape avec deux dérivés PEG-AF et PEG-Ce6. Le GO doublement

fonctionnalisé a ensuite été appliqué aux cellules HeLa pour étudier la PTT et la PDT pour le traitement du cancer. Un effet synergique a été observé. De plus, nous avons étudié la fonctionnalisation covalente du MoS_2 en utilisant la bénzoquinone. La conjugaison de petites molécules sur la surface du MoS_2 a été confirmée et nous avons exploré l'exfoliation en phase liquide du MoS_2 à l'aide de la bénzoquinone. Nos études fournissent plusieurs stratégies flexibles pour la préparation de conjugués GO doublement fonctionnels, ainsi que la fonctionnalisation covalente du MoS_2. En changeant les groupes fonctionnels, les matériaux préparés peuvent être appliqués à différents domaines. De plus, ces réactions peuvent être étendues à d'autres matériaux 2D pour une fonctionnalisation covalente.

Références

1. D. R. Dreyer, S. Park, C. W. Bielawski and R. S. Ruoff, "The chemistry of graphene oxide", *Chem. Soc. Rev.*, 2010, **39**, 228-240.

2. C. Martín, A. Ruiz, S. Keshavan, G. Reina, D. Murera, Y. Nishina, B. Fadeel and A. Bianco, "A Biodegradable Multifunctional Graphene Oxide Platform for Targeted Cancer Therapy", *Adv. Funct. Mater.*, 2019, **29**, 1901761-1901771.

3. I. A. Vacchi, S. Guo, J. Raya, A. Bianco and C. Menard-Moyon, "Strategies for the Controlled Covalent Double Functionalization of Graphene Oxide", *Chem. Eur. J.*, 2020, **26**, 6591 –6598

4. K. C. Mei, N. Rubio, P. M. Costa, H. Kafa, V. Abbate, F. Festy, S. S. Bansal, R. C. Hider and K. T. Al-Jamal, "Synthesis of double-clickable functionalised graphene oxide for biological applications", *Chem. Commun.*, 2015, **51**, 14981-14984.

5. A. Stergiou and N. Tagmatarchis, "Molecular Functionalization of Two‐Dimensional MoS_2 Nanosheets", *Chem. Eur. J.*, 2018, **24**, 18246-18257.

6. M. Vera-Hidalgo, E. Giovanelli, C. Navio and E. M. Perez, "Mild Covalent Functionalization of Transition Metal Dichalcogenides with Maleimides: A "Click" Reaction for 2H-MoS_2 and WS_2", *J. Am. Chem. Soc.*, 2019, **141**, 3767-3771.

7. D. Jaque, L. Martinez Maestro, B. del Rosal, P. Haro-Gonzalez, A. Benayas, J. L. Plaza, E. Martin Rodriguez and J. Garcia Sole, "Nanoparticles for photothermal therapies", *Nanoscale*, 2014, **6**, 9494-9530.

8. N. Frazier and H. Ghandehari, “Hyperthermia approaches for enhanced delivery of nanomedicines to solid tumors”, *Biotechnol. Bioeng.*, 2015, **112**, 1967-1983.

9. M. Yang, J. Ding, Y. Zhang, F. Chang, J. Wang, Z. Gao, X. Zhuang and X. Chen, “Activated macrophage-targeted dextran–methotrexate/folate conjugate prevents deterioration of collagen-induced arthritis in mice”, *J. Mater. Chem. B*, 2016, **4**, 2102-2113.

10. D. Chandrupatla, C. F. M. Molthoff, A. A. Lammertsma, C. J. van der Laken and G. Jansen, “The folate receptor β as a macrophage-mediated imaging and therapeutic target in rheumatoid arthritis”, *Drug Delivery Transl. Res.*, 2019, **9**, 366-378.

11. C. Chen, W. Kong, H. M. Duan and J. Zhang, “Theoretical simulation of reduction mechanism of graphene oxide in sodium hydroxide solution”, *Phys. Chem. Chem. Phys.*, 2014, **16**, 12858-12864.

12. S. Guo, Y. Nishina, A. Bianco and C. Ménard-Moyon, “A Flexible Method for Covalent Double Functionalization of Graphene Oxide”, *Angew. Chem., Int. Ed.*, 2020, **59**, 1542-1547.

13. S. Eigler, C. Dotzer, F. Hof, W. Bauer and A. Hirsch, “Sulfur species in graphene oxide”, *Chem. Eur. J.*, 2013, **19**, 9490-9496.

14. Z. Wang, Y. Dong, H. Li, Z. Zhao, H. B. Wu, C. Hao, S. Liu, J. Qiu and X. W. Lou, “Enhancing lithium–sulphur battery performance by strongly binding the discharge products on amino-functionalized reduced graphene oxide”, *Nat. Commun.*, 2014, **5**, 5002-5007.

15. X. Y. Wong, A. Sena-Torralba, R. Alvarez-Diduk, K. Muthoosamy and A. Merkoci, “Nanomaterials for nanotheranostics: tuning their properties according to disease needs”, *ACS Nano*, 2020, **14**, 2585-2627.

Chapter 1 Introduction

1.1 2D materials

In recent years, 2D materials have been raising a great interest due to a wide range of outstanding properties that make them materials with great potential applications in different fields covering energy storage,[1, 2] antibacterial,[3, 4] biosensing,[5] diagnosis and therapy,[6-9] and artificial organs.[10] Graphene family materials, including graphene, graphene oxide, reduced graphene oxide and graphene quantum dots, are one of the most studied 2D materials. Graphene is a nanomaterial made of a single atomic layer of sp^2-hybridized carbon atoms, in the form of a 2D hexagonal lattice. It was first isolated by Geim and Novoselov in 2004, allowing them to obtain the Nobel prize in Physics in 2010.[11, 12] The interest of research on graphene was soon rising up due to its unique properties, making it one of the most studied area until now. But the poor aqueous dispersibility and low degree of functionalization still hamper the application of graphene in some domains,[12] especially the biomedical domain covering the treatment of diseases. Following the isolation of graphene, other classes of 2D materials including layered nitrides, transition metal dichalcogenides (TMDs), transition metal oxides have gained increasing research interest, since they have unique electronic and photonic properties. Molybdenum disulfide is always used as the model for the study of the TMD material. We chose GO and MoS_2 as the materials for further research.

1.1.1 Graphene oxide

Graphene oxide (GO) is the oxidized form of graphene, consisting of a hexagonal ring-based carbon network with abundant oxygen-containing functional groups.[13] The study of graphene oxide was much earlier than the isolation of graphene and a reliable method was discovered by Brodie in 1895 by a oxidation treatment on graphite using potassium chlorate and fuming nitric acid.[14] The yellowish material was also called at the beginning graphite oxide ,[15] and it has attracted the interest of research for more than 160 years. However, the structure and properties of GO were started to be fully revealed in recent years with the help of modern analytical method.

Lerf and Klinowski proposed a GO model in 1998 based on the analysis of solid-state nuclear magnetic resonance (solid-state NMR),[16] which is the most accepted model until today. The GO is consisting of abundant epoxides and hydroxyl groups distributed on the basal plane of GO with carboxylic acids at the rims. This model was confirmed by adding more details to the structure of GO using multidimentsional ^{13}C solid-state NMR.[17] Besides the majority of epoxides and hydroxyls, carbon-centered radicals, endoperoxides, ketones and lactols are also identified.[18-20] Moreover, a dynamic structural model (DSM) was introduced by Dimiev *et al.*,[21, 22] which suggested a dynamic structure with undefined set of functional groups (Figure 1a). Instead of a static structure with a given set of

functional groups, the authors suggested that these functional groups are constantly developing and transforming in water. More defects were introduced to the structure of basal plane of GO during the oxidation procedure and with the involvement of water molecules, the surface transformation occurs, leading to a more complex form consistent on functional groups at the edges and accumulation of negative charges. This model would also explain the gradual degradation of GO in water and the consequent generation of an acidic solution. In addition, the formation of highly oxidized debris (oxidative debris, OD) was observed during the strong overoxidation.[23] These highly oxidized fragments are adsorbed onto the surface of GO flakes and contribute to most of the oxygenated functional groups. The cleavage/removal of OD by washing with alkaline solutions would lead to the reduction of GO.

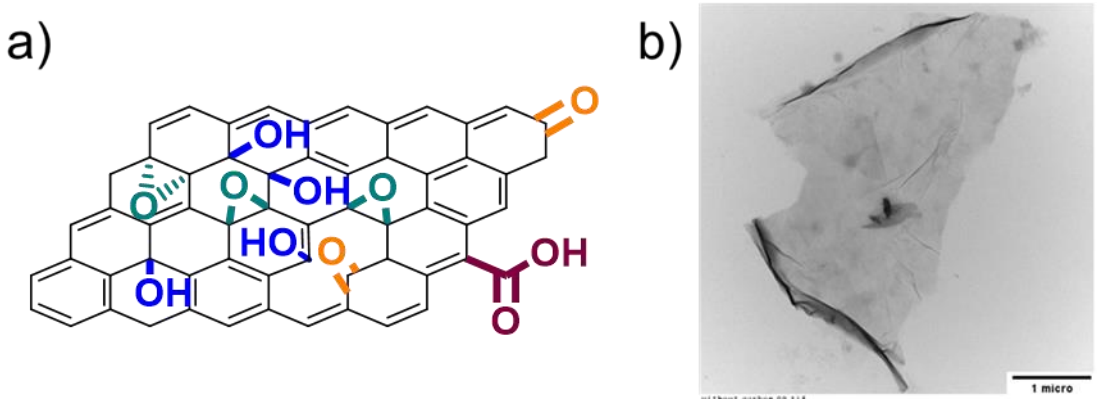

Figure 1.1 a) Graphene oxide molecular structure. The vicinal diols on GO are deoxygenated with the C-C bond cleavage and the formation ketone and acidic enol;[22] b) TEM image of graphene oxide.

Generally, the synthesis of GO is mainly based on an oxidative procedure from graphite. As mentioned above, the first reliable method was investigated by Brodie using potassium chlorate and fuming nitric acid.[14] Later this method was improved by Staudenmaier in 1898 adding concentrated sulfuric acid to the oxidation mixture, reduced the oxidation cycle.[24] In 1985, this protocol was further developed by Hummers and Offenman by introducing potassium permanganate as a strong oxidant with sodium nitrate and sulfuric acid.[25] The Hummers' method was then modified by replacing the sodium nitrate with phosphoric acid to avoid the production of toxic gases.[26] Moreover, hydrogen peroxide was also introduced to the reaction mixture to solubilized Mn species formed during the oxidation.[27] The modified Hummers' methods are the most used method of GO preparation.

Thanks to the unique structure of graphene oxide and the facility to prepare it, this material owns many excellent properties such as large surface area, satisfying water dispersibility,[28] good biodegradability,[29, 30] optical transparency and photoluminescence quenching,[31, 32] which are important for the applications especially in biomedical and biosensing fields. Many papers in the literature have reported the application of GO and its reduced form (rGO) in the treatment of cancer or other diseases as an excellent platform for targeted drug delivery,[33] diagnosis[34] and phototherapy.[35]

1.1.2 Functionalization of graphene oxide

Thanks to its properties, GO has become the mostly studied 2D material, especially for biomedical applications. To achieve better performances, the fine-designed modification of GO with diverse functional groups is required. Generally, chemical functionalization of GO, including covalent or non-covalent method, is considered as the best protocol to enhance the designed performance of GO complexes. The chemical modifications of GO allow to modulate the physicochemical properties and derivatize GO with different functional groups, which would greatly extend the applications in different areas.[36-39]

Noncovalent functionalization is always preferred in the literature as it is easy to perform and can diminish the alteration of the structure or physicochemical properties of GO, while introducing new functional groups on its surface.[38] Thanks to the similar basal plane as graphene, the high surface area of GO allows adsorption of a large amount of drugs,[6, 40] RNA[41, 42] or nanoparticles.[43] The presence of defects and the epoxides or hydroxides bound to the carbon atoms formed by the transformation of sp^2 carbon to sp^3 carbon are potentially beneficial for combining multiple interactions in the case of non-covalent fucntionalization.[38] Polymer wrapping, π–π interactions, electron donor−acceptor complexes, and van der Waals forces are involved in the non-covalent functionalization procedure.[44-46] These modifications of GO could lead to enhanced dispersibility, better biocompatibility and higher loading capacity of drugs or sensing probes.

However, the functionalization of GO through a non-covalent protocol affords complexes that are less stable than the covalent interactions. The unspecific leakage of a cargo adsorbed onto GO was observed in some cases, leading to an certain degree of toxicity of GO, especially in complex biological conditions.[47, 48] Compared to non-covalent complexation, the covalent functionalization enables to prepare more stable conjugates and minimize the release of molecules adsorbed onto the GO surface, especially for biomedical uses. The abundant oxygen-containing functional groups, including epoxides, hydroxyls and carboxyl groups at the edges, not only provide GO with unique properties, but also provide active sites for a specific chemical functionalization of GO surface. Several strategies have been reported to functionalize GO covalently by targeting different functional groups such as carboxylic acids,[49] epoxide rings[50] and hydroxyl groups,[51-53] which are the principal groups for the functionalization.

In most of the approaches, reported in the literature, the carboxylic acids located at the rim of GO are the prime targets for reaction. The carboxyl groups are normally first activated by coupling reagents or thionyl chloride followed by the amidation reaction with molecules containing free amines such as peptides, amino-terminal polyethylene glycol (PEG) or polyethyleneimine (PEI) chains (Scheme 1.1). Huang *et al.* reported a GO composite with an amino and a 6-carboxyfluorescein dual labeled DNA covalently attached via an amide bond.[54] The prepared nanomaterial was used as a molecular beacon and showed higher resistant to nonspecific response to untargeted DNA compared to noncovalent method. Similarly, Xu *et al.* functionalized GO with porphyrin using thionyl chloride.[55] A electron-transfer process was observed with a quenching of the photoexcited fluorescence state of the porphyrin.

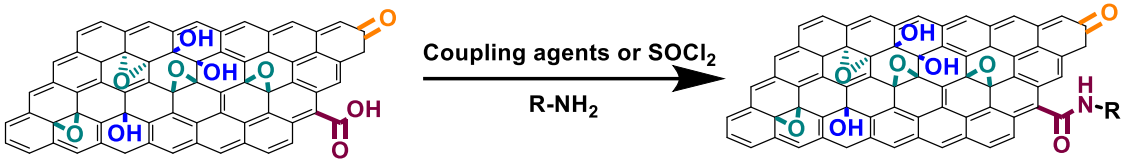

Scheme 1.1 Amidation reaction onto GO targeting the carboxyl groups. For the sake of clarity, only one functional group is drawn and the side reactions (e.g. epoxide ring opening, see below) are not considered.

Besides amidation, the esterification could also be performed on carboxylic acids. Yu *et al*. reported a work in which GO activated by $SOCl_2$ was able to bind with hydroxyl terminated poly(3-hexylthiophene) via ester bond formation, resulting in the highly dispersible hexylthiophene /GO hybrids in common organic solvents such as DMF and DMSO (scheme 1.2).[56]

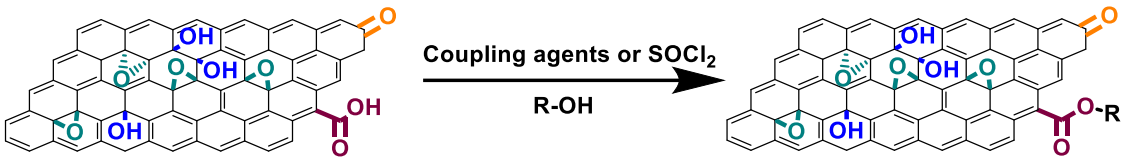

Scheme 1.2 Esterification reaction onto GO targeting the carboxyl groups. For the sake of clarity, only one functional group is drawn.

The epoxide ring opening reaction by nucleophilic attack is another important strategy to introduce functional groups onto GO under mild condition. Epoxy groups located at the basal plane of graphene are able to undergo a ring-opening reaction upon SN_2 nucleophilic attack with the α-carbon by amine or thiol groups.[50, 52] The formed covalent bond can be amine or thioether bonds, depending on the nucleophilic reagent ($R{-}NH_2$ or R−SH, respectively) together with a new hydroxyl group on the other side of the plane. Our group explored the chemical reactivity of epoxides towards amines with the help of solid-state NMR.[50] We proved that amine functions introduced onto GO are mostly grafted to the epoxy groups through ring opening but not to the carboxylic acids which are present only in a limited amount at the edge of GO. Although the reaction on carboxylic acid though amidation is widely used in literatures, the side reaction on epoxides is barely considered. Since the GO structure is extremely complex, it is crucial to control the derivatization to achieve a clarified structure.

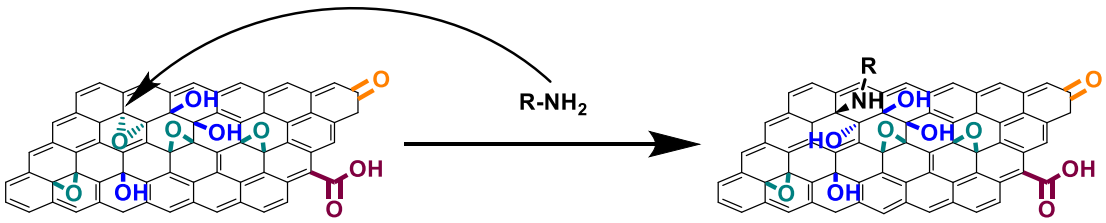

Scheme 1.3 Epoxide ring opening reaction on GO targeting the epoxide groups. For the sake of clarity, only one functional group is drawn.

The other abundant groups are the OH. Hydroxyl groups are localized on the basal surface of GO and can undergo different reactions. Organic compounds with an isocyanate group (−N=C=O) can be easily react with OH to form the urethane linkage and with the carboxyl groups forming an amide bond

(Scheme 1.4). Isocyanate compounds (R−N=C=O) have been proved to functionalize GO leading to amides or carbamates by targeting hydroxyls and carboxyl groups, respectively.[57] The formation of carbamates would remove the surface hydroxyls and edge carboxyl groups, making GO sheets less hydrophilic and more compatible with polar aprotic solvents.

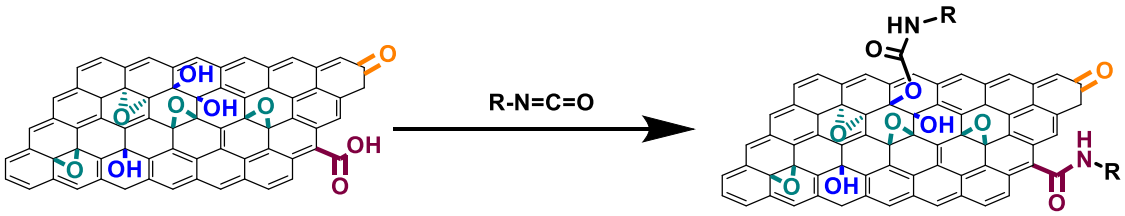

Scheme 1.4 Isocyanate reaction on GO targeting the hydroxyl groups and carboxylic acids. For the sake of clarity, only one functional group is drawn.

The hydroxyl groups could be also derivatized through Williamson reaction.[58-60] Sun *et al.* reported a strategy to increase the amount of carboxyl groups onto GO basal plane using chloroacetic acid in strong basic condition (Scheme 1.5).[59] The hydroxyl groups were deprotonated by sodium hydroxide and then react with chloroacetic acid forming an ether bond with a new carboxyl group introduced onto GO surface. However, the use of high amount of sodium hydroxide promotes the reduction of GO.

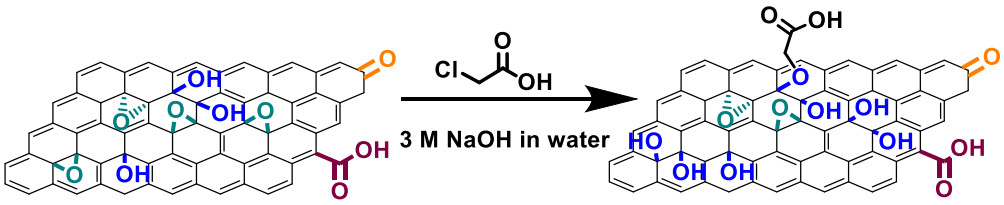

Scheme 1.5 Carboxylation reaction (Williamson reaction) on GO targeting the hydroxyl groups. For the sake of clarity, only one functional group is drawn.

Another approach to functionalize GO targeting hydroxyl groups is using the silanization reaction. Silanes are reactive towards the hydroxyl groups on GO forming C-O-Si bonds (Scheme 1.6). Abbas *et al.* introduced vinyltrimethoxysilane to GO by the silanization followed by a reduction reaction on the silane-GO network using a hydrazine/ammonia mixture.[61] The successful grafting of the silane agent created a spacer between the layers and the unreacted vinyl groups of the silane provided pendant reactive position for the crosslinking the silane-rGO network structure to other moieties.

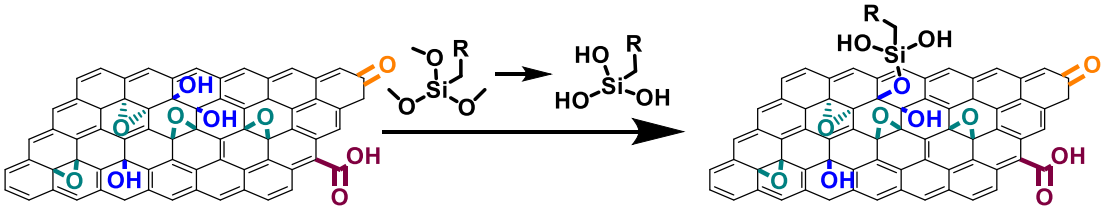

Scheme 1.6 Silanization reaction on GO targeting the hydroxyl groups. For the sake of clarity, only one functional group is drawn.

Boronic acid and its derivatives are likewise good functionalities for modification of vicinal OH onto GO (Scheme 1.7), since the boronic esters are responsive to reduced pH, overexpression of reactive oxygen species or the presence of other moieties such as specific proteins or carbohydrates.[62, 63] For example, He *et al.* prepared a boronic acid-grafted mesoporous silica nanoparticles incorporating (4-phenoxyphenyl)diphenylsulfonium triflate, a photoacid generator, which can produce strong acid conditions under irradiation, and doxorubicin (DOX) adsorbed onto the nanoparticles.[53] The nanoparticles were capped with folate (FA)-functionalized GO by the esterification between boronic acid and hydroxyls. The FA could target the folate receptor (FR) expressed on cancer cells. Using UV light, the photoacid generator provoked a pH jump, which induced the cleavage of the boroester linkers and thus resulted in the uncapping of pore gates, liberating doxorubicin, thus leading to a light triggered drug release targeting cancer cells.

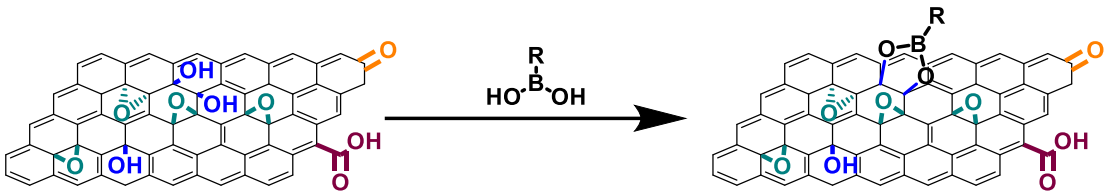

Scheme 1.7 Esterification reaction on GO targeting the hydroxyl groups using boronic acid. For the sake of clarity, only one functional group is drawn.

The covalent reactions described above allow to obtain diverse forms of functionalized GO. However, due to the variety of different oxygenated groups present on the surface of GO, the risk of side reactions is extremely high. Often the side reactions are not taken into consideration leading to final conjugates that are not correctly characterized and difficult to reproduce. In addition, the functionalization should be performed in mild conditions because GO is not stable at high temperature and it can be thermally reduced.

1.1.3 Application of GO in the treatment of diseases

Over the past few years, graphene oxide has shown its great potential as promising alternative for various biological applications including biosensing, imaging, antimicrobial effect, phototherapy and drug delivery, owing to its low intrinsic toxicity, good biodegradation, low cost for large-scale production, and versatile surface functionalization.[64, 65]

The infection of pathogenic microorganisms is one of the largest public health concerns worldwide, and the gradually enhancement of the resistance to typical antibacterial drugs in microbes makes the treatments sometimes infective.[66] Since the development of new antibiotics is difficult and usually takes long time, the study of new antibacterial antibiotic-free agents is meaningful for human health. Multifunctional graphene-based nanomaterials, especially graphene oxide, have shown a great potential as efficient antibacterial nanodrug with broad-spectrum activities against Gram-positive and Gram-negative bacteria.[67, 68] Multiple mechanisms are involved in the antibacterial mechanism

including the edge cutting effect,[67, 69] cell entrapment ability[70] and oxidative stress effect.[69] Among the graphene-based material, GO and its derivatives are considered as one of the most effective antibacterial nanomaterials (Figure 1.2).

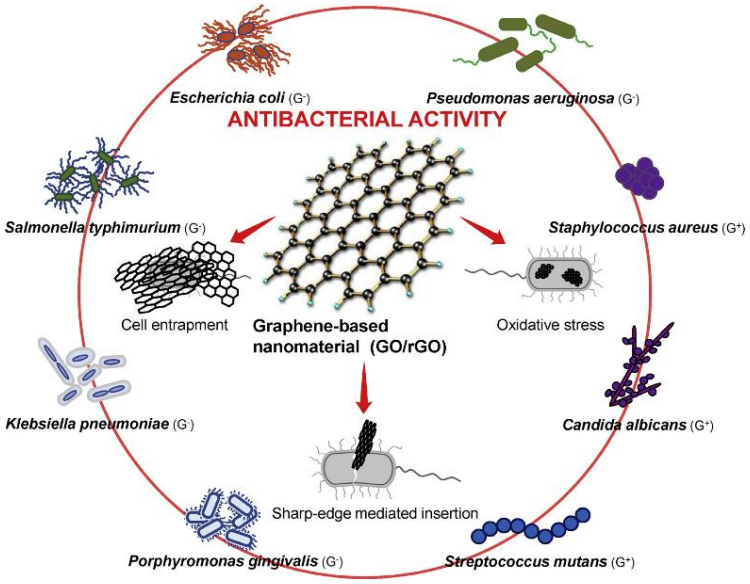

Figure 1.2 The various mechanisms of antibacterial activity in graphene-based nanomaterials. Adapted from reference [71].

For example, *Staphylococcus aureus* is associated with various human body infections and plays a key role in many human diseases such as nonalcoholic fatty liver disease and obesity.[72] With multiple antibiotic resistance, methicillin-resistant *S. aureus* (MRSA) is one of the major pathogens in hospital acquired infection.[73] De Moraes *et al.* prepared GO-Ag nanoparticles (GO-AgNPs) with strong antibacterial activity against MRSA.[74] The GO-AgNPs showed a minimal inhibitory concentration (MIC) against MRSA at 15 μg mL^{-1}, which is much lower than Ag nanoparticles alone. After 4 h contact with GO-AgNPs, 100% of MRSA cells were inactivated (Figure 1.3). A further modification of GO-AgNPs with chitosan led to a better anti-MRSA performance with the MIC lower than 1.5 μg mL^{-1}, againbetter than chitosan alone.[75]

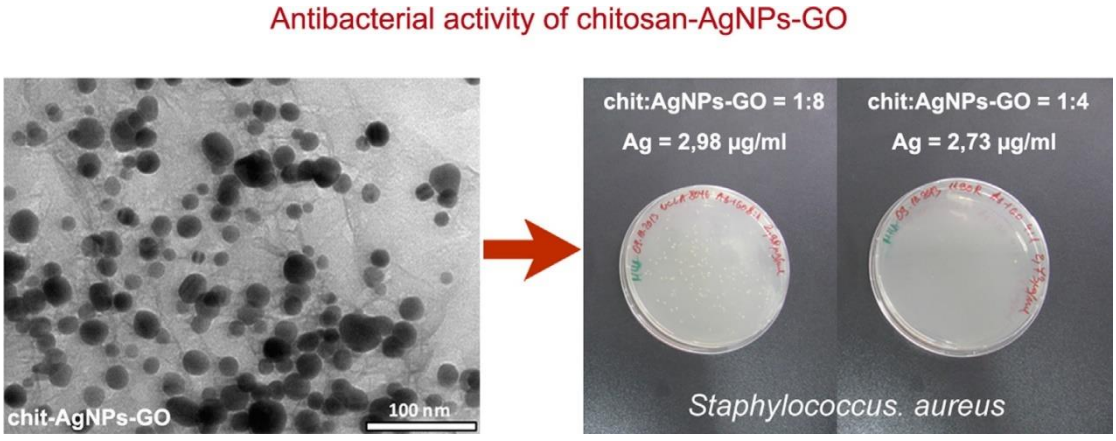

Figure 1.3 The TEM image (left) and antibacterial activity (right) of chitosan–AgNPs–GO nanohybrids. The right panel shows the agar plates inoculated with MRSA and chitosan–AgNPs–GO after 24 h. The nanohybrids

with the ratio of chitosan to AgNPs–GO = 1:4 possess a higher antibacterial activity than chitosan to AgNPs–GO = 1:8. Adapted from references [75].

In addition to the antibacterial properties of GO composites, this nanomaterial has been widely studied for the treatment of cancer. Since centuries, surgery, chemotherapy, and radiotherapy are still the most common cancer therapies. However, the possibility of recurrence after the treatment, and severe toxic side effects of the drugs of the irradiations demand for the developments of new strategies. GO provides an excellent platform for the development of theranostic nanomedicine, combining the diagnostic and therapeutic application in a simple and non-invasive way. GO can be derivatized with targeting groups, reporting groups and loaded with drugs in the same construction, achieving a multiple purpose in a single treatment.

For example, our group prepared a GO conjugate functionalized with the chemotactic peptide N-formyl-methionyl-leucyl-phenylalanine (GOfMLP), which could target different cancer cells.[76] GO was first covalently functionalized with 2,2'-(ethylenedioxy)bis(ethylamine) (diamino-TEG) via the epoxide ring opening reaction, leading to the introduction of primary amines. The fMLP peptide was then grafted to these free amines through the carbodiimide-mediated amidation. GOfMLP was finally loaded with DOX through physisorption, and this nanomaterial showed a targeted antitumor property.

The application of GO to cancer treatment can also help to overcome drug resistance. For instance, Feng *et al.* reported a work using pH-responsive a GO nanocomposite to deliver DOX into cancer cells.[77] Nano-GO (NGO) was functionalized with a PEG chain and a positively charged polyallylamine hydrochloride (PAH). PAH was then modified with 2,3-dimethylmaleic anhydride (DA). The obtained NGO-PEG-DA was stable and negatively charged under physiological pH (7.4), but it would rapidly convert into positively charged nanocarriers with markedly enhanced cellular uptake in a slightly acidic condition. When loaded with DOX, NGOPEG-DA/DOX complex showed a pH-depended cytotoxicity and it was able to effectively kill drug-resistant MCF-7/ADR cells. After combining with photothermal treatment (PTT) (see section 1.2.1), a higher killing efficiency was able to achieve. This strategy of combined PTT and chemotherapy offers an alternative method for cancer therapy with enhanced cell-killing ability against drug-resistant cancer cells without invasive operation.

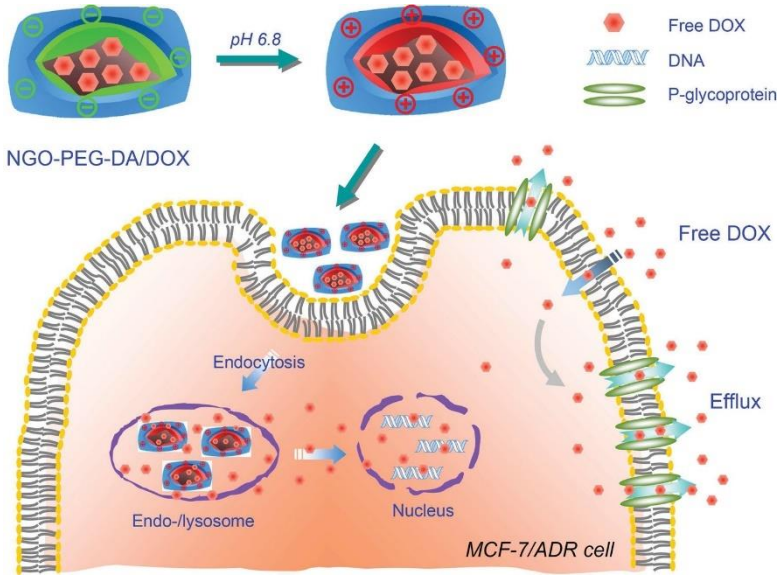

Figure 1.4 Illustration of the cellular uptake and intracellular acidic environment-triggered DOX release in NGO-PEG-DA/DOX complex. Adapted from reference [77].

GO-based nanomaterials are also used in the treatment of diseases which involve dysregulation of immune cells. For example, macrophages play an important role in the progression of myocardial infarction (MI) and cardiac repair. Two main phenotypes are involved in cardiac repair, the pro-inflammatory M1 macrophages, which can remove necrotic cells and debris, further initiating inflammatory reactions, and anti-inflammatory M2 macrophages that can produce anti-inflammatory cytokines. Han *et al.* explored GO as carrier of a plasmid DNA. GO was conjugated with PEI and a folic acid-PEG chain (FA-PEG), showing a high affinity for activated macrophages and a reduced intracellular reactive oxygen species (ROS) generation in immune-stimulated macrophages.[78] An interleukin(IL)-4 plasmid DNA, which propagates M2 macrophages, was then adsorbed onto GO conjugate via electrostatic interactions. The complex induced an early phenotype shift of macrophages from inflammatory M1 phase to reparative M2 phase, both *in vitro* and *in vivo* in mouse MI models, and thus enhanced secretion of cardiac repair-favorable cytokines (Figure 1.5). The combination of the anti-inflammatory properties of GO and IL-4 plasmid DNA led to an improvement left ventricular remodeling with a significant decreasing of fibrotic areas and the recovery of heart function.

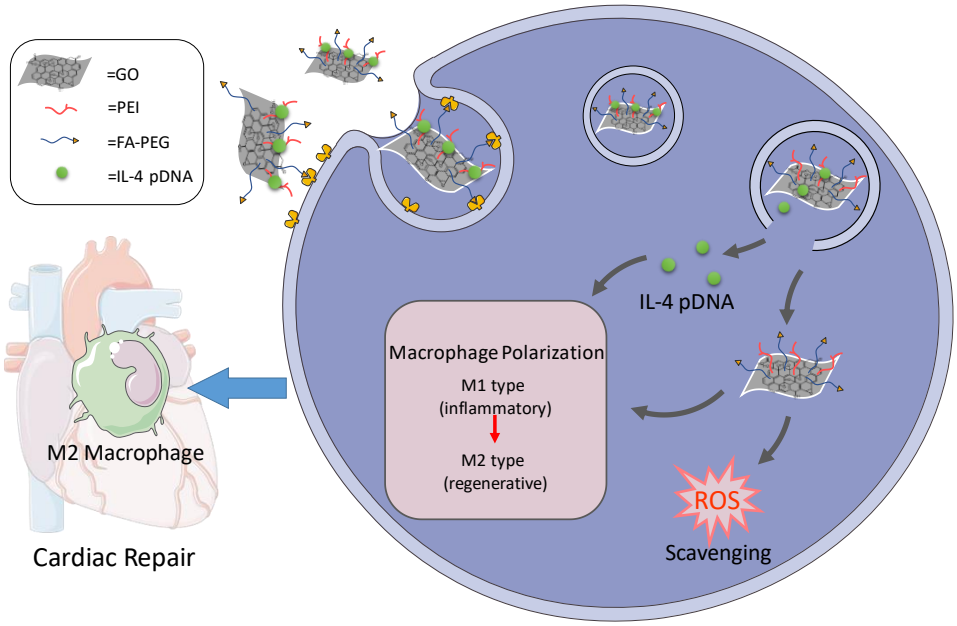

Figure 1.5. Proposed therapeutic mechanisms of IL-4 plasmid DNA (pDNA) adsorbed on functionalized GO in cardiac repair. Adapted from a reference [78].

In summary, based on the tremendous number of studies available, GO-based nanocomposites have shown their great potential in biomedical applications. Although there are still bias about the safety of GO, it is worth to further investigate this material as an alternative solution for disease treatment following a well-controlled preparation and functionalization.

1.1.4 Molybdenum disulfide

Following the rapidly increasing interests in the field of graphene-based materials, other 2D materials, including inorganic transition-metal dichalchogenides (TMDs), have recently received growing attention due to their potential application in optoelectronics, catalysis, electrochemistry, and medicine.[79-82] The bulk TMD materials are made of 3D crystalline solids with stacked structures and strong covalent bonds are stabilizing the basal plane made of different atoms with weak van der Waals interactions between each layers, which could be easily interrupted by exfoliation procedure for delamination of 3D crystals into 2D nanosheets (Figure 1.6). When the bulk TMDs are exfoliated to single or few layers, a change of some physical phenomena could be observed due to the quantum confinement effect and change of interlayer coupling as well as the lattice symmetry.[83]

Layered TMDs are a class of materials with MX_2 stoichiometry, where M refers to a transition metal typically from Groups 4-7 (e.g. Ti, Nb, Ta, Mo, or W) of the periodic table and X is a chalcogen atom

like S, Se or Te. Single layer TMDs have a thickness of 6-7 Å.[84] TMD monolayer is in a sandwich-like polymeric X-M-X form, with a plane of transition metal atoms in the middle and two layers of chalcogen atoms on the top and bottom.

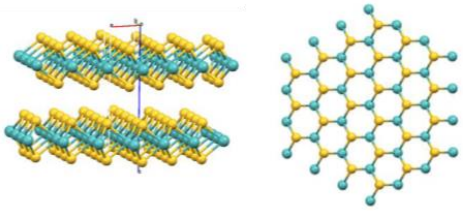

Figure 1.6 Crystal structures of bulk TMD (left) and the top-down view of the isolated TMD (right).

The layered TMDs exhibit disparate electronic properties depending on the coordination environment of transition metal and the electronic configuration, even if the stoichiometry is the same.[80] The coordination of metal atoms in layered TMDs can either be trigonal prismatic (2H polymorph), octahedral (1T polymorph) or rhombohedral symmetry (3R polymorph) (Figure 1.7).

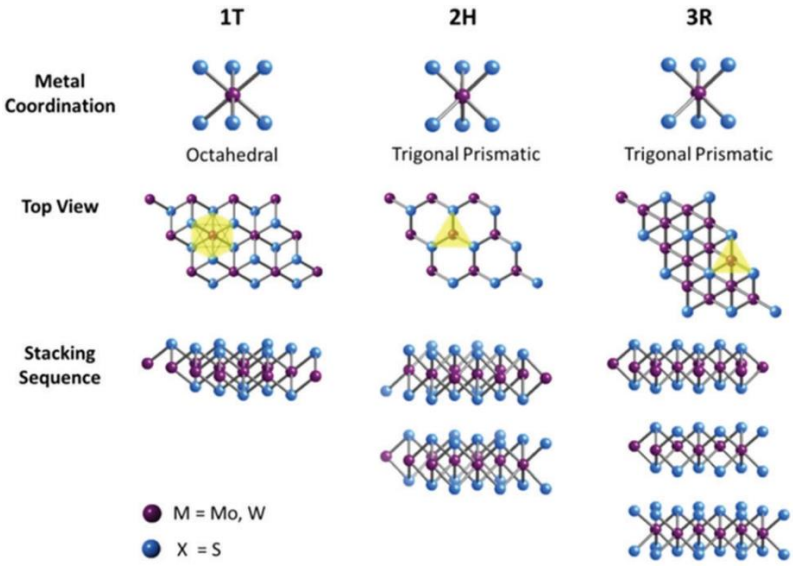

Figure 1.7 Metal coordination and stacking sequences of TMD structural unit cells. Adapted from reference [85].

Molybdenum disulfide (MoS_2) is one prototype of TMDs and acts as an excellent model system to explore the chemistry of 2D TMDs. In nature, the semiconductive 2H-polymorphic MoS_2 is predominant since it is thermodynamically stable, while the metallic 1T phase MoS_2 is less stable.[86]

1.1.5 Synthesis of MoS_2

Many protocols have been developed to prepare single and few layer MoS_2. In general, there are two main strategies of synthesis: top-down methods[87, 88] and bottom-up methods.[89] Mechanical cleavage is the most traditional method to isolate MoS_2, similarly to the isolation of graphene from graphite. The atomically thin flakes are peeled from the bulk MoS_2 crystals using a scotch tape. This is a straightforward method to exfoliate high quality MoS_2 since the morphology of the nanomaterial could be preserved without alerting the crystal structures. This method is normally used in research depending on intrinsic properties of MoS_2. But mechanical exfoliation is limited by a very low amount of obtained material and less control of the size of 2D nanosheet.

Liquid-phase exfoliation is the alternative solution to produce massive MoS_2 nanosheets. Different dispersive chemicals, including reaction reagents, solvents or surfactants, are required to weaken the interactions of the adjacent layers of bulk MoS_2,[90] leading to the isolation of a dispersion of monolayer or few layer MoS_2 (Figure 1.8). The liquid phase exfoliation could be directly performed by sonication of bulk MoS_2 in various solvent to prepare few layered nanosheets. Coleman's group reported that the solvent of exfoliation should have a similar surface tension as the minimal energy of TMDs to break the interactions between the layers. A surface tension of 44 mJ/m^2 was measured for MoS_2, which is similar to that of 1-methyl-2-pyrrolidone (NMP) that has a surface energy around 70 mJ/m^2.[91] However, NMP is toxic, unstable and difficult to remove completely.

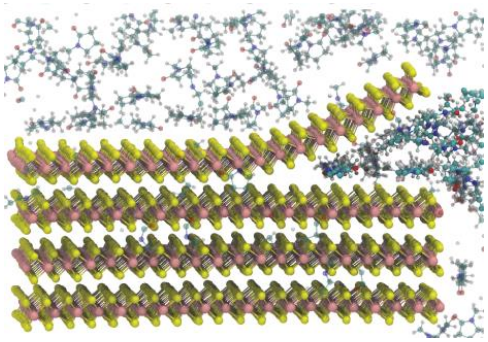

Figure 1.8 Liquid-phase exfoliation of MoS_2. Adapted from reference[88].

To overcome the disadvantage of NMP method, Zhou *et al.* used a mixture of water and ethanol to exfoliate MoS_2.[92]. With the volume ratio of ethanol/water of 45:55, exfoliated MoS_2 nanosheets were obtained.

Different surfactants are also used to exfoliate MoS_2 in liquid phase. Sodium cholate is one of the surfactants that leads to exfoliated MoS_2 nanosheets with good stability in water.[88, 93] Similarly,

Satheeshkumar *et al.* used amino acids to exfoliate the MoS_2 achieving the functionalization at the same time.[94]

The chemical exfoliation is another feasible method to prepare massive MoS_2 nanosheets in water. Two steps are involved in the chemical exfoliation procedure. The first step is to insert the intercalation compounds into the MoS_2 interlayers. The intercalation compound can be alkali metal ions or small molecule with Lewis base suitable reducing ability.[90] The compounds are inserted through chemical or electrochemical methods alone with expansion of the space between layers and generation of gas with water.[95] After sonication, bulk MoS_2 can be easily exfoliated.

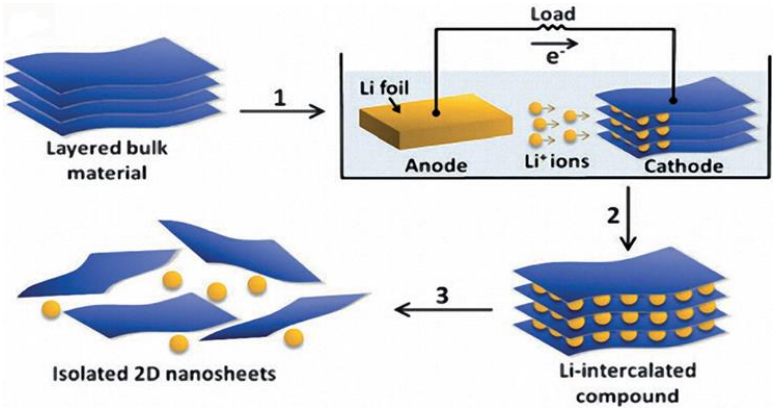

Figure 1.9 Electrochemical lithiation and exfoliation process for the fabrication of 2D nanosheets from layered bulk crystals. Adapted from reference [90].

Despite the top-down method, MoS_2 nanosheets can be also synthesized through bottom-up procedure. Chemical vapor deposition (CVD) and wet chemical synthesis are two main techniques. The bottom-up method allows to provide high-quality of MoS_2 nanosheets with controlled size and thickness but the extreme conditions of reaction limit the further application of this protocol for industrial production.

1.1.6 Functionalization of MoS_2

The functionalization of MoS_2 is now attracting more attention as it could help modify the intrinsic properties of exfoliated MoS_2 nanosheets, thus extending the applications. Similar to the modification on GO, MoS_2 can be functionalized through non-covalent or covalent methods.

Guan *et al.* reported a protocol to exfoliate and stabilize MoS_2.[96] MoS_2 was first exfoliated in water with the assistance of protein bovine serum albumin (BSA) under sonication. Then BSA was replaced with tris(hydroxymethyl)aminomethane (Tris) and this nanomaterial was stable in solution for 2.5 year.

Tris molecule was able to further react with polydopamine forming a universal platform for coating of other functional polymers onto the nanosheets. MoS_2 was also functionalized with other carbon nanomaterials. Baek *et al.* prepared a MoS_2-fullerene nanohybrids.[97] The supramolecular functionalization of suppressed photoinduced charge recombination and was beneficial for enhancing the incident photon-to-current efficiency of the hybrid.

To covalently functionalize MoS_2 at the edge and in-plane, three main strategies are commonly used: 1) chemistry at S vacancies, 2) direct C-S bond formation, and 3) coordination of S edges to metal centers.[98] To attach functional units to MoS_2, the reaction at sulfur vacancies is the most common explored strategy. The sandwiched three-atom-thick structure of MoS_2 often is disrupted and S and Mo vacancies exist, especially in the case of the liquid phase exfoliated MoS_2. Some studies reported functionalized MoS_2 by using thiols to fill the S-atom vacancies. Cho *et al.* functionalized MoS_2 with alkane thiol to prepare a field effect transistors (FETs).[99] The electrical characteristics of MoS_2 FETs changed dramatically due to the deposition of alkanethiol. However, this work did not provide a solid proof of covalent bonding of the thiol derivatives onto MoS_2. In fact, Chen *et al.* demonstrated for example that the SH group of cysteine was not covalently grafted onto MoS_2 surface.[100] Instead, MoS_2 facilitated the oxidation of cysteine to cystine during functionalization. Rather than coordinating as a thiol (cysteine) at S-vacancies in the MoS_2 conceived, cystine was simply physisorbed onto the nanosheet.

Recently, Vera-Hidalgo *et al.* reported a method of covalent functionalization on MoS_2 by directly formation of a S-C bond under mild condition based on the avidity of S as a soft nucleophile for soft electrophiles.[101] Maleimide derivatives were used for binding to MoS_2 following the Michael addition to S atoms (Figure 1.10).

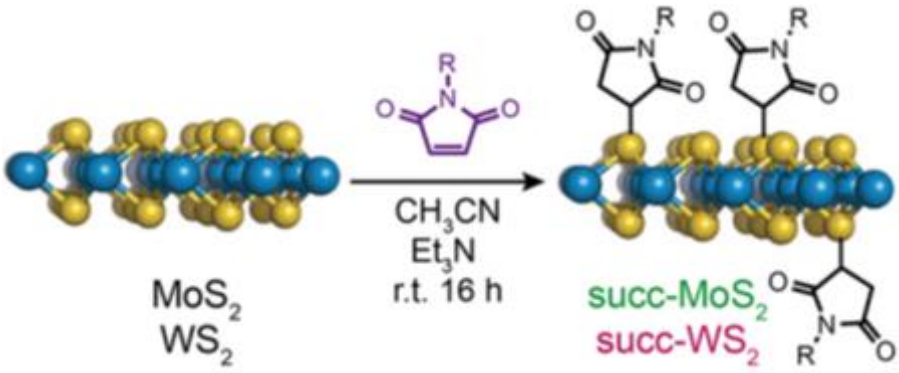

Figure 1.10 Functionalization of TMDs with maleimides. Adapted from reference [101].

Knirsch *et al.* discovered that aryl diazonium salts can be used for basal plane functionalization of MoS_2.[102] After the reaction with 4-methoxyphenyldiazonium tetrafluoroborate, MoS_2 nanosheets immediately flocculated, indicating a change in the surface properties of the material. The functionalized MoS_2 was characterized by several method and the degree of functionalization was considerably less than the 20%.

Metal salts can be also coordinated (formation of a dative bond) to the basal plane S atoms to form functionalized MoS_2.[103] Copper showed the maximum affinity for coordinating sulfur, while zinc was found to be less reactive. The prepared MoS_2 showed better dispersibility in more conventional solvents including acetone, rather than in highly toxic NMP.

In summary, GO and MoS_2 are two ideal materials for further research, especially in biology application. The numerous studies have proved that they are promising platform for several disease treatments as a drug deliver or by taking advantages of their intrinsic properties, such as photothermal property for phototherapy. To prepare a more performant nanomaterial, the functionalization is obligated. Several strategies have been established to functionalize these two materials but the method of double covalent functionalization still needs to be studied.

1.2 Photothermal therapy and photodynamic therapy

The phototherapy is a light-triggered therapeutic modality for various diseases and it has attracted tremendous scientific interest in the past decades, especially for cancer treatment. In comparison to conventional therapies, phototherapy is non-invasive, with minimal side effects and negligible drug resistance, making it a potential alternative for the replacement of traditional cancer treatment such as surgery, chemotherapy and radiotherapy as well as the treatment for other diseases. Photothermal (PTT) and photodynamic (PDT) therapies are two major types of light-activated therapies for disease treatment.

1.2.1 Introduction to PTT

PTT requires photothermal materials to convert the energy of absorbed photons to heat, resulting in a local hyperthermia, which leads to the death of cells by the triggering of necrosis or apoptosis depending on the local temperature increase. With a PTT-mediated heat up to 50 °C, this process induces an irreversible damage on cells, resulting in protein denaturation, collapse of cell membrane,

and dysfunction metabolism by affecting the activity of enzymes and mitochondria, leading to the necrosis of the cells.[104] However, the strong hyperthermia requires longer irradiation time, higher power and excess concentration of PTT agent. The temperature could also cause severe side effects to the surrounding tissue. If the increase of local temperature is lower, a reversible damage on cells can be induced by affecting the cell metabolism and DNA repair mechanisms.[104, 105] Although this mild hyperthermia could not directly kill the cell, the increased temperature could sensitize cells to the influence of other treatment.[106] The increased blood flow into the tumor tissue under mild hyperthermia could improve tissue hypoxia and can benefit the accumulation of the PTT agent at target tissue by enhanced permeability and retention (EPR) phenomenon. The membrane permeability is also affected and the increased temperature can help to disrupt the endosomes or lysosomes, releasing the loaded cargo into the cytoplasm.[107, 108] Overall, the mild hyperthermia can enhance the therapeutic efficiency.

The wavelength of irradiation is also very important for PTT. The light applied for the photothermal treatment usually located in a near-infrared window (NIR) between approximately 650 nm and 900 nm (Figure 1.11).[109] The irradiation with NIR light minimizes the acceleration of damage on normal tissues, thus reducing the side effects. When applied using PTT agents to the diseased tissues, NIR light can cause a local photothermal destruction without affecting normal tissue.[110]

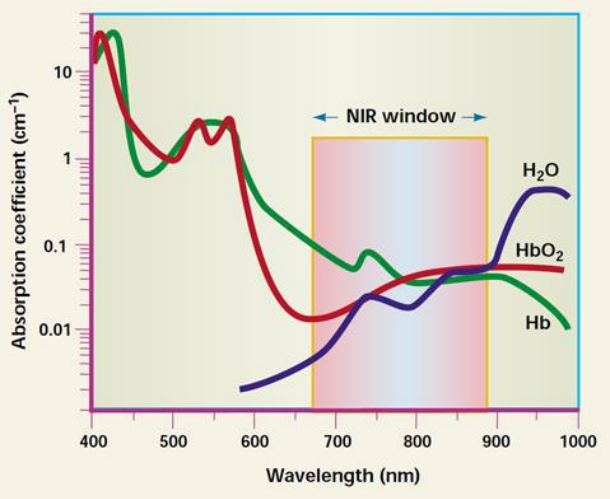

Figure 1.11 Biological absorbance of NIR radiation. Adapted from reference [109].

As graphene-based materials absorb a wide range of wavelengths, these materials are of extreme interest as efficient PTT agents. Among various graphene derivatives, GO is widely used for PTT due to its good water dispersibility, biocompatibility and easy functionalization.[35] In 2010, Yang *et al.* first applied GO to mice for *in vivo* cancer photothermal treatment.[111] Nano-GO sheets were covalently

modified with PEG. Due to EPR effect of tumors, the GO complex was highly accumulated into the tumor while the excess nanomaterial was renal excreted. After applying a 808 nm laser irradiation, an efficient ablation of tumor was observed without exhibiting noticeable toxicity to mice (Figure 1.12).

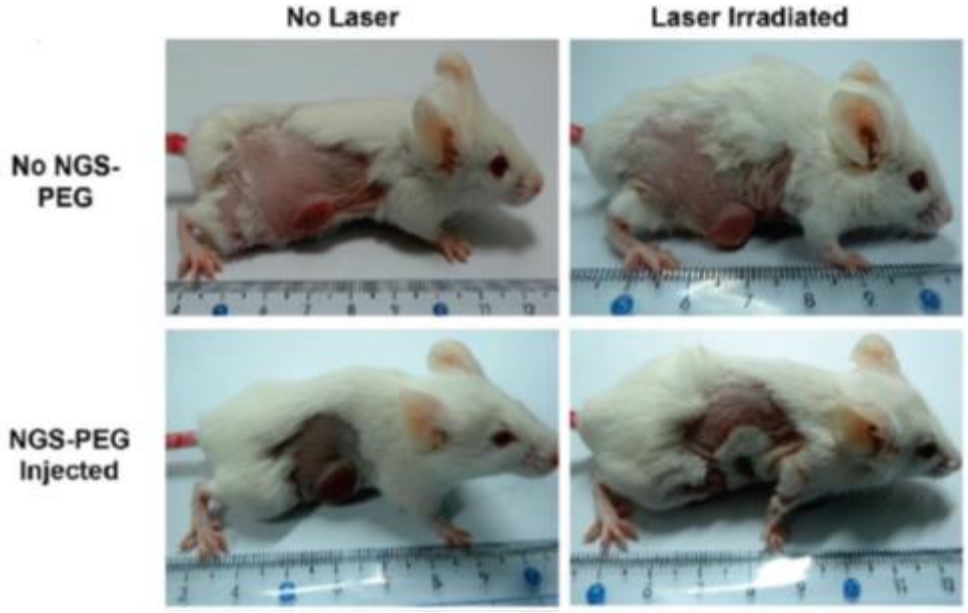

Figure 1.12 Representative photos of tumors on mice after the treatment with/without GO complex under laser irradiation. Adapted from reference [111].

As described before, GO is easily derivatized with different functionalities to achieve a multifunctional nanomaterial. When loaded with drug, targeting groups or other nanoparticles, the obtained GO conjugate can be used as a specific PTT agent towards diseased tissues combined with other treatment (chemotherapy when the drug is present on the complex) to achieve improved therapeutic efficiency.

Tao *et al.* loaded an immunostimulatory peptide on PEI and PEG modified GO through electrostatic interactions.[107] The cellular uptake of the GO complex by macrophages was enhanced by photothermal effect under a NIR laser irradiation. The secretions of TNF-α and IL-6 by macrophages were enhanced after applying of GO-peptides complex by 2.2 and 1.8-fold, respectively, in comparison with the non-irradiation control group. In *vivo*, the GO complex was injected intratumorally and it exhibited a satisfying growth inhibition up to 91% while less than 50% inhibition of the tumor growth was observed without PTT.

In view of these representative examples, lot of promises hold that GO can serve as an ideal nanoplatform for PTT treatment against several disease, thanks to its good photothermal efficiency and diverse methods for functionalization. However, the high irradiation power required for PTT

treatment can lead to sever side effect in clinical. Thus, the combination of PTT with other therapies is necessary.

1.2.2 Introduction to PDT

Unlike photothermal therapy which uses high energy to generate sufficient heat to increase the local temperature, PDT uses a lower energy radiation modality and can be repeated at the same site several times if required. The presence of adequate oxygen contents in tissues and of a photosensitizer (PS) is required in the photodynamic treatment. PS is stimulated with a specific wavelength of light (e.g. 660 nm). The excited electron in PS then transfer the absorbed energy to oxygen in the adjacent ground state tissue, leading to the generation of toxic ROS such as singlet oxygen ($^1O_2$), superoxide anion radical ($O_2^{\cdot-}$), and hydroxyl radicals ($^{\cdot}OH$).[112] ROS are highly reactive and are able to interfer with the biomolecules into the cells, inducing the cell apoptosis. [113]

ROS generation by excited PSs follows two types of photoreaction, obtaining different species of reactive oxygen (Figure 1.13). When stimulated, the first type of PSs can transfer an electron to other substrates, resulting in the formation of radicals including the superoxide anion radical.[114] The superoxide radical can be further converted to the more cytotoxic hydrogen peroxide and react with Fe^{2+} producing hydroxyl radicals through Haber–Weiss/Fenton reaction.[114] The second type PSs follows the energy transfer process with ground state molecular oxygen, also called triplet oxygen, giving the formation of singlet oxygen $^1O_2$.[115] However, the effective generation of $^1O_2$ requires an adequate concentration of oxygen at the reaction site. The continued irradiation would deplete the local oxygen and the following hypoxia effect in tissue is considered as one of the important factors relevant to the side effects observed in the PDT.[112, 116]

The most widely used PSs are porphyrin, chlorin, and bacteriochlorin.[117] These compounds have an aromatic structure that generates a strong absorption band between 600 and 800 nm, located in the optical NIR window for phototherapy.

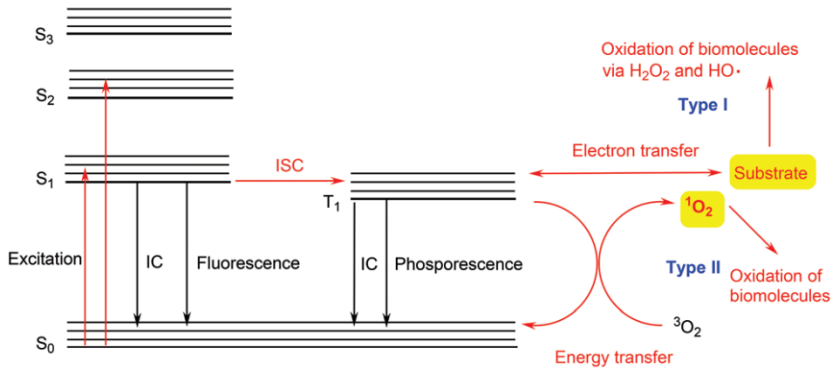

Figure 1.13 Processes relevant for the formation of ROS. Adapted from reference [112].

GO and its derivatives are considered ideal carriers for PS delivery, since it can complex of covalently bind PSs, overcoming the problem of hydrophobicity of such molecules that hampers they solubility in physiological solutions and limits their therapeutic effects. Huang *et al.* developed a GO complex functionalized with cancer cell targeting folic acid. The prepared material was then loaded with PS, chlorin e6 (Ce6), via hydrophobic interactions and π–π stacking.[118] The GO-FA-Ce6 complex enhanced the accumulation of Ce6 in tumor tissues, leading to a higher PDT efficacy in cancer cells under irradiation.

PDT has shown its great potential in the treatment for diverse diseases and many generations of PDT agents have been developed. But the demand of sufficient molecule oxygen limits the efficacy of this therapy. Although the hypoxia effect can be remised by better monitoring the irradiation time, it would be better to increase the local oxygen concentration *via* increased blood flow or applying oxygen-generation agents.

1.2.3 Synergistic therapy combining PTT and PDT

Synergistic therapy is one of promising ways to improve the treatment efficacy by integrating two or more therapeutic modes into a single application.[119] For the single photodynamic treatment, an important therapeutic problem is that the exhaust of tissue oxygen would exacerbate the local hypoxia leading to a side effect on the normal cells and decreasing the efficiency of singlet oxygen due to the insufficiency of molecular oxygen. The intra-treatment detection of $_1O^2$ could partially avoid such problems and enhanced PDT efficacy by monitoring the irradiation time.[116, 120] Thus, determining oxygen consumption and tissue oxygenation during the treatment is essential for the development of PDT. For PTT, a light with high intensity (normally higher than 0.5 W per cm^{-2}) is usually required for a sufficient increase of hyperthermia. But intense light irradiation might itself induce side effects to healthy tissues trespassed by light. So, the combination of PDT and PTT could lead to a better efficiency of disease treatment with minimal side effect.

In the literature we can find now numerous works describing the combination of these to therapeutic modalities.[35, 121] For example, Tian *et al.* first investigated the synergistic therapy by combining PTT and PDT using a GO nanocomposite.[122] The authors loaded Ce6 onto a PEG functionalized GO by π-π stacking. The cellular uptake of the Ce6 was significantly enhanced compared to free Ce6, increasing the photodynamic efficiency. The mild hyperthermia induced by PTT irradiation promoted then the delivery of Ce6 molecules at a much lower power density than PTT alone. This opens the way to build a multifunctional nanomaterial for enhanced cancer therapy under mild condition.

Overall, the combination of the two modalities could overcome the limitation of PTT and PDT alone, achieving a synergistic effect in disease therapy, and leading to a higher therapeutic efficacy with reduced side effects. Since GO is a good PTT material and has extraordinary loading efficiency for PDT reagents, it holds good promises possesses for future clinical translation.

1.3 Autoimmune diseases and their treatment using nanomaterial

1.3.1 Introduction of autoimmune disease and macrophages

Autoimmune diseases consist of a diversity of chronic inflammatory disorders where the immune system attacks specific cells, body tissues and organs of the host. Rheumatoid arthritis (RA) is a common polyarticular autoimmune inflammatory disease resulting in destruction of both cartilage and bone destruction within the synovial joints.[123] Normally, RA is characterized by the synovial inflammation and hyperplasia, autoantibody production, cartilage and bone destruction,[124] The symptoms caused by RA may lead to chronic pain, long-standing synovitis, progressive functional disability and greater morbidity.[125] The RA affects about 1% of the population globally and can present at any age.[126]

The pathogenesis of RA is complicated and usually associated with susceptibility genes, environmental stimulation, epigenetic modifications, and post-translational modifications.[125] But it still remains difficult to describe the full etiology of RA. Different types of tissues are enclosed within a fibrous capsule in the synovial joint, including synovial membrane and fluid, articular cartilage and bone. The tissues damage within the joint relates to the synovium inflammation[127, 128] and the subsequent increased fibroblast-like synoviocytes,[129, 130] the disorder of bone resorption and formation,[131, 132] the overexpression of proinflammation cadherins[133] and the imbalance of apoptosis.[134] The activation of the immune system is considered as the fundamental factor to the pathological changes within the synovial joints and the development of clinical features, including synovial hyperplasia, formation of invasive pannus tissue and progressive joint destruction.[135] Several environmental insults, including smoking, diet, obesity, infections and microbiota, can provoke an immune response, which leads to the generation of proinflammatory autoantigens and the subsequent production of rheumatoid factors.[136, 137]

For the immunopathogenesis of RA, T cells,[127] B cells,[128] synovial fibroblasts,[130, 138] osteoclasts,[132] and macrophages are involved in the generation of the disease. Among these cells, macrophages are considered as the central role in the progress of RA, due to their higher presence in the RA joints, their

activation and polarization after infection and their successful response to anti-rheumatic.[139, 140] The synovium-resident macrophages are seeded prior to differentiation from monocytes. The differentiation process can be prominent in response to macrophage depletion, inflammatory conditions or physiological stress, leading to activated macrophages.[139] The proinflammatory macrophages continue to release some proinflammatory factors such as tumor necrosis factor-α (TNF-α), interleukin(IL)-1β, IL-6, and matrix metalloproteinase (MMP), which constitute the pivotal event leading to chronic inflammation.

Folate receptors (FRs) β have been proved to be expressed on activated monocytes and macrophages in chronic inflammatory diseases including RA and they can be used as imaging and therapeutic target.[141] FRs are N-glycosylated proteins, with the relative molecular mass around 40 kDa. FRs show high binding affinity to folic acid (or folate) (Figure 1.14).[137]

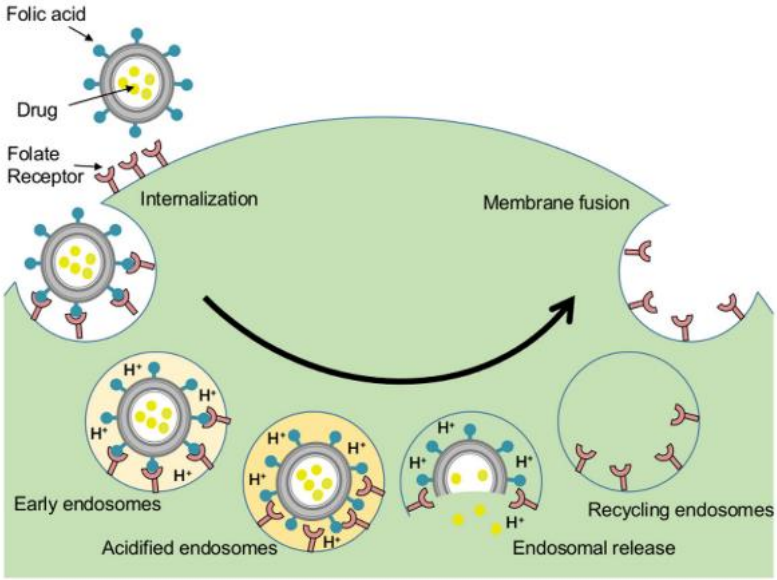

Figure 1.14. Schematic representation of folate mediated endocytosis. Adapted from reference [137].

1.3.2 RA therapy targeting FR β

The process of RA is commonly divided into two stages.[142] The first stage of RA development consists of promotion of protein citrullination in extraarticular sites and other autoimmune response to the environment acceleration such as smoking or infection, including formation of RF (rheumatoid factor), anti-citrullinated protein antibodies (ACPA), and anti-carbamylated proteins. However, only 40% of ACPA-positive arthralgia will eventually develop into the second stage of clinical RA, which consists on an unrelated self-limiting synovial inflammation and associated locally induced citrullination.[143]

Current treatment strategies for RA include nonsteroidal anti-inflammatory drugs (NSAIDs), glucocorticoids (GCs), disease-modifying anti-rheumatic drugs (DMARDs) and biologic response modifiers for the symptomatic relief or alter the disease process.[123] For example, methotrexate (MTX) is an antimetabolite-folate antagonist in DMARDs family and it has been widely used as the first-line antirheumatic agent due to its outstanding effectiveness.[144] However, the application of these drugs is strictly limited due to their severe side effects, such as cardiac complications, gastrointestinal damage and ulcers, along with immunosuppression that leads to the development of opportunistic infections. In order to overcome this shortcoming, the combination of different types of nanocarriers and drugs were applied to provide multifaceted solutions.[123]

To achieve better therapeutic effect, FR β is commonly used as the target for the specific treatment of macrophages in RA.[143] Since FA has a high affinity to FR on activated macrophages, FA-derivatized nanocomposite can be selectively internalized by macrophages though a receptor-mediated endocytosis. Chen *et al.* prepared a FA-PEG liposome encapsulating MTX and catalase (CAT).[145] The prepared liposome was able to target activated macrophages. The encapsulated CAT catalyzed the decomposition of hydrogen peroxide into oxygen and water, leading to the release of the encapsulated MTX. The liposome possesses a ROS-triggered drug release combined with an improved cellular uptake through folate-mediated endocytosis (Figure 1.15). The nanocomposite enhanced the accumulation of MTX in inflamed joints of mice, reinforced therapeutic efficacy and minimal toxicity toward major organs.

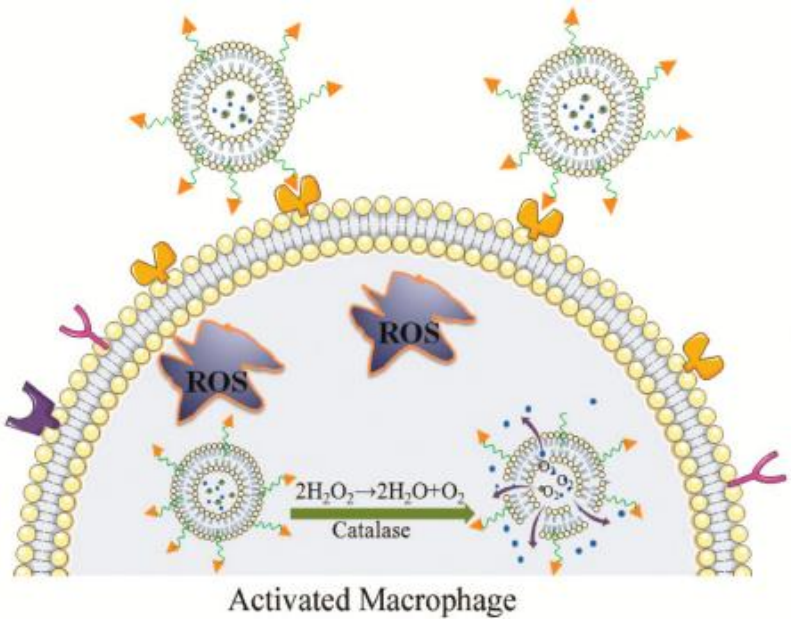

Figure 1.15 The prepared liposomes with folate targets the activated macrophages and processes a ROS-responsive drug releasing function for RA treatment. Adapted from reference [145].

However, no studies were reported using FR β-targeting GO for the treatment of RA. Since GO has been proved as a good platform for drug delivery and phototherapy, it is interesting to develop a folate-functionalized GO combined with PTT and PDT as a new RA therapeutic conjugate.

1.4 Objectives of this thesis

The main purpose of my thesis was to explore the possible therapeutic effect of GO conjugates functionalized with a targeting agent (FA) and a photosensitizer (Ce6) in the treatment of cancer cells and RA combining PTT and PDT. To achieve this objective, the thesis was divided into three main chapters. The second and fourth chapters concern the investigation of new methods for the double functionalization of GO and MoS_2, while the third chapter reports the preliminary results about the application of FR targeting GO-FA/Ce6 conjugate in the treatment of cancer cells, which overexpress FRs, and macrophages involved in RA pathology.

In chapter 2, I focused on the chemical modification of GO. In order to achieve a robust structure, we decided to optimize a method for the covalent double functionalization. Epoxides and hydroxyl groups were chosen as the targeting groups for the modification. The epoxide can be easily derivatized through a nucleophilic attack by a functional group bearing free amine or thiol. Then we performed a Williamson reaction between the hydroxyl groups and chloroacetic acid following the protocol published by other groups. To study the influence of strong alkaline solutions on GO, we used different the amounts of sodium hydroxide for the carboxylation step. We combined the epoxide ring opening reaction and the carboxylation followed by amidation to prepare the double functionalized GO in a stepwise procedure.

In addition to the Williamson reaction, we also explored the possibility to derivatize the hydroxyl groups with benzoquinone following Michael addition. Three different protocols were used to double functionalize GO in a three-step procedure. The prepared GO was characterized using different techniques.

In the third chapter of the thesis, I prepared a FA/Ce6 double functionalized GO through epoxide ring opening reaction by one-pot mixing a PEG with a terminal FA and a Boc protected PEG. Boc was then removed and Ce6 was covalently bound to GO. The prepared GO-FA/Ce6 conjugate was characterized by different methods to confirm the grafting of the two molecules. This as-prepared GO conjugate was applied first to cancer cells to evaluate the PTT/PDT efficiency *in vitro*. The cell viability was evaluated before and after the irradiation under 808 nm and 660nm for PTT and PDT, respectively.

Then the PTT and PDT were combined in order to achieve a better killing efficiency. The same conjugate was then used to study the behavior of macrophages, in view of the possibility to develop a treatment for RA.

Finally, since the MoS_2 can be also covalently functionalized through Michael addition, we started to explore the derivatization of MoS_2 using benzoquinone (chapter 3). Different functionalities were used to be covalently grafted onto MoS_2 in order to confirm the successful functionalization.

The thesis ends with chapter 5 on conclusion and perspectives.

1.5 References

1. L. Zhang, Y. Ding, C. Zhang, Y. Zhou, X. Zhou, Z. Liu and G. Yu, "Enabling Graphene-Oxide-Based Membranes for Large-Scale Energy Storage by Controlling Hydrophilic MicrostructuresEnabling Graphene-Oxide-Based Membranes for Large-Scale Energy Storage by Controlling Hydrophilic Microstructures", *Chem*, 2018, **4**, 1035-1046.
2. U. R. Farooqui, A. L. Ahmad and N. A. Hamid, "Graphene oxide: A promising membrane material for fuel cells", *Renewable Sustainable Energy Rev.*, 2018, **82**, 714-733.
3. X. Lu, X. Feng, J. R. Werber, C. Chu, I. Zucker, J. H. Kim, C. O. Osuji and M. Elimelech, "Enhanced antibacterial activity through the controlled alignment of graphene oxide nanosheets", *Proc. Natl. Acad. Sci. U. S. A.*, 2017, **114**, 9793-9801.
4. M. Y. Xia, Y. Xie, C. H. Yu, G. Y. Chen, Y. H. Li, T. Zhang and Q. Peng, "Graphene-based nanomaterials: the promising active agents for antibiotics-independent antibacterial applications", *J. Controlled Release*, 2019, **307**, 16-31.
5. F. Vulcano, A. Kovtun, C. Bettini, Z. Xia, A. Liscio, F. Terzi, A. Heras, A. Colina, B. Zanfrognini, M. Melucci, V. Palermo and C. Zanardi, "Dopamine-functionalized graphene oxide as a high-performance material for biosensing", *2D Materials*, 2020, **7**, 024007-024015.
6. D. K. Ji, C. Ménard-Moyon and A. Bianco, "Physically-triggered nanosystems based on two-dimensional materials for cancer theranostics", *Adv. Drug Delivery Rev.*, 2019, **138**, 211-232.
7. G. Reina, J. M. González-Dominguez, A. Criado, E. Vázquez, A. Bianco and M. Prato, "Promises, facts and challenges for graphene in biomedical applications", *Chem. Soc. Rev.*, 2017, **46**, 4400-4416.
8. B. Jana, G. Mondal, A. Biswas, I. Chakraborty, A. Saha, P. Kurkute and S. Ghosh, "Dual functionalized graphene oxide serves as a carrier for delivering oligohistidine- and biotin-tagged biomolecules into cells", *Macromol Biosci.*, 2013, **13**, 1478-1484.
9. B. Jana, A. Biswas, S. Mohapatra, A. Saha and S. Ghosh, "Single functionalized graphene oxide reconstitutes kinesin mediated intracellular cargo transport and delivers multiple cytoskeleton proteins and therapeutic molecules into the cell", *Chem. Commun.*, 2014, **50**, 11595-11598.

10. B. Han, Y. L. Zhang, L. Zhu, Y. Li, Z. C. Ma, Y. Q. Liu, X. L. Zhang, X. W. Cao, Q. D. Chen, C. W. Qiu and H. B. Sun, "Plasmonic-Assisted Graphene Oxide Artificial Muscles", *Adv. Mater.*, 2019, **31**, 1806386-18063892.

11. K. S. Novoselov, A. K. Geim, S. V. Morozov, D. Jiang, Y. Zhang, S. V. Dubonos, I. V. Grigorieva and A. A. Firsov, "Electric field effect in atomically thin carbon films", *Science*, 2004, **306**, 666-669.

12. G. Bottari, M. A. Herranz, L. Wibmer, M. Volland, L. Rodriguez-Perez, D. M. Guldi, A. Hirsch, N. Martin, F. D'Souza and T. Torres, "Chemical functionalization and characterization of graphene-based materials", *Chem. Soc. Rev.*, 2017, **46**, 4464-4500.

13. D. R. Dreyer, S. Park, C. W. Bielawski and R. S. Ruoff, "The chemistry of graphene oxide", *Chem. Soc. Rev.*, 2010, **39**, 228-240.

14. B. C. Brodie, "Note sur un nouveau procédé pour la purification et la désagrégation du graphite", *Ann. Chim. Phys.*, 1855, **45**, 351–353.

15. A. Hamwi and V. Marchand, "Some chemical and electrochemical properties of graphite oxide", *J. Phys. Chem. Solids*, 1996, **57**, 867-872.

16. A. Lerf, H. He, M. Forster and J. Klinowski, "Structure of Graphite Oxide Revisited", *J. Phys. Chem. B*, 1998, **102**, 4477-4482.

17. L. B. Casabianca, M. A. Shaibat, W. W. Cai, S. Park, R. Piner, R. S. Ruoff and Y. Ishii, "NMR-based structural modeling of graphite oxide using multidimensional ^{13}C solid-state NMR and ab initio chemical shift calculations", *J. Am. Chem. Soc.*, 2010, **132**, 5672-5676.

18. L. Yang, R. Zhang, B. Liu, J. Wang, S. Wang, M. Y. Han and Z. Zhang, "pi-conjugated carbon radicals at graphene oxide to initiate ultrastrong chemiluminescence", *Angew. Chem. Int. Ed.* , 2014, **53**, 10109-10113.

19. H. Pieper, S. Chercheja, S. Eigler, C. E. Halbig, M. R. Filipovic and A. Mokhir, "Endoperoxides Revealed as Origin of the Toxicity of Graphene Oxide", *Angew. Chem. Int. Ed.*, 2016, **55**, 405-407.

20. W. Gao, L. B. Alemany, L. Ci and P. M. Ajayan, "New insights into the structure and reduction of graphite oxide", *Nat. Chem.*, 2009, **1**, 403-408.

21. A. Dimiev, D. V. Kosynkin, L. B. Alemany, P. Chaguine and J. M. Tour, "Pristine graphite oxide", *J. Am. Chem. Soc.*, 2012, **134**, 2815-2822.

22. A. M. Dimiev, L. B. Alemany and J. M. Tour, Graphene oxide. "Origin of acidity, its instability in water, and a new dynamic structural model", *ACS Nano*, 2013, **7**, 576-588.

23. J. P. Rourke, P. A. Pandey, J. J. Moore, M. Bates, I. A. Kinloch, R. J. Young and N. R. Wilson, "The real graphene oxide revealed: stripping the oxidative debris from the graphene-like sheets", *Angew. Chem. Int. Ed.* , 2011, **50**, 3173-3177.

24. L. Staudenmaier, V"erfahren zur Darstellung der Graphitsäure", *Berichte der deutschen chemischen Gesellschaft*, 1898, **31**, 1481-1487.

25. W. S. Hummers and R. E. Offeman, "Preparation of Graphitic Oxide", *J. Am. Chem. Soc.*, 1958, **80**, 1339-1339.

26. D. C. Marcano, D. V. Kosynkin, J. M. Berlin, A. Sinitskii, Z. Sun, A. Slesarev, L. B. Alemany, W. Lu and J. M. Tour, "Improved synthesis of graphene oxide", *ACS Nano*, 2010, **4**, 4806-4814.

27. Y. Nishina and S. Eigler, "Chemical and electrochemical synthesis of graphene oxide - a generalized view", *Nanoscale*, 2020, **12**, 12731-12740.

28. O. C. Compton and S. T. Nguyen, "Graphene Oxide, Highly Reduced Graphene Oxide, and Graphene: Versatile Building Blocks for Carbon-Based Materials", *Small*, 2010, **6**, 711-723.

29. G. P. Kotchey, B. L. Allen, H. Vedala, N. Yanamala, A. A. Kapralov, Y. Y. Tyurina, J. Klein-Seetharaman, V. E. Kagan and A. Star, "The enzymatic oxidation of graphene oxide", *ACS Nano*, 2011, **5**, 2098-2108.

30. R. Kurapati, J. Russier, M. A. Squillaci, E. Treossi, C. Ménard-Moyon, A. E. Del Rio-Castillo, E. Vazquez, P. Samori, V. Palermo and A. Bianco, "Dispersibility-Dependent Biodegradation of Graphene Oxide by Myeloperoxidase", *Small*, 2015, **11**, 3985-3994.

31. H. Golmohammadi, E. Morales-Narváez, T. Naghdi and A. Merkoçi, "Nanocellulose in Sensing and Biosensing", *Chem. Mater.*, 2017, **29**, 5426-5446.

32. N. Cheeveewattanagul, E. Morales-Narváez, A.-R. H. A. Hassan, J. F. Bergua, W. Surareungchai, M. Somasundrum and A. Merkoçi, "Straightforward Immunosensing Platform Based on Graphene Oxide-Decorated Nanopaper: A Highly Sensitive and Fast Biosensing Approach", *Adv. Funct. Mater.*, 2017, **27**, 1702741-1702748.

33. T. Yin, J. Liu, Z. Zhao, Y. Zhao, L. Dong, M. Yang, J. Zhou and M. Huo, "Redox Sensitive Hyaluronic Acid-Decorated Graphene Oxide for Photothermally Controlled Tumor-Cytoplasm-Selective Rapid Drug Delivery", *Adv. Funct. Mater.*, 2017, **27**, 1604620-1604631.

34. E. Morales-Narváez and A. Merkoçi, "Graphene Oxide as an Optical Biosensing Platform: A Progress Report", *Adv. Mater.*, 2019, **31**, 1805043-1805054.

35. B. P. Jiang, B. Zhou, Z. Lin, H. Liang and X. C. Shen, "Recent Advances in Carbon Nanomaterials for Cancer Phototherapy", *Chem. Eur. J.*, 2019, **25**, 3993-4004.

36. P. Ji, W. Zhang, S. Ai, Y. Zhang, J. Liu, J. Liu, P. He and Y. Li, "Hybridization of graphene oxide into nanogels to acquire higher photothermal effects for therapeutic delivery", *Nanotechnology*, 2019, **30**, 115701-115710.

37. M. Wang, R. Jamal, Y. Wang, L. Yang, F. Liu and T. Abdiryim, "Functionalization of Graphene Oxide and its Composite with Poly(3,4-ethylenedioxythiophene) as Electrode Material for Supercapacitors", *Nanoscale Res. Lett.*, 2015, **10**, 370-381.

38. V. Georgakilas, J. N. Tiwari, K. C. Kemp, J. A. Perman, A. B. Bourlinos, K. S. Kim and R. Zboril, "Noncovalent Functionalization of Graphene and Graphene Oxide for Energy Materials, Biosensing, Catalytic, and Biomedical Applications", *Chem. Rev.*, 2016, **116**, 5464-5519.

39. F. Li, X. Jiang, J. Zhao and S. Zhang, "Graphene oxide: A promising nanomaterial for energy and environmental applications", *Nano Energy*, 2015, **16**, 488-515.

40. D. Chai, B. Hao, R. Hu, F. Zhang, J. Yan, Y. Sun, X. Huang, Q. Zhang and H. Jiang, "Delivery of Oridonin and Methotrexate via PEGylated Graphene Oxide", *ACS Appl. Mater. Interfaces*, 2019, **11**, 22915-22924.

41. G. Reina, N. D. Q. Chau, Y. Nishina and A. Bianco, "Graphene oxide size and oxidation degree govern its supramolecular interactions with siRNA", *Nanoscale*, 2018, **10**, 5965-5974.

42. N. D. Q. Chau, G. Reina, J. Raya, I. A. Vacchi, C. Ménard-Moyon, Y. Nishina and A. Bianco, "Elucidation of siRNA complexation efficiency by graphene oxide and reduced graphene oxide", *Carbon*, 2017, **122**, 643-652.

43. S. S. Bhosale, E. Jokar, A. Fathi, C.-M. Tsai, C.-Y. Wang and E. W.-G. Diau, "Functionalization of Graphene Oxide Films with Au and MoOx", *Adv. Funct. Mater.*, 2018, **28**, 1803200-1803207.

44. S. Omidi, A. Kakanejadifard and F. Azarbani, "Noncovalent functionalization of graphene oxide and reduced graphene oxide with Schiff bases as antibacterial agents", *J. Mol. Liq.*, 2017, **242**, 812-821.

45. D. Zaharie-Butucel, M. Potara, S. Suarasan, E. Licarete and S. Astilean, "Efficient combined near-infrared-triggered therapy: Phototherapy over chemotherapy in chitosan-reduced graphene oxide-IR820 dye-doxorubicin nanoplatforms", *J. Colloid Interface Sci.*, 2019, **552**, 218-229.

46. I. A. Lawal, M. M. Lawal, S. O. Akpotu, H. K. Okoro, M. Klink and P. Ndungu, "Noncovalent Graphene Oxide Functionalized with Ionic Liquid: Theoretical, Isotherm, Kinetics, and Regeneration Studies on the Adsorption of Pharmaceuticals", *Ind. Eng. Chem. Res.*, 2020, **59**, 4945-4957.

47. N. Luo, J. K. Weber, S. Wang, B. Luan, H. Yue, X. Xi, J. Du, Z. Yang, W. Wei, R. Zhou and G. Ma, "PEGylated graphene oxide elicits strong immunological responses despite surface passivation", *Nat. Commun.*, 2017, **8**, 14537.

48. B. Liu, S. Salgado, V. Maheshwari and J. Liu, "DNA adsorbed on graphene and graphene oxide: Fundamental interactions, desorption and applications", *Curr. Opin. Colloid Interface Sci.*, 2016, **26**, 41-49.

49. K. C. Mei, N. Rubio, P. M. Costa, H. Kafa, V. Abbate, F. Festy, S. S. Bansal, R. C. Hider and K. T. Al-Jamal, "Synthesis of double-clickable functionalised graphene oxide for biological applications", *Chem. Commun.*, 2015, **51**, 14981-14984.

50. I. A. Vacchi, C. Spinato, J. Raya, A. Bianco and C. Ménard-Moyon, "Chemical reactivity of graphene oxide towards amines elucidated by solid-state NMR", *Nanoscale*, 2016, **8**, 13714-13721.

51. I. A. Vacchi, J. Raya, A. Bianco and C. Ménard-Moyon, "Controlled derivatization of hydroxyl groups of graphene oxide in mild conditions", *2D Materials*, 2018, **5**, 35037-35047.

52. S. Guo, Y. Nishina, A. Bianco and C. Ménard-Moyon, "A Flexible Method for Covalent Double Functionalization of Graphene Oxide", *Angew. Chem., Int. Ed.*, 2020, **59**, 1542-1547.

53. D. He, X. He, K. Wang, Z. Zou, X. Yang and X. Li, "Remote-controlled drug release from graphene oxide-capped mesoporous silica to cancer cells by photoinduced pH-jump activation", *Langmuir*, 2014, **30**, 7182-7189.

54. P. J. Huang and J. Liu, "Molecular beacon lighting up on graphene oxide", *Anal. Chem.*, 2012, **84**, 4192-4198.

55. Y. Xu, Z. Liu, X. Zhang, Y. Wang, J. Tian, Y. Huang, Y. Ma, X. Zhang and Y. Chen, "A Graphene Hybrid Material Covalently Functionalized with Porphyrin: Synthesis and Optical Limiting Property", *Adv. Mater.*, 2009, **21**, 1275-1279.

56. D. Yu, Y. Yang, M. Durstock, J. B. Baek and L. Dai, “Soluble P3HT-grafted graphene for efficient bilayer-heterojunction photovoltaic devices”, *ACS Nano*, 2010, **4**, 5633-5640.

57. C. Hontoria-Lucas, A. J. López-Peinado, J. d. D. López-González, M. L. Rojas-Cervantes and R. M. Martín-Aranda, “Study of oxygen-containing groups in a series of graphite oxides: Physical and chemical characterization”, *Carbon*, 1995, **33**, 1585-1592.

58. I. A. Vacchi, S. Guo, J. Raya, A. Bianco and C. Menard-Moyon, “Strategies for the Controlled Covalent Double Functionalization of Graphene Oxide”, *Chem. Eur. J.*, 2020, **26**, 6591-6598.

59. X. Sun, Z. Liu, K. Welsher, J. T. Robinson, A. Goodwin, S. Zaric and H. Dai, “Nano-Graphene Oxide for Cellular Imaging and Drug Delivery”, *Nano Res.*, 2008, **1**, 203-212.

60. R. Yu, S. Zhang, Y. Luo, R. Bai, J. Zhou and H. Song, “Synthetic possibility of polystyrene functionalization based on hydroxyl groups of graphene oxide as nucleophiles”, *New J. Chem.*, 2015, **39**, 5096-5099.

61. S. S. Abbas, G. J. Rees, N. L. Kelly, C. E. J. Dancer, J. V. Hanna and T. McNally, “Facile silane functionalization of graphene oxide”, *Nanoscale*, 2018, **10**, 16231-16242.

62. N. Kamaly, B. Yameen, J. Wu and O. C. Farokhzad, “Degradable Controlled-Release Polymers and Polymeric Nanoparticles: Mechanisms of Controlling Drug Release”, *Chem. Rev.*, 2016, **116**, 2602-2663.

63. A. Stubelius, S. Lee and A. Almutairi, “The Chemistry of Boronic Acids in Nanomaterials for Drug Delivery”, *Acc. Chem. Res.*, 2019, **52**, 3108-3119.

64. N. Panwar, A. M. Soehartono, K. K. Chan, S. Zeng, G. Xu, J. Qu, P. Coquet, K. T. Yong and X. Chen, “Nanocarbons for Biology and Medicine: Sensing, Imaging, and Drug Delivery”, *Chem. Rev.*, 2019, **119**, 9559-9656.

65. R. Kurapati, F. Bonachera, J. Russier, A. R. Sureshbabu, C. Ménard-Moyon, K. Kostarelos and A. Bianco, “Covalent chemical functionalization enhances the biodegradation of graphene oxide”, *2D Materials*, 2017, **5**, 15020-15031.

66. K. E. Jones, N. G. Patel, M. A. Levy, A. Storeygard, D. Balk, J. L. Gittleman and P. Daszak, “Global trends in emerging infectious diseases”, *Nature*, 2008, **451**, 990-993.

67. O. Akhavan and E. Ghaderi, “Toxicity of graphene and graphene oxide nanowalls against bacteria”, *ACS Nano*, 2010, **4**, 5731-5736.

68. J. He, X. Zhu, Z. Qi, C. Wang, X. Mao, C. Zhu, Z. He, M. Li and Z. Tang, “Killing dental pathogens using antibacterial graphene oxide”, *ACS Appl. Mater. Interfaces*, 2015, **7**, 5605-5611.

69. S. Liu, T. H. Zeng, M. Hofmann, E. Burcombe, J. Wei, R. Jiang, J. Kong and Y. Chen, “Antibacterial activity of graphite, graphite oxide, graphene oxide, and reduced graphene oxide: membrane and oxidative stress”, *ACS Nano*, 2011, **5**, 6971-6980.

70. M. Dallavalle, M. Calvaresi, A. Bottoni, M. Melle-Franco and F. Zerbetto, “Graphene can wreak havoc with cell membranes”, *ACS Appl. Mater. Interfaces*, 2015, **7**, 4406-4414.

71. M. Y. Xia, Y. Xie, C. H. Yu, G. Y. Chen, Y. H. Li, T. Zhang and Q. Peng, “Graphene-based nanomaterials: the promising active agents for antibiotics-independent antibacterial applications”, *J. Control. Release*, 2019, **307**, 16-31.

72. J. K. Nicholson, E. Holmes, J. Kinross, R. Burcelin, G. Gibson, W. Jia and S. Pettersson, "Host-gut microbiota metabolic interactions", *Science*, 2012, **336**, 1262-1267.

73. M. C. Enright, D. A. Robinson, G. Randle, E. J. Feil, H. Grundmann and B. G. Spratt," The evolutionary history of methicillin-resistant Staphylococcus aureus (MRSA)", *Proc. Natl. Acad. Sci. U. S. A.*, 2002, **99**, 7687-7692.

74. A. C. de Moraes, B. A. Lima, A. F. de Faria, M. Brocchi and O. L. Alves, "Graphene oxide-silver nanocomposite as a promising biocidal agent against methicillin-resistant Staphylococcus aureus", *Int. J. Nanomedicine*, 2015, **10**, 6847-6861.

75. B. Marta, M. Potara, M. Iliut, E. Jakab, T. Radu, F. Imre-Lucaci, G. Katona, O. Popescu and S. Astilean, "Designing chitosan–silver nanoparticles–graphene oxide nanohybrids with enhanced antibacterial activity against Staphylococcus aureus", *Colloids Surf., A*, 2015, **487**, 113-120.

76. C. Martín, A. Ruiz, S. Keshavan, G. Reina, D. Murera, Y. Nishina, B. Fadeel and A. Bianco, "A Biodegradable Multifunctional Graphene Oxide Platform for Targeted Cancer Therapy", *Adv. Funct. Mater.*, 2019, **29**, 1901761-1901771.

77. L. Feng, K. Li, X. Shi, M. Gao, J. Liu and Z. Liu, "Smart pH-responsive nanocarriers based on nano-graphene oxide for combined chemo- and photothermal therapy overcoming drug resistance", *Adv. Healthc. Mater.*, 2014, **3**, 1261-1271.

78. J. Han, Y. S. Kim, M. Y. Lim, H. Y. Kim, S. Kong, M. Kang, Y. W. Choo, J. H. Jun, S. Ryu, H. Y. Jeong, J. Park, G. J. Jeong, J. C. Lee, G. H. Eom, Y. Ahn and B. S. Kim, "Dual Roles of Graphene Oxide To Attenuate Inflammation and Elicit Timely Polarization of Macrophage Phenotypes for Cardiac Repair", *ACS Nano*, 2018, **12**, 1959-1977.

79. B. Radisavljevic, A. Radenovic, J. Brivio, V. Giacometti and A. Kis, "Single-layer MoS_2 transistors", *Nat. Nanotechnol.*, 2011, **6**, 147-150.

80. M. Chhowalla, H. S. Shin, G. Eda, L. J. Li, K. P. Loh and H. Zhang, "The chemistry of two-dimensional layered transition metal dichalcogenide nanosheets", *Nat. Chem.*, 2013, **5**, 263-275.

81. B. Dou, J. Yang, R. Yuan and Y. Xiang, "Trimetallic Hybrid Nanoflower-Decorated MoS_2 Nanosheet Sensor for Direct in Situ Monitoring of H_2O_2 Secreted from Live Cancer Cells", *Anal. Chem.*, 2018, **90**, 5945-5950.

82. J. Wang, L. Liu, D. Ge, H. Zhang, Y. Feng, Y. Zhang, M. Chen and M. Dong, "Differential Modulating Effect of MoS_2 on Amyloid Peptide Assemblies", *Chem. Eur.J.*, 2018, **24**, 3397-3402.

83. K. F. Mak, C. Lee, J. Hone, J. Shan and T. F. Heinz, "Atomically thin MoS_2: a new direct-gap semiconductor", *Phys. Rev. Lett.*, 2010, **105**, 136805-136808.

84. S. Bertolazzi, J. Brivio and A. Kis, "Stretching and breaking of ultrathin MoS_2", *ACS Nano*, 2011, **5**, 9703-9709.

85. R. J. Toh, Z. Sofer, J. Luxa, D. "Sedmidubsky and M. Pumera, 3R phase of MoS_2 and WS_2 outperforms the corresponding 2H phase for hydrogen evolution", *Chem. Commun.*, 2017, **53**, 3054-3057.

86. E. Benavente, M. A. S. Ana, F. Mendiza´bal and G. Gonza´lez, "Intercalation chemistry of molybdenum disulfide", *Coord. Chem. Rev.*, 2002, **224**, 87-109.

87. J. N. Coleman, M. Lotya, A. O'Neill, S. D. Bergin, P. J. King, U. Khan, K. Young, A. Gaucher, S. De, R. J. Smith, I. V. Shvets, S. K. Arora, G. Stanton, H. Y. Kim, K. Lee, G. T. Kim, G. S. Duesberg, T. Hallam, J. J. Boland, J. J. Wang, J. F. Donegan, J. C. Grunlan, G. Moriarty, A. Shmeliov, R. J. Nicholls, J. M. Perkins, E. M. Grieveson, K. Theuwissen, D. W. McComb, P. D. Nellist and V. Nicolosi, "Two-dimensional nanosheets produced by liquid exfoliation of layered materials", *Science*, 2011, **331**, 568-571.

88. V. Sresht, A. Govind Rajan, E. Bordes, M. S. Strano, A. A. H. Pádua and D. Blankschtein, "Quantitative Modeling of MoS_2–Solvent Interfaces: Predicting Contact Angles and Exfoliation Performance using Molecular Dynamics", *J. Phys. Chem. C*, 2017, **121**, 9022-9031.

89. H. S. Matte, A. Gomathi, A. K. Manna, D. J. Late, R. Datta, S. K. Pati and C. N. Rao, "MoS_2 and WS_2 analogues of graphene", *Angew. Chem. Int. Ed.*, 2010, **49**, 4059-4062.

90. X. Zhang, Z. Lai, C. Tan and H. Zhang, "Solution-Processed Two-Dimensional MoS_2 Nanosheets: Preparation, Hybridization, and Applications", *Angew. Chem. Int. Ed.*, 2016, **55**, 8816-8838.

91. G. Cunningham, M. Lotya, C. S. Cucinotta, S. Sanvito, S. D. Bergin, R. Menzel, M. S. Shaffer and J. N. Coleman, "Solvent exfoliation of transition metal dichalcogenides: dispersibility of exfoliated nanosheets varies only weakly between compounds", *ACS Nano*, 2012, **6**, 3468-3480.

92. K. G. Zhou, N. N. Mao, H. X. Wang, Y. Peng and H. L. Zhang, "A mixed-solvent strategy for efficient exfoliation of inorganic graphene analogues", *Angew. Chem. Int. Ed.*, 2011, **50**, 10839-10842.

93. R. J. Smith, P. J. King, M. Lotya, C. Wirtz, U. Khan, S. De, A. O'Neill, G. S. Duesberg, J. C. Grunlan, G. Moriarty, J. Chen, J. Wang, A. I. Minett, V. Nicolosi and J. N. Coleman, "Large-scale exfoliation of inorganic layered compounds in aqueous surfactant solutions", *Adv. Mater.* , 2011, **23**, 3944-3948.

94. E. Satheeshkumar, A. Bandyopadhyay, M. B. Sreedhara, S. K. Pati, C. N. R. Rao and M. Yoshimura, "One-Step Simultaneous Exfoliation and Covalent Functionalization of MoS2by Amino Acid Induced Solution Processes", *ChemNanoMat*, 2017, **3**, 172-177.

95. E. Er, H.-L. Hou, A. Criado, J. Langer, M. Möller, N. Erk, L. M. Liz-Marzán and M. Prato, "High-Yield Preparation of Exfoliated 1T-MoS2 with SERS Activity", *Chem. Mater.*, 2019, **31**, 5725-5734.

96. G. Guan, M. You, X. Liu, Y. L. Wu, E. Ye and Z. Li, "Tris‐Stabilized MoS_2 Nanosheets with Robust Dispersibility and Facile Surface Functionalization", *Adv. Mater. Interfaces*, 2019, **6**.

97. J. Baek, T. Umeyama, W. Choi, Y. Tsutsui, H. Yamada, S. Seki and H. Imahori, "Formation and Photodynamic Behavior of Transition Metal Dichalcogenide Nanosheet-Fullerene Inorganic/Organic Nanohybrids on Semiconducting Electrodes", *Chem. Eur. J.*, 2018, **24**, 1561-1572.

98. A. Stergiou and N. Tagmatarchis, "Molecular Functionalization of Two-Dimensional MoS_2 Nanosheets", *Chem. Eur. J.*, 2018, **24**, 18246-18257.

99. K. Cho, M. Min, T. Y. Kim, H. Jeong, J. Pak, J. K. Kim, J. Jang, S. J. Yun, Y. H. Lee, W. K. Hong and T. Lee, "Electrical and Optical Characterization of MoS_2 with Sulfur Vacancy Passivation by Treatment with Alkanethiol Molecules", *ACS Nano*, 2015, **9**, 8044-8053.

100. X. Chen, N. C. Berner, C. Backes, G. S. Duesberg and A. R. McDonald, “Functionalization of Two-Dimensional MoS2 : On the Reaction Between MoS_2 and Organic Thiols”, *Angew. Chem., Int. Ed.*, 2016, **55**, 5803-5808.

101. M. Vera-Hidalgo, E. Giovanelli, C. Navio and E. M. Perez, “Mild Covalent Functionalization of Transition Metal Dichalcogenides with Maleimides: A "Click" Reaction for 2H-MoS_2 and WS_2”, *J. Am. Chem. Soc.*, 2019, **141**, 3767-3771.

102. K. C. Knirsch, N. C. Berner, H. C. Nerl, C. S. Cucinotta, Z. Gholamvand, N. McEvoy, Z. Wang, I. Abramovic, P. Vecera, M. Halik, S. Sanvito, G. S. Duesberg, V. Nicolosi, F. Hauke, A. Hirsch, J. N. Coleman and C. Backes, “Basal-Plane Functionalization of Chemically Exfoliated Molybdenum Disulfide by Diazonium Salts”, *ACS Nano*, 2015, **9**, 6018-6030.

103. C. Backes, N. C. Berner, X. Chen, P. Lafargue, P. LaPlace, M. Freeley, G. S. Duesberg, J. N. Coleman and A. R. McDonald, “Functionalization of liquid-exfoliated two-dimensional 2H-MoS_2”, *Angew. Chem. Int. Ed.*, 2015, **54**, 2638-2642.

104. K. F. Chu and D. E. Dupuy, “Thermal ablation of tumours: biological mechanisms and advances in therapy”, *Nat. Rev. Cancer*, 2014, **14**, 199-208.

105. S. Gao, M. Zheng, X. Ren, Y. Tang and X. Liang, “Local hyperthermia in head and neck cancer: mechanism, application and advance”, *Oncotarget*, 2016, **7**, 57367-57378.

106. D. de Melo-Diogo, R. Lima-Sousa, C. G. Alves and I. J. Correia, “Graphene family nanomaterials for application in cancer combination photothermal therapy”, *Biomater. Sci.*, 2019, **7**, 3534-3551.

107. Y. Tao, E. Ju, J. Ren and X. Qu, “Immunostimulatory oligonucleotides-loaded cationic graphene oxide with photothermally enhanced immunogenicity for photothermal/immune”, *Biomaterials*, 2014, **35**, 9963-9971.

108. H. Kim and W. J. Kim, “Photothermally controlled gene delivery by reduced graphene oxide-polyethylenimine nanocomposite”, *Small*, 2014, **10**, 117-126.

109. R. Weissleder, “A clearer vision for in vivo imaging”, *Nat. Biotechnol*, 2001, **19**, 316-317.

110. E. S. Day, J. G. Morton and J. L. West, “Nanoparticles for thermal cancer therapy”, *J. Biomech. Eng.*, 2009, **131**, 074001-074005.

111. K. Yang, S. Zhang, G. Zhang, X. Sun, S. T. Lee and Z. Liu, “Graphene in mice: ultrahigh in vivo tumor uptake and efficient photothermal therapy”, *Nano Lett.*, 2010, **10**, 3318-3323.

112. A. Wiehe, J. M. O'Brien and M. O. Senge, “Trends and targets in antiviral phototherapy”, *Photochem. Photobiol. Sci.*, 2019, **18**, 2565-2612.

113. S. S. Lucky, K. C. Soo and Y. Zhang, “Nanoparticles in photodynamic therapy”, *Chem. Rev.*, 2015, **115**, 1990-2042.

114. M. S. Baptista, J. Cadet, P. Di Mascio, A. A. Ghogare, A. Greer, M. R. Hamblin, C. Lorente, S. C. Nunez, M. S. Ribeiro, A. H. Thomas, M. Vignoni and T. M. Yoshimura, “Type I and Type II Photosensitized Oxidation Reactions: Guidelines and Mechanistic Pathways”, *Photochem. Photobiol.*, 2017, **93**, 912-919.

115. H. Kim, S. Beack, S. Han, M. Shin, T. Lee, Y. Park, K. S. Kim, A. K. Yetisen, S. H. Yun, W. Kwon and S. K. Hahn, “Multifunctional Photonic Nanomaterials for Diagnostic, Therapeutic, and Theranostic Applications”, *Adv. Mater.*, 2018, **30**, 1701460-1701492.

116. Josephine H. Woodhams, Alexander J. MacRobert and S. G. Bown, “The role of oxygen monitoring during photodynamic therapy and its potential for treatment dosimetry”, *Photochem. Photobiol. Sci.*, 2007, **6**, 1246–1256.

117. A. K. Mandal, T. Sahin, M. Liu, J. S. Lindsey, D. F. Bocian and D. Holten, “Photophysical comparisons of PEGylated porphyrins, chlorins and bacteriochlorins in water”, *New J. Chem.*, 2016, **40**, 9648-9656.

118. P. Huang, C. Xu, J. Lin, C. Wang, X. Wang, C. Zhang, X. Zhou, S. Guo and D. Cui, “Folic Acid-conjugated Graphene Oxide loaded with Photosensitizers for Targeting Photodynamic Therapy”, *Theranostics*, 2011, **1**, 240-250.

119. D. Zeng, L. Wang, L. Tian, S. Zhao, X. Zhang and H. Li, “Synergistic photothermal/photodynamic suppression of prostatic carcinoma by targeted biodegradable MnO_2”, nanosheets *Drug Delivery*, 2019, **26**, 661-672.

120. A. Looft, M. Pfitzner, A. Preuss and B. Roder, “In vivo singlet molecular oxygen measurements: Sensitive to changes in oxygen saturation during PDT”, *Photodiagnosis Photodyn. Ther.*, 2018, **23**, 325-330.

121. Z. Yang, Z. Sun, Y. Ren, X. Chen, W. Zhang, X. Zhu, Z. Mao, J. Shen and S. Nie, “Advances in nanomaterials for use in photothermal and photodynamic therapeutics”, *Mol. Med. Rep.*, 2019, **20**, 5-15.

122. B. Tian, C. Wang, S. Zhang, L. Feng and Z. Liu, “Photothermally enhanced photodynamic therapy delivered by nano-graphene oxide”, *ACS Nano*, 2011, **5**, 7000-7009.

123. N. Qamar, A. Arif, A. Bhatti and P. John, “Nanomedicine: an emerging era of theranostics and therapeutics for rheumatoid arthritis”, *Rheumatology (Oxford)*, 2019, **58**, 1715-1721.

124. I. B. McInnes and G. Schett, “The pathogenesis of rheumatoid arthritis”, *N. Engl. J. Med.*, 2011, **365**, 2205-2219.

125. S. Wang, J. Lv, S. Meng, J. Tang and L. Nie, “Recent Advances in Nanotheranostics for Treat-to-Target of Rheumatoid Arthritis”, *Adv. Healthc. Mater.*, 2020, **9**, 1901541-1901557.

126. I. B. McInnes and G. Schett, “Pathogenetic insights from the treatment of rheumatoid arthritis”, *The Lancet*, 2017, **389**, 2328-2337.

127. S. Alzabin and R. O. Williams, “Effector T cells in rheumatoid arthritis: lessons from animal models”, *FEBS Lett.*, 2011, **585**, 3649-3659.

128. W. Sun, N. Meednu, A. Rosenberg, J. Rangel-Moreno, V. Wang, J. Glanzman, T. Owen, X. Zhou, H. Zhang, B. F. Boyce, J. H. Anolik and L. Xing, “B cells inhibit bone formation in rheumatoid arthritis by suppressing osteoblast differentiation”, *Nat. Commun.*, 2018, **9**, 5127-5140.

129. N. C. Walsh, T. N. Crotti, S. R. Goldring and E. M. Gravallese, “Rheumatic diseases: the effects of inflammation on bone”, *Immunol. Rev.*, 2005, **208**, 228-251.

130. M. F. Bustamante, R. Garcia-Carbonell, K. D. Whisenant and M. Guma, “Fibroblast-like synoviocyte metabolism in the pathogenesis of rheumatoid arthritis”, *Arthritis Res. Ther.*, 2017, **19**, 110-121.

131. D. R. Haynes, E. Barg, T. N. Crotti, C. Holding, H. Weedon, G. J. Atkins, A. Zannetino, M. J. Ahern, M. Coleman, P. J. Roberts-Thomson, M. Kraan, P. P. Tak and M. D. Smith,

"Osteoprotegerin expression in synovial tissue from patients with rheumatoid arthritis, spondyloarthropathies and osteoarthritis and normal controls", *Rheumatology (Oxford)*, 2003, **42**, 123-134.

132. U. Steffen, G. Schett and A. Bozec, "How Autoantibodies Regulate Osteoclast Induced Bone Loss in Rheumatoid Arthritis", *Front. Immunol.*, 2019, **10**, 1483-1491.

133. H. P. Kiener, D. M. Lee, S. K. Agarwal and M. B. Brenner, "Cadherin-11 induces rheumatoid arthritis fibroblast-like synoviocytes to form lining layers in vitro", *Am. J. Pathol.*, 2006, **168**, 1486-1499.

134. R. M. Pope, "Apoptosis as a therapeutic tool in rheumatoid arthritis", *Nat. Rev. Immunol.*, 2002, **2**, 527-535.

135. M. Gallardo-Villagran, D. Y. Leger, B. Liagre and B. Therrien, "Photosensitizers Used in the Photodynamic Therapy of Rheumatoid Arthritis", *Int. J. Mol. Sci.*, 2019, **20**, 3339-3359.

136. D. E. Furst and P. Emery, "Rheumatoid arthritis pathophysiology: update on emerging cytokine and cytokine-associated cell targets", *Rheumatology (Oxford)*, 2014, **53**, 1560-1569.

137. E. Nogueira, A. C. Gomes, A. Preto and A. Cavaco-Paulo, "Folate-targeted nanoparticles for rheumatoid arthritis therapy", *Nanomedicine*, 2016, **12**, 1113-1126.

138. C. Carmona-Rivera, P. M. Carlucci, E. Moore, N. Lingampalli, H. Uchtenhagen, E. James, Y. Liu, K. L. Bicker, H. Wahamaa, V. Hoffmann, A. I. Catrina, P. Thompson, J. H. Buckner, W. H. Robinson, D. A. Fox and M. J. Kaplan, "Synovial fibroblast-neutrophil interactions promote pathogenic adaptive immunity in rheumatoid arthritis", *Sci. Immunol.*, 2017, **2**, 3358-3371.

139. I. A. Udalova, A. Mantovani and M. Feldmann, "Macrophage heterogeneity in the context of rheumatoid arthritis", *Nat. Rev. Rheumatol.*, 2016, **12**, 472-485.

140. S. Tardito, G. Martinelli, S. Soldano, S. Paolino, G. Pacini, M. Patane, E. Alessandri, V. Smith and M. Cutolo, "Macrophage M1/M2 polarization and rheumatoid arthritis: A systematic review", *Autoimmun Rev.*, 2019, **18**, 102397-102417.

141. W. Xia, A. R. Hilgenbrink, E. L. Matteson, M. B. Lockwood, J. X. Cheng and P. S. Low, "A functional folate receptor is induced during macrophage activation and can be used to target drugs to activated macrophages", *Blood*, 2009, **113**, 438-446.

142. L. Klareskog, J. Ronnelid, K. Lundberg, L. Padyukov and L. Alfredsson, "Immunity to citrullinated proteins in rheumatoid arthritis", *Annu. Rev. Immunol.*, 2008, **26**, 651-675.

143. D. Chandrupatla, C. F. M. Molthoff, A. A. Lammertsma, C. J. van der Laken and G. Jansen, "The folate receptor beta as a macrophage-mediated imaging and therapeutic target in rheumatoid arthritis", *Drug Delivery Transl. Res.*, 2019, **9**, 366-378.

144. J. M. Kremer, A. S. Russell, P. Emery, C. Abud-Mendoza, J. Szechinski, R. Westhovens, T. Li, X. Zhou, J. C. Becker, R. Aranda, C. Peterfy and H. K. Genant, "Long-term safety, efficacy and inhibition of radiographic progression with abatacept treatment in patients with rheumatoid arthritis and an inadequate response to methotrexate: 3-year results from the AIM trial", *Ann. Rheum. Dis.*, 2011, **70**, 1826-1830.

145. M. Chen, J. C. K. Amerigos, Z. Su, N. E. I. Guissi, Y. Xiao, L. Zong and Q. Ping, "Folate Receptor-Targeting and Reactive Oxygen Species-Responsive Liposomal Formulation of Methotrexate for Treatment of Rheumatoid Arthritis", *Pharmaceutics*, 2019, **11**, 582-604.

Chapter 2 The covalent double functional on GO

2.1 Introduction

Since GO possesses many extraordinary properties such as good water dispersibility, rapid biodegradability and low toxicity, it has become the mostly studied 2D material, especially for biomedical applications.[1] To achieve better performances of this material, the modification of GO with diverse functional groups is required. Non-covalent functionalization onto GO is generally preferred since this method is easy to perform and will not alter the morphology and the intrinsic physicochemical property of GO. However, covalent derivatization provides the possibility to form more robust GO hybrids endowed of different functional groups. Several methods have been developed to covalently modify GO through the oxygenated functions on its surface,[2] such as carboxylic acids,[3] epoxide rings[4] and hydroxyl groups. [5, 6]

Compared to mono-functionalization, the covalent double functionalization of GO allows to better control the specific attachment of distinct molecules or nanoparticles through different reactions. Since a variety of different oxygenated groups is present on GO, it is challenging to develop strategies for covalent double functionalization without affecting other functional groups or to avoid side reactions. Only few strategies for the covalent double functionalization of GO have been reported so far.[7] One simple strategy is based on “one-pot” method. One paper described the double functionalization on GO using a mixture of octa-arginine and amino-polyethylene glycol through amidation.[7] However, concomitant side reactions may render this procedure difficult to control. Also, the one-pot strategy usually targets only one functional group on GO leading to a lower efficiency of modification. Another strategy for a double functionalization is to develop a stepwise procedure by targeting different functional groups onto GO, such carboxyl groups and epoxide rings.[3] This kind of functionalization allows better controlling the conjugation of the two molecules compared to a one-pot strategy. But the percentage of the original COOH on GO is rather low (around 3.5%)[4] leading to low loading efficiency.

In our group, we have done a lot of work on multi-functionalization of GO targeting the epoxides and hydroxyl groups.[5] But the efficiency of the derivation on hydroxyl groups is always lower than the opening of epoxides, which is always the first step of functionalization. A possible solution to increase the grafting of functionalities after epoxide ring opening is to derivatize alcohol functions with another function, which is more reactive than hydroxyl groups.

2.2 Objectives of this chapter

The objectives of this chapter are to devise an efficient strategy for the covalent double functionalization of GO by targeting two different functional groups in mild conditions. The epoxides

and hydroxyls are two main functional group on GO surface and can be grafted with different molecule through stepwise reactions. For this reason, we chose these two groups as targets for the covalent double functionalization.

The epoxide ring opening reaction was first performed to graft one functional group. To further attach another molecule, the hydroxyl groups were derivatized with chloroacetic acid or benzoquinone. The application of chloroacetic acid was aiming to introduce more carboxyl groups onto GO. A second functional molecule bearing an amine moiety was then covalently bound to GO through amidation reaction with these new carboxyl groups. To clarify the impact of different amount of alkaline solution on GO functionalization, we prepared carboxylated GO using different molarities of sodium hydroxide. Besides the derivatization of the hydroxyls with chloroacetic acid, we also explored the protocol to covalently double functionalize GO through the combination of an epoxide ring opening reaction and a Michael addition to the hydroxyl groups on benzoquinone which can be further derivatized with molecules through another Michael addition.

2.3 Combination of epoxide opening and carboxylation

The GO sample for all the experiments was obtained from Prof. Yuta Nishina (University of Okayama, Japan). Generally, large GO flakes (30 μm) were prepared following a modified Hummers' method. Then, by using a jet mill with a 0.1 mm nozzle, GO with an average lateral size of 1 μm was obtained.[6]

We first explored the method of double functionalization though the combination of the epoxide ring opening reaction and carboxylation of GO. Although there are already many articles reporting that GO could be partially reduced during carboxylation using chloroacetic acid and sodium hydroxide,[9, 10] the effect of this deoxygenation effect on the efficiency of GO functionalization is still unclear. Moreover, various concentrations of sodium hydroxide solutions were reported (from 123 mM to 4 M), with 3 M being the most commonly used. To better understand if the carboxylation reaction is appropriate for the covalent double functionalization of GO, we started the reaction with a high amount of sodium hydroxide.

2.3.1 Carboxylation of GO with high amount of sodium hydroxide

Carboxylation of hydroxyl groups can be performed either before or after the epoxide ring opening. We first derivatized hydroxyl groups onto GO with chloroacetic acid in strong basic conditions following the protocol published by other groups to increase the amount of carboxylic acids.[11] Briefly, pristine GO was dispersed in 3 M sodium hydroxide solution followed by the immediate addition of chloroacetic acid (Scheme 2.1). After washing and dialysis, the resulting GO **1** was characterized by XPS, TGA, FT-IR and TEM.

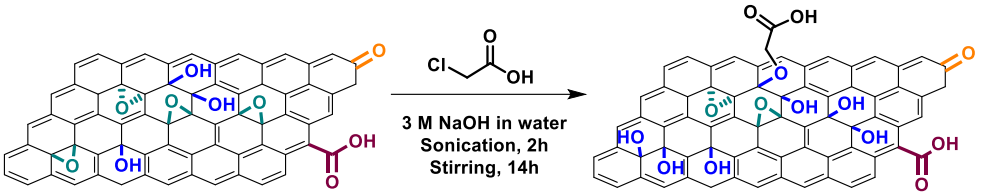

1

Scheme 2.1. Carboxylation reaction onto GO. For the sake of clarity, only one hydroxyl group is derivatized and the epoxide rings are closed. The epoxide ring opening by sodium hydroxide is under an equilibrium and part of the C-O$^-$ groups can close again to form the three atom ring.[12, 13]

XPS is the method of choice to prove the information on the chemical composition of the surface of GO (Figure 2.1). The atomic percentage composition of pristine GO and GO **1** was calculated (Figure 2.1a and d, respectively). As presented in Figure 2.1, the C/O ratio for the starting GO was calculated as 2.6, while for GO **1**, it resulted 3.0. The increase of the C/O ratio after carboxylation revealed that there was a partial reduction of GO during the reaction,[14] indicating that part of the oxygen-containing functional groups such as epoxides and hydroxyls were removed in basic condition. The deconvolution of the high-resolution C 1s spectra also supported the reduction of GO. C 1s spectrum of pristine GO exhibited two major peaks which could be assigned to the carbon atoms from C-C bond at 284.8 eV and C-O bond from alcohols and epoxides at 286.6 eV (Figure 1b). The small peak located in the 288.3 to 289.1 eV region could be deconvoluted into two components: carbon atoms from the carboxyl groups in the range from 288.7 eV to 289.1 eV, and the atoms from the carbonyl groups from 288.1 eV to 288.3eV. However, a significant change in the C 1s spectrum was observed after the reaction (Figure 1e). The component of the carboxyl groups on GO increased from 3.9% to 6.2%, proving the successful modification of the starting GO with additional carboxylic acids. As indicated from the C/O ratio, a significant decrease of the C-O component from 44.0% to 28.7% was also observed after the carboxylation, confirming the partial removal of the oxygen-containing functional groups during the reaction.[15] The XPS spectra showed that some labile oxygenated groups and oxidative debris[16] were likely to be removed from the GO surface during the treatment with a high concentration of sodium hydroxide. Part of the epoxide rings were probably opened by OH^- and the hydroxyl groups could be further reduced by OH^- assisted with Na^+ and water molecules, resulting in the formation of CO_2, vacancy defects and extension of conjugation, as previously reported (Scheme 2.2).[17, 18] The partial reduction of GO affects its intrinsic properties and decrease the amount of hydroxyl groups on GO. This unexpected deoxygenation of GO would lead to a lower amount of COOH groups introduced by carboxylation procedure, thus decreasing the loading of molecules through amidation following this strategy. The high-resolution O 1s peak was deconvoluted into three components: C=O (531.4-530.3 eV), C-O (533.0-532.0 eV) and H_2O (535.2-534.8 eV). The increase of the C=O component from 5.0% to 5.7% after carboxylation was not very significant, probably due to contribution of the chloroacetic moiety in both peaks (Figure 2.1 f).

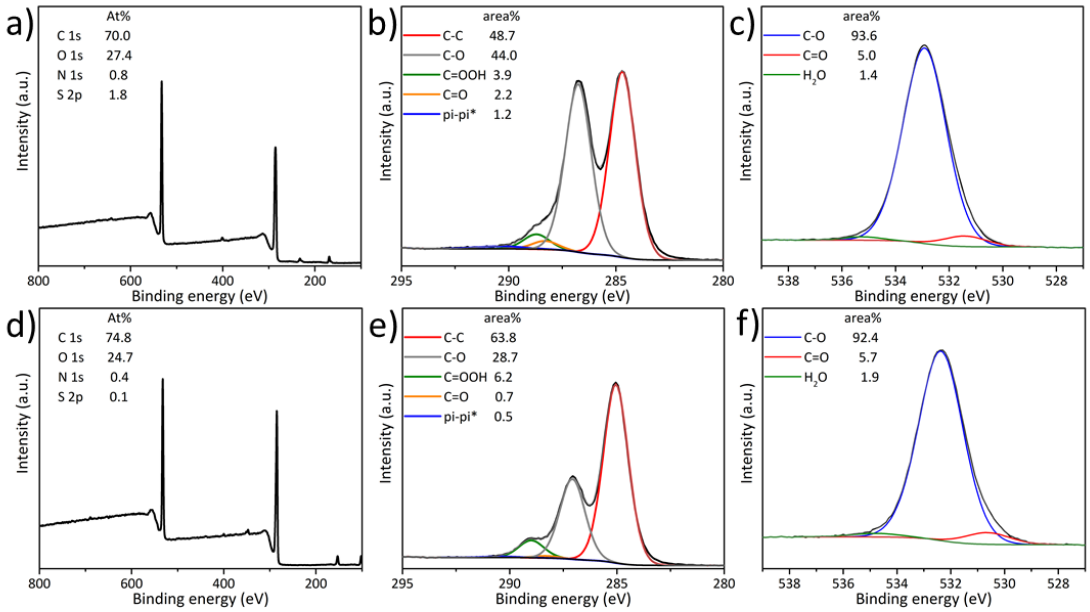

Figure 2.1. XPS survey spectra (a, d), high resolution C 1s (b, e) and O 1s (c, f) spectra of pristine GO (top row) and GO **1** (bottom row).

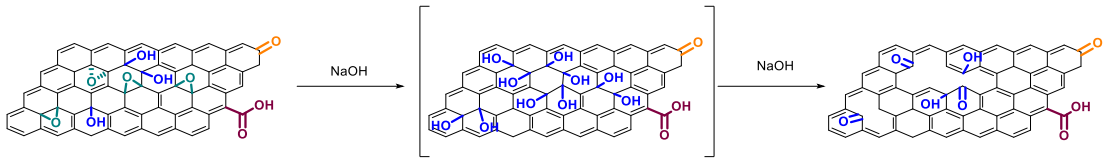

Scheme 2.2. Deoxygenation of GO under alkaline solution.[17, 18]

The reduction of GO was corroborated by thermogravimetric analysis under inert atmosphere (Figure 2.2a). The TGA curve of the pristine GO showed two main weight losses. The first weight loss from 30-100°C can be assigned to the removal of physisorbed water,[4] while the second weight loss from 150 to 200 °C is due to the decomposition of labile oxygenated groups. As evidently showed in Figure 2a, the TGA curve of GO **1** present a higher thermal stability in the 150-200°C region and a lower total weight loss at 800°C. The increase of the thermal stability could be attributed to the partial reduction of GO by removal of some labile oxygen-containing groups.[18]

Then we performed the attenuated total reflectance (ATR) FT-IR spectroscopy on pristine GO and GO **1** (Figure 2.2b). In the spectrum of the starting GO, a broad peak around 3400 cm^{-1} was observed and it could be assigned to the O-H stretching of the adsorbed water and the hydroxyl functions of GO.[19] The band at 1723 cm^{-1} in GO **1** was attributed to the stretching of C=O groups while the peak at 1619 cm^{-1} corresponded to the H-O-H bending vibration of water molecules and the skeletal C=C bond vibrations of the graphitic domains. The band at 1371 cm^{-1} could be assigned to the O-H bending vibration. The C-O-C vibration band of the epoxides was located at 1232 cm^{-1} and the peak at 1143

cm^{-1} was assigned to the C-O stretching. After the carboxylation, the stretching band of C=O at 1723 cm^{-1} was still present as well as the O-H stretching at ~ 3400 cm^{-1}.

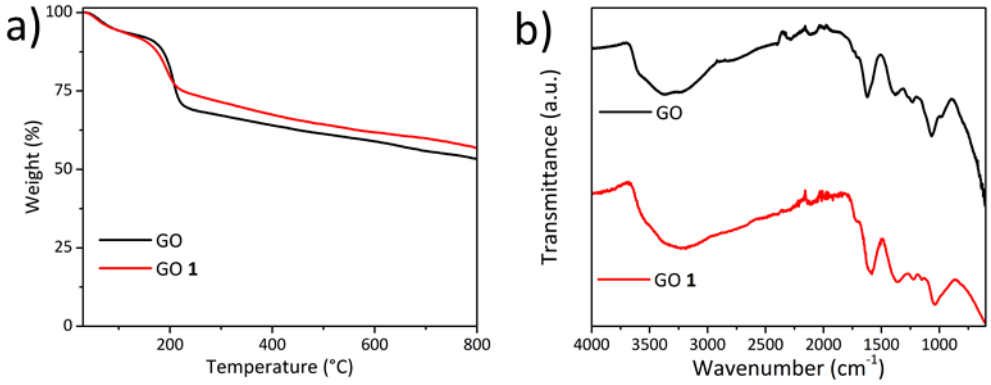

Figure 2.2. a) TGA of the pristine GO and GO **1** performed in inert atmosphere. b) FT-IR spectra of the pristine GO and GO **1**.

The morphology of GO was characterized by TEM (Figure 2.3). The GO sheets have an average lateral dimension around 1 μm and a wavy shape with folded edges. After carboxylation, the morphology of GO was not affected significantly.

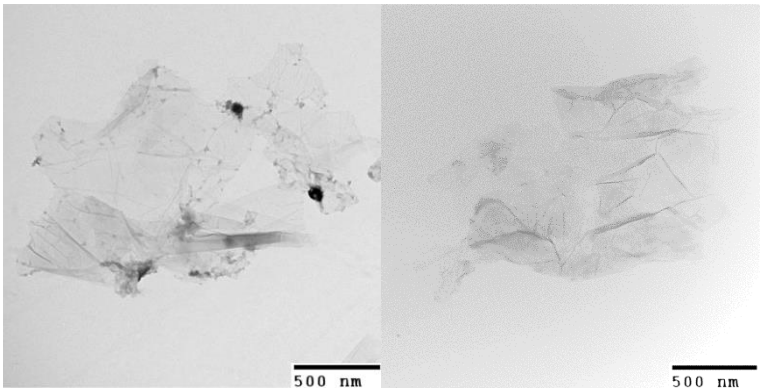

Figure 2.3. TEM images of GO (left) and GO **1** (right).

Although there are many literatures published applying the carboxylation method for GO surface modification using chloroacetic acid and sodium hydroxide with high concentration, the partial reduction of the material and the removal of the oxygen functional groups were never clearly mentioned. On the other hand, the reduction of GO in strong alkaline solution at room temperature has been reported by several groups,[16-18, 20] and it has been proved as an efficient way to produce reduced GO.[4, 21] Since these oxygenated groups are crucial for the functionalization on GO, we continued studying the impact of the reduction on the efficiency of double functionalization.

2.3.2 Double functionalization of GO combining opening of epoxides and carboxylation with high amount of sodium hydroxide

To better understand the effect of the partial reduction on GO double functionalization, we decided to combine an epoxide ring opening reaction and the carboxylation of GO followed by an amidation (Scheme 2.3). *O*-(2-aminoethyl)-*O'*-[2-(Boc-amino)ethyl]decaethylene glycol (BocNH-PEG_{10}-NH_2) was chosen as the functional group since the amine moiety can open the epoxide ring with high efficiency and it can also react with the carboxyl groups onto GO in the presence of activating agents (EDC/NHS) to achieve the double functionalization. The amount of amino-PEG groups grafted onto GO can be evaluated using the colorimetric Kaiser test after Boc-deprotection.[22, 23] The epoxide ring opening reaction was first performed since the epoxides easily react with amines through a nucleophilic addition forming a C-N bond and a new hydroxyl group on the opposite site of the plane, which can benefit of a further derivatization with chloroacetic acid. For this purpose, pristine GO was mixed with BocNH-PEG_{10}-NH_2 in water and stirred for 3 days at room temperature (Scheme 2.3). After washing and dialysis, GO **2** was obtained. The functionalities on GO **2** were determined by a Kaiser test after Boc deprotection and the amount of free amines was estimated to be 59 μmol/g, proving that the PEG chain was successfully grafted onto GO (Figure 2.4a). For the carboxylation procedure, GO **2** was mixed with chloroacetic acid in the presence of 3 M sodium hydroxide under bath sonication following the protocol described above, leading to GO **3** (Scheme 2.3). We cannot exclude that chloroacetic acid may also react with the secondary amine of the PEG chain introduced after the epoxide ring opening. However, the close proximity of this secondary amine with the surface of GO likely hampers such derivatization due to steric inaccessibility. The Kaiser test of Boc-deprotected GO **3** revealed that the amount of amines decreased to 14 μmol/g after the carboxylation (Figure 2.4a), indicating that the PEG chain may be partially removed due to partial reduction of GO during the carboxylation step. GO **3** was further reacted with BocNH-PEG_{10}-NH_2 through amidation in the presence of EDC/NHS, giving the double functionalized GO **4**. An increase of the amount of primary amines was measured by the Kaiser test (27 μmol/g), confirming that the PEG chain was linked to GO through amidation of the carboxyl groups (Figure 2.4a). Meanwhile, a control reaction was performed by directly grafting BocNH-PEG_{10}-NH_2 on GO **2** through amidation obtaining GO **4-CTR** (Scheme 2.3b). The Kaiser test value (62 μmol/g) showed a little increase compared to GO **2** (Figure 2.3a), thus confirming that there is only a limited amount of carboxyl groups at the edges of GO and that the reaction with chloroacetic acid allows to introduce more COOH moieties on GO.

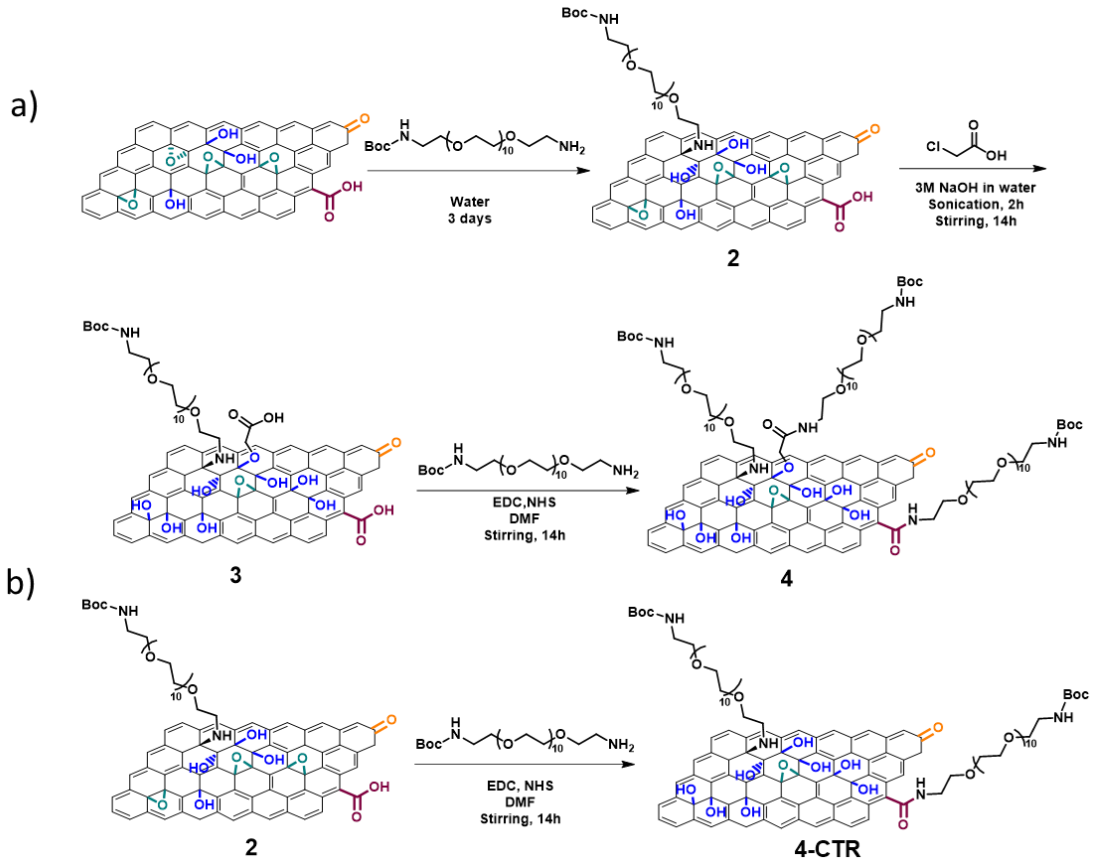

Scheme 2.3. a) Double functionalization of GO combining the epoxide ring opening reaction and the carboxylation reaction. b) Control reaction of the double functionalized GO. For the sake of clarity, only one type of functional group is derivatized.

The thermogravimetric analysis further confirmed the partial removal of the oxygenated functional groups on GO during the carboxylation step in the presence of the high concentration of sodium hydroxide (Figure 2.4b). Compared to pristine GO, PEG modified GO **2** displayed another weight loss in the region between 200 and 400°C, contributed by the thermal degradation of the PEG covalently bound to GO. However, after the carboxylation reaction, the thermal stability GO **3** of was enhanced with a lower weight loss compared to GO **2**, probably due to the deoxygenation under high concentration of sodium hydroxide. For the double functionalized GO **4**, a higher weight loss was observed in the temperature region between 200 and 400°C, indicating that more PEG chains were functionalized onto GO surface. Overall, the TGA results corresponded to the results obtained by Kaiser test, confirming the successful double functionalization of GO through the combination of epoxide ring opening reaction and carboxylation followed by amindation. The additional carboxyl groups introduced to GO surface may help increase the grafting of the second functional group. Nevertheless, the distinct increasing of thermal instability after the carboxylation on GO **2** revealed that some functionalities were partially removed in the strong basic condition.

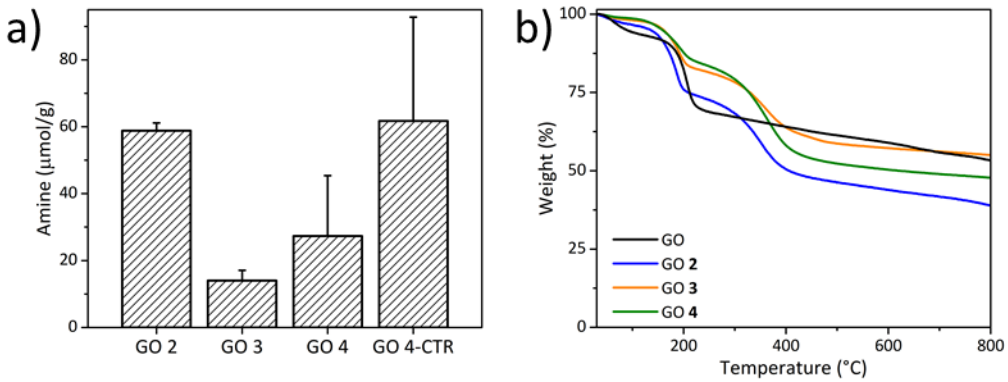

Figure 2.4. a) Kaiser test of GO **2**, GO **3,** GO **4** and GO **4-CTR** after Boc deprotection, and b) TGA of GO **2**, GO **3** and GO **4** performed in inert atmosphere.

The XPS analysis also confirmed the removal of some functional groups during the reaction (Figure 2.5). After the carboxylation step, the percentage of nitrogen atom on GO **3** increased from 1.0% to 1.8% compared to GO **2** due to the partial deoxygenation on GO. After the amidation reaction, the %N in GO **4** increased to 2.1%, proving that more PEG chains were grafted onto GO surface.

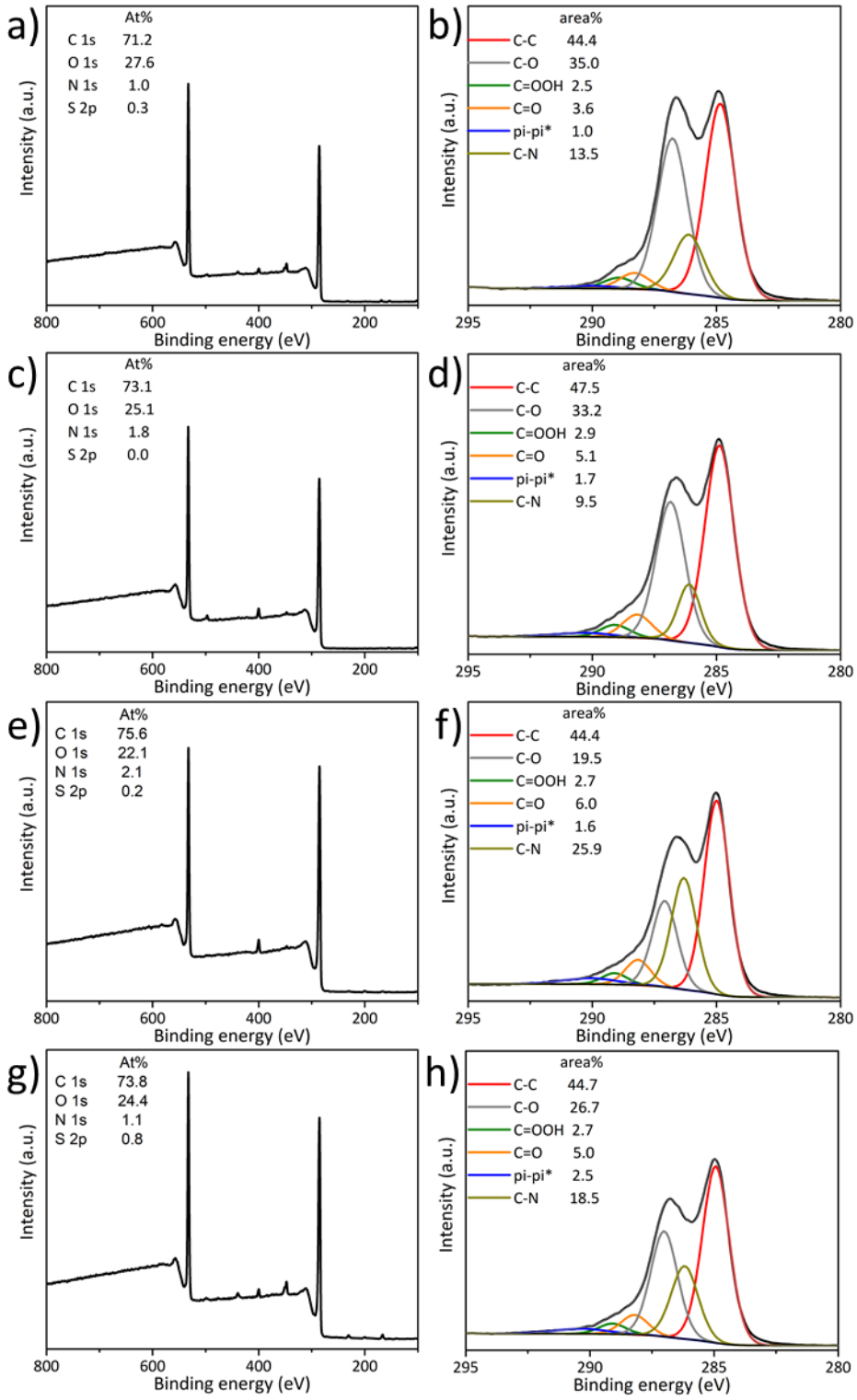

Figure 2.5. XPS survey spectra (a, c, e, g) and high resolution C 1s (b, d, f, h) spectra of GO **2** (a, b), GO **3** (c, d), GO **4** (e, f) and GO **4-CTR** (g, h).

With a combined epoxide ring opening followed by a carboxylation/amidation, a stepwise double GO functionalization was successfully achieved. But, the partial reduction of GO resulted in a lower efficiency of total functionalization and limited to a certain extent this method for further applications.

2.3.3 Double functionalization of GO combining opening of epoxides and carboxylation with a reduced amount of sodium hydroxide

To reduce the severe reduction of GO during the carboxylation process, we decided to perform this reaction using a lower amount of sodium hydroxide. The carboxylation of GO was operated in a sodium hydroxide solution at different pH: at pH 9 (10^{-5} M of NaOH in water) and at pH 13 (0.1 M of aqueous NaOH), leading to GO **5a** and GO **5b**, respectively. Both samples were characterized by XPS (Figure 2.6). However, the C 1s spectra indicated a lower efficiency of carboxylation using lower concentrations of sodium hydroxide. Based on the deconvolution of C 1s spectra, it is not evident to conclude that more carboxyl groups were introduced onto GO surface in both pH conditions. Additionally, the area of carbon from C-O component in GO **5a** decreased to 39.7% compared to pristine GO (44.0%), revealing that even at pH 9 GO was slightly reduced during the functionalization. A more pronounced reduction was instead observed in GO **5b** with the C-O component decreased to 35.0% due to the higher pH. The C/O ratio calculated from the survey spectra are consistent with the results from the high-resolution C 1s spectra. The C/O ratio increased from 2.6 for the pristine GO to 2.8 for GO **5a** and 3.0 for GO **5b**.

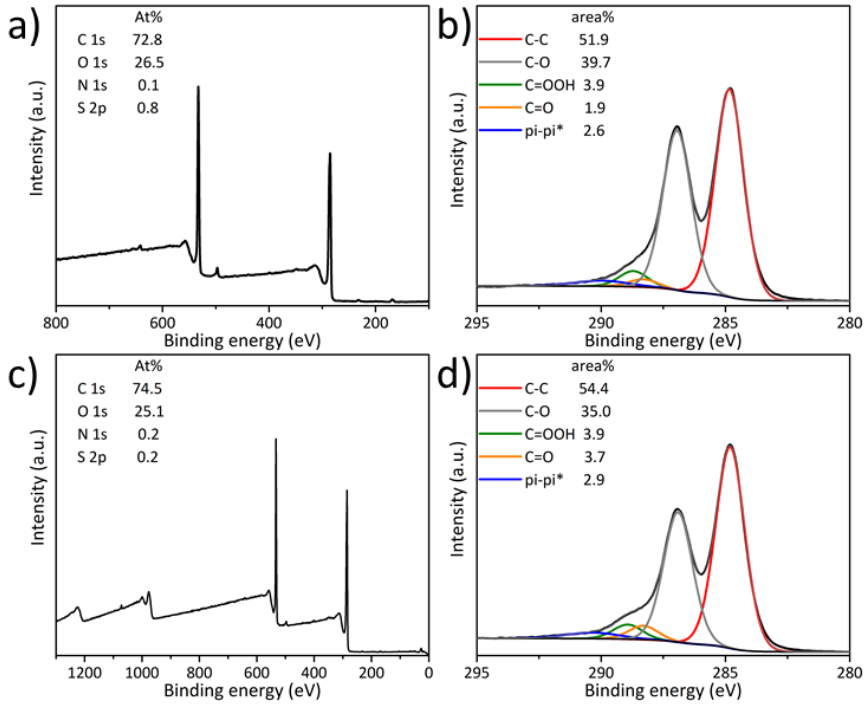

Figure 2.6. XPS survey spectra (a, c) and high resolution C 1s (b, d) spectra of GO **5a** (top row) and GO **5b** (bottom row).

The slight reduction of GO **5a** and GO **5b** were also confirmed by TGA (Figure 2.7). Both GO samples showed a slightly increased thermal stability around 200°C, which could be assigned to the partial removal of labile oxygen-containing groups, in agreement with the XPS data.

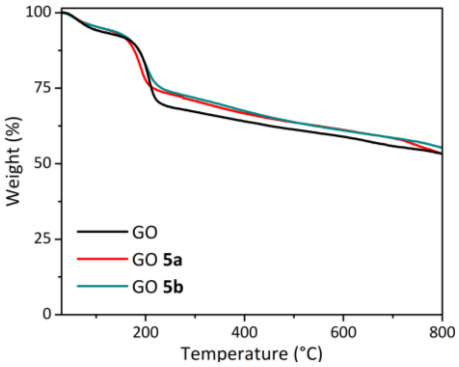

Figure 2.7. TGA of the pristine GO, GO **5a** and GO **5b** performed in inert atmosphere.

In order to further understand the carboxylation reaction using low concentration of sodium hydroxide, we decide to characterize the pristine GO and GO **5a** by quantitative ^{13}C direct polarization (DP) solid state MAS-NMR (Figure 2.8). A control reaction was also performed by stirring GO at the same pH but without adding chloroacetic acid giving GO **5a-CTR** (see section 2.5 Materials and methods). A detailed analysis of ^{13}C spectra is shown in Figure 2.8 with a line shape fitting using a CSA (Chemical Shift Anisotropy) model. The intensities for inner components of each broad bands were obtained (Table 2.1). The strong bands located at 60.1 ppm and 69.8 ppm can be assigned to the abundant epoxides and hydroxyl groups, respectively, and the strong peak at ~ 130 ppm is from C=C bonds.[4, 24, 25] However, the peak of the carboxyl groups located around 164 ppm is almost negligible due to the limited amount of carboxyl groups of pristine GO compared to other functional groups. Unfortunately, the carboxylation reaction did not increase the signal of the carboxyl groups, proving the inefficiency of the reaction at a lower pH.

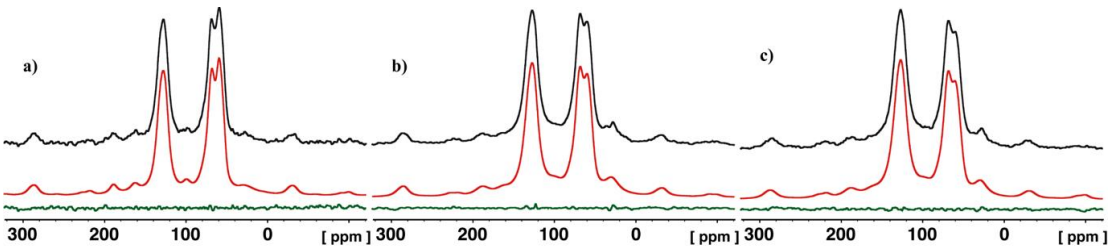

Figure 2.8. ^{13}C DP/MAS line shape analysis (experimental black, calculated red, difference green). a) pristine GO, b) GO **5a** and c) GO **5a-CTR**.

The ^{13}C DP/MAS NMR spectra also confirmed the slight reduction of GO in the basic condition. The intensity of the peaks of the epoxides decreased to 16% in GO **5a** and GO **5a-CTR** comparing to

pristine GO (22%), while hydroxyls showed a little increase from 20% in pristine GO to 23% in GO **5a** and 22% in GO **5a-CTR**, respectively (Table 2.1). The difference in the areas of the epoxides and the hydroxyls could be assigned to the opening of a small proportion of the epoxides by sodium hydroxide. The fitting of the C=C signal evidenced two peaks at ca. 126 and 132 ppm that could be ascribed to graphitic localized clusters of C=C and to the other C=C in proximity of oxygenated groups, respectively (Table 2.1).

Table 2.1. Percentages of the different peaks for pristine a) GO, b) GO **5a** and c) GO **5a-CTR** obtained from the quantitative ^{13}C NMR spectra.

a)

δ (ppm)	%
190.2	2
164.0	3
132.3	23
126.7	17
100.4	2
78.3	4
69.8	20
60.1	22
55.0	2
27.0	4

b)

δ (ppm)	%
189.7	3
164.5	2
131.8	25
125.9	18
100.4	3
80.8	2
70.2	23
60.4	16
55.9	2
30.6	6

c)

δ (ppm)	%
189.9	3
164.4	2
131.3	28
125.6	18
99.0	3
81.1	2
70.3	22
60.3	16
55.1	2
29.9	5

To confirm whether more carboxyl groups were however covalently linked onto GO surface, the carboxylated GO samples prepared at pH 9 (GO **5a**) and pH 13 (GO **5b**) were derivatized with *N*-Boc-2,2′-(ethylenedioxy)diethylamine (Boc-TEG-NH_2) (Scheme 2.4). Since the reduction of GO was not severe at pH 9 and pH 13, we assumed it was possible to perform the carboxylation keeping the epoxide group that can be susceptible to the following ring opening reaction. GO **5a** and GO **5b** were first functionalized Boc-TEG-NH_2 through a nucleophilic epoxide ring opening, obtaining GO **6a** and GO **6b**, respectively. Then, Boc-TEG-NH_2 was grafted on GO **6a** and GO **6b** by amidation of the carboxyl groups of GO in the presence of activating reagents (EDC/NHS), giving the double functionalized GO **7a** and GO **7b**.

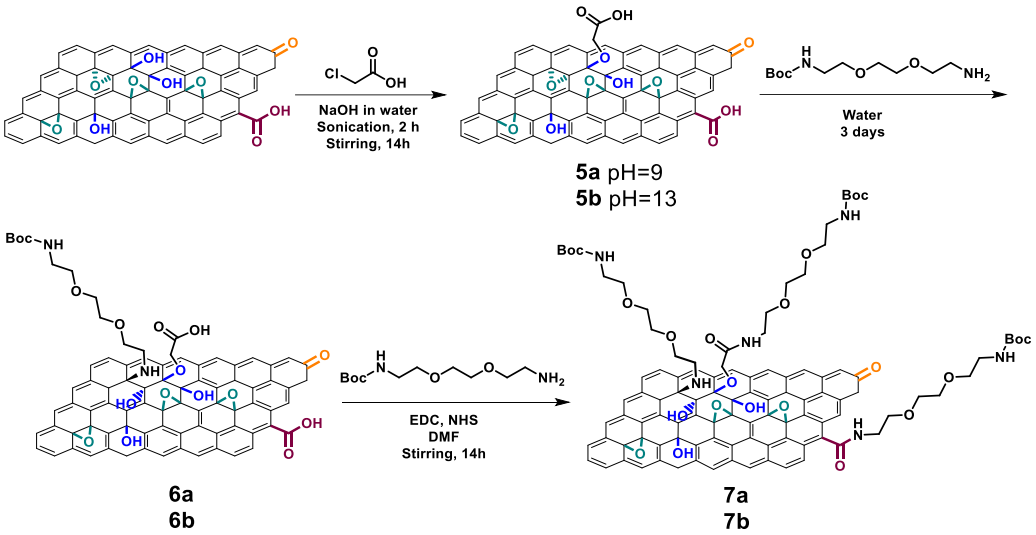

Scheme 2.4. Double functionalization of GO combining the carboxylation reaction using reduced amount of sodium hydroxide and epoxide ring opening reaction, followed by amidation. For the sake of clarity, only one type of functional group is derivatized.

The GO samples were characterized by XPS (Figure 2.9). The significant increase of the %N values for GO **6a** and GO **6b** proving that Boc-TEG-NH_2 was successfully introduced on GO through epoxide ring opening (Table 2.2). However, we could not observe a significant increase of the %N after the amidation reaction, indicating that there was little Boc-TEG-NH_2 added to monofunctionalized GO through amidation, likely due to the low amount of the carboxylic groups onto GO surface. These results were supported by the Kaiser test. The amount of amines in GO **6a** and GO **6b** were calculated after Boc deprotection, as shown in Table 2.2. However, both double functionalized GO **7a** and GO **7b** did not present a higher amount of amines compared to the monofunctionalized GO, confirming the low efficiency of the second step of functionalization. The slight decrease of the amine level after the amidation was likely caused by the removal of some PEG chains physisorbed onto GO by DMF.

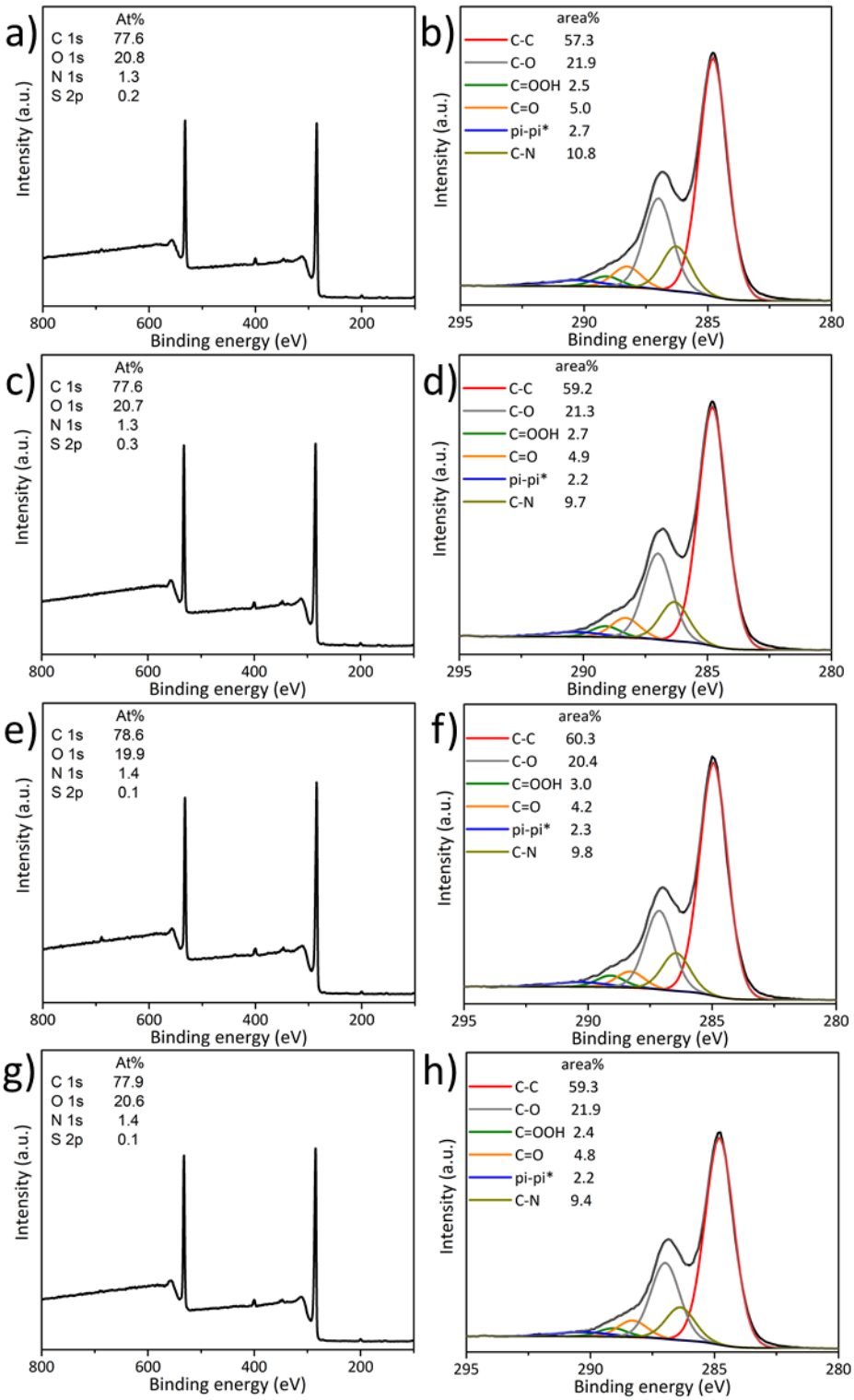

Figure 2.9. XPS survey spectra (a, c, e, g) and high resolution C 1s (b, d, f, h) spectra of GO **6a** (a, b), GO **6b** (c, d), GO **7a** (e, f) and GO **7b** (g, h).

By studying this alternative strategy using a lower amount of sodium hydroxide, the reduction of GO was limited compared to the common method used in previous publications.[26] Nevertheless, the

carboxylation was not efficient, thus limiting the scope of the double functionalization strategy based on carboxylation followed by epoxide ring opening.

Table 2.2. Percentage of nitrogen element and amount of amines on GO samples assessed by XPS and the Kaiser test, respectively.

Sample	%N	Amine (μmol/g)
5a	0.1	
6a	1.3	105
7a	1.4	75
5b	0.2	
6b	1.3	99
7b	1.4	75

2.3.4 Conclusion

In summary, we studied the possibility to combine the epoxide ring opening reaction and the carboxylation followed by the amidation reaction to prepare a multifunctional platform under controlled chemical approaches. To further optimize the condition of the carboxylation, we investigated the influence of different amounts of sodium hydroxide on GO structure. The GO was successfully derivatized with chloroacetic acid with a clear increase of the carboxyl groups observed, but a concomitant partial reduction of GO. GO was then doubly functionalized in a stepwise procedure by combining an epoxide ring opening, the carboxylation and an amidation reaction. The high concentration of sodium hydroxide used in the carboxylation step provoke however a significant reduction of the material accompanied by the removal of some functionalities during the carboxylation step. Although it was possible to attach two functional groups by combining carboxylation with epoxide ring opening reaction, the total level of functionalization is much lower compared to a direct epoxide ring opening.

In the following study, we found that the derivation of hydroxyl with carboxyl groups occurred only under strong basic condition. Indeed, with a lower amount of sodium hydroxide, GO was not significantly reduced due to a small proportion of the epoxides being opened by sodium hydroxide. But the introduction of carboxylates was negligible in these milder conditions and it would not help for the introduction of the second functional group.

Overall, our results demonstrate that the carboxylation is not a suitable approach for the functionalization of GO due to the partial reduction of GO in strong basic solution and it can be hardly applied to achieve an efficient double functionalization of GO for further modifications. This work shows that it is very important to consider side reactions that were barely mentioned in the previous

literature. The control of the derivatization of GO is crucial, in particular for biological purpose. The surface modification would tune the intrinsic properties of GO, affecting the loading effencency and other factors which are important for its application in biosensing and disease treatment as drug nanocarriers. This part of work has already published in Nanoscale Advances.

2.4 Combining the opening of epoxides and benzoquinone-mediated Michael addition reaction

In the previous part, we investigated the carboxylation reaction on GO and used this reaction in the double functionalization of GO. However, the strong basic condition provoked the severe reduction on GO, thus decreased the total loading efficiency.

In this section we have explored a new strategy, inspired by work of functionalization on nanodiamonds using benzoquinone by Purtov *et al.*[27] Benzoquinone is widely used as coupling agent to obtain protein-protein or protein-polysaccharide conjugates.[28] A polysaccharide or a protein is activated with benzoquinone in a mild alkaline solution and then mixed with a second biomolecule. The conjugation takes place through a Michael addition between benzoquinone and the amine or hydroxyl groups on the protein or the sugar chain. For example, nanodiamond-protein covalent complexes have been prepared using benzoquinone as crosslinker.[27, 29] Since there are abundant hydroxyl groups onto GO, it is possible to use benzoquinone in the functionalization of GO.

Aiming to develop an efficient double functionalization of GO in mild condition, we combined the epoxide ring opening reaction and Michael addition using benzoquinone.

2.4.1 Double functionalization through epoxide ring opening reaction and Michael addition of benzoquinone

We first decided to double functionalize GO with Boc-PEG_{10}-NH_2 and benzoquinone following a three-step procedure illustrated in Scheme 2.5. Briefly, Boc-PEG_{10}-NH_2 was firstly introduced onto GO through nucleophilic attack of the amine group on the epoxide with the formation of a C-N bond and a new hydroxyl group. Then, the hydroxyl groups of the mono-functionalized GO **8** were derivatized with benzoquinone, giving GO **9**. Subsequently Boc-PEG_{10}-NH_2 was covalently reacted to benzoquinone moiety onto GO **9** through another Michael addition, leading to the double functionalized GO **10**.

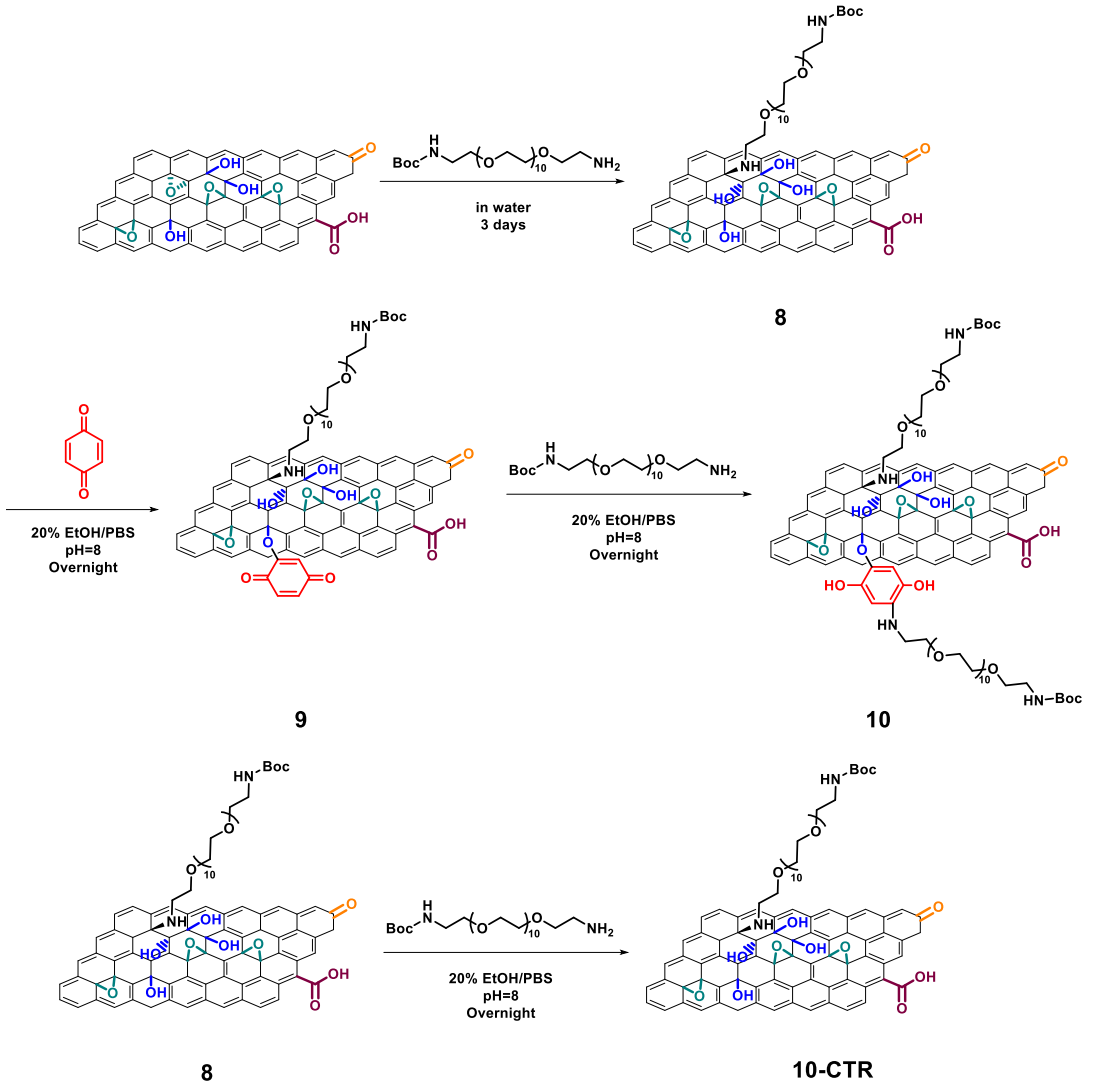

Scheme 2.5. Double functionalization of GO with Boc-PEG$_{10}$-NH$_2$. For the sake of clarity, only one epoxide and one hydroxyl group are derivatized.

The mono-functionalized GO **8** was characterized by XPS (Figure 2.10). Compared to starting GO, the nitrogen atom increased from 0.7% to 1.0% after the first step of functionalization, indicating the presence of Boc-PEG$_{10}$-NH$_2$ on GO (Figure 2.10a and c). The deconvolution of the high-resolution C 1s peak of GO **8** showed an increasing area of C-N bond after the derivation of GO with PEG chain, which further supports the presence of PEG onto GO (Figure 2.10d). Following the deprotection of Boc, the amines can be further functionalized with molecules of interest in mild conditions through an amidation reaction.

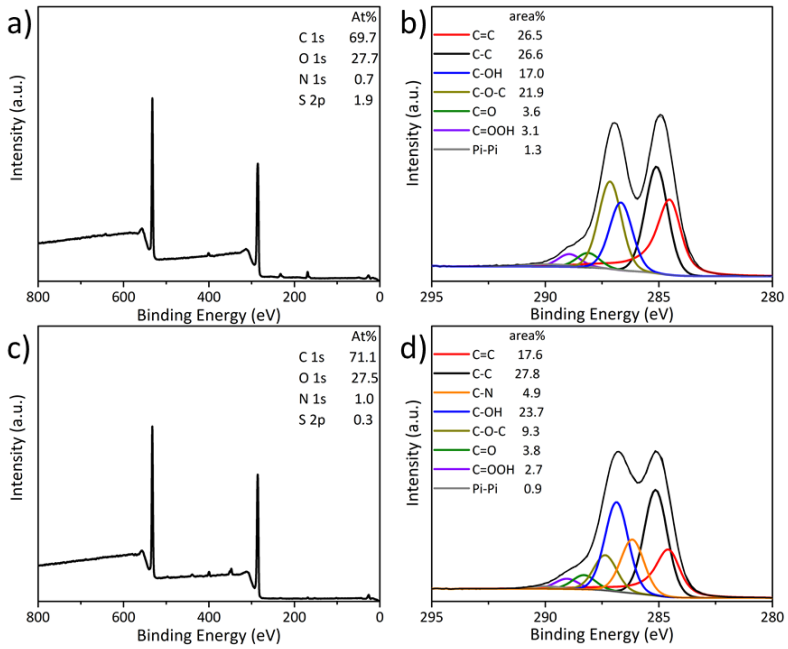

Figure 2.10. XPS survey spectra (a, c) and high resolution C1s (b, d) of GO (top row) and GO **8** (bottom row).

To perform the second step of functionalization, the hydroxyl groups of the mono-functionalized GO **8** were derivatized with benzoquinone (Scheme 2.5). The nucleophilic attack of the hydroxyls on benzoquinone resulted in a 2-substituted hydroquinone grafted onto GO. The hydroquinone moiety was self-oxidized by the excess of free benzoquinone to get benzoquinone-functionalized GO **9** ready for the subsequent functionalization with amine derivatives (Scheme 2.6).[28]

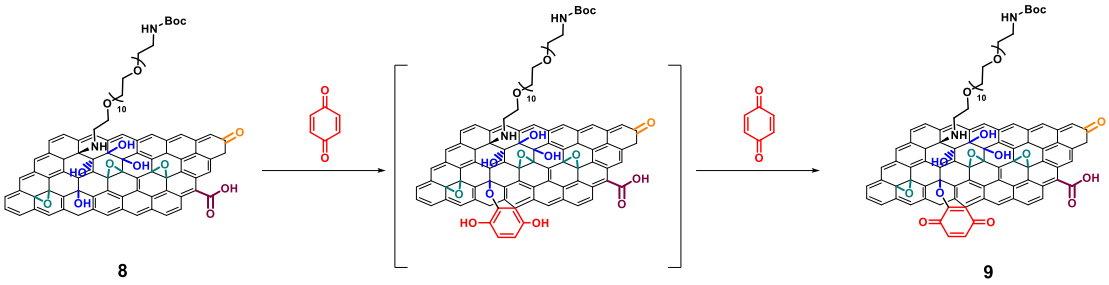

Scheme 2.6. Mechanism of Michael addition between benzoquinone and the hydroxyl groups onto GO **8** leading to GO **9**. For the sake of clarity, only one epoxide and one hydroxyl group are derivatized.

GO **9** was characterized by XPS (Figure 2.11) and C/O ratio calculated from survey spectrum increased from 2.6 to 3.1 (Figure 2.11), compared with GO **8** (Figure 2.10). the area of the C-OH and C-O-C in the detailed analysis of the C1s spectrum changed from 23.7% and 9.7% to 5.0% and 22.0%, in comparison with GO **8** respectively. These changes could be explained by the grafting of benzoquinone onto GO, which was further used for the second functionalization. An unexpected reduction of GO was also observed during the reaction. Compared to GO **8**, the percentage of nitrogen atoms decreased from 1.0% to 0.7% due to the slight reduction of GO and the removal of physisorbed PEG chain (Figure 2.10 c and 2.11 a). The benzoquinone-activated GO **9** was then reacted with Boc-PEG_{10}-NH_2 giving

double functionalized GO **10** (Scheme 2.5). The increase of nitrogen atom was observed by XPS from 0.7% to 1.4% providing a solid evidence that there is additional Boc-PEG_{10}-NH_2 grafted onto GO (Figure 2.11a and b). Moreover, the detailed analysis of the C 1s peak clearly showed the increase of C-O and C-N peaks after the introduction of PEG chain through the Michael addition with a significant change of line shape (Figure 2.11d and e). A control reaction was performed by directly mixing GO **8** with Boc-PEG_{10}-NH_2, leading to conjugate GO **10-CTR** (Scheme 2.5). The percentage of nitrogen atoms was 1.1% and the C-N and C-O components in C 1s spectrum were lower than GO **10** (Figure 2.11), which indicates a low tendency of the PEG chain to adsorb onto GO, thus confirming the covalent linkage in the case of GO **10**. The amine was deprotected through cleavage of Boc group using 2 M HCl in dioxane on an aliquot sample. The colorimetric Kaiser test in GO **10** confirmed the presence of free amines (35 µmol/g), while in GO **10-CTR** there was only 17 µmol/g, giving an additional evidence of successful covalent functionalization.

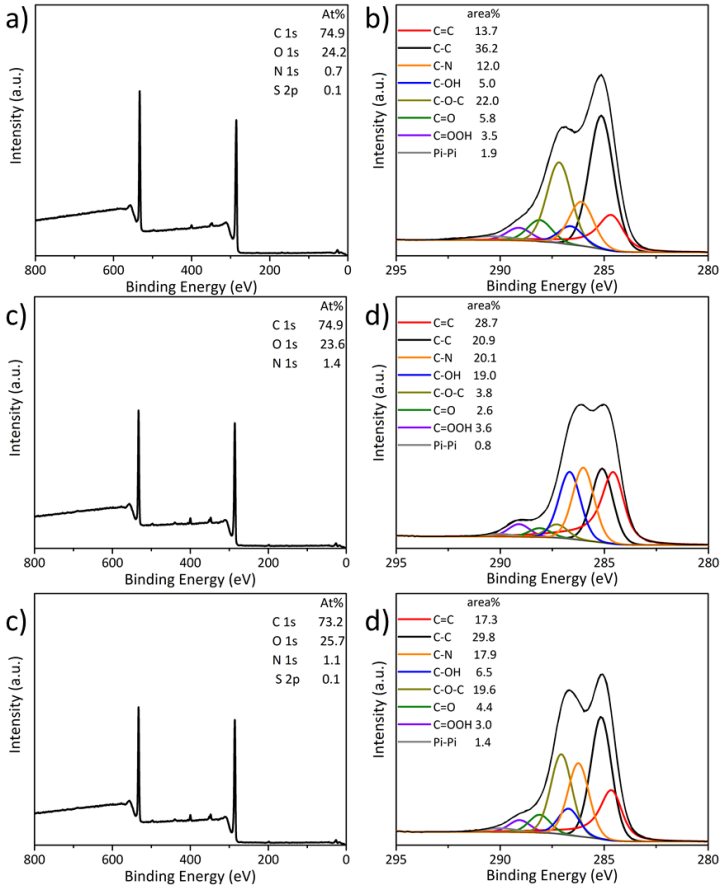

Figure 2.11. XPS survey spectra (a, c, e) and high resolution C 1s (b, d, f) spectra of GO **9** (a, b), GO **10** (c, d) and GO **10-CTR** (e, f).

Next, we performed TGA of GO before and after functionalization in inert atmosphere at a heating rate of 10°C·min^{-1} (Figure 2.12). The weight loss below 100°C was attributed to the desorption of water adsorbed onto GO surface. Compared to the starting GO, the functionalized GO **8**, GO **10**, and GO **10-CTR** presented a slightly lower weight loss below 100°C which could be assigned to the effect of the covalent functionalization. The TGA curve of pristine GO only showed one main weight loss at

around 200°C, which is caused by the removal of labile oxygenated functional groups, while the functionalized GO samples experienced two main weight loss. The starting GO exhibited a higher weight loss around 200°C compared to functionalized GO samples due to the higher amount of labile oxygenated functional groups before chemical modification. Moreover, the weight loss of GO **10** is lower than GO **8** and GO **10-CTR** around 200°C, due to the derivation on hydroxyl groups which would increase the thermostability. The gradual weight loss above 250°C can be ascribed to the decomposition of more stable oxygen-containing groups. A second main weight loss was observed in GO **8**, GO **10**, and GO **10-CTR** in the region of temperature between 200°C and 400°C that could be attributed to the loss of covalently grafted Boc-PEG_{10}-NH_2. As shown in figure 2.12, the characteristic temperature of Boc-PEG_{10}-NH_2 thermal decomposition is around 233°C, which consists of the second weight loss observed in GO **8**, GO **10**, and GO **10-CTR**. After the double functionalization, the higher weight loss in GO **10** compared to GO **8** can be explained by the additional presence of Boc-PEG_{10}-NH_2 introduced through the Michael addition between benzoquinone and amine moiety on PEG chain. The derivative of TGA curves clearly showed the significant difference of weight loss between GO **8** and GO **10** at the temperature between 200°C and 400°C. Compared to GO **8**, only a slight increase in GO **10-CTR** was observed, indicating that most of the Boc-PEG_{10}-NH_2 was covalently bound to GO rather than adsorbed. Overall, the TGA results confirmed the successful double functionalization of GO with Boc-PEG_{10}-NH_2 in a stepwise procedure.

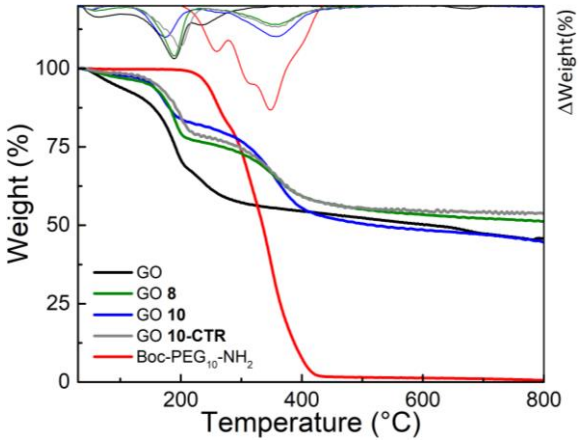

Figure 2.12. TGA of GO, GO **8**, GO **10**, GO **10-CTR** and Boc-PEG_{10}-NH_2.

With this strategy, we successfully grafted Boc-PEG_{10}-NH_2 onto GO through epoxide ring opening and Michael addition reaction in different steps. But with this strategy, the two Boc protected derivative cannot be functionalized selectively, which would limit the application of this method. To overcome this problem, it is necessary to add orthogonally protected amines.

2.4.2 Double functionalization of GO with Boc-PEG$_{10}$-NH$_2$ and 3-(pentafluorothio)-DL-phenylalanine

In the previous part, we successfully double functionalized GO with Boc-PEG$_{10}$-NH$_2$ in a stepwise procedure combining epoxide ring opening reaction and Michael addition of benzoquinone. However only one functional molecule was used in that protocol. To further investigate the method for GO double functionalization, we decided to derivatize GO with different functional molecules through the opening of epoxides and Michael addition.

The protocol of double functionalization was similar to the previous one. We first prepared the Boc-PEG$_{10}$-NH$_2$ functionalized GO **8** through epoxide ring opening reaction. The presence of PEG chain can be characterized by TGA and XPS, and after Boc-deprotection, the free amine can be further modified. Then the hydroxyl groups on GO **8** were derivatized with benzoquinone obtaining GO **9** as described before. To double functionalize GO, 3-(pentafluorothio)-DL-phenylalanine was covalently bound onto GO as the second functional group, giving GO **11** (Scheme 2.7). We decided to choose this phenylalanine derivative because it contains a free amine which can covalently link to the benzoquinone moiety present in GO **9** via a Michael addition reaction, while the COOH moiety in 3-(pentafluorothio)-DL-phenylalanine can be further functionalized by amidation or esterification. In addition, the pentafluorothio group in 3-(pentafluorothio)-DL-phenylalanine can facilitate the characterization by XPS and FT-IR because the fluorine atoms are often used as chemical tags for XPS as the F 1s core-level transition has a high photoemission cross-section (three times higher than that of carbon).[30] To clarify if GO **9** was covalently functionalized with 3-(pentafluorothio)-DL-phenylalanine through Michael addition to benzoquinone derivative, a control reaction was performed by mixing GO **8** directly with 3-(pentafluorothio)-DL-phenylalanine. After carefully washing and dialysis, GO **11-CTR** was obtained (Scheme 2.7).

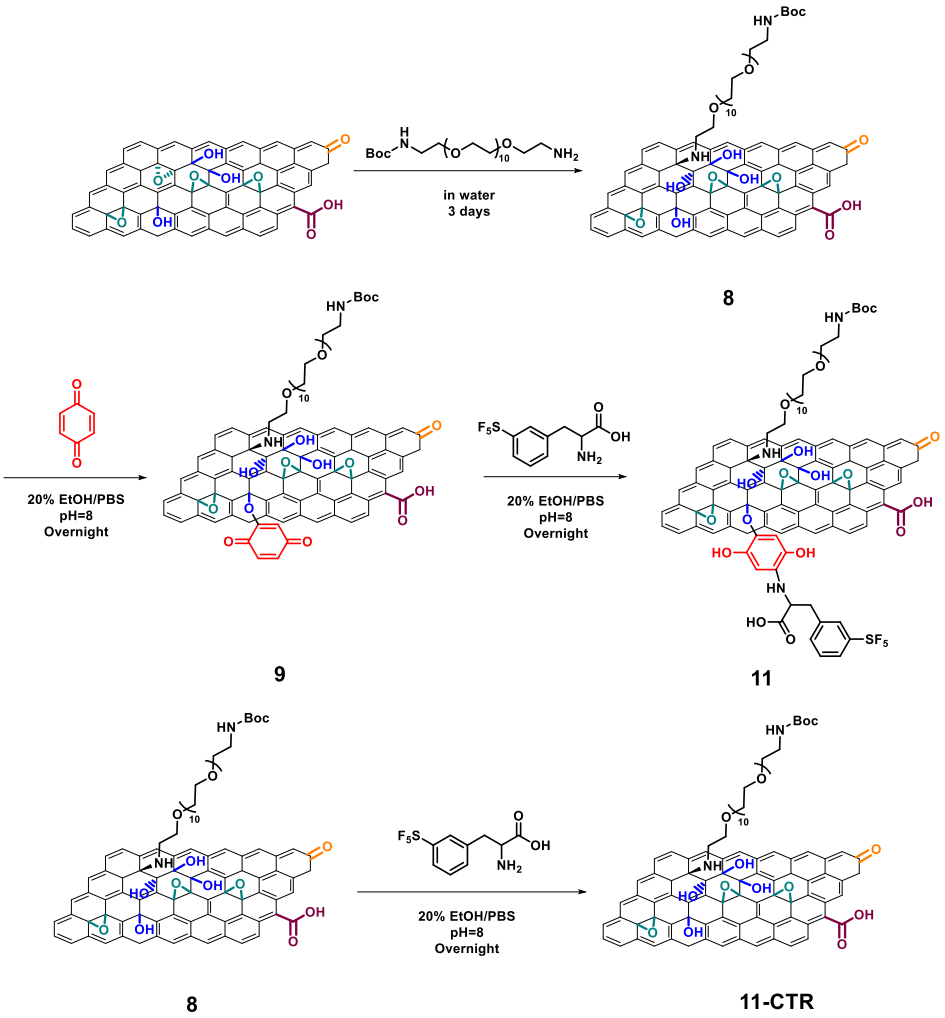

Scheme 2.7. Double functionalization of GO. For the sake of clarity, only one epoxide and one hydroxyl group are derivatized.

Since GO **8** and GO **9** were well-studied in the previous part, we directly performed the characterized on GO **11**. The double functionalized GO **11** was first characterized with XPS. A significant signal from fluorine atoms was recorded by XPS in the survey spectrum (2.7%) (Figure 2.13d), while no fluorine was detected in the all GO precursor conjugates. An increase of sulfur atom was also observed after the double functionalization from 0.1% to 0.9% (Figure 2.13a and d) indicating the successful introduction of the 3-(pentafluorothio)-phenylalanine moiety onto GO **9**. The detailed analysis of the S 2p peak further confirmed the presence of 3-(pentafluorothio)-DL-phenylalanine on double functionalized GO. In the monofunctionalized GO **9**, only one peak at 168.4 eV was recorded in S 2p spectrum, which was assigned to the sulfur atoms in S-O bond from organosulfate groups introduced onto GO surface during the exfoliation of graphite (Figure 2.13c).[31] After the Michael addition between 3-(pentafluorothio)-phenylalanine and benzoquinone, a new peak appeared at 173.0 eV which could be contributed by sulfur atom in S-F bond from the pentafluorothiol moiety (Figure 2.13 f).[33] The presence of the S-F component was indicative of the presence of 3-(pentafluorothio)-phenylalanine onto GO, thus confirming the successful double functionalization on GO with two different molecules. In the control sample GO **11-CTR**, the fluorine element was calculated as 1.3% which was much lower

than GO **11** (Figure 2.13). In S 2p spectrum, there was only one peak at 168.4 eV from S-O bond while the S-F peak was almost negligible compared to S-O peak (Figure 2.13), which indicates a low tendency of the phenylalanine derivative to adsorb onto GO **8**, thus confirming the covalent linkage in the case of GO **11**. In addition, the secondary amine formed during the opening of epoxide by Boc-PEG_{10}-NH_2 could undergo side reactions with benzoquinone. The activation of GO may not target only the hydroxyl groups, but also this secondary amine on monofunctionalized GO.

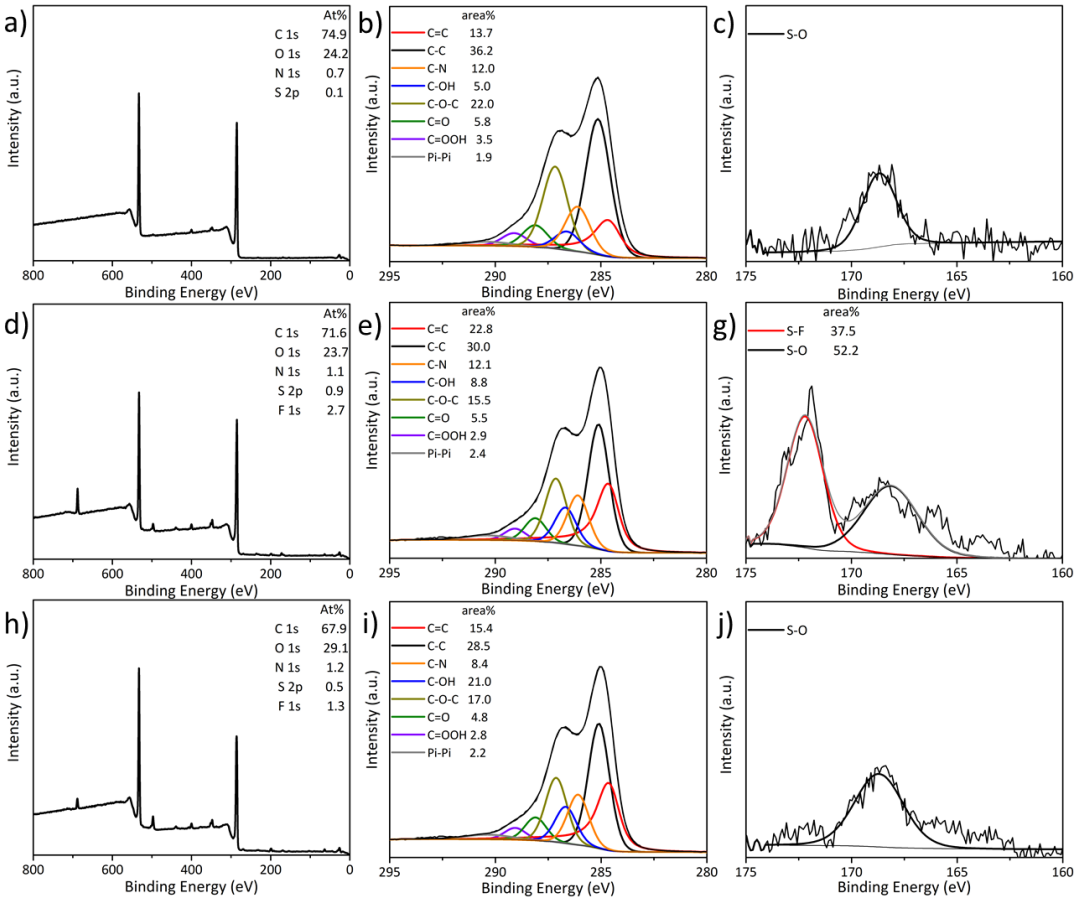

Figure 2.13. XPS survey spectra (a, d, h), high resolution C1s (b, e, i) and S2p (c, f, j) spectra of GO **9** (top row), GO **11** (middle row) and GO **11-CTR** (bottom row).

2.4.3 Double functionalization with Boc-aminoethanethiol and 3-(pentafluorothio)-DL-phenylalanine

In the previous part, we successfully modified GO with two different functional molecules in a stepwise procedure. But in the first step of functionalization, a secondary amine isformed during the nucleophilic addition of Boc-PEG_{10}-NH_2 to epoxides. Benzoquinone is also able to react with secondary amines through Michael addition. Although the close proximity of the secondary amine with the surface of GO could hamper the Michael addition to benzoquinone due to the steric inaccessibility, we still cannot exclude the possibility that benzoquinone might react with these secondary amines of the PEG chain introduced after the epoxide ring opening. Thus, it was unclear

whether only hydroxyl groups onto GO were derivatized by benzoquinone. For this reason, we shifted to another strategy by replacing the Boc-PEG_{10}-NH_2 with Boc-aminoethanethiol in the first step of the double functionalization (Scheme 2.8).

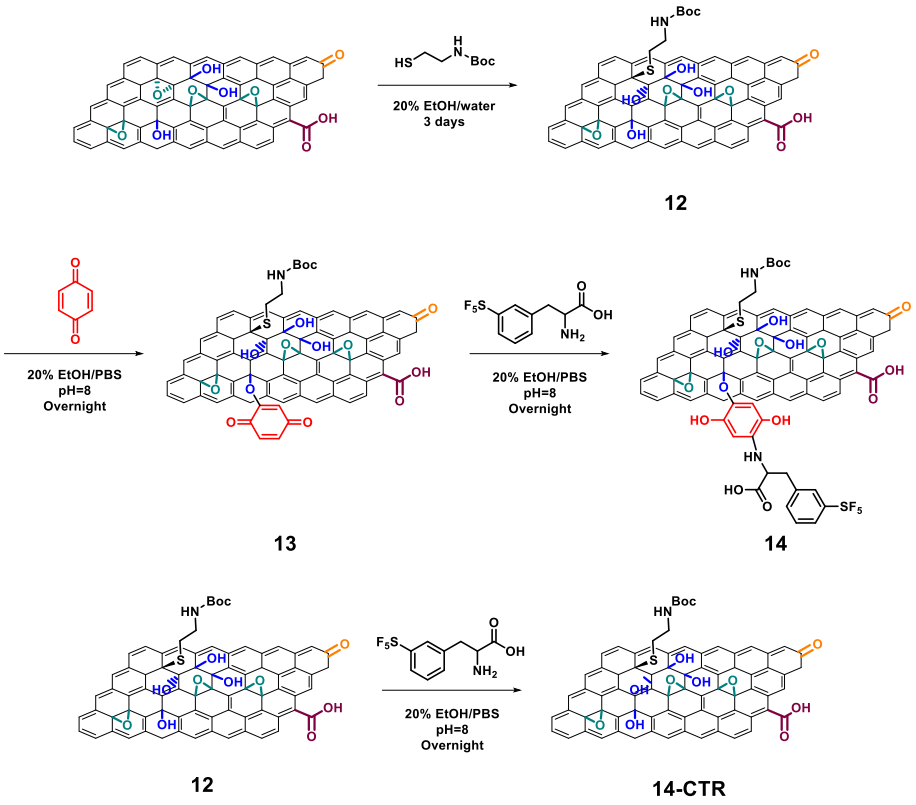

Scheme 2.8. Double functionalization of GO. For the sake of clarity, only one epoxide and one hydroxyl group are derivatized.

The Boc-aminoethanethiol was first grafted onto GO through nucleophilic attack of the thiol group on the epoxide leading to ring opening and formation of a thioether bond and new hydroxyl groups.[33] The mono-functionalized GO **12** was characterized by XPS (Figure 2.14). Compared to starting GO, the amount of sulfur atoms in monofunctionalized GO **12** increased from 0.5% to 1.4% and the nitrogen increased from 0.4% to 1.1%, indicating the successful complexing of Boc-aminoethanethiol onto GO (Figure 2.14a and d). The detailed analysis of the high resolution S 2p peak of GO **12** showed a new peak appeared at 164.0 eV, which could be assigned to the formation of new S-C bond, proving the introduction of Boc-aminoethanethiol through epoxide opening,[33] while in pristine GO there is only S-O peak organosulfate groups (Figure 2.14c and f). The presence of the new peak from S-C bond thus confirmed the functionalization of GO. The colorimetric Kaiser test was then performed to evaluate the amine introduced to the GO. The amine was deprotected through cleavage of Boc group using 2 M HCl in dioxane on an aliquot sample and the amount of free amines was calculated as 34 µmol/g, further confirming the successful mono-functionalization through the epoxide ring opening using thiol derivatives. The amines can be further functionalized with molecules of interest in mild conditions through an amidation reaction.

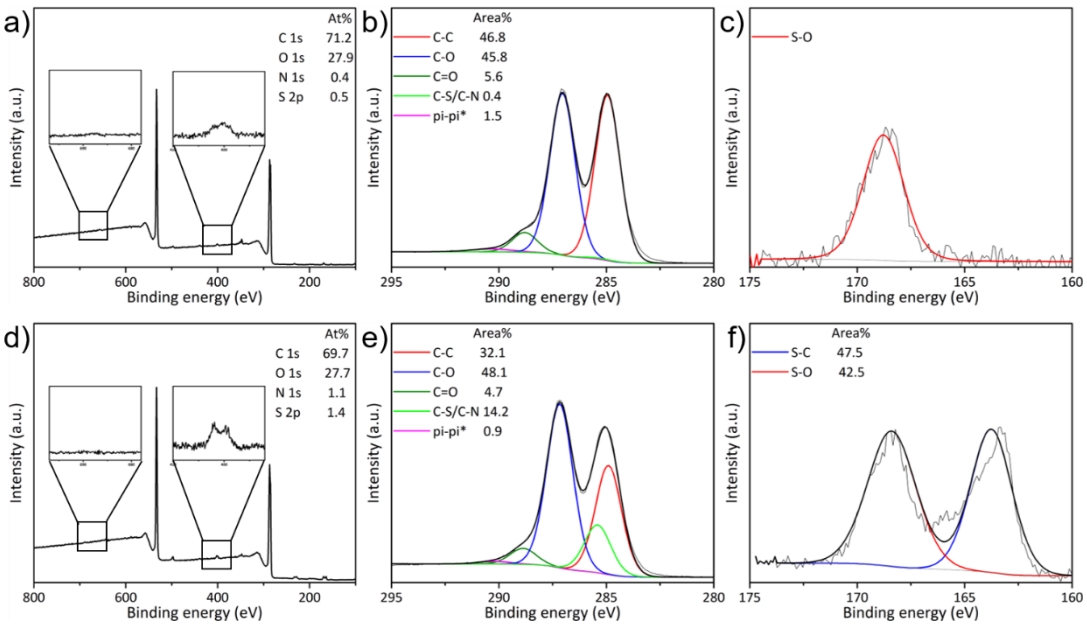

Figure 2.14. XPS survey spectra (a, d) with a zoom on the N 1s peaks (inset), high resolution C 1s (b, e) and S 2p (c, f) spectra of GO (top row) and GO **12** (bottom row).

The hydroxyl groups on mono-functionalized GO **12** were then activated with benzoquinone (Scheme 2.8), leading to GO **13**. GO **13** was characterized by XPS (Figure 2.15). After the deconvolution of the C1s spectrum, the area of the C-C, C=O, and π-π* peaks increased from 32.1%, 4.7% and 0.9% to 51.5%, 6.1% and 2.9%, respectively (Figure 2.15b), compared with GO **12** (Figure 2.14e).

The benzoquinone-derivatized GO **13** was reacted with 3-(pentafluorothio)-DL-phenylalanine giving double functionalized GO **14** (Scheme 2.8). In the previous part, we have proved that 3-(pentafluorothio)-DL-phenylalanine can facilitate the characterization of the double functionalization. The presence of fluorine was again confirmed by XPS (1.6%) after the addition of the phenylalanine derivative, while no signal of fluorine was recorded in the GO precursor conjugates (Figure 2.14a, 2.14d, 2.15a and 2.15d). An increase of the sulfur atom also observed from 0.5% in GO **13** to 0.7% in GO **14**, thus confirming the presence of the 3-(pentafluorothio)-phenylalanine moiety after the double functionalization. The high-resolution S 2p spectrum clearly showed the presence of a new peak at 173.0 eV (Figure 2.15c and f) after the double functionalization. The three main peaks were deconvoluted into three peaks at 164.5 eV (S-C), 168.0 eV (S-O), and 173.0 eV(S-F).[32] As mentioned before, the S-O peak came from the organosulfates introduced during the preparation of GO and the C-S-C peak belongs to the Boc-cysteamine. The appearance of the S-F peak confirmed the successful double functionalization onto GO. A control reaction was performed by directly mixing GO **12** with 3-(pentafluorothio)-phenylalanine, leading to conjugate GO **14-CTR** (Scheme 2.14). The resulting GO **14-CTR** was characterized using XPS (Figure 2.15). The signal of fluorine is much lower than GO **14** and the S-F peak in S 2p spectrum was almost negligible (Figure 2.15 h), confirming the covalent functionalization of 3-(pentafluorothio)-DL-phenylalanine on GO **14** rather than physisorbtion.

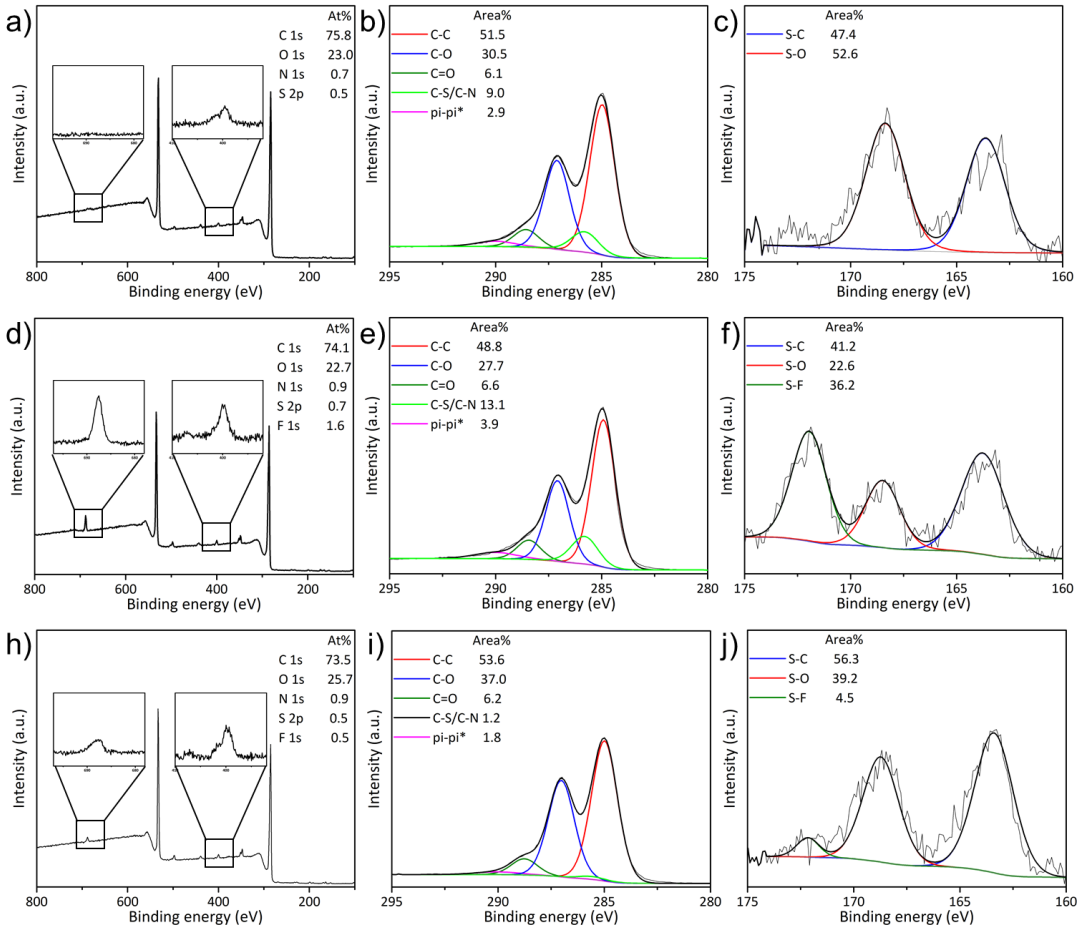

Figure 2.15. XPS survey spectra (a, d) with a zoom on the F 1s (left inset) and N1s peaks (right inset), high resolution C1s (b, e) and S 2p (c, f) spectra of GO **13** (top row), GO **14** (middle row) and GO **14-CTR** (bottom row).

Then some additional characterizations were performed on the different GO conjugates using complementary analytical and microscopic techniques. Attenuated total reflectance (ATR FT-IR) spectroscopy confirmed the double functionalization of GO (Figure 2.16a). The O–H stretching vibrations of adsorbed water and hydroxyl functions of GO can be found in the spectrum with a broad band centred at around 3400 cm^{-1} and there is also a band at 1620 cm^{-1}, which could be assigned to H–O–H bending vibrations of water molecules and skeletal vibrations of unoxidized graphitic domains.[19] The C–O–C vibration band of epoxides (at 1232 cm^{-1}) is small and covered by other unassigned bands. The band at 1371 cm^{-1} is ascribed mainly to the bending vibration of the O–H groups of GO. In GO **12** and GO **14** spectra, new bands appeared at 2850–2970 cm^{-1} which could be assigned to the stretching bands of alkyl groups of the Boc-aminoethanethiol moiety.[34] The appearance of a strong band at 842 cm^{-1} corresponded to the characteristic S–F stretching from 3-(pentafluorothio)-phenylalanine, proving successfully modification on GO with phenylalanine derivative.[35] In the control sample GO **14-CTR**, the peak at 842 cm^{-1} was much lower than GO **14** due to the very low amount of phenylalanine derivative adsorbed onto GO. FT-IR spectra further confirmed the covalent

double functionalization of GO through the epoxide ring opening using Boc-aminoethanethiol and the benzoquinone-related Michael addition of 3-(pentafluorothio)-phenylalanine.

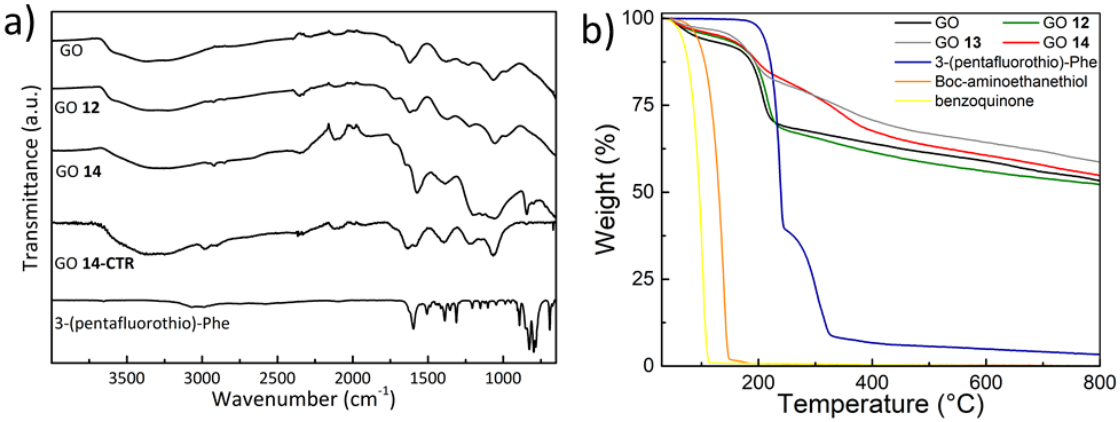

Figure 2.16. (a) FT-IR spectra of GO, GO **12**, GO **14**, GO **14-CTR**, and 3-(pentafluorothio)-phenylalanine and (b) TGA of GO, GO **12**, GO **13**, GO **14**, 3-(pentafluorothio)-phenylalanine, Boc-aminoethanethiol, and benzoquinone.

Next, GO samples before and after functionalization were characterized by TGA in inert atmosphere at a heating rate of 10°C·min^{-1} (Figure 2.16b). The weight loss of the functionalized GO **12**, GO **13**, and GO **14** was slightly lower than the starting GO below 100°C, which is similar to what we observed for GO **8**, GO **9** and GO **10**. The mono-functionalized GO **12** present a higher weight loss compared to GO due to the presence of Boc-aminoethanethiol. In the double functionalized GO **3**, a second peak of thermal decomposition was observed at the temperature between 200°C and 400°C, which could be assigned to the loss of covalently grafted 3-(pentafluorothio)-phenylalanine. For 3-(pentafluorothio)-phenylalanine alone, two main weight losses were recorded. The first thermal decomposition occurred at 233°C followed by a secondary weight loss at 300°C. However, a lower weight loss was observed both in GO **13** and GO **14** at 200°C in comparison to GO and GO **12**, due to the much lower amount of labile oxygenated groups such as hydroxyls after the derivatization of the OH groups with benzoquinone. The weight loss difference between GO **2** and GO **3** at high temperature is indicative of the presence of 3-(pentafluorothio)-phenylalanine. Overall, the TGA results showed an evident proof for the successful double functionalization of GO with two different molecules having distinct thermal properties.

The presence of quinone moiety onto GO was confirmed by analysis of the electrochemical redox behavior of GO, benzoquinone, GO **13**, and GO **14** (Figure 2.17). Because of the high dispersibility of pristine GO in the electrolyte, GO could be easily leached out from the glassy carbon electrode in the electrolyte solution. Therefore, we used slightly dehydrated GO for comparison by refluxing GO in water for 1 h to partially reduce its hydrophilicity. Thermally treated GO showed no clear redox peak (Figure 2.17a). Benzoquinone showed oxidation at 0.53 V and reduction at 0.48 V (Figure 2.17b). Similarly, GO **13** and GO **14** showed oxidation (at 0.52 and 0.51 V) and reduction (at 0.45 and 0.44 V) peaks, respectively (Figure 2.17 c and d), suggesting successful functionalization of GO with benzoquinone.

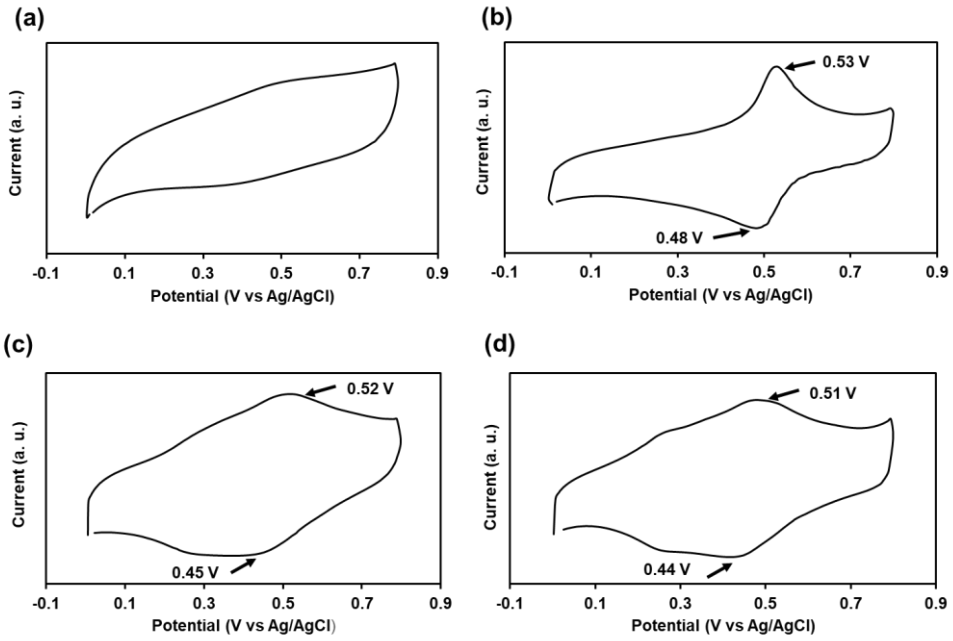

Figure 2.17. Cyclic voltammogram of (a) GO, (b) benzoquinone, (c) GO **13**, and (d) GO **14**. Scan rate: 50 $mV \cdot s^{-1}$, Electrolyte: 0.5 M H_2SO_4.

Finally, the characterization by TEM and AFM showed that the morphology of the GO sheets was preserved after the double functionalization process (Figure 2.18). Indeed, both starting GO and GO **14** have wrinkled sheets with folded edges with a similar lateral size dimension. AFM showed an increase of the thickness from 0.8 to 1.2 nm due to functionalization. Hence, the epoxide ring opening reaction and the Michael addition did not affect the morphology of GO, while increasing the thickness.

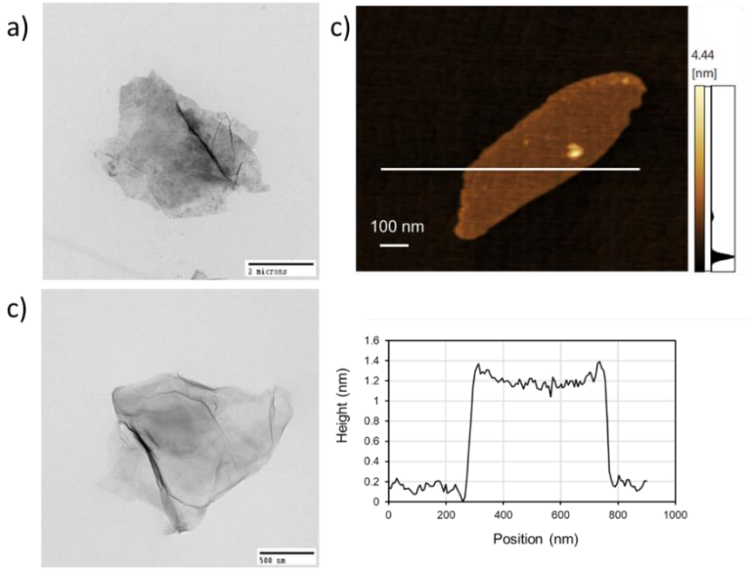

Figure 2.18. TEM images of GO (a) and GO **14** (b) and AFM image and cross section analysis of GO **14** (c). After functionalization, the thickness of GO **14** increased to 1.2 nm while the general thickness of GO is around 0.8 nm.[36, 37]

2.4.4 Conclusion

In summary, we developed a simple method for the double functionalization of GO in mild conditions targeting the epoxides and hydroxyl groups that are present in large amount on the basal plane of the material. Three different protocols were developed using different functional molecules. In the first protocol, Boc-PEG_{10}-NH_2 was introduced onto GO surface by a nucleophilic opening of the epoxides with the free amine moiety obtaining the mono-functionalized GO. An C-N bond and a hydroxyl group were formed during the reaction. The mono-functionalized GO, with more OH groups compared to pristine GO, was derivatized through Michael addition using benzoquinone, which is very reactive toward nucleophiles. Finally, an additional Boc-PEG_{10}-NH_2 was added to GO-benzoquinone complex through Michael addition between the amine and the benzoquinone moiety. Then in the second protocol, we double functionalized GO with different molecules by replacing the Boc-PEG_{10}-NH_2 with 3-(pentafluorothio)-phenylalanine in the last step of modification. However, as benzoquinone was assumed to be reactive with the secondary amines formed during the epoxide ring opening using Boc-PEG_{10}-NH_2, we decided to use a thiol-containing molecule for the opening of epoxides in the first step. The mono-functionalized GO was activated with benzoquinone followed by a Michael addition between the benzoquinone and 3-(pentafluorothio)-phenylalanine. The covalent functionalization of GO was confirmed by XPS, FT-IR, TGA, cyclic voltammetry, TEM, and AFM. The strategy we developed for the double functionalization is simple and robust. GO was efficiently functionalized with two different functional groups in mild condition. The functional groups onto GO can be further modified with biologically active molecules through amidation for instance. Compared with other covalent multi-functionalization protocols, the benzoquinone-based method is performed in mild conditions without heating or without adding metal catalysts. The morphology of the sheets is preserved and the functionalization does not cause reduction of GO which is especially appropriate for the conjugation of temperature- and pH-sensitive functional groups. This part of work has already published in Angewandte Chemie.[6]

2.5 Material and methods

Materials

All the chemicals and solvents were obtained from commercial suppliers and used without purification. *O*-(2-aminoethyl)-*O′*-[2-(Boc-amino)ethyl]decaethylene glycol (BocNH-PEG_{10}-NH_2) was purchased from Polypure AS. The solvents used during the reaction were analytical grade. Water was purified by a Millipore filter system MilliQ®.

Preparation of GO suspensions

GO suspensions were prepared by sonication in a water bath (20 W, 40 kHz) with a controlled temperature between 20°C and 30°C.

Dialysis

For dialysis, MWCO 12,000-14,000 Da membranes were purchased from Spectrum Laboratories, Inc.

Thermogravimetric analysis

Thermogravimetric analysis (TGA) was performed on a TGA1 (Mettler Toledo) apparatus from 30°C to 900°C with a ramp of 10°C·min^{-1} under N_2 atmosphere with a flow rate of 50 mL·min^{-1} and platinum pans.

Transmission electron microscopy

Transmission electron microscopy (TEM) analysis was performed on a Hitachi H600 with an accelerating voltage of 75 kV. The samples were dispersed in water/ethanol (1:1) at a concentration of 16 μg·mL^{-1} and the suspensions were sonicated for 10 min. Ten microliters of the suspensions were drop-casted onto a copper grid (Formvar film 300 Mesh, Cu from Electron Microscopy Sciences) and left for evaporation under ambient conditions.

Attenuated total reflectance-FTIR

ATR-FTIR was performed using a Thermo Scientific Nicolet™ 6700 FT-IR spectrometer equipped with an ATR accessory (diamond ATR polarization accessory with 1 reflection top-plate and pressure arm). The pressure arm was used for all solid samples at a force gauge setting between 100 and 120 units. The number of scans was set at 30. Samples were loaded on the reflection top-plate at a quantity sufficient enough to cover the entire diamond surface.

^{1}H NMR

^{1}H liquid-state NMR spectra were recorded in deuterated solvents using Bruker Avance I - 300 MHz. Chemical shifts are reported in ppm using the residual signal of deuterated solvent as reference. The resonance multiplicity is described as s (singlet), t (triplet), dd (doublet of doublet), dt (doublet of triplet). Coupling constants (J) are given in Hz.

X-ray photoelectron spectroscopy

X-ray photoelectron spectroscopy experiments were performed on a Thermo Scientific KAlpha X-ray photoelectron spectrometer with a basic chamber pressure of 10^{-8}-10^{-9} bar and an Al anode as the X-ray source (1486 eV). The samples were analyzed as powder pressed onto a scotch tape (3MTM EMI Copper Foil Shielding Tape 118). Spot size of 400 μm was used for analysis. The survey spectra are an average of 10 scans with a pass energy of 200.00 eV and a step size of 1 eV. The high resolution spectra are an average of 10 scans with a pass energy of 50 eV and a step size of 0.1 eV. The pass energy of 50.00 eV corresponds to Ag $3d_{5/2}$ full width line at half maximum (FWHM) of 1.3 eV. A pass energy of 50.00 eV for the high resolution spectra was applied because lower pass energies have shown no improvement in FWHM for graphene materials on Thermo Scientific K-ALPHA.[38] For each

sample, the analysis was repeated three times. A flood gun was turned on during analysis. We grouped the functional groups of C 1s spectra to avoid imprecision due to the proximity of the peak values, since the binding energy values in the literature were too spread. Therefore, the C 1s spectra were deconvoluted in C=OOH (288.7-289.1 eV) for carboxyl groups, C=O (288.1-288.3eV) for carbonyl groups, C-O (286.2-287.2 eV) for hydroxyls and epoxides and C-C (284.4-285.3 eV) for sp^2 and sp^3 carbon atoms. For data analysis, the software casaXPS (2.3.18) was used. A Shirley background subtraction was applied. A line-shape 70% Gaussian/30% Lorenzian [GL(30)] was selected for all peaks. The full width at half maximum was constrained to be the same for all peaks, apart for the pi-pi* peak because it is a broad signal. Similarly, the O 1s spectra were deconvoluted in C=O (531.4-530.3 eV), C-O (533.0-532.0 eV) and H_2O (535.2-534.8 eV).

Solid-State NMR

^{13}C solid-state NMR experiments were performed at room temperature on an AVANCE 300 MHz wide-bore spectrometer (Bruker™) operating at a frequency of 75.52 MHz for ^{13}C. All the samples were spun at 12 kHz in a double resonance MAS (Magic Angle Spinning) probe designed for 4 mm o.d. zirconia rotors (closed with Kel-F caps). All spectra were acquired following the Hahn's spin-echo experiment pulse scheme[39] as it allows to get undistorted line shapes and flat baselines that are prerequisites for quantitative analysis. Echo times were synchronized with the rotation (echo time = 2 rotation periods = 166.67 µs) and durations were 2.73 µs and 5.46 µs for $\pi/2$ and π pulses respectively. Proton decoupling during acquisition was done using SPINAL-64 decoupling[40] at a 73 kHz RF field. Spectral width was set to 50 kHz and 65536 transients per FID were acquired on 8192-time domain points except for pristine GO where only 7168 transients per FID were added. In order to achieve quantitative results a series of longitudinal relaxation times (T1) measurements were carried out (Inversion-Recovery method, data not shown). With the longest T1 being below 300 ms we could safely use a recycling delay of 2 s for all spin-echoes experiments. Together with a relatively high amount of sample inside the rotors (80 µL active volume) it allowed to get rather noiseless spectra in a reasonable time (ca. 12 h). A 150 Hz Lorentzian filter was applied prior to Fourier transform without zero filling. Chemical shifts were given respective to tetramethysilane (TMS) using adamantane as a secondary reference. Spectral deconvolutions were obtained using the solid line shape analysis tool (SOLA) inside the TopSpin 4.0.8 software (Bruker™). Here the CSA (Chemical Shift Anisotropy) subroutine was employed in order to get intensities (Table S1) for the minimal set of 10 sites needed to get a rather good agreement between experimental and synthetic spectra (lower traces in Figure S4 correspond to their difference).

Thin layer chromatography

Thin layer chromatography (TLC) was performed on pre-coated aluminum plates with 0.20 mm Macherey-Nagel silica gel 60 with fluorescent indicator UV_{245}.

Chromatographic purification

Chromatographic purification was performed using silica gel (Sigma-Aldrich, 40-63 μm, 230-400 mesh).

LC/MS analyses

LC/MS analyses were performed on a LC/MS instrument equipped with a Thermo Scientific VANQVISH Flex UHPLC (Hypers II GOLD column, 50×2.1 mm, 1.9 μm) integrated with a Thermo Scientific LCQ Fleet ion-trap. Deconvolution of the data was performed in MagTran 1.03 (Amgen, Thousand Oaks, CA).

Atomic force microscopy

Atomic force microscopy (AFM) was performed by SHIMADZU SPM-9700HT. The sample was dispersed in ethanol, and spin-coated on mica substrate.

Cyclic voltammetry

Cyclic voltammetry (CV) was performed with a Solartron SI1287 electrochemical workstation. Each sample was diluted in NMP (20 $mg \cdot mL^{-1}$), then 3 μL of the sample was dropped off on a glassy carbon electrode. After drying under vacuum for 30 min, CV was performed from 0 to 0.8 V at the scan rate of 50 $mV \cdot s^{-1}$ in 0.5 M H_2SO_4 electrolyte using counter Pt electrode and reference Ag/AgCl electrode. The CV data were taken up at the 2^{nd} cycle.

Quantitative Kaiser test protocol

Three solutions were prepared separately:

- (I): 10 g of phenol in 20 mL of absolute ethanol.

- (II): 2 mL of potassium cyanide 1 mM (aqueous solution) dissolved in 98 mL of pyridine.

- (III): 1 g of ninhydrin in 20 mL of absolute ethanol.

Functionalized graphene oxide was carefully weighted in a haemolysis test tube with a approximate mass of 300 μg. Then, 75 μL of solution (I), 100 μL of solution (II), and 75 μL of solution (III) were added to the testing tube and heating at 120 °C for 5 min in a heating block (Bioblock Scientific). The suspension was immediately diluted with 4450 μL of 60% ethanol. After centrifugation at 15000 rpm, the supernatant was collected and analyzed by UV-Vis spectroscopy. The absorbance at 570 nm was correlated to the amount of free amine functions on the graphene surface using the equation:

NH loading (μmol/g) = $[Abssample - Absblank]$ × diluition (mL) × 10^6 / (Extinction coefficient × sample weight (mg))

Dilution is 5 mL and extinction coefficient is 15000 $m^{-1}cm^{-1}$.

The blank was prepared exactly the same way but without graphene oxide.

The Kaiser test is repeated at least three times for each sample to ensure reproducibility.

Synthesis of the building blocks, precursors and final GO conjugates

***tert*-Butyl (2-(2-(2-aminoethoxy)ethoxy)ethyl)carbamate (Boc-TEG-NH_2)**

To a cooled solution (0°C) of 30.0 g (202.5 mmol) 2,2'-(ethylenedioxy)bis(ethylamine) in 200 mL of chloroform, a solution of 4.425 g (20.3 mmol) di-*tert*-butyl dicarbonate in 200 mL of chloroform was added dropwise under inert atmosphere. After complete addition after 2 h, the water-ice bath was removed and the mixture was allowed to warm to room temperature and it was stirred for 24 h. The organic solvent was removed under vacuum to give 4.5 g of a colorless oil. ^{1}H NMR (300 MHz, $CDCl_3$) δ 5.13 (s, 1H), 3.57 (s, 4H), 3.48 (dt, J = 9.3, 5.2 Hz, 4H), 3.26 (dd, J = 10.4, 5.3 Hz, 2H), 2.82 (t, J = 5.2 Hz, 2H), 1.39 (s, 9H) ppm. The ^{1}H NMR data were consistent with a previous work.[41]

Preparation of GO

A stirred suspension of graphite (3 g) in 95 wt% H_2SO_4 (75 mL) was gradually treated with the required amount of $KMnO_4$ (12 g) while keeping the temperature below 10°C, and the obtained mixture was stirred at 35°C for 2 h and then diluted with water (75 mL) under vigorous stirring. The resulting suspension was treated with 30 wt% H_2O_2 (7.5 mL), and the solids were separated and purified via repeated centrifugation and resuspension in water. The concentration of GO dispersion was adjusted to 1 wt%, then subjected to wet jet mill (0.1 mm nozzle) at 150 MPa.

Preparation of GO 1

1.2 g of sodium hydroxide was dissolved in 6 mL of water using a water bath sonication. 4 mL of GO suspension at a concentration of 5 $mg \cdot mL^{-1}$ was added to the NaOH solution. 1 g of chloroacetic acid were immediately added to the mixture and the suspension was bath sonicated for 2 h with a controlled temperature between 16 and 30°C. The mixture was then stirred at room temperature overnight and filtered over a polytetrafluoroethylene (PTFE) Millipore® membrane with 0.1 µm pore size. The GO on the membrane was collected and dispersed in water, sonicated in a water bath and filtered again. This sequence was repeated 3 times with water and 3 times with methanol. The resulting solid was dispersed in water and the suspension was dialyzed in water for 3 days. After lyophilization, GO **1** was obtained.

Preparation of GO 2

To a suspension of GO (50 mg) in 50 mL of water, 100 mg of Boc-PEG_{10}-NH_2 was added to the solution and bath sonicated for 10 min. The mixture was then stirred at room temperature for 3 days

and filtered over a PTFE filter membrane with 0.1 µm pore size. The solid on membrane was collected and washed with water and methanol for 3 times each. The solid was dispersed in water, the suspension was dialyzed in water for 3 days, and lyophilized to obtain GO **2**.

Preparation of GO 3

The preparation of GO **3** was similar to the preparation of GO **1**. Briefly, 1.8 g of sodium hydroxide was dissolved in 15 mL of water using water bath sonication. Then, 30 mg of GO **2** was added to the NaOH solution, followed by the immediate addition of 1.5 g of chloroacetic acid. The suspension was bath sonicated for 2 h with a controlled temperature below 30°C. The mixture was then stirred at room temperature overnight, filtered over a PTFE membrane, and washed with water and methanol for 3 times each. The solid was dispersed in water, the suspension was dialyzed in water for 3 days and lyophilized to obtain GO **3**.

Preparation of GO 4

To a suspension of GO **3** (10 mg) in 10 mL DMF, 3.8 mg of 1-ethyl-3-(3-dimethylaminopropyl)carbodiimide hydrochloride (EDC) were added. The suspension was stirred for 30 min. Then 5.8 mg of *N*-hydroxysuccinimide (NHS) were added. After stirring for 30 min, 20 mg of Boc-PEG_{10}-NH_2 were added and the suspension was bath sonicated for 10 min. The mixture was then stirred under argon atmosphere at room temperature overnight and filtered over a PTFE filter membrane with 0.1 µm pore size. The solid on membrane was collected and washed with water and methanol for 3 times each. The solid was dispersed in water, the suspension was dialyzed in water for 3 days and lyophilized to obtain GO **4**.

Preparation of GO 4-CTR

To a suspension of GO **2** (10 mg) in 10 mL DMF, 3.8 mg of EDC were added. The suspension was stirred for 30 min. Then, 5.8 mg of NHS were added. After stirring for 30 min, 20 mg of Boc-PEG_{10}-NH_2 were added and the suspension was bath sonicated for 10 min. The mixture was then stirred under argon atmosphere at room temperature overnight and filtered over a PTFE filter membrane with 0.1 µm pore size. The solid on membrane was collected and washed with water and methanol for 3 times each. The solid was dispersed in water, the suspension was dialyzed in water for 3 days and lyophilized to obtain GO **4-CTR**.

Preparation of GO 5a and GO 5b

The preparation of GO **5a** and GO **5b** is similar to GO **1**. Briefly, two different concentrations of NaOH solution was prepared (pH=9 for GO **5a**, and pH=13 GO **5b**). 6 mL of GO suspension at a concentration of 5 $mg \cdot mL^{-1}$ were added to 9 mL NaOH solution. 3 g of chloroacetic acid were immediately added and the suspension was bath sonicated for 10 min with a controlled temperature below 30°C. The mixture was then stirred at room temperature overnight, filtered over a PTFE membrane, and washed with water and methanol for 3 times each. The solid was dispersed in water, the suspension was dialyzed in water for 3 days and lyophilized, obtaining GO **5a** and GO **5b**.

Preparation of GO 6a and GO 6b

To a suspension of GO **5a** (20 mg) in 20 mL of water, 40 mg of Boc-TEG-NH_2 were added to the solution. The suspension was bath sonicated for 10 min, stirred at room temperature for 3 days, and filtered over a PTFE filter membrane with 0.1 µm pore size. The solid on membrane was collected and washed with water and methanol for 3 times each. The solid was dispersed in water, the suspension was dialyzed in water for 3 days and lyophilized to obtain GO **6a**. The preparation of GO **6b** was similar starting from GO **5b**.

Preparation of GO 7a and GO 7b

To a suspension of GO **6a** (10 mg) in 10 mL of DMF, 3.8 mg of EDC were added. The suspension was stirred for 30 min. Then, 5.8 mg of NHS were added. After stirring for 30 min, 20 mg of Boc-TEG-NH_2 were added and the suspension was bath sonicated for 10 min. The mixture was then stirred under argon atmosphere at room temperature for 3 days and filtered over a PTFE filter membrane with 0.1 µm pore size. The solid on membrane was collected and washed with water and methanol for 3 times each. The solid was dispersed in water, the suspension was dialyzed in water for 3 days and lyophilized to obtain GO **7a**. The preparation of GO **7b** was similar starting from GO **6b**.

Preparation of GO 5-CTR

GO **5a-CTR** was obtained following the protocol for the preparation of GO **5a** without adding chloroacetic acid.

Synthesis of (*tert*-butoxycarbonyl)aminoethanethiol

To a solution of aminoethanethiol hydrochloride (5.9 g, 50 mmol, 1 eq.) in dichloromethane (100 mL), triethylamine (8.4 mL, 60 mmol, 1.2 eq.) was added dropwise and the solution was stirred at room temperature for 15 min. A solution of di-*tert*-butyl dicarbonate (12.0 g, 55.0 mmol, 1.1 eq.) in dichloromethane (20 mL) was added dropwise over a period of 4 h. The reaction was monitored by TLC stained with a ninhydrin solution. After stirring for 5 h the solvent was removed under reduced pressure. The residue was dissolved in DCM and extracted with a saturated aqueous solution of sodium carbonate and then with water. The organic phase was collected, dried with anhydrous Na_2SO_4, and the solvent was removed under reduced pressure. The residue was purified by chromatography on silica gel using dichloromethane as eluent to give (*tert*-butoxycarbonyl)aminoethanethiol as colorless oil (3.8 g, 64% yield). ^{1}H NMR (400 MHz, $CDCl_3$): δ=4.88 (bs, 1H), 3.28 (t, *J* = 6.5 Hz, 2H), 2.62 (dt, *J* = 8.5, 6.5 Hz, 2H), 1.42 (s, 9H), 1.32 ppm (t, *J* = 8.5 Hz, 1H). ESI-MS: *m/z* = 177.6 $[M+H]^+$.

Preparation of GO 8

To a suspension of GO (10 mg) in water (4 mL), a solution of Boc-PEG_{10}-NH_2 (50 mg) in water (1 mL) was added dropwise under stirring. The mixture was stirred under argon atmosphere at room

temperature for 3 days and then filtered over a polytetrafluoroethylene (PTFE) Millipore® membrane with 0.1 µm pore size. The solid on the membrane was collected and dispersed in water, sonicated in a water bath and filtered again over a PTFE membrane. This sequence was repeated 3 times with water and 3 times with ethanol. The resulting solid was dispersed in water and dialyzed in water for 3 days. After lyophilization, GO **8** was obtained.

Preparation of GO 9

To a suspension of GO **8** (10 mg) in phosphate-buffered saline (PBS) solution (4 mL, 0.02 M, pH=8), a solution of benzoquinone (50 mg) in ethanol (1 mL) was added dropwise under stirring. The mixture was stirred under argon atmosphere at room temperature overnight and then filtered over a PTFE membrane with 0.1 µm pore size. The solid on the membrane was collected and dispersed in water, sonicated in a water bath and filtered again over a PTFE membrane. This sequence was repeated 3 times with water and 3 times with ethanol. The resulting solid was dispersed in water and dialyzed in water for 3 days. After lyophilization, GO **9** was obtained.

Preparation of GO 10

To a suspension of GO **9** (10 mg) in PBS (4 mL, 0.02 M, pH=8), a solution of Boc-PEG_{10}-NH_2 (50 mg) in ethanol (1 mL) was added dropwise under stirring. The mixture was stirred under argon atmosphere at room temperature overnight and then filtered over a PTFE membrane with 0.1 µm pore size. The solid on the membrane was collected and dispersed in water, sonicated in a water bath and filtered again over a PTFE membrane. This sequence was repeated 3 times with water and 3 times with ethanol. The resulting solid was dispersed in water and dialyzed in water for 3 days. After lyophilization, GO **10** was obtained.

Preparation of GO 10-CTR

GO **10-CTR** was obtained following the protocol for the preparation of GO **10** but starting from GO **8**

Preparation of GO 11

To a suspension of GO **9** (10 mg) in PBS (4 mL, 0.02 M, pH=8), a solution of 3-(pentafluorothio)-DL-phenylalanine (50 mg) in ethanol (1 mL) was added dropwise under stirring. The mixture was stirred under argon atmosphere at room temperature overnight and then filtered over a PTFE membrane with 0.1 µm pore size. The solid on the membrane was collected and dispersed in water, sonicated in a water bath and filtered again over a PTFE membrane. This sequence was repeated 3 times with water and 3 times with ethanol. The resulting solid was dispersed in water and dialyzed in water for 3 days. After lyophilization, GO **11** was obtained.

Preparation of GO 11-CTR

GO **11-CTR** was obtained following the protocol for the preparation of GO **11** but starting from GO **8**

Preparation of GO 12

To a suspension of GO (10 mg) in water (4 mL), a solution of (*tert*-butoxycarbonyl)aminoethanethiol (50 mg) in ethanol (1 mL) was added dropwise under stirring. The mixture was stirred under argon atmosphere at room temperature for 3 days and then filtered over a polytetrafluoroethylene (PTFE) Millipore® membrane with 0.1 µm pore size. The solid on the membrane was collected and dispersed in water, sonicated in a water bath and filtered again over a PTFE membrane. This sequence was repeated 3 times with water and 3 times with ethanol. The resulting solid was dispersed in water and dialyzed in water for 3 days. After lyophilization, GO **12** was obtained.

Preparation of GO 13

To a suspension of GO **12** (10 mg) in phosphate-buffered saline (PBS) solution (4 mL, 0.02 M, pH=8), a solution of benzoquinone (50 mg) in ethanol (1 mL) was added dropwise under stirring. The mixture was stirred under argon atmosphere at room temperature overnight and then filtered over a PTFE membrane with 0.1 µm pore size. The solid on the membrane was collected and dispersed in water, sonicated in a water bath and filtered again over a PTFE membrane. This sequence was repeated 3 times with water and 3 times with ethanol. The resulting solid was dispersed in water and dialyzed in water for 3 days. After lyophilization, GO **13** was obtained.

Preparation of GO 14

To a suspension of GO **13** (10 mg) in PBS (4 mL, 0.02 M, pH=8), a solution of 3-(pentafluorothio)-DL-phenylalanine (50 mg) in ethanol (1 mL) was added dropwise under stirring. The mixture was stirred under argon atmosphere at room temperature overnight and then filtered over a PTFE membrane with 0.1 µm pore size. The solid on the membrane was collected and dispersed in water, sonicated in a water bath and filtered again over a PTFE membrane. This sequence was repeated 3 times with water and 3 times with ethanol. The resulting solid was dispersed in water and dialyzed in water for 3 days. After lyophilization, GO **14** was obtained.

Preparation of GO 14-CTR

GO **14-CTR** was obtained following the protocol for the preparation of GO **14** but starting from GO **12**

2.6 References

1. S. S. Nanda, G. C. Papaefthymiou and D. K. Yi, “Functionalization of Graphene Oxide and its Biomedical Applications”, *Crit. Rev. Solid State Mater. Sci.*, 2015, **40**, 291-315.

2. X. Lu, X. Feng, J. R. Werber, C. Chu, I. Zucker, J. H. Kim, C. O. Osuji and M. Elimelech, “Enhanced antibacterial activity through the controlled alignment of graphene oxide nanosheets”, *Proc. Natl. Acad. Sci. U S A*, 2017, **114**, 9793-9801.

3. K. C. Mei, N. Rubio, P. M. Costa, H. Kafa, V. Abbate, F. Festy, S. S. Bansal, R. C. Hider and K. T. Al-Jamal, "Synthesis of double-clickable functionalised graphene oxide for biological applications", *Chem. Commun.*, 2015, **51**, 14981-14984.

4. I. A. Vacchi, C. Spinato, J. Raya, A. Bianco and C. Ménard-Moyon, "Chemical reactivity of graphene oxide towards amines elucidated by solid-state NMR", *Nanoscale*, 2016, **8**, 13714-13721.

5. I. A. Vacchi, S. Guo, J. Raya, A. Bianco and C. Menard-Moyon, "Strategies for the Controlled Covalent Double Functionalization of Graphene Oxide", *Chem. Eur. J.*, 2020, **26**, 6591-6598.

6. S. Guo, Y. Nishina, A. Bianco and C. Ménard-Moyon, "A Flexible Method for Covalent Double Functionalization of Graphene Oxide", *Angew. Chem., Int. Ed.*, 2020, **59**, 1542-1547.

7. M. Y. Xia, Y. Xie, C. H. Yu, G. Y. Chen, Y. H. Li, T. Zhang and Q. Peng, "Graphene-based nanomaterials: the promising active agents for antibiotics-independent antibacterial applications", *J. Controlled Release*, 2019, **307**, 16-31.

8. R. Imani, S. Prakash, H. Vali and S. Faghihi, "Polyethylene glycol and octa-arginine dual-functionalized nanographene oxide: an optimization for efficient nucleic acid delivery", *Biomater Sci*, 2018, **6**, 1636-1650.

9. T. Yin, J. Liu, Z. Zhao, Y. Zhao, L. Dong, M. Yang, J. Zhou and M. Huo, "Redox Sensitive Hyaluronic Acid-Decorated Graphene Oxide for Photothermally Controlled Tumor-Cytoplasm-Selective Rapid Drug Delivery", *Adv. Funct. Mater.*, 2017, **27**, 1604620.

10. K.-W. Park, "Carboxylated graphene oxide–Mn_2O_3 nanorod composites for their electrochemical characteristics", *J. Mater. Chem. A*, 2014, **2**, 4292–4298.

11. X. Sun, Z. Liu, K. Welsher, J. T. Robinson, A. Goodwin, S. Zaric and H. Dai, "Nano-Graphene Oxide for Cellular Imaging and Drug Delivery", *Nano. Res.*, 2008, **1**, 203-212.

12. J.-L. Han, D. Zhang, W. Jiang, Y. Tao, M.-J. Liu, M. R. Haider, R.-Y. Ren, H.-c. Wang, W.-L. Jiang, Y.-C. Ding, Y.-N. Hou, B. Zhang, H.-Y. Cheng, X. Xia, Z. Wang and A.-J. Wang, "Tuning the functional groups of a graphene oxide membrane by ·OH contributes to the nearly complete prevention of membrane fouling", *J. Membr. Sci.*, 2019, **576**, 190-197.

13. T. Taniguchi, S. Kurihara, H. Tateishi, K. Hatakeyama, M. Koinuma, H. Yokoi, M. Hara, H. Ishikawa and Y. Matsumoto, "pH-driven, reversible epoxy ring opening/closing in graphene oxide", *Carbon*, 2015, **84**, 560-566.

14. P. Zhang, Z. Li, S. Zhang and G. Shao, "Recent Advances in Effective Reduction of Graphene Oxide for Highly Improved Performance Toward Electrochemical Energy Storage", *Energy Environ. Mater.*, 2018, **1**, 5-12.

15. M. Shams, L. M. Guiney, L. Huang, M. Ramesh, X. Yang, M. C. Hersam and I. Chowdhury, "Influence of functional groups on the degradation of graphene oxide nanomaterials", *Environ. Sci.: Nano*, 2019, **6**, 2203-2214.

16. J. P. Rourke, P. A. Pandey, J. J. Moore, M. Bates, I. A. Kinloch, R. J. Young and N. R. Wilson, "The real graphene oxide revealed: stripping the oxidative debris from the graphene-like sheets", *Angew. Chem., Int. Ed.*, 2011, **50**, 3173-3177.

17. C. Chen, W. Kong, H. M. Duan and J. Zhang, "Theoretical simulation of reduction mechanism of graphene oxide in sodium hydroxide solution", *PCCP*, 2014, **16**, 12858-12864.

18. A. M. Dimiev, L. B. Alemany and J. M. Tour, "Graphene oxide. Origin of acidity, its instability in water, and a new dynamic structural model", *ACS Nano*, 2013, **7**, 576-588.

19. T. Szabó, O. Berkesi and I. Dékány, "DRIFT study of deuterium-exchanged graphite oxide", *Carbon*, 2005, **43**, 3186-3189.

20. X. Fan, W. Peng, Y. Li, X. Li, S. Wang, G. Zhang and F. Zhang, "Deoxygenation of Exfoliated Graphite Oxide under Alkaline Conditions: A Green Route to Graphene Preparation", *Adv. Mater.*, 2008, **20**, 4490-4493.

21. H. Wang, Q. Zhang, X. Chu, T. Chen, J. Ge and R. Yu, "Graphene oxide-peptide conjugate as an intracellular protease sensor for caspase-3 activation imaging in live cells", *Angew. Chem., Int. Ed.*, 2011, **50**, 7065-7069.

22. E. Kaiser, R. L. Colescott, C. D. Bossinger and P. I. Cook, "Color test for detection of free terminal amino groups in the solid-phase synthesis of peptides", *Anal. Biochem.*, 1970, **34**, 595-598.

23. M. A. Lucherelli, J. Raya, K. F. Edelthalhammer, F. Hauke, A. Hirsch, G. Abellan and A. Bianco, "A Straightforward Approach to Multifunctional Graphene", *Chem. Eur. J.*, 2019, **25**, 13218-13223.

24. A. Lerf, H. He, M. Forster and J. Klinowski, "Structure of Graphite Oxide Revisited", *J. Phys. Chem. B*, 1998, **102**, 4477-4482.

25. W. Cai, R. D. Piner, F. J. Stadermann, S. Park, M. A. Shaibat, Y. Ishii, D. Yang, A. Velamakanni, S. J. An, M. Stoller, J. An, D. Chen and R. S. Ruoff, "Synthesis and solid-state NMR structural characterization of 13C-labeled graphite oxide", *Science*, 2008, **321**, 1815-1817.

26. R. Bhaskar, H. Joshi, A. K. Sharma and A. K. Singh, "Reusable Catalyst for Transfer Hydrogenation of Aldehydes and Ketones Designed by Anchoring Palladium as Nanoparticles on Graphene Oxide Functionalized with Selenated Amine", *ACS Appl. Mater Interfaces*, 2017, **9**, 2223-2231.

27. K. V. Purtov, A. I. Petunin, A. E. Burov, A. P. Puzyr and V. S. Bondar, "Nanodiamonds as carriers for address delivery of biologically active substances", *Nanoscale Res. Lett.*, 2010, **5**, 631-636.

28. J. Brandt, L.-O. Andersson and J. Porath, "Covalent attachment of proteins to polysaccharide carriers by means of benzoquinone", *Biochim. Biophys. Acta, Protein Struct.*, 1975, **386**, 196-202.

29. S. Suliman, Z. Xing, X. Wu, Y. Xue, T. O. Pedersen, Y. Sun, A. P. Doskeland, J. Nickel, T. Waag, H. Lygre, A. Finne-Wistrand, D. Steinmuller-Nethl, A. Krueger and K. Mustafa, "Release and bioactivity of bone morphogenetic protein-2 are affected by scaffold binding techniques in vitro and in vivo", *J. Controlled Release*, 2015, **197**, 148-157.

30. K. A. Wepasnick, B. A. Smith, J. L. Bitter and D. Howard Fairbrother, "Chemical and structural characterization of carbon nanotube surfaces", *Anal. Bioanal. Chem.*, 2010, **396**, 1003-1014.

31. S. Eigler, C. Dotzer, F. Hof, W. Bauer and A. Hirsch, "Sulfur species in graphene oxide", *Chem. Eur. J.*, 2013, **19**, 9490-9496.

32. H. R. Thomas, A. J. Marsden, M. Walker, N. R. Wilson and J. P. Rourke, "Sulfur-functionalized graphene oxide by epoxide ring-opening", *Angew. Chem., Int. Ed.*, 2014, **53**, 7613-7618.

33. Z. Wang, Y. Dong, H. Li, Z. Zhao, H. B. Wu, C. Hao, S. Liu, J. Qiu and X. W. Lou, "Enhancing lithium-sulphur battery performance by strongly binding the discharge products on amino-functionalized reduced graphene oxide", *Nat. Commun.*, 2014, **5**, 5002-5007.

34. D. A. Jasim, C. Ménard-Moyon, D. Begin, A. Bianco and K. Kostarelos, "Tissue distribution and urinary excretion of intravenously administered chemically functionalized graphene oxide sheets", *Chem. Sci.*, 2015, **6**, 3952-3964.

35. R. Winter, P. G. Nixon, G. L. Gard, D. J. Graham, D. G. Castner, N. R. Holcomb and D. W. Grainger, "Self-Assembled Organic Monolayers Terminated in Perfluoroalkyl Pentafluoro-λ^6-sulfanyl (-SF_5) Chemistry on Gold", *Langmuir*, 2004, **20**, 5776-5781.

36. H. Kinoshita, Y. Nishina, A. A. Alias and M. Fujii, "Tribological properties of monolayer graphene oxide sheets as water-based lubricant additives", *Carbon*, 2014, **66**, 720-723.

37. J. W. Suk, R. D. Piner, J. An and R. S. Ruoff, "Mechanical properties of monolayer graphene oxide", *ACS Nano*, 2010, **4**, 6557-6564.

38. I. A. Vacchi, J. Raya, A. Bianco and C. Ménard-Moyon, "Controlled derivatization of hydroxyl groups of graphene oxide in mild conditions", *2D Mater.*, 2018, **5**, 035037.

39. E. L. Hahn, "Spin echoes", *Phys. Rev.* **1950**, *80*, 580-594.

40. B. M. Fung, A. K. Khitrin, K. Ermolaev, “An improved broadband decoupling sequence for liquid crystals and solids”, *J. Magn. Reson.* **2000**, *142*, 97-101.

41. G. Pastorin, W. Wu, S. Wieckowski, J.-P. Briand, K. Kostarelos, M. Prato, A. Bianco. “Double functionalization of carbon nanotubes for multimodal drug delivery”, *Chem. Commun.* **2006**, *11*, 1182-1184.

Chapter 3 The PTT and PDT of FA/Ce6 double functional GO on cancer cells and macrophages

3.1 Introduction

In the first chapter I have described the great potential of GO and its derivatives in optical, electrochemical and biological applications, especially in disease treatments. Many literature has proposed GO as an ideal nanoplatform for drug delivery and as an efficient material for phototherapy, including PTT and PDT, thanks to its good photothermal effect, low cytotoxicity and high loading efficiency.[1] However, the photosensitizers for PDT were non-covalently loaded onto GO, especially in the cases of small molecule derivativess.[2] The covalent multi-functionalization of GO with targeting groups and photosensitizers would allow us to prepare a more stable nanostructure in physiological conditions with high molecular loading.

GO functionalization with affinity ligands enables the specific recognition of the multifunctional nanomaterial by target cells or biomarkers, resulting in the accumulation at the disease site and in an improved cellular uptake of GO complexes[3] to tackle various diseases, such as cancer[4] and neurodegeneration.[5] Cancer is among the leading causes of death and morbidity globally. The radiotherapy and chemotherapy often do not lead to satisfactory therapeutic result, due to the side effect from the low specificity against cancer cells, enzymatic deactivation and increased efflux of the drug.[6-8] Thus, the development of targeted drug delivery and non-invasive treatment with less side effects is important for cancer therapy. FRs are highly expressed in various types of human cancers and are widely used as ideal biomarkers for cancer therapy.[9] The FRs, and in particular FR-β, are also highly expressed on joint activated macrophages in RA, making them widely used biomarker for the theragnostic of RA treatment.[10]

3.2 Objectives of this chapter

The objectives of this chapter are to investigated the application of multi-functionalized GO conjugates in the treatment of cancer and RA, combining PTT and PDT. A FA/Ce6 double-functionalized GO was first prepared. The FA was chosen as the targeting groups towards cancer cells and macrophages and it was covalently bounded onto GO surface. Ce6 was selected as photosensitizer for photodynamic treatment. This molecule can generate singlet oxygen under laser irradiation at 660 nm. Instead of physiosorbed onto the surface, Ce6 was covalently grafted onto GO-FA nanomaterial through a PEG linker. The successful conjugation of FA and Ce6 was confirmed by UV-Vis, fluorescence spectroscopy and immunostaining. The photothermal effect and ROS generation in solution were evaluated.

Then, the prepared GO-FA/Ce6 was first applied to HeLa cells, to evaluate the cytotoxicity and uptake of the material. Afterwards, PTT and PDT efficiency of the nanoplatform was explored using 808 nm and 660 nm laser irradiation, respectively. The treatment combining the PTT and PDT was also evaluated to study synergistic effect for cancer therapy. As the HeLa cells showed a high resistance to the treatment with the multi-functionalized GO, MCF-7 was eventually used to evaluate the anti-cancer property of GO-FA/Ce6. Finally, preliminary data on macrophages towards future application to treat RA are also summarized.

3.3 Preparation of FA/Ce6 double-functionalized GO

While developing the strategies for controlled functionalization of GO by reacting epoxides and hydroxyl groups with appropriate functions, we also prepared a FA/Ce6 multi-functional GO using a mixture of two amine-terminated PEG chains only targeting the epoxides. The GO sample was again obtained from Prof. Yuta Nishina (University of Okayama, Japan). This material has an average lateral size of 1 μm. The functionalities were grafted onto GO in three steps. In the first step, GO was derivatized using an equimolar mixture of two free amine terminated PEG ligands, namely Boc-PEG$_{10}$-NH$_2$ and FA-PEG$_{10}$-NH$_2$, by opening the epoxides. The Boc protecting group was then removed and Ce6 was conjugated to the free amine through amidation reaction (Scheme 3.1).

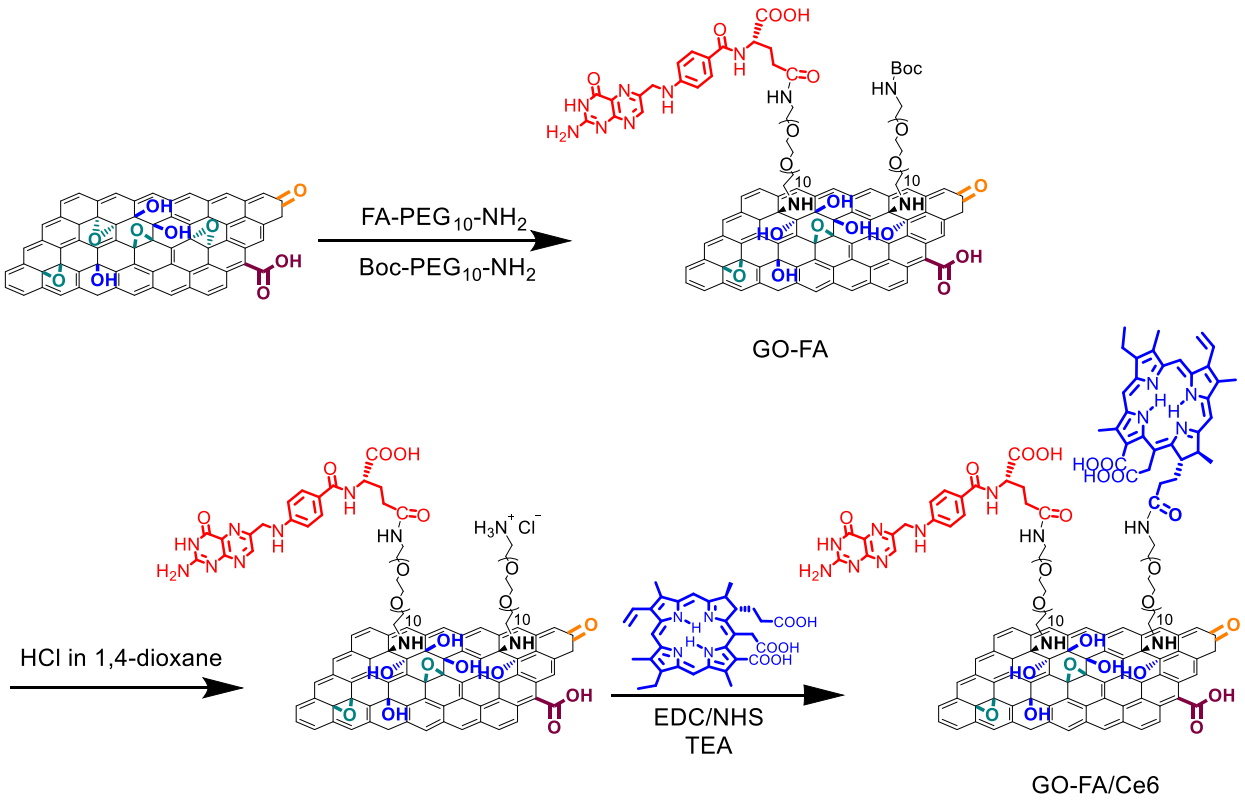

Scheme 3.1 The preparation of GO-FA/Ce6 nanocomplex.

This protocol is simple and easy to perform in comparison with the strategies targeting selectively two functional groups onto GO. Here, the FA was first conjugated on Boc-PEG_{10}-NH_2 by amidation reaction followed by the Boc-deprotection, giving FA-PEG_{10}-NH_2.

3.3.1 Synthesis of FA-PEG_{10}-NH_2

To introduce the targeting ligand for cancer cells and macrophages onto GO, we designed and synthesized a FA-PEG_{10}-NH_2 derivative according to the literature (Scheme 3.2).[11, 12] The mono-protected PEG diamine (Boc-PEG_{10}-NH_2 commercially available) chain was chosen as a linker connecting FA and GO. The PEG could also enhance the water dispersibility due to its hydrophilic character. The synthesis of FA-PEG_{10}-NH_2 was started with the conjugation of FA to Boc-PEG_{10}-NH_2 by amidation in the presence of the coupling agents NHS/EDC. After Boc-deprotection, the FA-PEG_{10}-NH_2 was obtained in 51% yield.

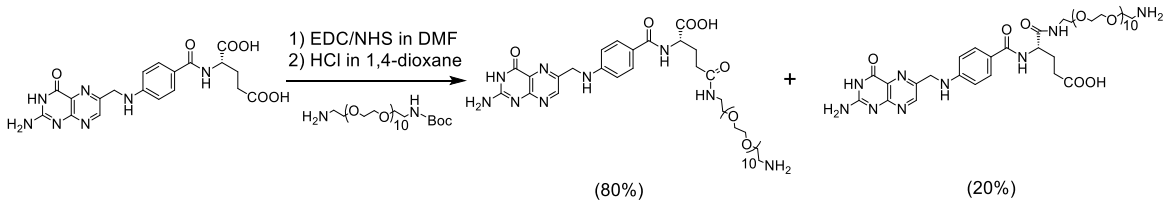

Scheme 3.2 The synthesis of FA-PEG_{10}-NH_2

As there are two carboxylic acids in the glutamic acid moiety of FA, the PEG ligand can react either with the α- or γ-COOH or both, while only the FA-γ-PEG conjugate has the affinity towards FRs. It has already been reported that the γ-COOH is more reactive in the amidation reaction with over 80% γ-conjugation in FA-mono-PEG derivative (Scheme 3.2).[13] The high-performance liquid chromatography (HPLC) clearly showed the presence of FA-mono-PEG-Boc conjugation and the FA linked with two PEG chains (Figure 3.1a). After column chromatography purification, FA-PEG-Boc was obtained pure.

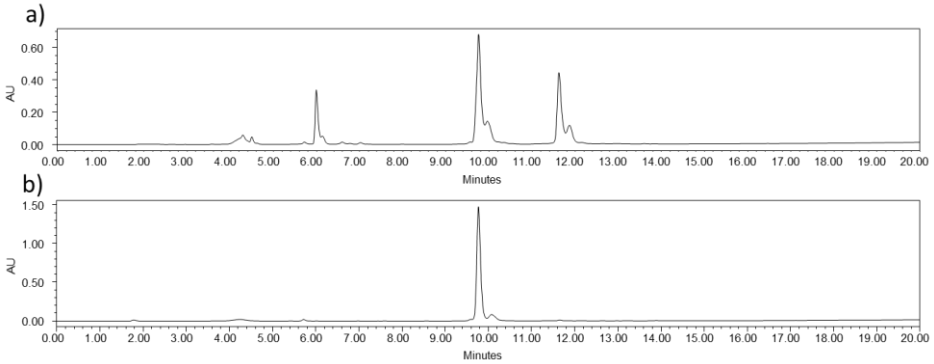

Figure 3.1 HPLC of FA-PEG-Boc reaction mixture a) before and b) after silica chromatography purification.

After Boc-deprotection using HCl, the obtained FA-PEG-NH_2 was then used for the preparation of FA/Ce6 double functionalized GO.

3.3.2 Synthesis and characterization of GO-FA/Ce6

Since Ce6 has three carboxyl groups and it is sensitive to light, we decided to graft it directly to the amino groups of PEG, instead of synthesizing the ligand Ce6-PEG_{10}-NH_2 like FA-PEG_{10}-NH_2. Boc-PEG_{10}-NH_2 was chosen as precursor, as the free amine is able to undergo a nucleophilic attack towards the epoxides, and the primary amine after the Boc-cleavage could be further functionalized with Ce6 via amidation reaction. GO was first stirred with an equimolar mixture of Boc-PEG_{10}-NH_2 and FA-PEG_{10}-NH_2 giving FA double-functionalized GO-FA with the second PEG chain protected by Boc. This conjugate was characterized by UV-Vis, TGA and immunostaining. In the UV-Vis spectra, GO-FA showed an additional peak at 290 nm belonging to FA moiety in comparison with GO (Figure 3.2a). The thermogravimetric analysis confirmed the presence of PEG functional groups onto GO after the epoxide ring opening reaction (Figure 3.2b). Compared to pristine GO, the two PEGs provoke a second weight loss in the region between 200 and 400°C, likely due to the contribution of the thermal degradation of Boc-PEG_{10}-NH_2 and FA-PEG_{10}-NH_2 covalently bound to GO, similarly to the results reported in Chapter two (Figure 2.4b).

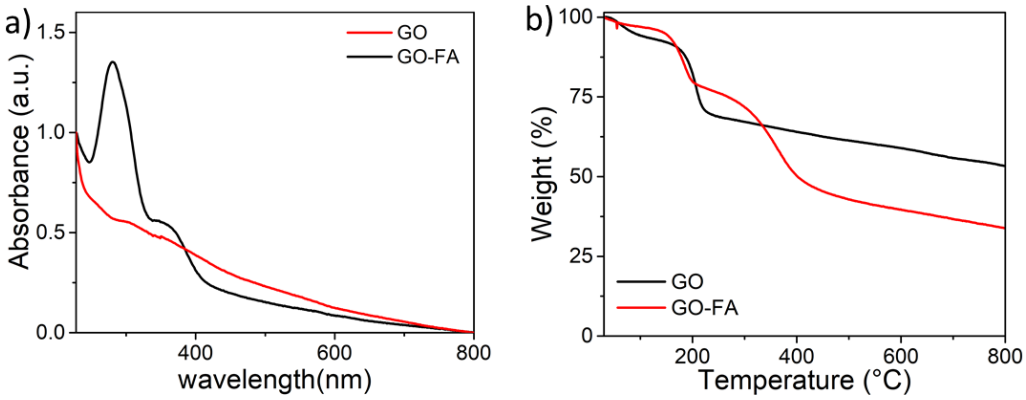

Figure 3.2 a) UV-Vis spectra of GO and GO-FA**,** and b) TGA curves of GO and GO-FA performed in inert atmosphere.

Immunostaining further supported the presence of FA onto GO-FA conjugate. For this analysis, two antibodies were used for the staining. The GO-FA was deposited on a TEM grid. After coating with acetylated BSA (1%) to block the non-specific binding, the anti-FA antibody (a mouse folic acid specific monoclonal antibody, FA1) was dropped on the top of the grid and incubated for 30 min. After washing, the grid was then incubated with a secondary antibody, which can specifically recognize the anti-FA antibody. The secondary is coupled to 10-nm gold nanoparticles and it could be identified by TEM with high contrast. In the TEM image of GO-FA immunostaining, many gold nanoparticles were observed, revealing that large quantity of FA were grafted onto GO surface (Figure 3.3a). To confirm

that the gold nanoparticles were not nonspecifically adsorbed onto GO, a control sample without FA was prepared by stirring GO with Boc-PEG_{10}-NH_2, giving GO-Boc (called GO-FA-CTR). The immunostaining of GO-Boc showed only few gold nanoparticles present on GO (Figure 3.3b), confirming that the secondary antibody was bounded to anti-FA antibody onto GO-FA sheets rather than simply nonspecifically physisorbed. Moreover, another prilary antibody, hRANK-M331 antibody (a mouse IgG1 monoclonal antibody against the human protein RANK-M331) was used for the immunostaining followed by the secondary antibody bearing gold nanoparticle. The hRANK-M331 antibody does not have affinity for FA, but it can be recognized by the secondary antibody. The TEM image showed no gold nanoparticles onto GO-FA incubated with hRANK-M331 and the secondary antibody (Figure 3.3c), proving that FA molecules are present on GO.

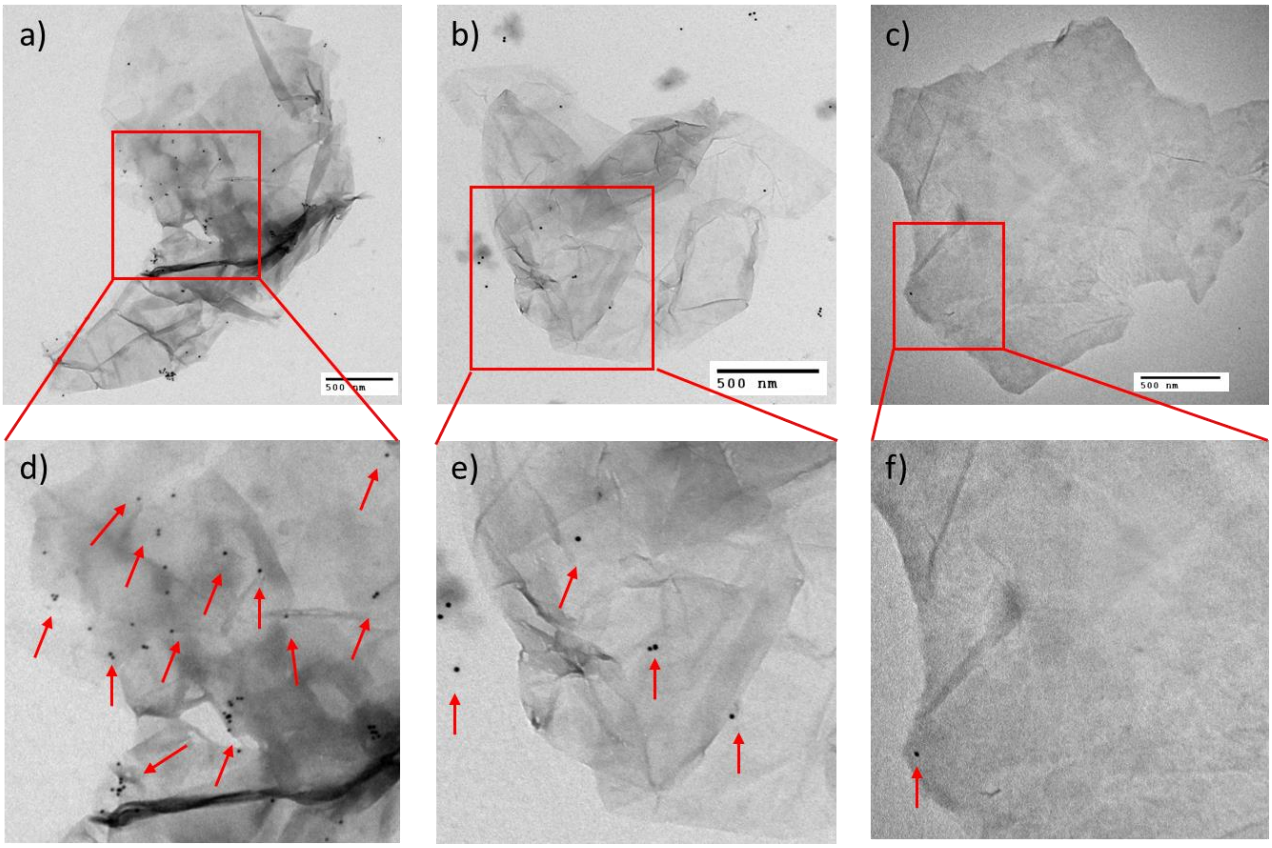

Figure 3.3 TEM images (a, b, c) and magnified images (d, e, f) illustrating the immunostaining experiments on a, d) GO-FA**,** b, e) GO-FA-CTR using anti-FA antibody and secondary antibody, and c, f) GO-FA using the non-specific antibody hRANK-M331. The gold nanoparticles are pointed out with red arrows.

The double-functionalized GO-FA was then used to prepare the final functional GO-FA/Ce6. Boc group on Boc-PEG_{10} moiety was removed using HCl, and the free amine was reacted with Ce6 using EDC/NHS coupling agents, giving GO-FA/Ce6. The conjugation of Ce6 was characterized by UV-Vis and fluorescence spectroscopy. In the UV-Vis spectra, GO-FA/Ce6 present a new characteristic peak centered at 420 nm belonging to Ce6 compared to GO-FA (Figure 3.4a) with a red shift observed compared to Ce6 alone due to the strong interaction between Ce6 and GO.[14, 15]The amount of Ce6

loaded on the double functional GO was determined by UV-Vis through a standard curve method and the concentration corresponded to 3 μmol/g (Figure 3.4b). The fluorescence spectroscopy confirmed the loading of Ce6. A stronger fluorescent emission was also observed in GO-FA/Ce6 centered at 650 nm with an excitation wavelength at 420 nm, indicating again the presence of Ce6. A control sample was prepared by mixing GO-FA with Ce6 before Boc-deprotection giving GO-FA/Ce6-CTR. However, the fluorescence of GO-FA/Ce6-CTR was significantly lower than the covalent functionalized GO-FA/Ce6, proving that a higher loading efficiency of Ce6 through amidation (Figure 3.4c).

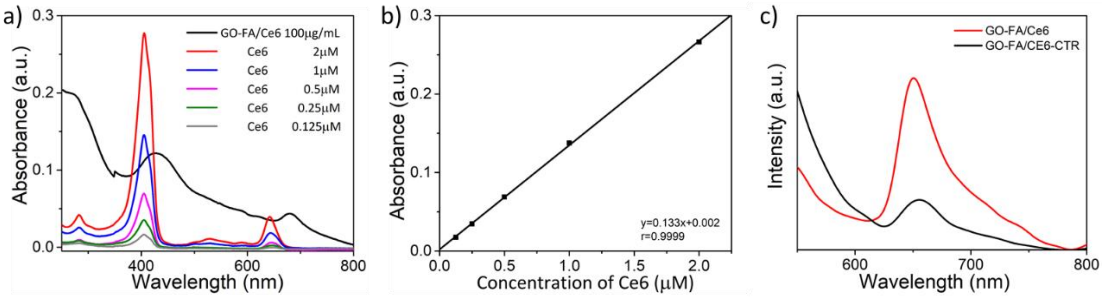

Figure 3.4 a) UV-Vis spectrua of GO-FA/Ce6 and Ce6 spectra at different concentration, b) standard curve of Ce6, and c) fluorescence spectra of GO-F/Ce6 and GO-FA/Ce6-CTR.

Overall, the FA and Ce6 double-functionalized GO was prepared and characterized by different methods. The photothermal effects and ROS generation of GO-FA/Ce6 were then evaluated.

3.3.3 Evaluation of the photothermal property of GO-FA/Ce6 and ROS generation

Thanks to its broad absorbance profile, GO is considered a good photothermal material for various disease treatments. The photothermal effect induced by NIR laser irradiation at 808 nm with a power density of 2 W·cm^{-2} in 1 mL GO-FA/Ce6 aqueous dispersion was first investigated by monitoring the temperature at various concentrations of the conjugate (5, 25, 50, and 100 μg·mL^{-1}). (Figure 3.5a). The temperature increased immediately when applied the irradiation and a concentration dependence was observed. At a highest concentration of 100 μg·mL^{-1}, the temperature increased 10 ℃ from room temperature in 6 min, which could induce an irreversible damage on cells. If the concentration decreased to 50 μg·mL^{-1}, the temperature increased 6 ℃. At a lower concentration of 25 μg·mL^{-1}, the temperature increased around 4℃ within 6 min, which is enough to induce a mild hyperthermia affecting the cell metabolism and DNA repair mechanisms, while minimizing the cytotoxicity induced by the nanomaterial.

The generation of ROS by GO-FA/Ce6 was subsequently evaluated using dihydrorhodamine 123 (DHR123) test by fluorescence spectroscopy. DHR123 is a non-fluorescent dye and after it is oxidized by ROS, it is transformed into the fluorescent rhodamine 123, with a high red emission. As shown in Figure 3.5b, the fluorescent emission of DHR123 was almost negligible in water solution and the addition of 10 μg·mL^{-1} GO-FA/Ce6 did not change the fluorescence of this dye. After low-power irradiation with a 660 nm laser at the power of 0.2 W·cm^{-2}, a significant increase of the fluorescence

intensity was observed (Figure 3.5b), due to the generation of ROS by Ce6. DHR123 alone did not show an increase of fluorescence after the irradiation (Figure 3.5c), indicating that DHR123 was stable when exposed to 660 nm laser. The ROS generated by Ce6 alone were also detected by DHR123. Surprisingly, the generation of ROS by GO-FA/Ce6 was slightly higher than Ce6 alone at the same concentration (Figure 3.5c). The higher ROS production in GO-FA/Ce6 could due to the extra ROS generated by GO under exposure to laser light.

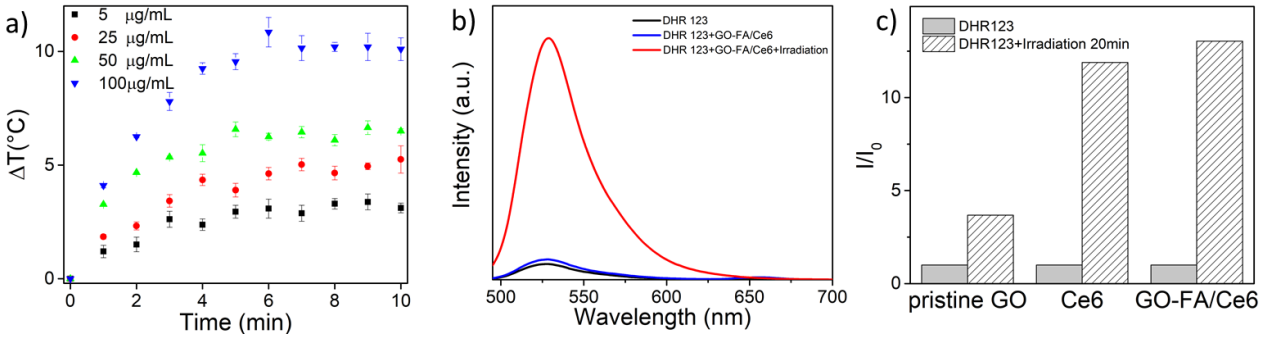

Figure 3.5 a) Temperature increase in water at different concentrations of GO-FA/Ce6due to photothermal effect under irradiation, b) DHR123 test for ROS generation by GO-FA/Ce6, and c) normalized DHR123 test for ROS generation by GO, Ce6 and GO-FA/Ce6.

3.3.4 Conclusion

In summary, we prepared a FA/Ce6 double-functionalized GO. FA- and Boc- terminated PEG ligands were used to open the epoxides onto GO surface. The Ce6 was then covalently bound to GO after the Boc-cleavage. The conjugation of FA and Ce6 was confirmed by different methods and the loading efficiency of Ce6 was higher than simple physisorption. The prepared double functional GO displayed good photothermal properties and higher ROS generation than Ce6 alone. The GO-FA/Ce6 was then tested *in vitro* for photothermal and photodynamic treatments of cancer cells and macrophages.

3.4 PTT and PDT of GO-FA/Ce6 on cancer cells

For the therapeutic use of the double functional GO, we firstly applied the GO-FA/Ce6 on cancer cells. HeLa human cervical cancer cells were chosen because of the high-level expression of FR, which would enhance the cellular uptake of GO-FA/Ce6 through a receptor-mediated endocytosis. Several articles have reported the application of GO-based nanomaterials to HeLa cells to study the anticancer capacity obtaining interesting results. Therefore, we have considered HeLa as appropriate for the evaluation of the efficacy of PTT and PDT by our photo-responsive GO complex. Alternatively, MCF-7, a breast cancer cell line, is also a commonly used model cell line for to study the effect of nanomaterials on cancer. The choice of two cell lines was to prevent the possibility that PTT and PDT

accelerate the cytoprotective mechanisms to preserve cancer cells from hyperthermia and ROS production, becoming resistant to the treatments.[16-18]

The initial biocompatibility study of a nanomaterial is commonly performed *in vitro*, to determine the dose-dependent toxicity of nanoparticles as well as the killing efficiency of the treatments. Different assays such as MTT, MTS, and alamarBlue, are used to measure the viability of the cells after incubation with nanomaterials alone, and after the irradiation for PTT and PDT. Thus, we first started with the evaluation of the cytotoxicity and cellular uptake of GO-FA/Ce6 on Hela cells.

3.4.1 Cytotoxicity and uptake of GO-FA/Ce6 on Hela cells

To explore the anti-cancer property of the double functional GO, the cytotoxicity of the GO-FA/Ce6 was assessed to determine an appropriate concentration for further PTT and PDT experiments. HeLa cells were seed in the 96-well plate with a density of 2000 cells per well. Different concentrations of GO-FA/Ce6 were prepared in cell culture media and applied to cells 24 h after seeding. The samples were incubated for 24 h and removed. The alamarBlue™ cell viability assay was used to evaluate the cytotoxicity of GO-FA/Ce6 on Hela cells (Figure 3.6).

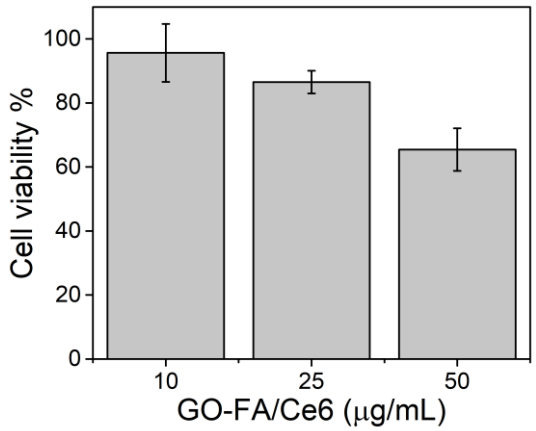

Figure 3.6 cytotoxicity of GO-FA/Ce6 on Hela cells.

GO-FA/Ce6 exhibited a dose-dependent cytotoxicity to HeLa cells. The double functional GO present negligible toxicity at the concentration of 5 and 25 $\mu g \cdot mL^{-1}$ with the cell viability higher than 86%. However, GO-FA/Ce6 was more toxic against HeLa cells at the highest concentration tested (50 $\mu g \cdot mL^{-1}$). Although GO is considered as a nanomaterial with good biocompatibility, even at high concentration, the cytotoxicity may differ due to the size, purity and different functionalities loaded onto GO. According to the cytotoxicity results, the concentration of 25 $\mu g \cdot mL^{-1}$ was chosen for further studies.

The cellular uptake of GO-FA/Ce6 by HeLa cells was then measured, with the help of Giacomo Reina, a post-doctoral fellow in our group. Due to the strong fluorescent emission of Ce6 covalently bound to GO, the conjugate could be tracked by confocal microscopy (Figure 3.7). CellMask green due was applied to identify the morphology of the cell membranes. The confocal images clearly show that GO-FA/Ce6 is internalized by HeLa cells already after 4 h. The emission from Ce6 was visible in compartments that likely correspond to endosomes, indicating the FR-mediated internalization. After 8 h incubation, more GO-FA/Ce6 is present in the cytoplasmic vesicles. However, the fluorescence of Ce6 decreased after 24 h incubation, likely due to a degradation of Ce6 in HeLa cells after 24 hours.

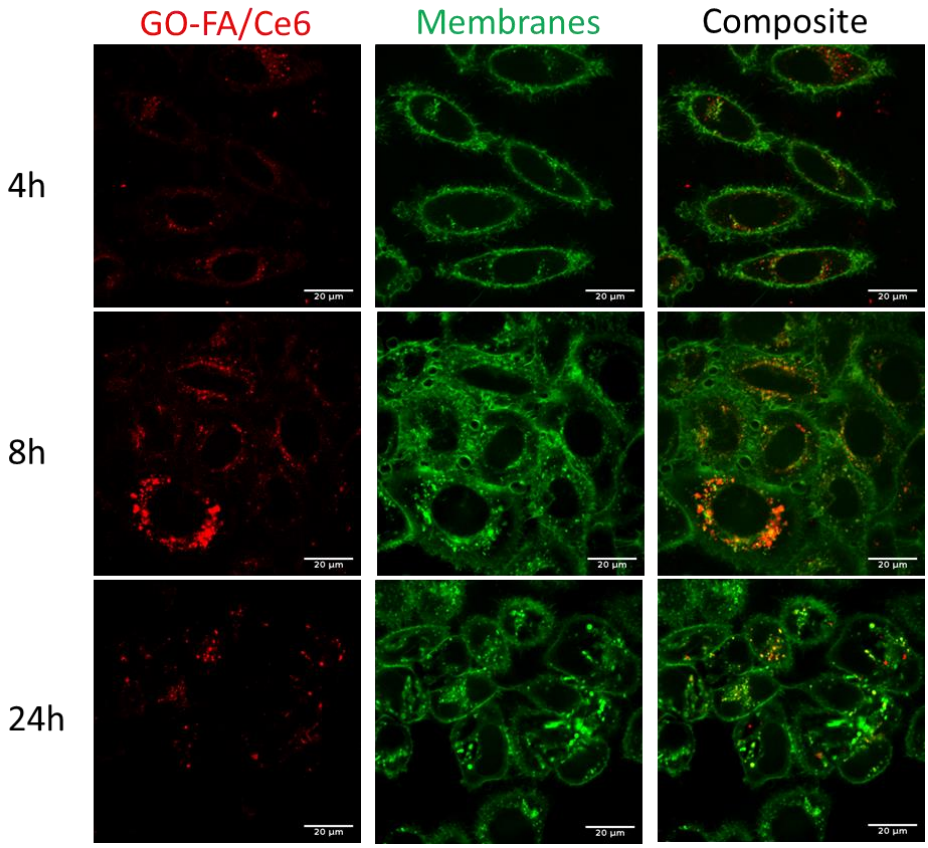

Figure 3.7 Confocal microscopy images of cellular uptake of GO-FA/Ce6 by HeLa cells.

After the evaluation of cytotoxicity and cellular uptake of GO-FA/Ce6, the effect of PTT and PDT were studied.

3.4.2 PTT and PDT effects of GO-FA/Ce6 on HeLa cells

To explored the potential of GO-FA/Ce6 in phototherapy against cancer cells, the cell viability of HeLa after photothermal and photodynamic treatments was evaluated by alamarBlue assay. In order to understand the influence of laser irradiation on cells, the analysis of the intrinsic cytotoxicity of illumination on HeLa cells was performed without applying the nanomaterial. A 808 nm laser at a

power density of 2 W·cm^{-2} was used for PTT and a 660 nm laser at a power density of 0.2 W·cm^{-2} was applied for PDT. The viability of cells exposed to irradiation without GO is shown in Figure 3.8. Both lights exert a minimal toxicity on HeLa cells following a time-depend manner. The 808 nm laser at 2 W·cm^{-2} has a negligible toxic effect on HeLa with a cell viability still more than 90% after 20 min irradiation. However, the 660 nm laser at 0.2 W·cm^{-2} provoked a higher mortality. After 10 min irradiation, the viability of HeLa was around 93%, while it decreased to 80% after the exposure to the laser for 20 min. Thus, we decided to select the irradiation time of 10 min to minimize the intrinsic toxicity of the laser treatment in the next experiments.

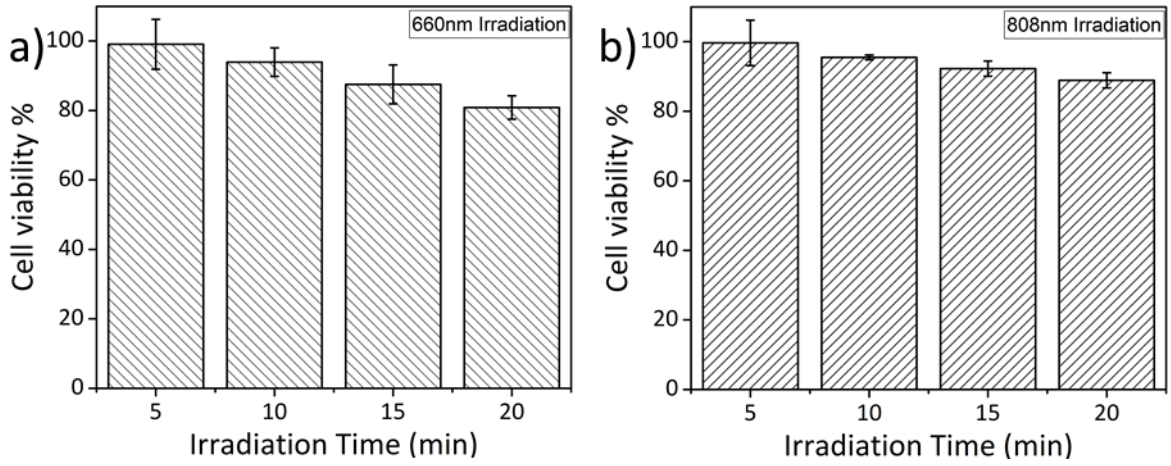

Figure 3.8 Cell viability of Hela cells after irradiation using a 808 nm laser at the power density of 2 W·cm^{-2} (left) and a 660 nm laser at the power density of 0.2 W·cm^{-2} (right).

Subsequently, PTT and PDT experiments on HeLa cells incubated with GO-FA/Ce6 were performed. A dispersion of GO-FA/Ce6 at a concentration of 25 μg·mL^{-1} in cell culture medium was applied to HeLa cells 24 h after seeding the cells into 96-well plates. The nanomaterial was removed after 24 h incubation and fresh cell medium was added. The cells were immediately irradiated for 5 min and 10 min with the 808 nm and the 660 nm lasers. The alamarBlue assay was then performed and the results are reported in Figure 3.9. Both PTT and PDT showed good killing efficiency against HeLa cells, proving that the GO-FA/Ce6 can be used for photothermal and photodynamic treatment in cancer therapy. A time-depended phototoxicity behavior was also observed. After irradiation for 10 min, the viability of HeLa cells decreased to 48% under the exposure to 808 nm laser for PTT, while the viability remained little higher (55%) in the case of PDT. When the time of irradiation was shortened to 5 min, the photo-triggered cytotoxicity by GO-FA/Ce6 was decreased in both photothermal and photodynamic conditions.

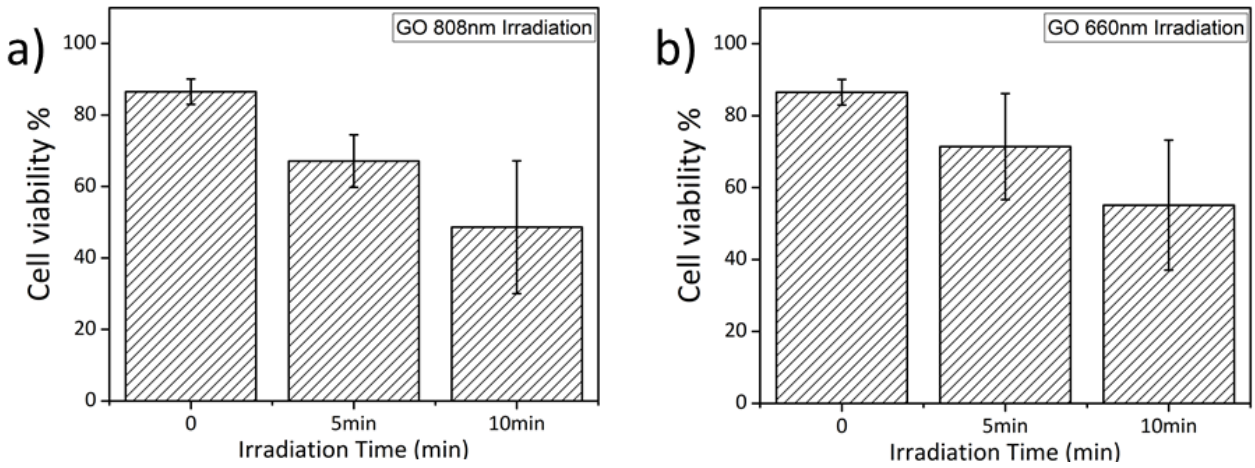

Figure 3.9 Cell viability of Hela cells irradiated using a) a 808 nm and b) a 660 nm laser after the incubation with GO-FA/Ce6 for 24 h.

Since a higher accumulation of GO-FA/Ce6 was observed inside HeLa cells 8 h after applying the nanomaterial, the irradiation experiments were then optimized by reducing the incubation time of the GO conjugate to 4 and 8 h in order to achieve a higher photodynamic efficiency. The alamarBlue assay was used again to evaluate the cell viability after the treatment (Figure 3.10). An unexpected increase of cell viability was observed after laser irradiation in the presence of GO-FA/Ce6. Compared to the control without irradiation, the cell viability increased to 104% and 99% under 660 nm and 808 nm irradiation, respectively, after 4 h incubation with GO-FA/Ce6. Meanwhile, after 8 h incubation, the cell viability increased to 111% and 102% after the illumination of 660 nm and 808 nm laser. The results indicated that the application of laser irradiation did not induce the cytotoxicity on HeLa cells as we observed in the experiment at 24 h incubation. In the contrary, it seems that the HeLa cells have developed the resistance against the photothermal and photodynamic treatment. The hyperthermia and ROS probably accelerated the metabolism activity in HeLa cells.[16, 18, 19] To understand if the readout of the viability test had some interference with the material, another cell viability assay, MTS, was performed to evaluate the phototriggered toxicity of GO-FA/Ce6. An increase of cell viability was also observed using MTS. The influence of the enhanced cellular metabolism was lower than alamarBlue, but still higher than the group without irradiation (Figure 3.10).

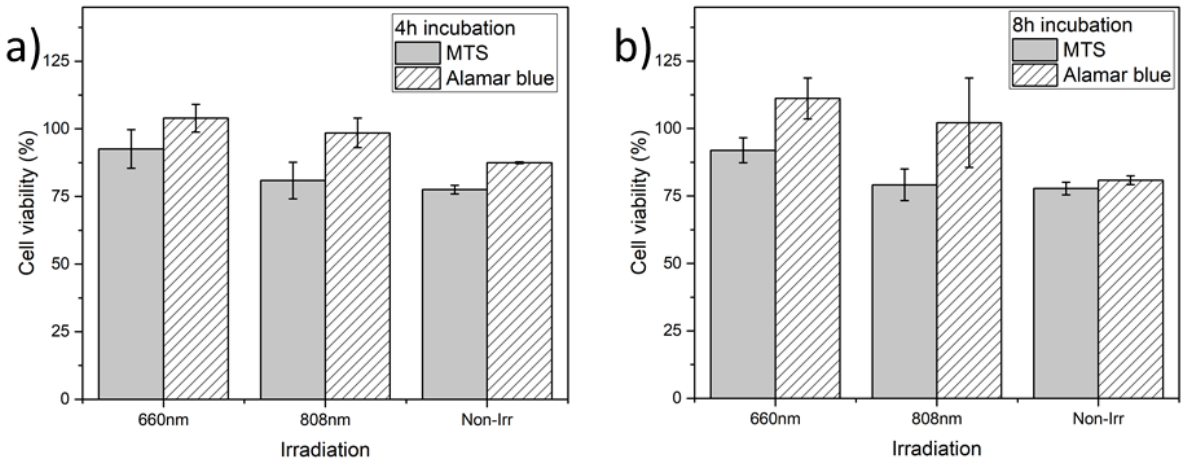

Figure 3.10 Cell viability of Hela cells irradiated using a 808 nm and a 660 nm laser after the incubation with GO-FA/Ce6 for a) 4 h and b) 8 h. HeLa cells incubated with GO-FA/Ce6 for 4 and 8 h (Non-IRR) were used as control.

Considering that the HeLa cells seemed to have developed a resistance to ROS and hyperthermia, the alamarBule and MTS assay did not allow us to demonstrate properly the killing efficiency in our experiments. Therefore, we decided to use another cell line, MCF-7, for the application of GO-FA/Ce6 in cancer phototherapy.

3.4.3 Cellular uptake and cytotoxicity of GO-FA/Ce6 on MCF-7

The cellular uptake of GO-FA/Ce6 by MCF-7 cells was first evaluated using confocal microscopy, by tracking the fluorescence of Ce6 on GO (Figure 3.11). CellMask green was again applied for better identification of the cell membranes. Similar to HeLa cells, GO-FA/Ce6 was already internalized by MCF-7 cells in 4 h. A higher accumulation of GO-FA/Ce6 was observed in the cytoplasmic compartments 8 h after the treatment with the nanomaterial. The Ce6 displayed lower fluorescence intensity after 24 h incubation likely due to degradation to a certain extent.. Thus, it was more efficient to perform the photothermal and photodynamic experiments after 4 and 8 h incubation with the double functional GO.

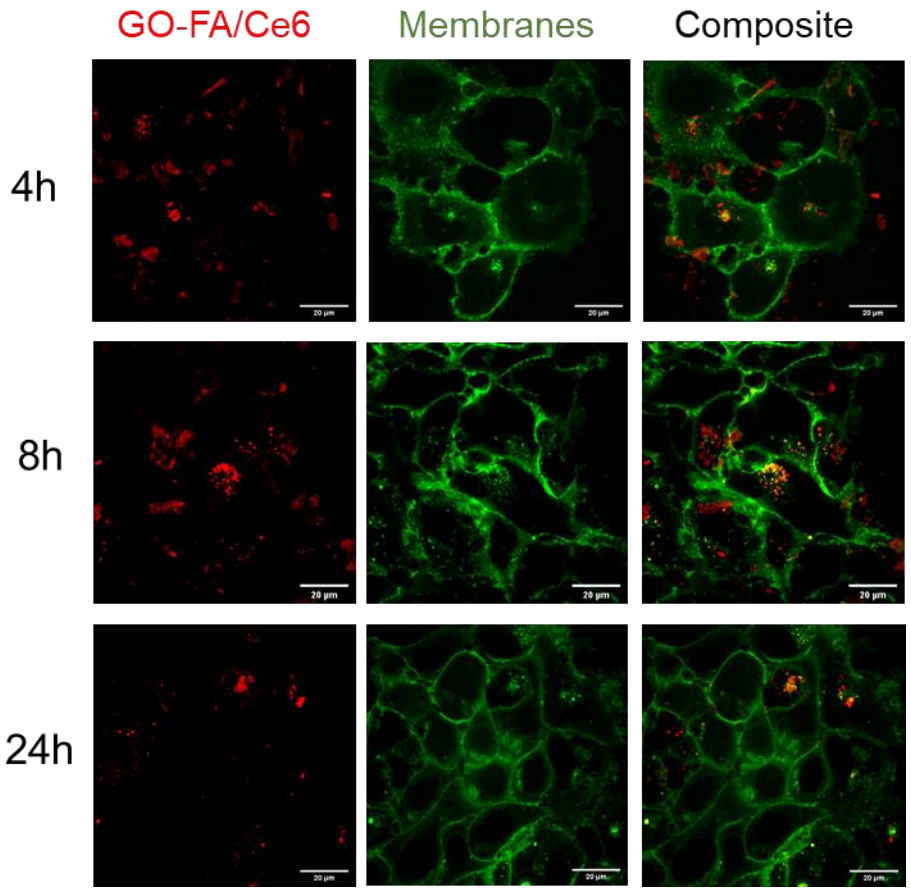

Figure 3.11 Confocal microscopy images of cellular uptake of GO-FA/Ce6 by MCF-7 cells.

Cytotoxicity of GO-FA/Ce6 on MCF-7 cells was also evaluated after the incubation for 4 and 8 h. The MTS assay was performed and the results are shown in Figure 3.12. The double functional GO shows both time-dependent and dose-dependent toxicity on MCF-7 cells. In the group of cells at 4 h incubation, the GO platform presents no cytotoxicity at the concentration of 10 and 25 $\mu g \cdot mL^{-1}$ with the cell viability around 100%, while a a 85% cell viability was observed when the concentration increased to 50 $\mu g \cdot mL^{-1}$. The longer incubation time would increase the cytotoxicity of the nanomaterial. However, at 25 $\mu g \cdot mL^{-1}$, the cell viability decreased to 89%, remaining still acceptable for next tests. The standard deviation is rather high meaning that the difference in the percentage at the two time-points is not statistically significant. At 50 $\mu g \cdot mL^{-1}$ there is no difference in cell viability at 4 and 8h.

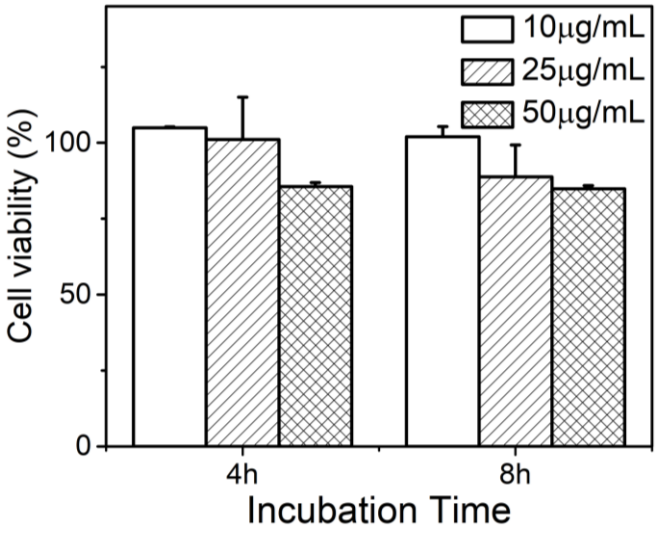

Figure 3.12 Cytotoxicity of GO-FA/Ce6 on MCF-7 cells.

3.4.4 PTT and PDT effects of GO-FA/Ce6 on MCF-7 cells

To study the photo-induced cytotoxicity of GO-FA/Ce6 on MCF-7, the cell viability was evaluated by MTS assay after irradiation using 660 nm and 808 nm laser in the presence of GO-FA/Ce6 (Figure 3.13). Similar to the results obtained with HeLa cells, MCF-7 showed a higher cell viability after the photodynamic treatment in the presence of GO-FA/Ce6, indicating that the ROS generated by Ce6 would promote the intracellular metabolism activity. The irradiation with 808 nm after 4 h incubation exhibited a slight killing efficiency against MCF-7 with a decreased viability down to 87%. However, the material showed no better hyperthermia-induced toxicity after 8 h incubation. The confocal microscopy had already demonstrated that more GO-FA/Ce6 was accumulated in the cytoplasm after 8 h. Since the hyperthermia induced by GO derivatives follows a dose-dependent manner, a higher killing efficiency by photothermal treatment was expected due to more GO material internalized by MCF-7. Thus, it seems that MTS assay did not reveal the influence of PTT and PDT on MCF-7 cells. We are in a situation similar to HeLa cells. The MTS test is likely no appropriate to evaluate the efficiency of phototherapy.

We decided to explore an alternative test corresponding to the Live/Dead assay. The LIVE/DEAD® Viability/Cytotoxicity assay kit is a two-color fluorescence cell viability test based on the simultaneous determination of live and dead cells with two probes measuring the intracellular esterase activity (calcein AM) and plasma membrane integrity (ethidium homodimer, EthD-1). A clear photo-triggered cytotoxicity was observed in this case (Figure 3.13). The 808 m irradiation induced a high killing efficiency by GO-FA/Ce6 against MCF-7 cells and the cell viability significantly decreased to 54% (after 4 h incubation) and to 51% (after 8 h incubation). The efficiency of the photodynamic treatment exhibited also an incubation-time-dependent killing efficiency, because of the different concentration of Ce6 in the cytoplasm. After 4 h incubation followed by the 660 nm irradiation, the cell viability

decreased to 82% compared to the non-irradiated group (101%). A lower viability (68%) was observed in the group with longer incubation time, revealing a higher PDT efficiency.

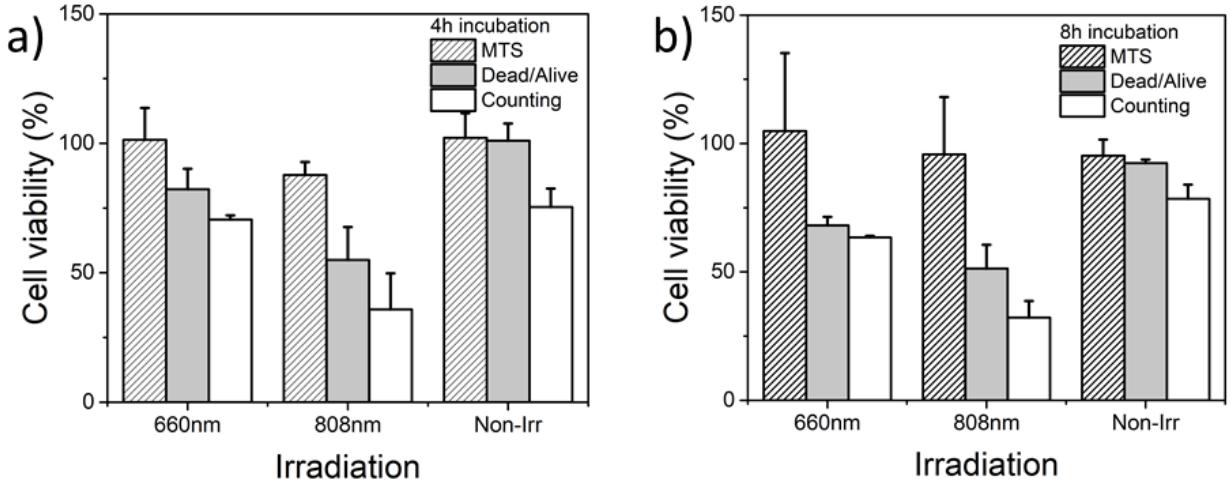

Figure 3.13 Viability of MCF-7 cells incubated with GO-FA/Ce6 for a) 4 h and b) 8 h, after photothermal and photodynamic treatment.

This kit can be also used for the staining of live and dead cells (Figure 3.14). The live cells were stained in green and the dead cells were red. The fluorescent microscopy images clearly show the change of live and dead cell numbers according to the different treatments. Compared to the control group, the images of both photothermal and photodynamic treated cells display less cells. The 808 nm laser irradiated cells are much less in comparison to other treated groups, which was consistent with the results of cell viability experiment. With the Live/Dead staining, the number of live cells can be easily counted on the pictures. After analysis of at least 6 images for each group, the cell viability by counting was calculated (Figure 3.13). A lower viability was obtained in comparison with Live/Dead assay probably due to the inhomogeneous distribution of the cells on the plates. However, both analyses allow to prove the effects of PPT and PDT on MCF-7 cultures with GO-FA/Ce6.

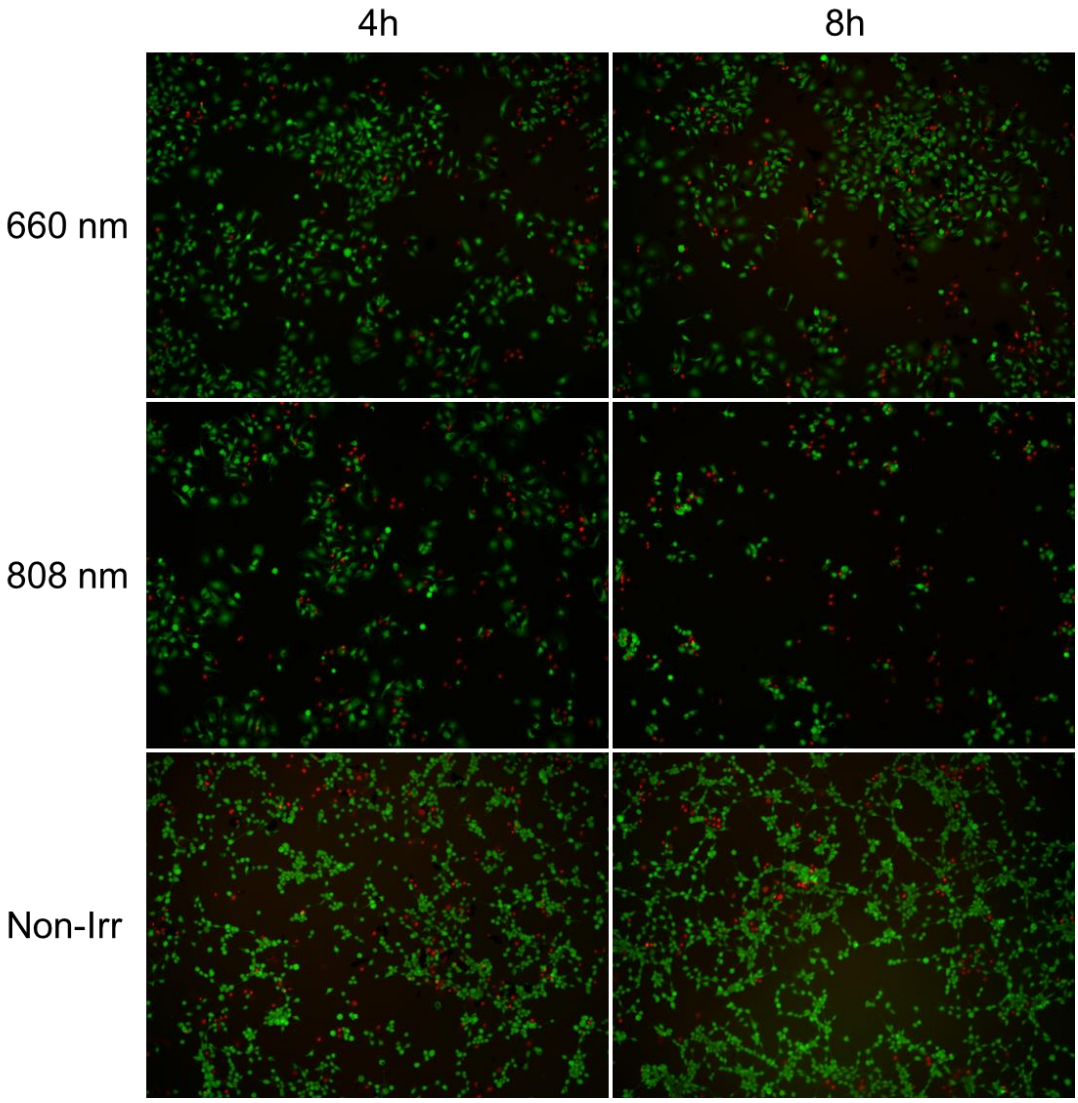

Figure 3.14 Fluorescence images of calcein-AM (green) and EthD-1 (red) double stained cells after different treatments. MCF-7 cells incubated with GO-FA/Ce6 for 4 and 8 h (Non-Irr) were used as control.

Next, we measured the cytotoxicity on MCF-7 of the combined PTT and PDT treatment with GO-FA/Ce6 using the Live/Dead assay (Figure 3.15). Cells were incubated with GO-FA/Ce6 for 4 and 8 h before removal of the nanomaterials and addition of fresh cell culture medium. The cells were then treated with a 808 nm laser irradiation for PTT followed by 660 nm irradiation for PDT. In the cells after 4 h incubation, no synergistic effect was observed. However, 77% of MCF-7 cells were killed by the two laser-induced cytotoxic effect after 8 h incubation, which is much higher than photothermal treatment alone with 49% of cell death and photodynamic treatment with only 32% of cell death, revealing that a synergistic effect was achieved by using two laser wavelengths in the presence of GO-FA/Ce6.

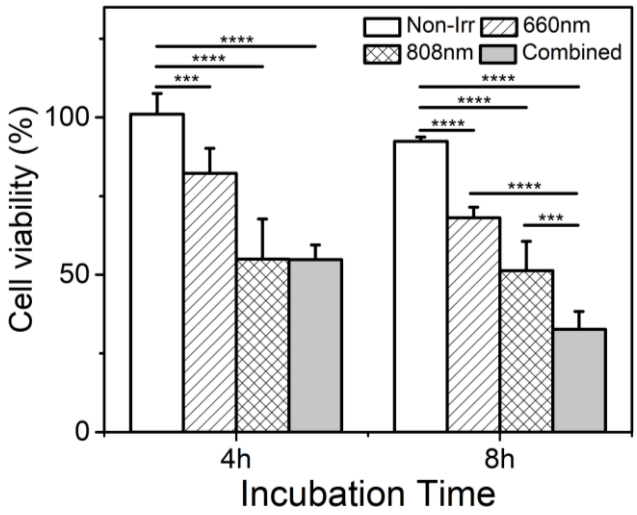

Figure 3.15 Comparison of MCF-7 viability following PTT, PDT and combed phototherapy after the incubation with GO-FA/Ce6 for 4 and 8 h. MCF-7 cells incubated with GO-FA/Ce6 for 4 and8 h (Non-IRR) were used as control.

The Live/Dead cell staining also proved that a higher killing efficiency was achieved through the synergistic effect of PTT and PDT after 8 h incubation (Figure 3.16). A lower number of cells was observed in the group of 8 h incubation, consistent with the cell viability experiments.

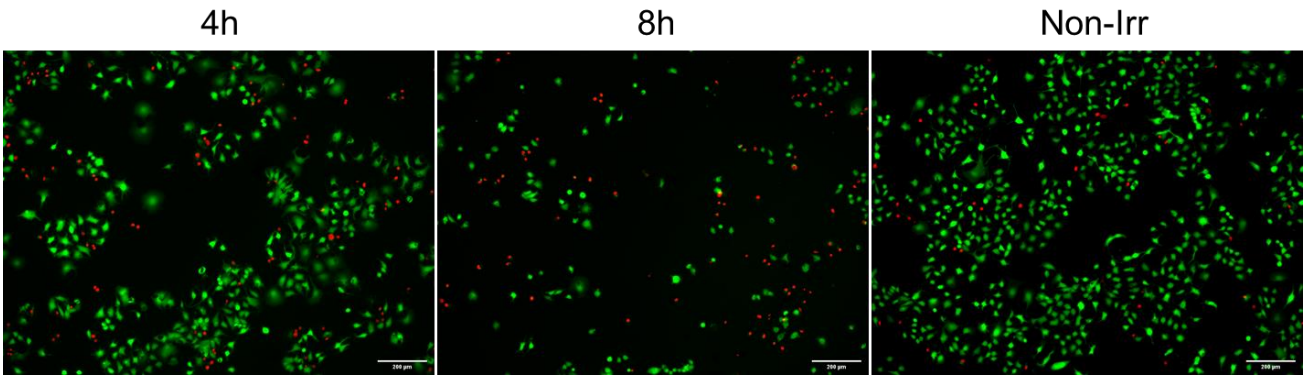

Figure 3.16 Comparison of MCF-7 cell viability following PTT, PDT and combing phototherapy after the incubation with GO-FA/Ce6 for 4 and 8 h. MCF-7 cells incubated with GO-FA/Ce6 for 4/8 h (Non-Irr) were used as control.

Overall, the therapeutic effect of PTT and PDT was measured by the Live/Dead assay. An incubation-time dependent cytotoxicity triggered by light was observed. By combining the PTT and PDT, a synergistic cancer therapy was achieved, resulting in a satisfactory killing efficiency of MCF-7 cells.

3.5 PTT and PDT of GO-FA/Ce6 on macrophages

The GO-FA/Ce6 has shown its good potential in the treatment of cancer cells by combing PTT and PDT to achieve a synergetic effect in killing cancer cells. The activated macrophages in rheumatoid arthritis joint also overexpress folate receptor β (FRβ), making the macrophages a target for RA therapy.[20] RAW 264.7 cells are a macrophage-like cell line derived from mice and can be used as a model for RA research.[21, 22] The FRβ on RAW 264.7 cells could specifically recognize FA-conjugated nanomaterials leading to a receptor-mediated endocytosis.

Therefore, we decided to apply GO-FA/Ce6 on RAW 264.7 to study the double functional GO for RA phototherapy. The initial biocompatibility study of a nanomaterial is commonly performed *in vitro*, to determine the dose-dependent toxicity of nanoparticles as well as the killing efficiency of the treatments. Different assays such as MTS and Live/Dead were used to measure the viability of the cells after incubation with nanomaterials alone, and after the irradiation for PTT and PDT. First of all, we evaluated the cytotoxicity of GO-FA/Ce6 on RAW 264.7 cells. This part of work was performed with the help of Dr Zhengmei Song in our group.

3.5.1 Cytotoxicity of GO-FA/Ce6 on RAW 264.7 cells

Cytotoxicity of GO-FA/Ce6 on RAW 264.7 cells was evaluated after the incubation for 24 h with MTS assay (Figure 3.17a). The double functional GO shows no effects on RAW 264.7 cells even at the highest concentration of 50 $\mu g \cdot mL^{-1}$. In all conditions, the cell viability was around 100%, indicating that the RAW cells have a good tolerance against GO-FA/Ce6.

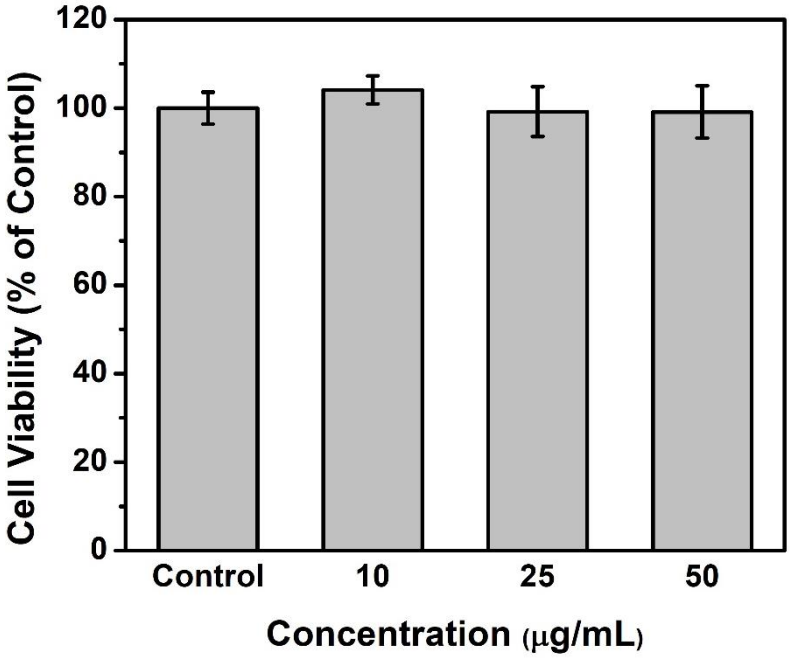

Figure 3.17 Cytotoxicity of GO-FA/Ce6 on RAW 264.7 cells.

3.5.2 PTT and PDT effects of GO-FA/Ce6 on RAW 264.7 cell

To study the photo-induced cytotoxicity of GO-FA/Ce6 on RAW 264.7 cells, the cell viability was evaluated by Live/Dead assay after irradiation using 660 nm and 808 nm laser in the presence of GO-FA/Ce6 (Figure 3.18). Compared to the results of cytotoxicity measured by MTS, the Live/Dead assay showed a lower cell viability at around 85% in the group without irradiation, both after 4 h and 8 h incubation. After applying the 660 nm and 808 nm irradiation, a clear photo-triggered cytotoxicity was observed (Figure 3.18). The 808 nm irradiation induced a sufficient killing efficiency by GO-FA/Ce6 against RAW 264.7 cells and the cell viability significantly decreased to 25% (after 4 h incubation) and to 20% (after 8 h incubation), revealing that these are more sensitive to the hyperthermia induced by photothermal effect of GO-FA/Ce6. The efficiency of the photodynamic treatment on RAW 264.7 cells was lower than PTT. After the irradiation of 660 nm laser, the cell viability decreased to 72% and the incubation-time-dependent killing efficiency was not observed. The low killing efficiency of PDT in RAW cells was probably due to the high resistance of macrophages to ROS.[23] To overcome this problem, we have planned to combined the PTT with PDT to obtain a synergistic effect. The hyperthermia would sensitize cells to the influence of other treatment leading to a higher therapeutic effect after PDT.[24, 25] This part of work is currently ongoing.

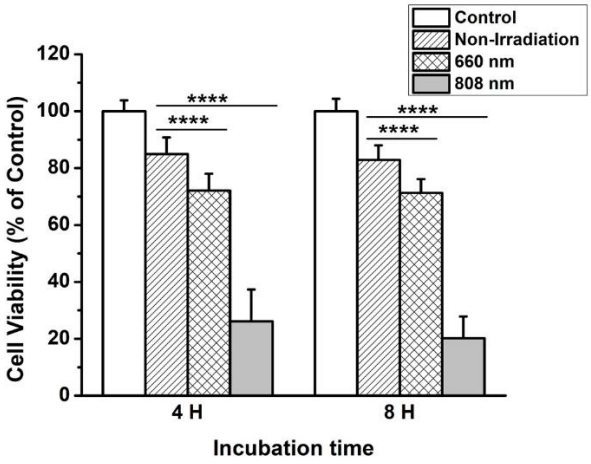

Figure 3.18 Viability of RAW 264.7 cells incubated with GO-FA/Ce6 for a) 4 h and b) 8 h, after separated photothermal and photodynamic treatment.

The fluorescence staining of live and dead cells is shown in Figure 3.19. The live cells are stained in green and the dead cells are in red. The fluorescence microscopy images clearly show the change of live and dead cell numbers according to the different treatments. Compared to the control group and the non-irradiated group, the images of both photothermal and photodynamic treated cells display less cells. The 808 nm laser irradiated cells are much less in comparison to other groups, which was consistent with the results of cell viability experiment. While in 660 nm laser irradiated groups showed

a higher the cell number compared to 808 nm irradiated groups, but still lower than the non-irradiated group.

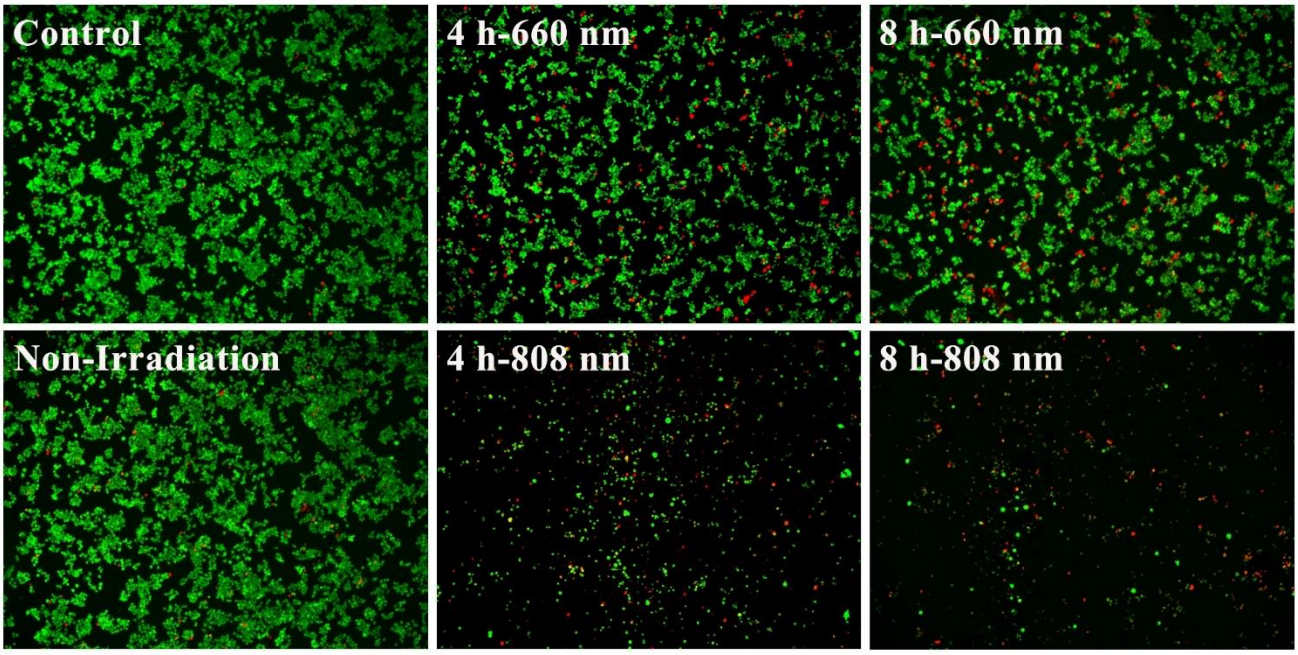

Figure 3.19 Fluorescence images of calcein-AM (green) and EthD-1 (red) double stained cells after different treatments. RAW 264.8 cells incubated with GO-FA/Ce6 for 4 and 8 h (Non-Irr) were used as control.

Overall, the therapeutic effect of PTT and PDT was measured by the Live/Dead assay. The RAW 264.8 cells present a higher sensitivity to photothermal treatment in comparison with cancer cells but also a resistance against photodynamic treatment. Further experiments need to be finish to evaluate the synergistic effect by combining PTT and PDT in the treatment of macrophages-associated RA.

3.6 Conclusions

In summary, a FA/Ce6 double-functionalized GO was successfully prepared and used for *in vitro* PTT/PDT synergistic cancer therapy using HeLa and MCF-7 cells. GO-FA/Ce6 exhibited good photothermal converting property and high ROS generation effect. The nanomaterial was able to penetrate quickly cancer cells due to the FR-mediated endocytosis. However, the metabolism based alamarBlue and MTS assays seems not to evidence eff on cell viability, likely due to an enhanced cellular metabolism activity after phototherapy. The Live/Dead assay was then used and GO-FA/Ce6 exhibited high killing efficiency on MCF-7 cells. Furthermore, a higher therapeutic efficiency was achieved by combining photothermal and photodynamic treatment, leading to satisfactory antitumor efficacy. Preliminary experiments using PTT and PDT alone were also performed on RAW 264.7 cells. The macrophages showed a higher sensitivity to PTT with a sufficient killing efficiency after

irradiation but also a resistance against ROS was observed. The synergistic effect of combining PTT and PDT still needs further experiments.

3.7 Material and methods

Materials

All the chemicals and solvents were obtained from commercial suppliers and used without purification. *O*-(2-aminoethyl)-*O'*-[2-(Boc-amino)ethyl]decaethylene glycol (BocNH-PEG_{10}-NH_2) was purchased from Polypure AS. Folic acid (FA) was purchased ACROS. Carbodiimide hydrochloride (EDC·HCl) and N-hydroxysuccinimide (NHS) were purchased from Alfa Aesar. The solvents used during the reaction were analytical grade. Water was purified by a Millipore filter system MilliQ®.

Preparation of GO suspensions

The pristine GO was obtained from Prof. Yuta Nishina (University of Okayama, Japan). All GO suspensions were prepared by sonication in a water bath (20 W, 40 kHz) with a controlled temperature between 20°C and 30°C.

Dialysis

For dialysis, MWCO 12,000-14,000 Da membranes were purchased from Spectrum Laboratories, Inc.

Thermogravimetric analysis

Thermogravimetric analysis (TGA) was performed on a TGA1 (Mettler Toledo) apparatus from 30°C to 900°C with a ramp of 10°C·min^{-1} under N_2 atmosphere with a flow rate of 50 mL·min^{-1} and platinum pans.

Transmission electron microscopy

Transmission electron microscopy (TEM) analysis was performed on a Hitachi H600 with an accelerating voltage of 75 kV. The samples were dispersed in water/ethanol (1:1) at a concentration of 16 μg·mL^{-1} and the suspensions were sonicated for 10 min. Ten microliters of the suspensions were drop-casted onto a copper grid (Formvar film 300 Mesh, Cu from Electron Microscopy Sciences) and left for evaporation under ambient conditions.

Thin layer chromatography

Thin layer chromatography (TLC) was performed on pre-coated aluminum plates with 0.20 mm Macherey-Nagel silica gel 60 with fluorescent indicator UV_{245}.

Chromatographic purification

Chromatographic purification was performed using silica gel (Sigma-Aldrich, 40-63 μm, 230-400 mesh).

HPLC

High-performance liquid chromatography analyses were performed on a Waters Alliance e2695 instrument, with integrated autosampler and a Waters 2998 PDA detector, using a Macherey–Nagel Nucleosil 100–5 C 18 column 4.6x125 mm (gradient: 0-100% of A and 100-0% of B in 20 min at 1.2 mL/min flow rate). Eluents for HPLC: A = H_2O+0.1% TFA, and B = MeCN+0.08% TFA.

LC/MS analyses

LC/MS analyses were performed on a LC/MS instrument equipped with a Thermo Scientific VANQVISH Flex UHPLC (Hypers II GOLD column, 50×2.1 mm, 1.9 μm) integrated with a Thermo Scientific LCQ Fleet ion-trap. Deconvolution of the data was performed in MagTran 1.03 (Amgen, Thousand Oaks, CA).

UV-Vis analyses

UV-Vis absorption spectra were recorded on a Cary 5000 UV-Vis-NIR spectrophotometer using 1 cm path quartz glass cuvettes and were corrected for the baseline and the solvent. The temperature was controlled at 25 °C using a Peltier system.

Immunostaining

A suspension GO-FA/Ce6 was deposited on a TEM grid. The grid was first verified by TEM that the functionalized carbon nanomaterials were well dispersed. The grid with nanomaterial was then re-hydrated by deposition of the grid on a drop of water (300 µL) for 15 min. The grid was then incubated in 40 µL acetylated BSA (1% in PBS) for 45 min. Then the grid was deposited on a 40 µL drop of anti-FA antibody [using mouse monoclonal folic acid antibody (FA1) stock solution (7 mg/mL), ref. NB100-72975] and incubated for 2 h (dilution 1/50 with 0.1% acetylated BSA in PBS). The antibody was removed and washed with PBS (4 times for 10 min each time) and with water (4 times for 10 min each time) by deposition of the grid on 300 µL PBS or water. Incubation of the grid with secondary antibody (using anti-mouse antibody coupled to 10-nm gold nanoparticles) for 2 h (dilution 1/50 in 0.1% acetylated BSA in PBS, centrifuging the antibody 2 min at 10 000g before dilution) was performed by deposition of the grid on a 40 µL drop. The grid was washed with PBS (3 times for 10 min each time) and with water (3 times for 10 min each time) by dropping the grid on 300 µL PBS or water. The immunostaining was evaluated by TEM. Two control samples were performed, using GO without FA (GO-FA-CTR) followed by the incubation of anti-FA antibody and secondary antibody, and using hRANK-M331 antibody (mouse IgG1monoclonal antibody against human RANK-M331, dilution 1/20 in 0.1% acetylated BSA in PBS) instead of anti-FA antibody on GO-FA followed by the incubation of secondary antibody.

Fluorescence measurements

Fluorescence measurements were performed in a water suspension at a concentration of 10 μg·mL^{-1} with a Jasco FP8003 fluorimeter using a swig xenon 450 W lamp and were corrected for the baseline and the solvent. The excitation wavelength was 420 nm and the emission range was measured between 520 nm and 800 nm.

Photothermal experiments

Different concentrations of GO-FA/Ce6 in water were prepared through sonication. The photothermal conversion of the carbon nanomaterial suspensions was examined by monitoring the temperature increase during irradiation using a 808 nm laser at a power density of 2 W·cm^{-2} from 0 to 15 min. The distance between laser and sample was kept constant at 3 cm. Each photothermal experiment was repeated three times. The temperature was monitoring using an infrared thermal imaging camera by recording the maximum temperatures in the images.

ROS generation assay

Dihydrorhodamine-123 (DHR123) purchased from Sigma-Aldrich was used to evaluate ROS generation in water solution. Light-triggered generation of ROS oxidizes DHR123 to fluorescent rhodamine 123. In a typical assay, a suspension of GO-FA/Ce6 (10 μg·mL^{-1}) was prepared in water and DHR123 (final concentration at 20 nM) was added. Then, the mixture was irradiated under 660 nm a laser (0.2 W·cm^{-2}) for 10 min and the emission intensity in the range from 495 nm to 900 nm was recorded with excitation at 485 nm.

Cell Culture

Cervical carcinoma cells (HeLa), Human Caucasian breast adenocarcinoma (MCF-7) and RAW 264.7 macrophages were cultured in high-glucose Dulbecco's modified Eagle medium (H-DMEM) with 10 μg/mL gentamycin (Lonza BioWhittaker), 10 mM N-(2-hydroxyethyl)-piperazine-N′-ethanesulfonic acid (Lonza BioWhittaker), 0.05 mM β-mercaptoethanol (Lonza BioWhittaker) and 10% fetal bovine serum (FBS). HeLa cells were maintained under a humidified atmosphere of 5% CO_2 at 37 °C, and the culture medium was changed every 2 days.

Cell viability assay

AlamarBlue assay, MTS assay and Live/Dead assay were performed to measure the cell viability according to the manufacturer's instructions.

For the AlamarBlue assay, HeLa cells were seeded in a 96-well plate at a density of 2×10^3 cells/well. The cells were adhered to the plate for 24 h and then exposed to different concentration of GO-FA/Ce6 for 4/8/24 h, as indicated. AlamarBlue reagent in cell culture media (10% v/v solution) was added to each well 24 h after the removal of GO nanomaterial. After 2 h of incubation at 37 °C, UV-Vis adsorption was measured at wavelength of 570 nm and 620 nm with a microplate reader (Thermo

Scientific, Multiskan FC). AlamarBlue solution in the cell culture media alone was included as blank. The experiments were performed with at least three replicates. Results were expressed as percentage cell viability versus control.

For MTS assay, HeLa, MCF-7 and RAW 264.7 cells were seeded in a 96-well plate at a density of 2×10^3 cells/well, 6×10^3 cells/well and 1×10^4, respectively. The cells after the treatment with GO were incubated with MTS solution in cell culture media (10% v/v solution) for 30 min at 37 °C. UV-Vis adsorption was measured at wavelength of 590 nm with a microplate reader, and MTS in the cell culture medium alone was included as blank. The experiments were performed with at least three replicates. Results were expressed as percentage cell viability versus control.

For Live/Dead assay, a solution A (2 μM calcein AM), solution B (4 μM EthD-1) and a working solution (2 μM calcein AM and 4 μM EthD-1) were freshly prepared before adding to the cells. MCF-7 and RAW 264.7 cells after the treatment with GO were incubated with the working solution for 40-50 min at room temperature. Three control samples were also performed using solution A, solution B and the working solution. Fluorescence was measured at the respective excitation and emission wavelength of 480 nm and 571 nm for calcein AM and 528 nm and 671 nm for EthD-1, using a Tecan Infinite F200 plate reader. The cell viability was calculated according to the manufacturer's instructions.

Confocal imaging

Confocal images were obtained with a Zeiss Axio Observer Z1 spinning disk confocal microscope equipped with a 63 or 100 × oil objective. z-Stacking was recorded with 0.3 μm interplanar distance. The fluorescence signal from CellMask (Sigma-Aldrich) was obtained using a 488 nm laser excitation and recording in the green channel (505-555 nm), whereas GO-FA/Ce6 were recorded using a 405 nm laser excitation in the far-red (FR) channel (665−715 nm). Images were then treated with ImageJ software.

***In vitro* PDT and PTT experiments**

Hela cells (2.0×10^3/well), MCF-7 cells (6.0×10^3/well) or RAW 264.7 (1.0×10^4/well) were seeded on a 96-well microplate (Greiner bio-one, Germany) for 24 h. The cells were incubated with GO-FA/Ce6 for 4/8/24 h and the nanomaterial removed afterwards. Samples with a total volume of 100 μL of cell culture media in 96-well plates were irradiated for 5/10 min with a 660 nm laser (0.2 $W\cdot cm^{-2}$) for PDT or with a 808 nm (2 $W\cdot cm^{-2}$) for PTT. After 24 h incubation, the culture media were removed and the cell viability was measured using different assay.

***In vitro* combined PDT and PTT experiments**

MCF-7 cells (6.0×10^3/well) were seeded on a 96-well microplate (Greiner bio-one, Germany) for 24 h. The cells were incubated with GO-FA/Ce6 for 4/8 h and the nanomaterial removed afterwards. Samples with a total volume of 100 μL of cell culture media in 96-well plates were irradiated with a 808 nm (2 $W\cdot cm^{-2}$) for PTT for 10 min followed by a 660 nm laser (0.2 $W\cdot cm^{-2}$) irradiation for PDT.

After 24 h incubation, the culture media were removed and the cell viability was measured using Live/Dead assay.

Fluorescence microscopy imaging

The cells treated with irradiation were stained with Live/Dead kit following the same protocol described in the cell viability part. The images were taken by fluorescence microscopy using a ZIESS APRES-VENTE MICROSCOPIE

Statistical analysis

Results are presented as mean ± standard deviation of at least three independent experiments. The numbers of samples per group in each experiment are indicated in the corresponding figure legends as "n". Differences between groups were evaluated with the Student's t-test for two groups. *, **, *** and ****denote the p-values less than 0.05, 0.01, 0.001 and 0.0001, respectively.

Synthesis of the building blocks, precursors and final GO conjugates

FA-PEG$_{10}$-Boc

A 441 mg (1 mmol) of folic acid and 200 μL triethylamine (TEA) were dissolved in 5 mL of DMSO by continuous stirring in room temperature for 10 min under argon atmospheres. The solution was cooled to 4 ℃ and EDC·HCl (191 mg, 1 mmol) and NHS (143 mg, 1.2 mmol) were added and the mixture was stirred for 24 h. The mixture was dropped to cold 200 mL DCM and the precipitate filtered over a polytetrafluoroethylene (PTFE) Millipore® membrane with 0.1 μm pore size obtaining a yellowish solid. The precipitation was washed with DCM and re-dissolved in 5 mL DMSO under argon atmospheres. The solution was cooled to 4℃ and 644 mg of Boc-PEG$_{10}$-NH$_2$ (1mmol) were added and the mixture was stirred for 24 h. The mixture was then dropped to cold diethyl ether with continuous stirring. The diethyl ether was removed and washed again with cold diethyl ether to afford a yellowish oily product. The crude product was purified by silica chromatography using acetone/DCM/EtOH/H_2O/TEA=3/2/1/0.7/0.3 as eluant, to eliminate the side product and then changing to acetone/DCM/EtOH/H_2O/TEA=2/2/2/0.7/0.3 obtaining the desired product. After drying in vacuum, a yellowish solid corresponding to FA-PEG$_{10}$-Boc was obtained. LC-MS (ESI): *m/z* calculated for $C_{48}H_{77}N_9O_{18}$ 1067.54, found 1068.08 $[M + H]^+$. HPLC (tR=9.8 min over 20 min of gradient: 0-100% of A and 100-0% of B in 20 min at 1.2 mL/min flow rate, A = H_2O+0.1% TFA, eluent B = MeCN+0.08% TFA).

Preparation of GO-FA

To a suspension of GO (80 mg) in 16 mL of water, 230 mg of Boc-PEG_{10}-NH_2 and 230 mg of FA-PEG_{10}-NH_2 was added to the solution and bath sonicated for 10 min. The mixture was then stirred at room temperature for 3 days and filtered over polytetrafluoroethylene (PTFE) Millipore® membrane with 0.1 μm pore size. The solid on the membrane was collected and dispersed in water, sonicated in a water bath and filtered again. This sequence was repeated 3 times with water. The solid was finally dispersed in water. The suspension was dialyzed in water for 3 days, and lyophilized to obtain GO-FA.

Preparation of GO-FA-CTR

The preparation of GO-FA-CTR was similar to the preparation of GO-FA. To a suspension of GO (20 mg) in 5 mL of water, 125 mg of Boc-PEG_{10}-NH_2 was added to the solution and bath sonicated for 10 min. The mixture was then stirred at room temperature for 3 days and filtered over a PTFE filter membrane with 0.1 μm pore size. The solid on membrane was collected and washed with water for 3 times. The solid was finally dispersed in water, the suspension was dialyzed in water for 3 days, and lyophilized to obtain GO-FA-CTR.

Preparation of GO-FA/Ce6

The GO-FA was first deprotected using HCl. To a suspension of GO-FA (60 mg) in 30 mL of 1,4-dioxane and sonicated for 10 min. Thirty mL of 4 M HCl in 1,4-dioxane was added and sonicated for 5 min. The suspension was stirred for 17 h and filtered over a PTFE filter membrane with 0.1 μm pore size. The solid on membrane was collected and washed with water for 3 times. The solid was dried under vacuum.

Eighty mg Ce6 were dissolved in 1 mL of DMF with 20 μL TEA and stirred in ice bath for 10 min. EDC·HCl (28.2 mg) was added to the solution and stirred for 1 h in ice bath. Then 23.1 mg of NHS was added to the mixture and stirred for 17 h at 4 ℃. The mixture was dropped to a 9 mL DMF suspension of 20 mg Boc-deprotected GO-FA and stirred for 17 h. The mixture was filtered over a PTFE filter membrane with 0.1 μm pore size. The solid on membrane was collected and washed with DMF and water for 3 times each. The solid was finally dispersed in water, the suspension was dialyzed in water for 3 days, and lyophilized to obtain GO-FA/Ce6.

Preparation of GO-FA/Ce6-CTR

GO-FA/Ce6-CTR was obtained following the protocol for the preparation of GO-FA/Ce6 but directly using GO-FA for the reaction without Boc-deprotection. Forty mg Ce6 were dissolved in 1 mL of DMF with 10 μL TEA and stirred in ice bath for 10 min. EDC·HCl (14.1 mg) was added to the solution and stirred for 1 h in ice bath. Then 11.5 mg of NHS was added to the mixture and stirred for 17 h at 4 ℃. The mixture was dropped to a 4 mL DMF suspension of 10 mg GO-FA and stirred for 17 h. The mixture was filtered over a PTFE filter membrane with 0.1 μm pore size. The solid on membrane was collected and washed with DMF and water for 3 times each. The solid was finally dispersed in water, the suspension was dialyzed in water for 3 days, and lyophilized to obtain GO-FA/Ce6-CTR.

3.7 References

1. S. S. Nanda, G. C. Papaefthymiou and D. K. Yi, “Functionalization of Graphene Oxide and its Biomedical Applications”, *Crit. Rev. Solid State Mater. Sci.*, 2015, **40**, 291-315.

2. P. Huang, C. Xu, J. Lin, C. Wang, X. Wang, C. Zhang, X. Zhou, S. Guo and D. Cui, “Folic Acid-conjugated Graphene Oxide loaded with Photosensitizers for Targeting Photodynamic Therapy”, *Theranostics*, 2011, **1**, 240-250.

3. N. Karki, H. Tiwari, C. Tewari, A. Rana, N. Pandey, S. Basak and N. G. Sahoo, “Functionalized graphene oxide as a vehicle for targeted drug delivery and bioimaging applications”, *J. Mater. Chem. B*, 2020, **8**, 8116-8148.

4. B. P. Jiang, B. Zhou, Z. Lin, H. Liang and X. C. Shen, “Recent Advances in Carbon Nanomaterials for Cancer Phototherapy”, *Chem. Eur. J.*, 2019, **25**, 3993-4004.

5. Q. Chen, Y. Du, K. Zhang, Z. Liang, J. Li, H. Yu, R. Ren, J. Feng, Z. Jin, F. Li, J. Sun, M. Zhou, Q. He, X. Sun, H. Zhang, M. Tian and D. Ling, “Tau-Targeted Multifunctional Nanocomposite for Combinational Therapy of Alzheimer's Disease”, *ACS Nano*, 2018, **12**, 1321-1338.

6. M. Suggitt and M. C. Bibby, “50 Years of Preclinical Anticancer Drug Screening: Empirical to Target-Driven Approaches”, *Clin. Cancer Res.*, 2005, **11**, 971 – 981.

7. M. Król, K.M. Pawłowski, K. Majchrzak, K. Szyszko and T. Motyl, “Why chemotherapy can fail?”, *Pol. J. Vet. Sci.*, 2010, **13**, 399-406.

8. D. Kim, S. Park, H. Yoo, S. Park, J. Kim, K. Yum, K. Kim and H. Kim, “Overcoming anticancer resistance by photodynamic therapy-related efflux pump deactivation and ultrasound-mediated improved drug delivery efficiency”, *Nano Converg*, 2020, **7**, 30.

9. K. Vinothini, N. K. Rajendran, A. Ramu, N. Elumalai and M. Rajan, “Folate receptor targeted delivery of paclitaxel to breast cancer cells via folic acid conjugated graphene oxide grafted methyl acrylate nanocarrier”, *Biomed Pharmacother*, 2019, **110**, 906-917.

10. E. Nogueira, A. C. Gomes, A. Preto and A. Cavaco-Paulo, “Folate-targeted nanoparticles for rheumatoid arthritis therapy”, *Nanomedicine*, 2016, **12**, 1113-1126.

11. A. Li Volsi, C. Scialabba, V. Vetri, G. Cavallaro, M. Licciardi and G. Giammona, “Near-Infrared Light Responsive Folate Targeted Gold Nanorods for Combined Photothermal-Chemotherapy of Osteosarcoma”, *ACS Appl. Mater. Interfaces*, 2017, **9**, 14453-14469.

12. J. Liu, W. E. Hennink, M. J. van Steenbergen, R. Zhuo and X. Jiang, “A facile modular approach toward multifunctional supramolecular polyplexes for targeting gene delivery”, *J. Mater. Chem. B*, 2016, **4**, 7022-7030.

13. A. Gabizon, A. T. Horowitz, D. Goren, D. Tzemach, F. Mandelbaum-Shavit, M. M. Qazen and S. Zalipsky, “Targeting folate receptor with folate linked to extremities of poly(ethylene glycol)-grafted liposomes: in vitro studies”, *Bioconjug Chem*, 1999, **10**, 289-298.

14. K. H. Choi, K. C. Nam, G. Cho, J. S. Jung and B. J. Park, “Enhanced Photodynamic Anticancer Activities of Multifunctional Magnetic Nanoparticles (Fe_3O_4) Conjugated with Chlorin e6 and Folic Acid in Prostate and Breast Cancer Cells”, *Nanomaterials (Basel)*, 2018, **8**.

15. P. Li, G. Zhou, X. Zhu, G. Li, P. Yan, L. Shen, Q. Xu and M. R. Hamblin, “Photodynamic therapy with hyperbranched poly(ether-ester) chlorin(e6) nanoparticles on human tongue carcinoma CAL-27 cells”, *Photodiagn. Photodyn. Ther.*, 2012, **9**, 76-82.

16. W. H. Chen, G. F. Luo, Q. Lei, S. Hong, W. X. Qiu, L. H. Liu, S. X. Cheng and X. Z. Zhang, “Overcoming the Heat Endurance of Tumor Cells by Interfering with the Anaerobic Glycolysis Metabolism for Improved Photothermal Therapy”, *ACS Nano*, 2017, **11**, 1419-1431.

17. X. W. Liu, Y. Su, H. Zhu, J. Cao, W. J. Ding, Y. C. Zhao, Q. J. He and B. Yang, “HIF-1alpha-dependent autophagy protects HeLa cells from fenretinide (4-HPR)-induced apoptosis in hypoxia”, *Pharmacol. Res.*, 2010, **62**, 416-425.

18. A. P. Castano, T. N. Demidova and M. R. Hamblin, “Mechanisms in photodynamic therapy: part two—cellular signaling, cell metabolism and modes of cell death”, *Photodiagn. Photodyn. Ther.*, 2005, **2**, 1-23.

19. Z. Xie, T. Fan, J. An, W. Choi, Y. Duo, Y. Ge, B. Zhang, G. Nie, N. Xie, T. Zheng, Y. Chen, H. Zhang and J. S. Kim, “Emerging combination strategies with phototherapy in cancer nanomedicine”, *Chem. Soc. Rev.*, 2020, DOI: 10.1039/d0cs00215a.

20. D. Chandrupatla, C. F. M. Molthoff, A. A. Lammertsma, C. J. van der Laken and G. Jansen, “The folate receptor beta as a macrophage-mediated imaging and therapeutic target in rheumatoid arthritis”, *Drug Delivery Transl. Res.*, 2019, **9**, 366-378.

21. X. Sun, S. Dong, X. Li, K. Yu, F. Sun, R. J. Lee, Y. Li and L. Teng, “Delivery of siRNA using folate receptor-targeted pH-sensitive polymeric nanoparticles for rheumatoid arthritis therapy”, *Nanomedicine*, 2019, **20**, 102017-102027.

22. M. Chen, J. C. K. Amerigos, Z. Su, N. E. I. Guissi, Y. Xiao, L. Zong and Q. Ping, “Folate Receptor-Targeting and Reactive Oxygen Species-Responsive Liposomal Formulation of Methotrexate for Treatment of Rheumatoid”, *Pharmaceutics*, 2019, **11**, 582-604.

23. L. Virag, R. I. Jaen, Z. Regdon, L. Bosca and P. Prieto, “Self-defense of macrophages against oxidative injury: Fighting for their own survival”, *Redox Biol.*, 2019, **26**, 101261-101269.

24. D. de Melo-Diogo, R. Lima-Sousa, C. G. Alves and I. J. Correia, “Graphene family nanomaterials for application in cancer combination photothermal therapy”, *Biomater. Sci.*, 2019, **7**, 3534-3551.

25. R. Di Corato, G. Bealle, J. Kolosnjaj-Tabi, A. Espinosa, O. Clement, A. K. Silva, C. Menager and C. Wilhelm, “Combining magnetic hyperthermia and photodynamic therapy for tumor ablation with photoresponsive magnetic liposomes”, *ACS Nano*, 2015, **9**, 2904-2916.

Chapter 4 Benzoquinone-assisted covalent functionalization and liquid phase exfoliation of MoS_2

4.1 Introduction

The study of 2D layered nanomaterials has been inspired by the successful isolation of graphene. Among the large family of 2D nanomaterials, transition metal dichalcogenides (TMDs) have attracted increasing interest due to their unique structures and properties, leading to a vast potential for different applications in electronic devices, optoelectronics, sensing, drug delivery and energy storage.[1] However, the development of effective methods for high-quality TMDs preparation is still a major focus of the current experimental research.[2-4] Moreover, the chemical functionalization of TMDs allows to introduce modification of the intrinsic properties and extension of the applications.[5, 6] In the meantime, TDM functionalization could facilitate the synthesis of higher quantities of 2D TMDs.[5, 7]

MoS_2 is one of the main TDM materials for studying their chemistry and applications, and it has received a lot of interest by many researchers working at the cross field between physics, chemistry, biology and material science.[6] MoS_2 is constituted by two polymorphs, namely the semiconducting 2H MoS_2 and metallic 1T MoS_2. The 2H MoS_2 is thermodynamically stable, while the 1T-MoS_2 is metastable.[8] Therefore, natural MoS_2 is predominantly in 2H polymorph form. The isolation of the type of 2D MoS_2 nanosheet polymorph depends on the exfoliation procedure. 1T MoS_2 nanosheets are usually prepared *via* a "harsh" chemical exfoliation procedure,[7] while the mechanical or liquid phase exfoliation preserve the natural more stable polymorph 2H.[9] Recently, Pérez *et al.* reported a strategy for covalent functionalization of 2H MoS_2 using maleimides under mild condition.[10] The authors exploited the soft nucleophilicity of sulfur atoms on MoS_2 to react with maleimide derivatives following Michael addition. The covalent conjugation of different maleimides onto MoS_2 surface was confirmed by the authors using different characterization methods.

In the previous part, we have already proved that benzoquinone can covalently bounded onto GO surface through a Michael addition reacting with the hydroxyl groups. The benzoquinone derivatives can further react with electrophiles *via* another Michael addition. This inspired us to develop a protocol for covalent functionalization of MoS_2 with benzoquinone though Michael addition under mild condition.

4.2 Objectives of this chapter

The aim of this chapter is to develop an efficient strategy for the covalent functionalization of MoS_2 nanosheets by exploring the S atoms as mild nucleophiles for Michael addition. MoS_2 was isolated

s*via* a surfactant-assisted liquid phase exfoliation. To further attach the functional groups onto MoS_2, benzoquinone was used as the electrophiles reacting with S atoms through Michael addition, leading to the formation of C-S bond. The benzoquinone derivatized MoS_2 nanosheets were then functionalized with two different functional molecules through another Michael addition.

Besides exploring the functionalization of MoS_2 using benzoquinone, we were also interested to developed a protocol combining the exfoliation and benzoquinone derivatization in one step. Thus, we isolated the MoS_2 nanosheets from bulk material directly with benzoquinone *via* liquid phase exfoliation, in order to obtain a nanomaterial with good water dispersibility and highly reactive sites for further modification.

4.3 Covalent functionalization of MoS_2 using benzoquinone

4.3.1 Liquid-phase exfoliation and characterization of MoS_2

MoS_2 nanosheets were prepared with the collaboration of Dr. Dingkun Ji through a surfactant mediated liquid exfoliation method. Briefly, bulk MoS_2 was mixed with sodium cholate using ball milling. Then the mixture was transferred into water and the exfoliation of MoS_2 was carried out by bath sonication. The prepared MoS_2 was characterized by TEM (Figure 4.1a) The nanosheets have an average lateral size around 200 nm, with a distribution between 50 and 400 nm.

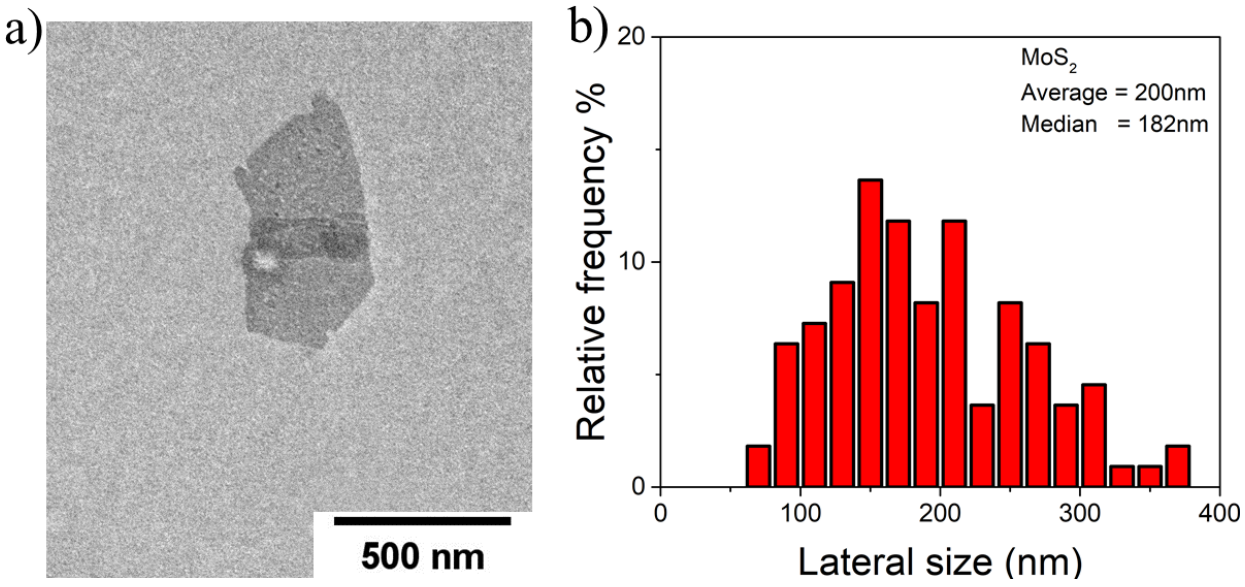

Figure 4.1 TEM image (a) and size distribution (b) of MoS_2 nanosheets exfoliated using sodium cholate.

Then, MoS_2 nanosheets were characterized by XPS (Figure 4.2). From the survey spectrum (Figure 4.2a), Mo, S, O and C elements were identified. The liquid-phase exfoliated MoS_2 displayed a S:Mo ratio of approximately 1.6:1, showing the existence of S vacancies on the surface of the nanomaterial. The sodium cholate was adsorbed onto MoS_2 nanosheets after exfoliation, leading to the high

emission of signal from carbon and oxygen elements in the XPS. As we did not observe sodium in XPS survey, sodium cholate is likely transformed into its acid derivative (cholic acid) due to hydrolysis, leading to removal of Na^+ during the washing procedure. The calculated amount of sodium cholate onto MoS_2 is 1.0 mmol·g^{-1}. However, XPS is a surface sensitive method and the intensity of the emission of the different elements might be difficult to quantify precisely in a heterogeneous nanomaterial.[11] Therefore, the amount of sodium cholate onto MoS_2 surface might be different from other technique (e.g. TGA). In the Mo 3d XPS spectrum (Figure 4.2b) of MoS_2, two peaks were observed at 229.5 and 232.7 eV, coming from Mo $3d_{5/2}$ and Mo $3d_{3/2}$ orbitals, respectively, indicating that Mo atoms were in 4^+ oxidation state in the 2H polymorph form.[12] The third peak centered at 226.4 eV was signal from S 2s photoelectrons. In the S 2p spectrum (Figure 4.2c), the peaks at 163.2 eV and 162.0 eV were contributed by the S^{2-} $2p_{1/2}$ and S^{2-} $2p_{3/2}$ orbitals. The C 1s spectrum showed the components of C-C (284.6 eV), C-O (286.4 eV) and C=O (288.6 eV) from sodium cholate adsorbed onto MoS_2 (Figure 4.2d).

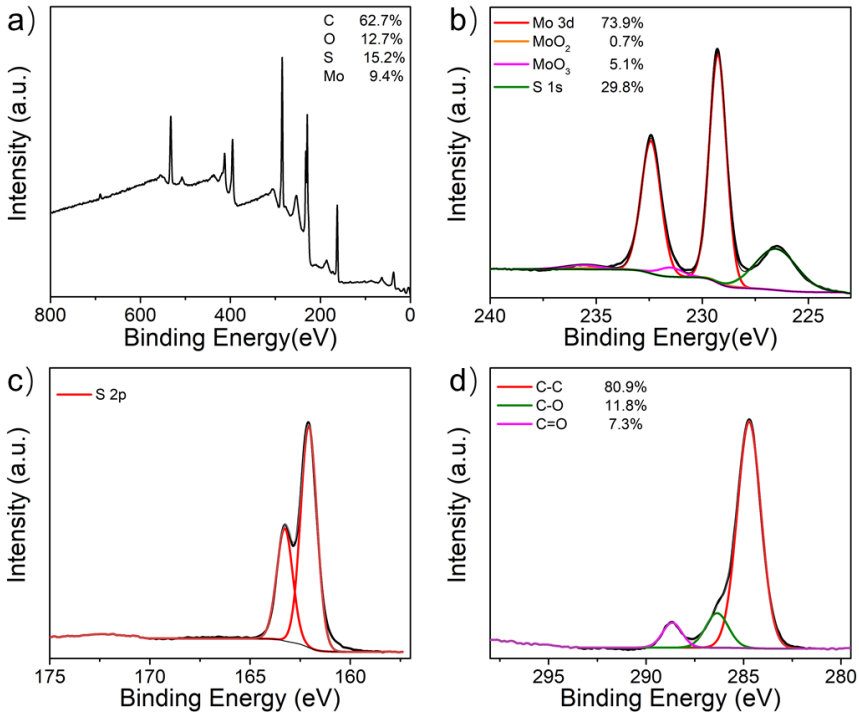

Figure 4.2 XPS survey spectra (a), high resolution Mo 3d (b), S 2p (c) and C 1s (d) spectra of MoS_2.

Subsequently, the prepared MoS_2 nanosheets were used for the study of covalent functionalization using benzoquinone.

4.3.2 Functionalization of MoS_2 with benzoquinone and 3-(pentafluorothio)-DL-phenylalanine

In chapter 2, we successfully functionalized GO using benzoquinone through Michael addition. 3-(Pentafluorothio)-DL-phenylalanine was chosen as the functional group since the fluorine atoms could facilitate the sensitivity of XPS characterization and the amine group was able to react with the benzoquinone moiety on nanosheets by Michael addition. Here we decided to use a similar procedure

to functionalize MoS_2 as illustrated in Scheme 4.1 (top). Briefly, MoS_2 was derivatized by benzoquinone through nucleophilic addition with the formation of S-C bond, obtaining benzoquinone functionalized MoS_2 **1**. Then, 3-(pentafluorothio)-DL-phenylalanine was covalently linked to benzoquinone moiety on MoS_2 **1** through a second Michael addition, leading to the phenylalanine derivatized MoS_2 **2**.

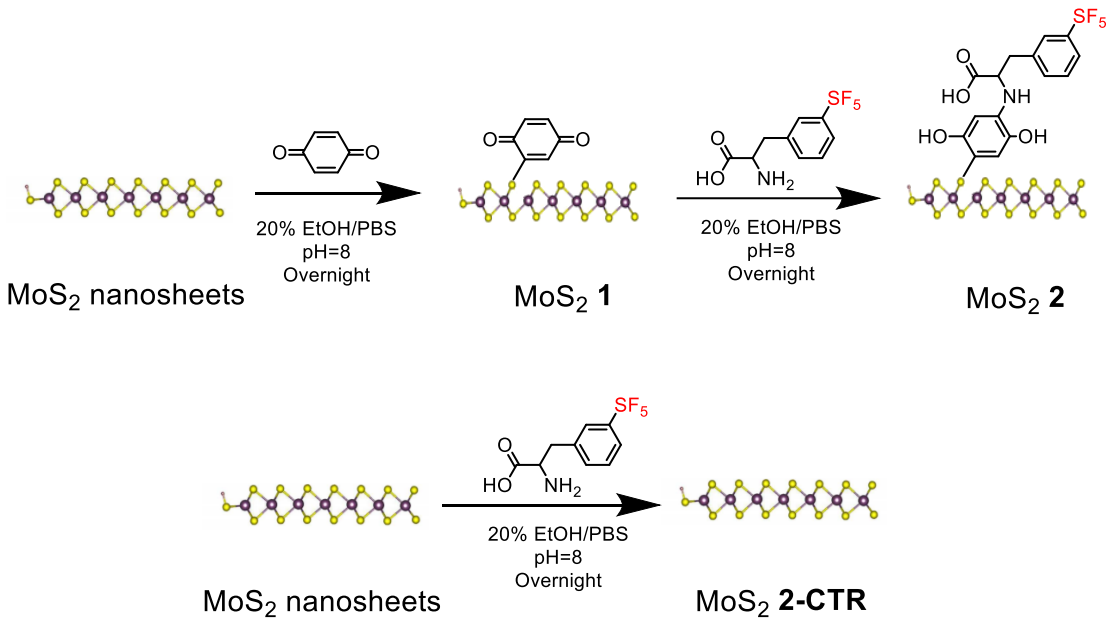

Scheme 4.1 Functionalization of MoS_2 using benzoquinone and 3-(pentafluorothio)-DL-phenylalanine. For the sake of clarity, only one S atom is derivatized.

Compared to pristine MoS_2, benzoquinone functionalized MoS_2 **1** displayed a good dispersibility in water (Figure 4.3a). It could be also well-redispersed after excessive washing followed by lyophilization, while the liquid exfoliated MoS_2 nanosheets tended to form aggregates (Figure 4.3b).

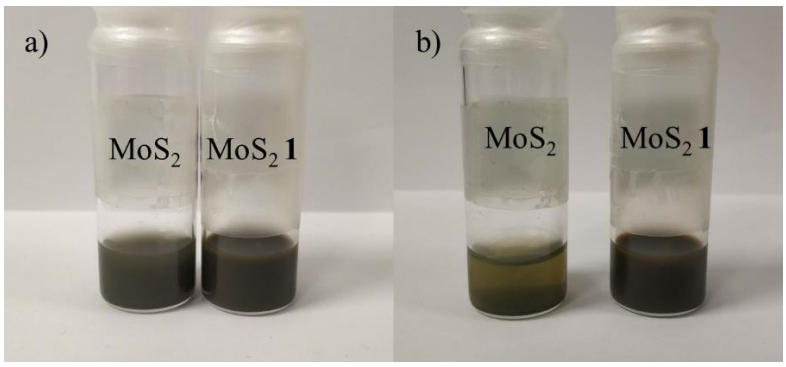

Figure 4.3 Water dispersions of MoS_2 and MoS_2 **1** before (a) and after (b) excessive washing and lyophilization.

MoS_2 **1** was then characterized by XPS (Figure 4.4). Compared to the starting MoS_2, a higher content of C and O atoms were detected in the benzoquinone functionalized MoS_2, due to the introduction of quinone moiety onto MoS_2. As the C and O atoms are coming from cholic acid and benzoquinone,

we can calculate the theoretical ratio between these two compounds as 1.1 ([benzoquinone]/[cholate acid]). The amount of benzoquinone on MoS_2 correspond to 0.95 $mmol \cdot g^{-1}$ with a molar loading efficiency of 34.8%. The cholic acid was calculated at 0.87 $mmol \cdot g^{-1}$, indicating that partial cholic acid was removed during the reaction with benzoquinone. After the detailed analysis of Mo 3d spectrum in MoS_2 **1**, a new doublet of Mo 3d peaks with the Mo 3d ($3d_{5/2}$ centered at 230.4 eV and $3d_{3/2}$ centered at 233.6 eV) was introduced, in order to obtain a better fitting in the deconvolution procedure. As a nucleophile in the Michael addition, the electrons are transferred from the basal plane of MoS_2 to benzoquinone molecules. Therefore, the peaks of Mo 3d would shift to a higher binding energy. However, Pérez *et al.*[10] reported that the components at a lower binding energy were assigned to the reaction between maleimide and MoS_2, while the components at a higher binding energy were coming from the oxidation of MoS_2. In our experiments, the oxidation of MoS_2 was not significant and no component was observed at a lower binding energy. In the meantime, these peaks were unnecessary in the deconvolution of MoS_2 samples exfoliated by sodium cholate. The generation of new fitting components was probably due to the formation of Mo-S-benzoquinone (Mo-S-C in Figure 4.4c) linkage *via* Michael addition. The C 1s spectrum showed an increasing area of carbon atoms in C=O bond compare to the starting MoS_2 from 7.3% to 8.5%, while the C-N/C-S component was also observed, indicating the conjugation of benzoquinone on MoS_2. In the high-resolution of S 2p spectrum, the pristine MoS_2 exhibited only one doublet of S 2p peaks with the S $2p_{3/2}$ centered at 162.1 eV. While, MoS_2 **1** showed a different line shape with another doublet with the S $2p_{3/2}$ centered at 163.2 eV which could be assigned to C-S bond in addition of the intrinsic doublet of S 2p peaks from MoS_2, confirming that benzoquinone was covalently attached to MoS_2.

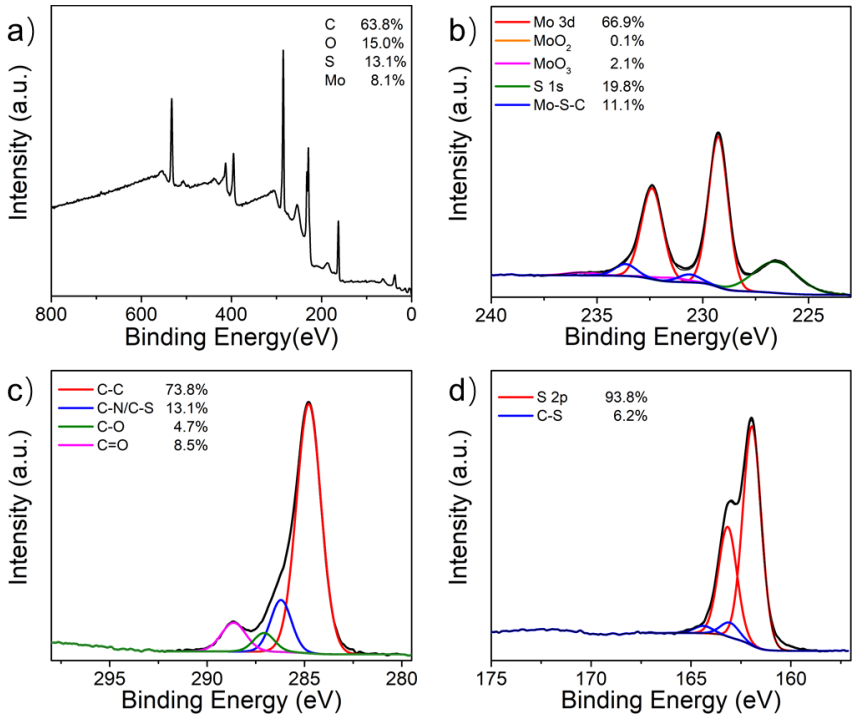

Figure 4.4 XPS survey spectra (a), high resolution Mo 3d (b), C 1s (c) and S 2p (d) spectra of MoS_2 **1**.

The presence of benzoquinone on MoS_2 surface was corroborated by thermogravimetric analysis under inert atmosphere (Figure 4.5). The TGA curve of the pristine MoS_2 showed a total 9% weight loss at 600°C. In MoS_2, a higher weight loss was observed (13%). The decrease of the thermal stability could be attributed to decomposition of benzoquinone grafted on the MoS_2 nanosheets. However, the TGA did not allow to provide the information about the ratio between sodium cholate and benzoquinone.

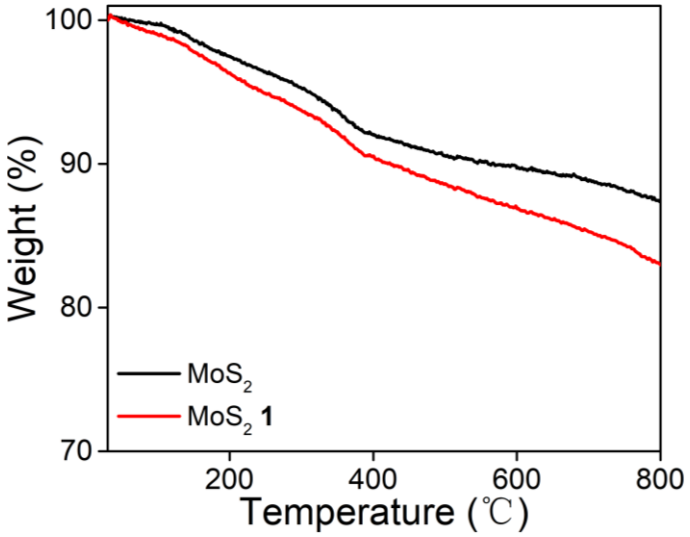

Figure 4.5 TGA of the pristine MoS_2 and MoS_2 **1** performed in inert atmosphere.

Once confirming that benzoquinone was successfully grafted onto MoS_2, the derivatization of MoS_2 **1** with 3-(pentafluorothio)-DL-phenylalanine was then performed. MoS_2 **1** was first dispersed in PBS/EtOH solution and stirred with 3-(pentafluorothio)-DL-phenylalanine overnight. After carefully washing and centrifugation, the phenylalanine derivative functionalized MoS_2 **2** was obtained. To clarify if the 3-(pentafluorothio)-DL-phenylalanine was covalently bounded onto MoS_2 through Michael addition, a control sample was also prepared by simply mixing the pristine MoS_2 nanosheets with 3-(pentafluorothio)-DL-phenylalanine in the absence of benzoquinone, giving MoS_2 **2-CTR** (Scheme 4.1 bottom).

The conjugation of 3-(pentafluorothio)-DL-phenylalanine was characterized by XPS. A significant signal from fluorine atoms was collected by XPS in the survey spectrum (3.1%) (Figure 4.6a), while no fluorine was detected in the all MoS_2 precursor conjugates, indicating the successful introduction of the 3-(pentafluorothio)-phenylalanine moiety onto MoS_2 **2**. The high-resolution spectrum of the S 2p peak further confirmed the presence of 3-(pentafluorothio)-DL-phenylalanine on MoS_2 **2**. Besides the peaks contributed by the S 2p from MoS_2 and atoms from S-C bond, a broad peak centered at 172.5 eV was recorded, which could be assigned to sulfur atom in S-F bond from the pentafluorothiol moiety (Figure 4.6g). However, the S-F peak was much smaller, since the introduced S atoms *via* Michael addition was relatively low in comparison with the intrinsic S elements in MoS_2. In the control sample MoS_2 **2-CTR**, the content of fluorine element calculated from survey spectrum was

0.4%, which was much lower than MoS_2 **2** (Figure 4.6b). In S 2p spectrum, only one doublet of S-Mo from MoS_2 was recorded and the S-F peak was almost negligible (Figure 4.6h), which further proved a low amount of the phenylalanine derivative physisorbed onto MoS_2. The XPS data confirmed the covalent conjugation of 3-(pentafluorothio)-DL-phenylalanine onto MoS_2 **1** thought the Michael addition on benzoquinone moieties.

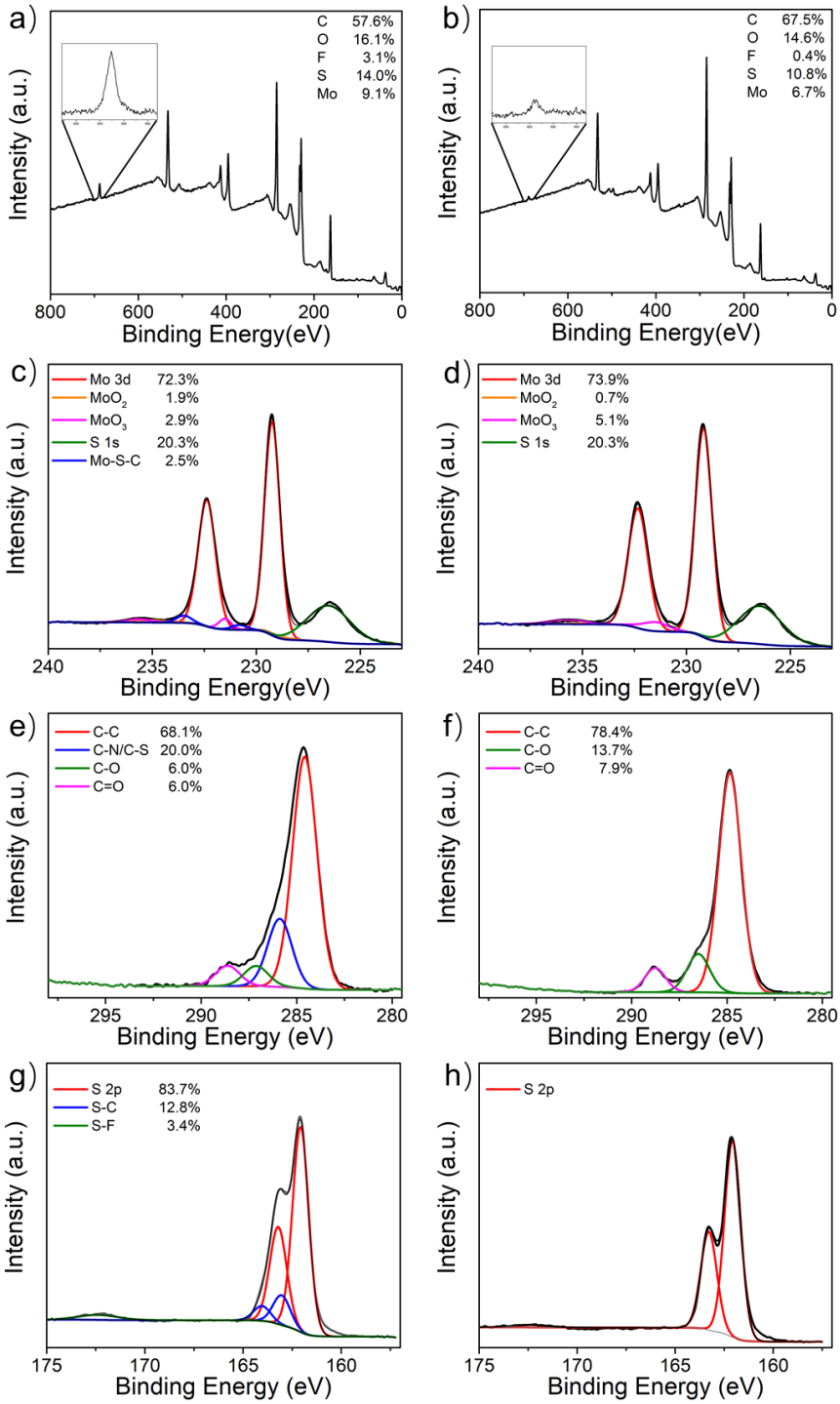

Figure 4.6. XPS survey spectra (a, b) with a zoom on the F 1s peaks (inset), high resolution Mo 3d (c, d), C 1s (e, f) and S 2p (g. h) spectra of MoS_2 **2** (a, c, e, g) and MoS_2 **2-CTR** (b, d, f, h).

ATR FT-IR were also performed on the different MoS_2 samples to confirm the covalent functionalization through benzoquinone (Figure 4.7). In comparison with starting material, a sharp peak was observed in MoS_2 **1** at 1656 cm^{-1}, which could be assigned to the C=O stretching on benzoquinone. And the peak at 1595 was contributed by the C=C stretching.[13] The appearance of the strong band at 817 cm^{-1} corresponds to the alkene =C−H bending mode in benzoquinone.[10] However, the expeted peak at 741 cm^{-1} (red arrow in Figure 4.7b) assigned to a S-C stretching vibration[14] was almost negligible. The less intense signal from S-C band was probably due to the overlapping by the C-H peak and the relatively low amount of benzoquinone covalently linked to MoS_2. After the functionalization of 3-(pentafluorothio)-phenylalanine, a strong band at 782.3 cm^{-1} was recorded, which is the characteristic S–F stretching, proving successfully modification on MoS_2 with phenylalanine derivative. In the control sample MoS_2 **2-CTR**, the peaks at 782.3 cm^{-1} and 817 cm^{-1} were insignificant compared with those on MoS_2 **2**, due to the low tendency of benzoquinone and phenylalanine derivative to physisorb onto MoS_2. The FT-IR spectra confirmed the covalent functionalization of MoS_2 through the benzoquinone-mediated Michael addition of 3-(pentafluorothio)-phenylalanine.

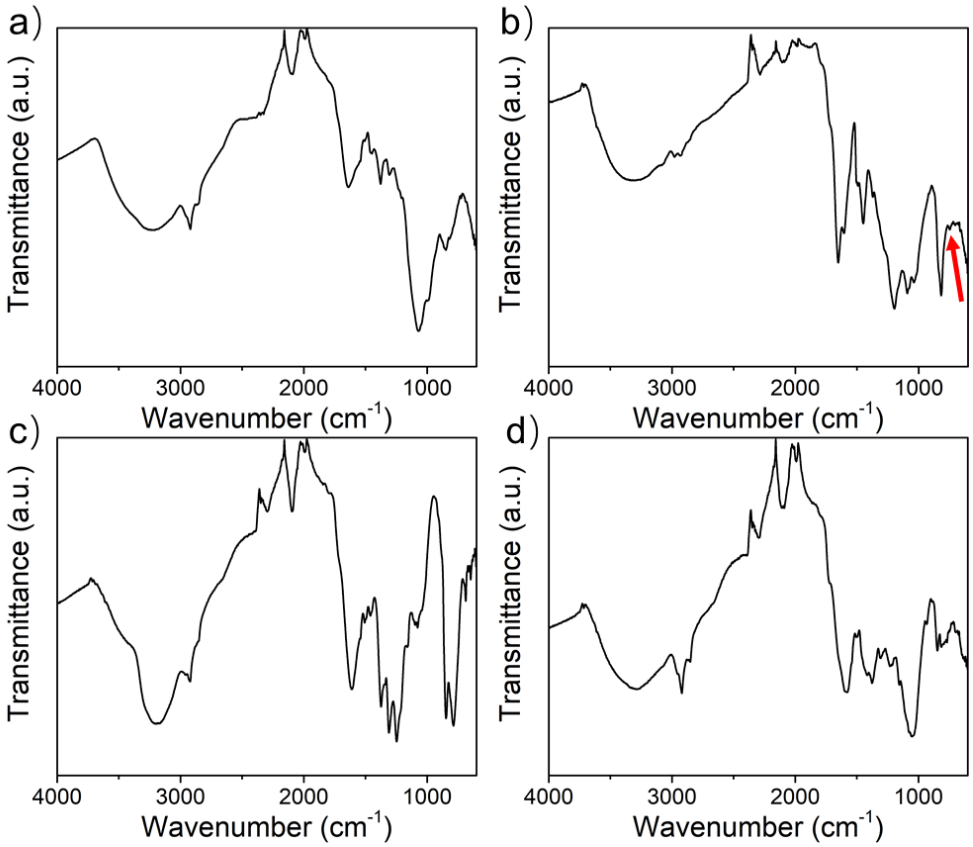

Figure 4.7. FT-IR spectra of MoS_2 (a), MoS_2 **1** (b), MoS_2 **2** (c) and MoS_2 **2-CTR** (d).

With this protocol, the liquid exfoliated MoS_2 was successfully derivatized with benzoquinone and the resulting material could be easily functionalized with 3-(pentafluorothio)-phenylalanine. The free amine on the phenylalanine was able to link to benzoquinone moiety onto MoS_2 and the carboxylic

acid can be further modified with other functional molecules by amidation. To further expend the usage of this strategy, we decided to functionalize MoS_2 with Boc-PEG_{10}-NH_2 using benzoquinone method.

4.3.3 Functionalization of MoS_2 with Boc-PEG_{10}-NH_2

In the previous section, we developed a method for covalent functionalization of MoS_2 through a benzoquinone mediated Michael addition. To further explore the method for MoS_2 functionalization with different molecules, we decided to modify MoS_2 **1** with Boc-PEG_{10}-NH_2.

The protocol of functionalization was similar to the previous one. In this case Boc-PEG_{10}-NH_2 was bound onto MoS_2 **1** targeting the benzoquinone groups, obtaining MoS_2 **3** (Scheme 4.2, top). To clarify if MoS_2 **1** was covalently functionalized with Boc-PEG_{10}-NH_2 through Michael addition towards benzoquinone derivative, a control reaction was performed by mixing the starting MoS_2 directly with Boc-PEG_{10}-NH_2. After carefully washing and centrifuging, MoS_2 **3-CTR** was obtained (Scheme 4.2, bottom).

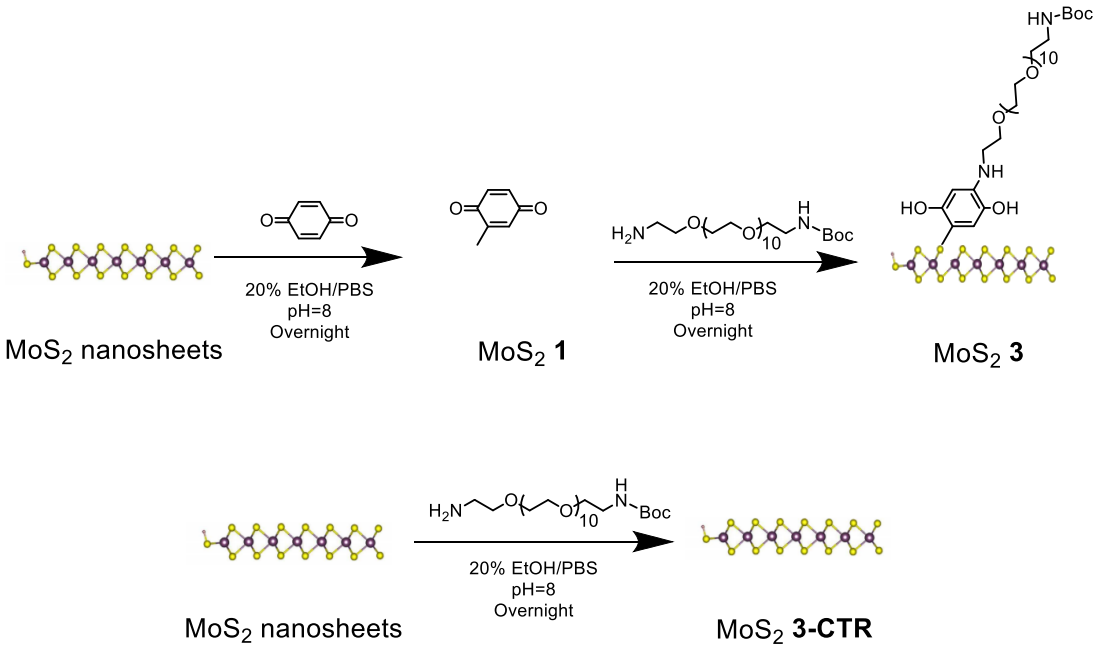

Scheme 4.2. Functionalization of MoS_2 using benzoquinone and Boc-PEG_{10}-NH_2. For the sake of clarity, only one S atom is derivatized.

MoS_2 derivations before and after functionalization were first characterized by TGA (Figure 4.8). The TGA curve of benzoquinone functionalized MoS_2 **1** showed a gradual weight loss as described before. However, MoS_2 **3** exhibited a higher thermal stability at the temperature below 300 ℃ probably due to the derivation on benzoquinone which would increase the thermostability. A major weight loss was observed in the region of temperature between 300°C and 400°C in MoS_2 **3** after the functionalization of Boc-PEG_{10}-NH_2, which could be attributed to the loss of covalently grafted Boc-PEG_{10}-NH_2. The major weight loss at 300°C and 400°C was also observed in our previous work

described in chapter 2. The characteristic temperature of Boc-PEG_{10}-NH_2 thermal decomposition starts around 233°C and this was consisting of the major weight loss observed in MoS_2 **3**. The total weight loss of MoS_2 **3** was also higher than MoS_2 **1**, which further confirming the successful modification of MoS_2 with Boc-PEG_{10}-NH_2. In the control sample MoS_2 **3-CTR**, the nanomaterial also underwent a major weight loss in the region of temperature between 300°C and 400°C, revealing that the PEG chain could also adsorbed onto MoS_2 surface by simply stirring starting MoS_2 with Boc-PEG_{10}-NH_2 in the absence of benzoquinone. But the weight loss contributed by the decomposition of Boc-PEG_{10}-NH_2 in MoS_2 **3-CTR** was much lower than MoS_2 **3**, leading to a higher thermal stability at the temperature 600 ℃. The TGA results revealed that more PEG linkage was covalently bounded onto MoS_2 surface *via* Michael addition toward benzoquinone derivatives on the nanomaterial.

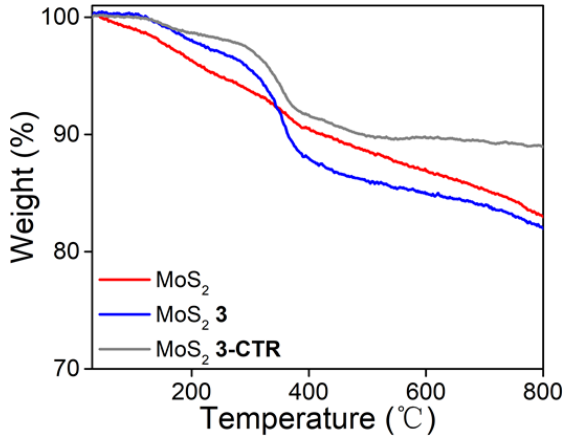

Figure 4.8 TGA of the MoS_2 **1**, MoS_2 **3** and MoS_2 **3-CTR** performed in inert atmosphere.

Then, we characterized PEG functionalized MoS_2 nanosheets by XPS. The C/O ratio was first calculated from survey spectra. The C/O ratio of MoS_2 **3** decreased from 4.4 to 2.7 after the conjugation of Boc-PEG_{10}-NH_2 onto MoS_2 **1** surface *via* Michael addition. The decreasing of C/O ratio indicated that the PEG derivatives were successfully linked on MoS_2 surface. However, the C/O ratio of MoS_2 **3-CTR** only showed a slight decrease from 4.9 to 4.4 in comparison with starting MoS_2 nanosheets. The C/O ratio in control sample did not undergo a significant change as MoS_2 **3,** due to a lower amount of PEG chains adsorbed onto MoS_2 compared to the covalently modification, which corroborated with the results obtained from TGA. However, it is difficult to characterize the amount of PEG chains loaded on MoS_2 by measuring the content of nitrogen by survey spectrum since there is also a strong emission from Mo atoms at binding energy around 399 eV which would overlap the signal of N element. Both in the starting MoS_2 and MoS_2 **1**, a strong emission of photoelectrons was recorded around 400 eV in the survey spectra. Since no nitrogen-containing molecules were used during the exfoliation procedure or in the conjugation of benzoquinone onto MoS_2 surface, the intensity around 400 eV should come from the Mo 3p. For this reason, the ratio of nitrogen atoms in MoS_2 nanosheets would not reveal the amount of PEG chains in our study. The detailed analysis of the C 1s spectrum of MoS_2 **3** clearly showed the increase of C-O and C-N/C-S components after the introduction of PEG chain through the Michael addition, resulting in a significant change of line

shape in comparison with MoS_2 **1** (Figure 4.9e and Figure 4.4c), further confirming the successful conjugation of Boc-PEG_{10}-NH_2 onto MoS_2 surface *via* benzoquinone-associated Michael addition. In the control sample MoS_2 **3-CTR,** the C-N and C-O components in C 1s spectrum were lower than MoS_2 **3** (Figure 4.9), which indicated a low tendency of the PEG chain to adsorb onto GO.

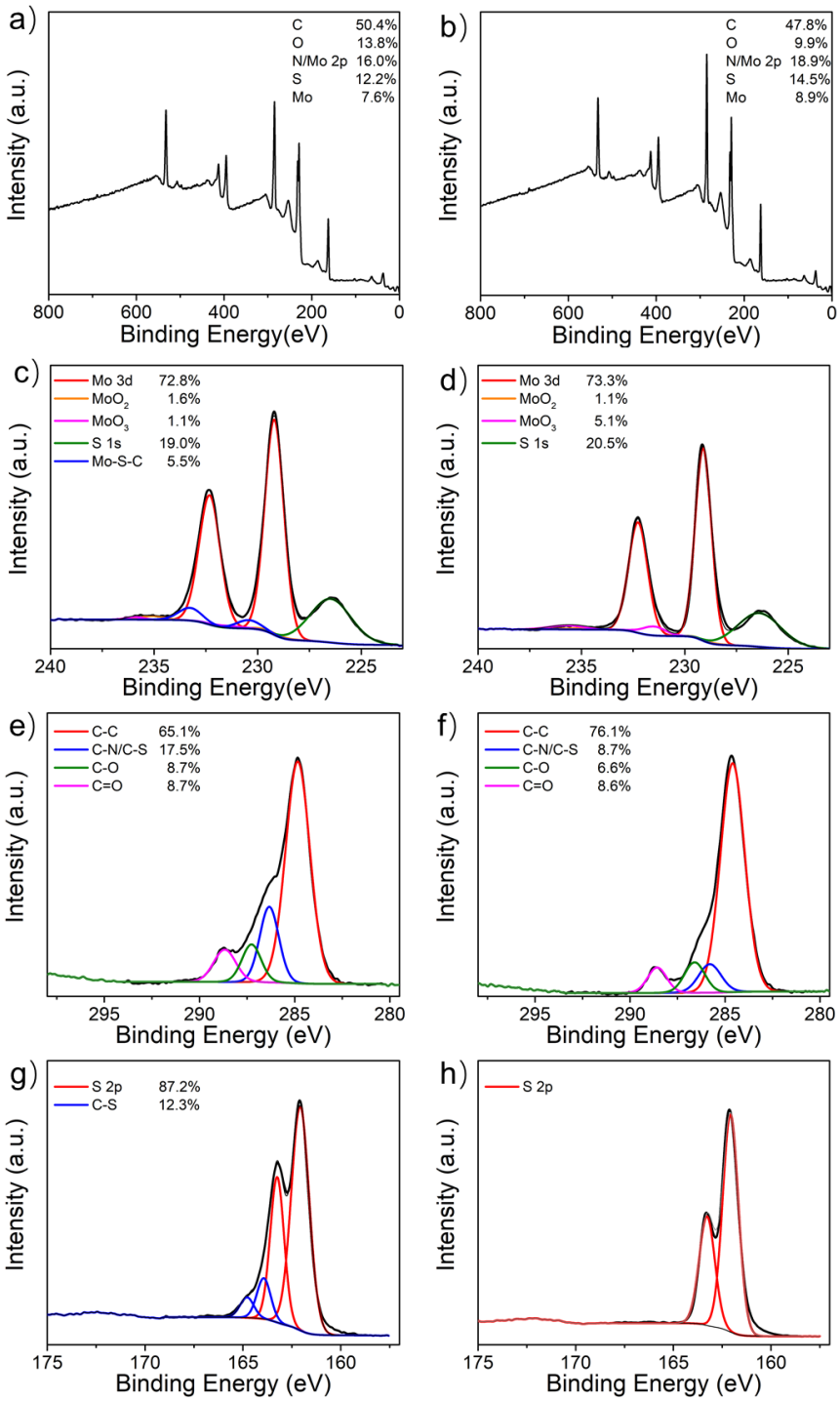

Figure 4.9 XPS survey spectra (a, b), high resolution of Mo 3d (c, d), C 1s (e, f) and S 2p (g. h) spectra of MoS_2 **3**(a, c, e, g) and MoS_2 **3-CTR** (b, d, f, h).

4.3.4 Conclusion

In summary, we developed a simple method for the covalent functionalization of MoS_2 in mild conditions *via* benzoquinone-mediated Michael addition inspired by our previous study of covalent functionalization on GO and the work published by Pérez *et al.*[10] The 2D MoS_2 nanosheets were isolated *via* surfactant-assisted liquid phase exfoliation. To achieve the covalent functionalization on MoS_2, the sulfur atoms were explored as a mild nucleophile and reacted with benzoquinone forming a C-S bond. Benzoquinone components covalently grafted onto MoS_2 surface were then were derivatized with two different molecules, 3-(pentafluorothio)-DL-phenylalanine and Boc-PEG_{10}-NH_2 through the Michael addition between free amine and benzoquinone. The two molecules conjugated on MoS_2 were confirmed by TGA, XPS and FT-IR. The strategy we developed for the covalent functionalization on MoS_2 is simple to perform. GO was efficiently functionalized with different functional groups in mild condition resulting in a higher loading efficiency than simple physisorbtion. The carboxylic acid on 3-(pentafluorothio)-DL-phenylalanine and the free amine on the PEG derivative after Boc-deprotection can be modified with diverse functional molecules through reactions such as amidation for different applications.

4.4 Benzoquinone-assisted liquid phase exfoliation of MoS_2

In the previous part, we investigated the Michael addition on MoS_2 using benzoquinone and explored this reaction in the covalent functionalization of MoS_2. During the preparation of benzoquinone modified MoS_2, we found that the water dispersibility of the benzoquinone derivatized MoS_2 was improved compared to pristine MoS_2 nanosheets. After washing and lyophilizing, the benzoquinone derivatized MoS_2 could still be easily redispersed while aggregations could be observed in the MoS_2 nanosheets exfoliated using sodium cholate. This suggested that benzoquinone could also acted as an exfoliation reagent in liquid phase to produce 2D MoS_2 nanosheets, producing good water dispersibility as well as benzoquinone moieties covalently bounded onto MoS_2 surface, which could be used for further functionalization.

4.4.1 Exfoliation and characterization of MoS_2 nanosheets assisted by benzoquinone

For this purpose, we explored a method to isolate 2D MoS_2 nanosheets directly with benzoquinone by liquid exfoliation. The procedure was similar to the protocol using sodium cholate. Briefly, bulk MoS_2 powder was mixed with benzoquinone by ball milling. The mixture was transferred into water and sonicated for 2 h in ice bath in order to control the temperature under 26 °C. After centrifugation, the supernatant was collected, filtered through a membrane and washed with water and ethanol and benzoquinone-exfoliated MoS_2-Q was prepared. MoS_2-Q nanosheets displayed a good dispersibility in water at a concentration of 2 $mg \cdot mL^{-1}$ (Figure 4.10).

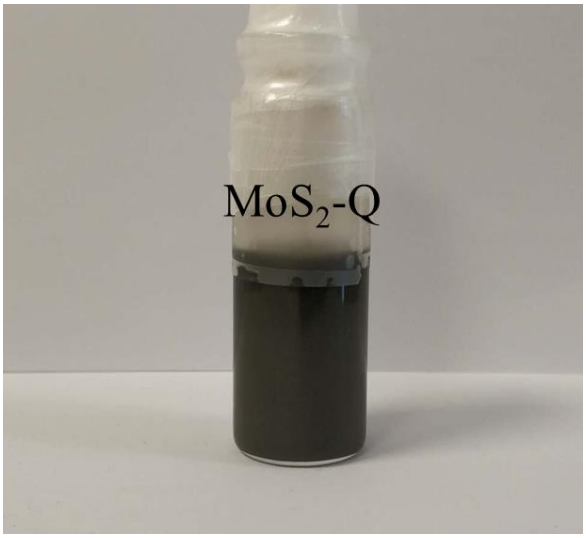

Figure 4.10 Water dispersions of MoS_2-Q.

The MoS_2-Q was first characterized by TEM (Figure 4.11a) The MoS_2-Q nanosheets processed an average size around 120 nm. The lateral size distribution was calculated from TEM images by measuring more than 150 sheets. The histogram plot of this distribution shows values ranging between 25 and 400 nm (Figure 4.11b).

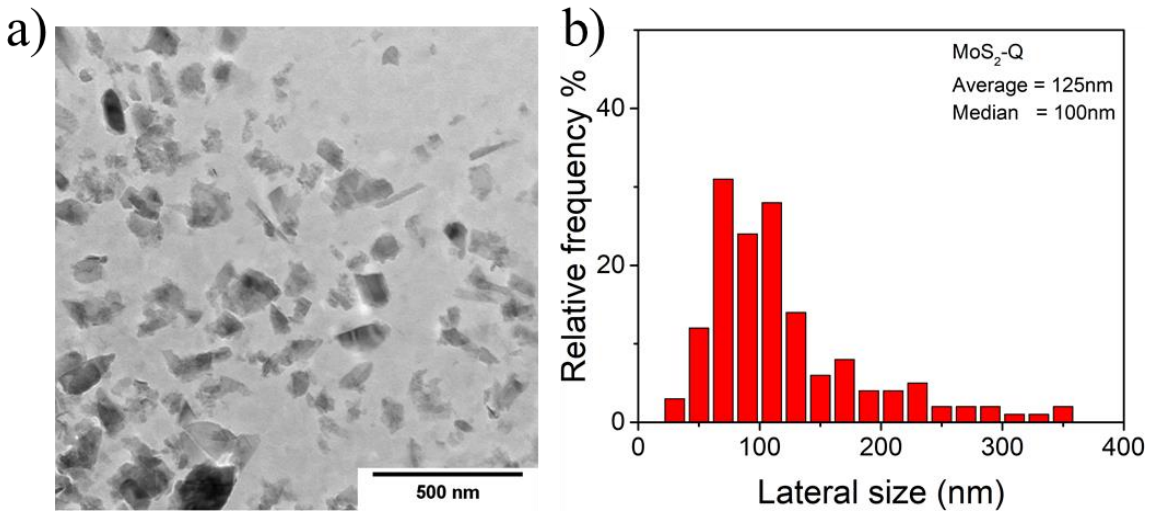

Figure 4.11 a) TEM and b) size distribution of MoS_2-Q nanosheets exfoliated using benzoquinone.

Then, MoS_2 nanosheets were characterized by XPS (Figure 4.12). From the survey spectrum (Figure 4.12a), high components of carbon and oxygen elements were observed due to the benzoquinone molecule anchored onto the MoS_2 surface and the amount of benzoquinone on MoS_2 was 6.6 $mmol \cdot g^{-1}$. The exfoliated MoS_2-Q displayed a S:Mo ratio of approximately 1.6:1 which is similar with the sodium cholate exfoliated MoS_2. In the Mo 3d XPS spectrum (Figure 4.12b) of MoS_2-Q, two peaks from Mo $3d_{5/2}$ and Mo $3d_{3/2}$ orbitals were observed at 229.3 and 232.4 eV, respectively, revealing that the 2H polymorph form was preserved in the isolated MoS_2-Q nanosheets. The doublet peaks

contributed by Mo-S-benzoquinone (Mo-S-C component) were also recorded with a higher area ratio in comparison with MoS_2 **1**, indicating that more benzoquinone molecules were covalently grafted onto MoS_2 surface by direct exfoliation method using benzoquinone. The third peak centered at 226.4 eV is signal from S 2s photoelectrons. In the high-resolution of S 2p spectrum (Figure 4.12d), the MoS_2-Q showed a different line shape compared to MoS_2 exfoliated with sodium cholate. After deconvolution of S 2p spectrum, the doublet of S 2p peaks with the S 2p3/2 centered at 162.7 eV was obtained, which could be assigned to S atoms in C-S bond formed during the exfoliation procedure, proving that the benzoquinone was covalently bound onto MoS_2 surface. The detailed analysis of C 1S spectrum further supported the exist of C-N/C-S bond in MoS_2-Q nanosheets (Figure 4.12c). The deconvolution results showed a strong peak of C-S component in MoS_2-Q, leading to the change of line shape compared to MoS_2 exfoliated with sodium cholate, thus confirming that benzoquinone was conjugated to the S atoms onto MoS_2. The amount of benzoquinone calculated from S 2p spectrum was 1.5 mmol·gram^{-1}, lower than the results based on survey, revealing that part of benzoquinone molecule might be physisorbed onto MoS_2.

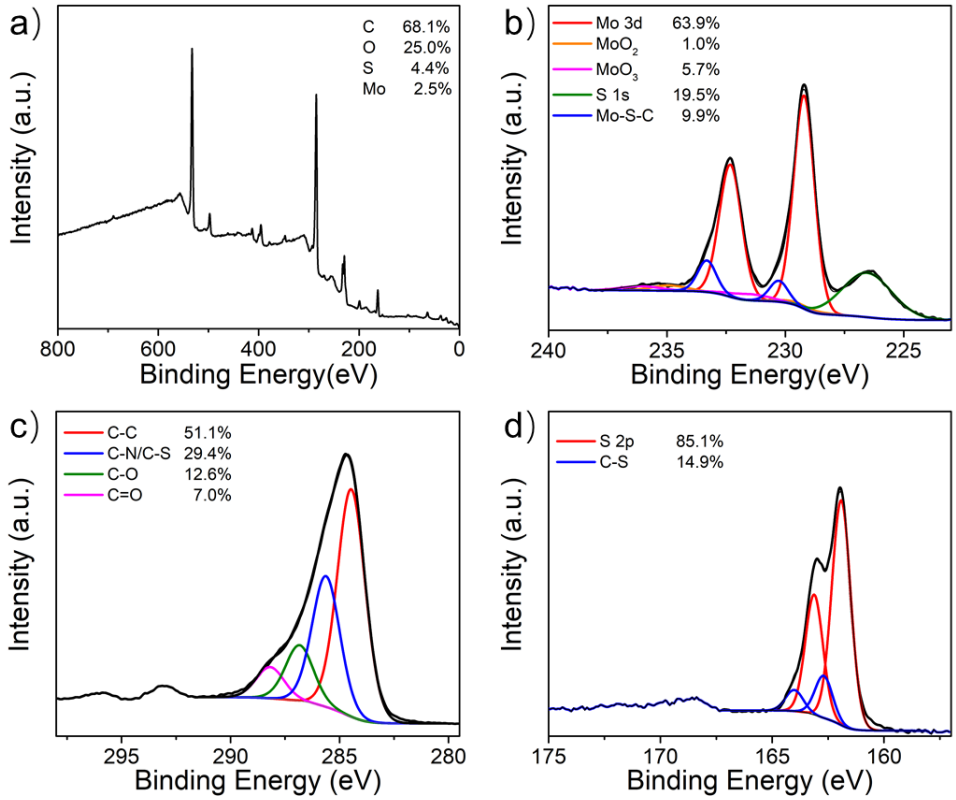

Figure 4.12 XPS survey spectra (a), high resolution Mo 3d (b), C 1s (c) and S 2p (d) spectra of MoS_2-Q.

In addition, the MoS_2-Q was characterized by TGA (Figure 4.13). The TGA curve of MoS_2-Q also showed a gradual weight loss as observed in MoS_2 exfoliated with sodium cholate and MoS_2 **1**. However, MoS_2-Q exhibited a higher rate of weight loss in the region of temperature between 200 °C and 400 °C, which was not observed in starting MoS_2 or MoS_2 **1**. The residue weight at 600 °C of MoS_2-Q was also lower than MoS_2 exfoliated with sodium cholate and MoS_2 **1** due to the higher amount of benzoquinone loaded onto MoS_2 surface which was consistent with XPS results. The

amount on benzoquinone on MoS_2 correspond to 2.3 mmol·g^{-1}, lower than the result calculated from XPS due to the depth of detection in XPS.

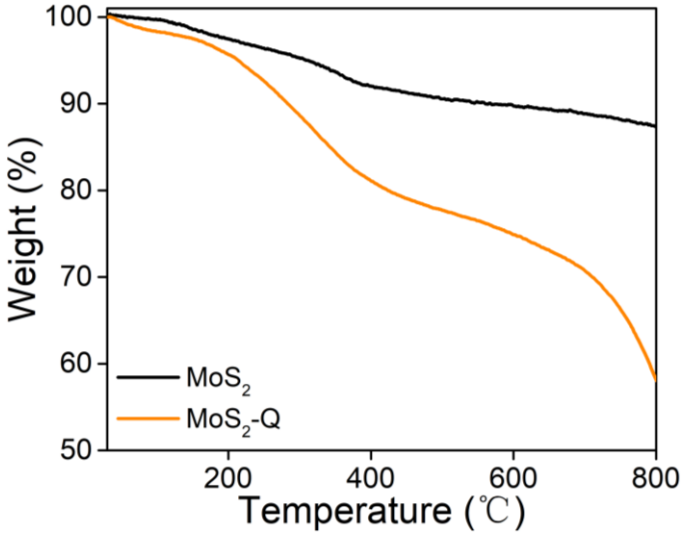

Figure 4.13 TGA of the pristine MoS_2-Q and MoS_2 (exfoliated with sodium cholate) performed in inert atmosphere.

4.4.2 Conclusion

Overall, we developed a protocol for liquid phase exfoliation of MoS_2 nanosheets assisted by benzoquinone. The prepared MoS_2-Q was well dispersed in water at high concentration. Some preliminary characterization methods were performed including XPS, TEM and TGA. The MoS_2-Q nanosheets preserved 2H polymorph form. The XPS data revealed that benzoquinone was covalently grafted onto MoS_2 surface with the formation of C-S bond. Although the prepared MoS_2 nanosheets need further characterization, our protocol of MoS_2 nanosheets exfoliation directly using benzoquinone holds a good potential in the preparation of MoS_2 nanosheet with reactive benzoquinone derivatives.

4.5 Material and methods

Materials

All the chemicals and solvents were obtained from commercial suppliers and used without purification. *O*-(2-aminoethyl)-*O'*-[2-(Boc-amino)ethyl]decaethylene glycol (BocNH-PEG_{10}-NH_2) was purchased from Polypure AS. 3-(pentafluorothio)-DL-phenylalanine was obtained from Alfa Aesar. Bulk MoS_2 was ordered from Acros Organics. The solvents used during the reaction were analytical grade. Water was purified by a Millipore filter system MilliQ®.

Thermogravimetric analysis

Thermogravimetric analysis (TGA) was performed on a TGA1 (Mettler Toledo) apparatus from 30°C to 900°C with a ramp of 10°C·min^{-1} under N_2 atmosphere with a flow rate of 50 mL·min^{-1} and platinum pans.

Transmission electron microscopy

Transmission electron microscopy (TEM) analysis was performed on a Hitachi H600 with an accelerating voltage of 75 kV. The samples were dispersed in water at a concentration of 20 μg·mL^{-1} and the suspensions were sonicated for 10 min. Ten microliters of the suspensions were drop-casted onto a copper grid (Formvar film 300 Mesh, Cu from Electron Microscopy Sciences) and left for evaporation under ambient conditions. All the images were treated with Fiji (ImageJ) software.

Attenuated total reflectance-FTIR

ATR-FTIR was performed using a Thermo Scientific Nicolet™ 6700 FT-IR spectrometer equipped with an ATR accessory (diamond ATR polarization accessory with 1 reflection top-plate and pressure arm). The pressure arm was used for all solid samples at a force gauge setting between 100 and 120 units. The number of scans was set at 30. Samples were loaded on the reflection top-plate at a quantity sufficient enough to cover the entire diamond surface.

X-ray photoelectron spectroscopy

X-ray photoelectron spectroscopy experiments were performed on a Thermo Scientific KAlpha X-ray photoelectron spectrometer with a basic chamber pressure of 10^{-8}-10^{-9} bar and an Al anode as the X-ray source (1486 eV). The samples were analyzed as powder pressed onto a scotch tape (3MTM EMI Copper Foil Shielding Tape 118). Spot size of 400 μm was used for analysis. The survey spectra are an average of 10 scans with a pass energy of 200.00 eV and a step size of 1 eV. The high resolution spectra of C1s, F1s and Mo 3d are an average of 10 scans with a pass energy of 50 eV and a step size of 0.1 eV, while the spectra of S 2p are an average of 20 scans. For each sample, the analysis was repeated three times. A flood gun was turned on during analysis. We grouped the functional groups of C 1s spectra to avoid imprecision due to the proximity of the peak values, since the binding energy values in the literature were too spread. Therefore, the C 1s spectra were deconvoluted in C=O (288.1-289.0 eV) for carbonyl groups and carboxyl groups, C-O (286.2-287.2 eV) for hydroxyls and epoxides, C-N/C-S (285.3-286.2 eV) for the carbon atoms in C-N or C-S bond formed during the functionalization and C-C (284.4-285.3 eV) for sp^2 and sp^3 carbon atoms. For data analysis, the software casaXPS (2.3.18) was used. A Shirley background subtraction was applied. A line-shape 70% Gaussian/30% Lorenzian [GL(30)] was selected for all peaks. The full width at half maximum was constrained to be the same for all peaks. The Mo 3d spectra were deconvoluted in Mo 3d (229.0-229.4 eV for $3d_{5/2}$ and 223.2-223.6 eV for $3d_{3/2}$), MoO_2 (234.9-235.3 eV for $3d_{5/2}$ and 229.0-229.4 eV for $3d_{3/2}$), MoO_3 (231.5-231.9 eV for $3d_{5/2}$ and 235.7-236.1 eV for $3d_{3/2}$) and Mo-S-C (230.0-230.6 eV for $3d_{5/2}$ and 233.3-237.0 eV for $3d_{3/2}$) for Mo-S-benzoquinone. The S 2p spectra were

deconvoluted in S 2p (163.05- 163.35 eV for $2d_{1/2}$ and 161.8-162.2 eV for $2p_{3/2}$), S-C (163.8- 164.6 eV for $2d_{1/2}$ and 162.6-163.4 eV for $2p_{3/2}$), and S-F (172.0-172.8 eV).

Synthesis of MoS_2 nanosheets, precursors and final MoS_2 conjugates

Preparation of MoS_2 nanosheets *via* sodium cholate-associated liquid phase exfoliation

Exfoliation of bulk MoS_2 was performed in MilliQ water in the presence of surfactant. Five hundred mg of bulk MoS_2 powder were mixed with 250 mg sodium cholate and milled for 2 h at 100 rmp with a Rescht Planetary Ball Mill PM 100. The powder was transferred to 400 mL Milli-Q water and sonicated at 37 MHz with 100% power for 3 h in ice bath to control the temperature under 26 °C. The obtained black suspension was centrifuged at 1500 rpm for 90 minutes and the supernatant was collected. The MoS_2 suspension was filtered over a polytetrafluoroethylene (PTFE) Millipore® membrane with 0.1 µm pore size and the precipitate was washed with 200 mL Milli-Q water for 3 times to remove the excess of sodium cholate. The precipitate was collected and redispersed it in Milli-Q water, giving a MoS_2 suspension at 2 $mg \cdot mL^{-1}$.

Preparation of MoS_2 1

Twenty mg of MoS_2 nanosheets dispersion (10 mL) was diluted with PBS (pH=8) and ethanol, giving a final concentration of MoS_2 at 1 $mg \cdot mL^{-1}$ in 20% EtOH/PBS. One hundred mg of benzoquinone waere then added to MoS_2 with continuous stirring. The mixture was stirred overnight. The suspension of MoS_2 nanosheets was divided into several tubes and centrifuged for 15 min at 13200 rpm. The supernatant was removed and the precipitate was redispersed in 20% EtOH/water and centrifuged again. The washing procedure repeated 6 times and the color of supernatant changed from brown to colorless. No benzoquinone in the supernatant after washing was detected by HPLC. The precipitate was collected and dispersed in water and lyophilized, obtaining benzoquinone derivatized MoS_2 **1**.

Preparation of MoS_2 2

Five mg of MoS_2 **1** was dispersed in 5 mL 20% EtOH/PBS, giving a final concentration of 1 $mg \cdot mL^{-1}$. 25 mg of 3-(pentafluorothio)-DL-phenylalanine was added to the solution and bath sonicated for 10 min. The mixture was then stirred at room temperature overnight. The suspension of MoS_2 nanosheets was centrifuged for 15 min at 13200 rpm and the precipitate was washed with 20% EtOH/water for 6 times. The colorless supernatant after washing was collected and checked with HPLC to confirm that there were no phenylalanine derivatives in the solution. The precipitate was collected and dispersed in water and lyophilized, obtaining 3-(pentafluorothio)-phenylalanine functionalized MoS_2 **2**.

Preparation of MoS_2 2-CTR

The preparation of control sample MoS_2 **2-CTR** was similar with to the synthesis of MoS_2 **2** but starting with MoS_2 without benzoquinone. Five mg starting MoS_2 nanosheets were dispersed in 5 mL 20% EtOH/PBS. Twenty-five mg of 3-(pentafluorothio)-DL-phenylalanine were added to the solution followed by bath sonicated for 10 min. The mixture was then stirred overnight. Afterwards, the suspension of MoS_2 nanosheets was centrifuged for 15 min at 13200 rpm and the precipitate was washed with 20% EtOH/water for 6 times. The precipitate was collected, dispersed in water and lyophilized, obtaining MoS_2 **2-CTR**.

Preparation of MoS_2 3

To a suspension of MoS_2 **1** (5 mg) in 4 mL 20% EtOH/PBS, a solution of Boc-PEG_{10}-NH_2 (25 mg) in 20% EtOH/PBS (1 mL) was added dropwise under stirring. The mixture was stirred at room temperature overnight and then centrifuged for 15 min at 13200 rpm. The supernatant was removed and the precipitate was redispersed in 20% EtOH/water and centrifuged again. The washed procedure was repeated for 6 times to remove the PEG chains. The precipitate was collected, dispersed in water and lyophilized, obtaining PEG functionalized MoS_2 **3**.

Preparation of MoS_2 3-CTR

The preparation of MoS_2 **3-CTR** followed the same procedure as MoS_2 **3**. To a suspension of pristine MoS_2 nanosheets (5 mg) in 4 mL 20% EtOH/PBS, a solution of Boc-PEG_{10}-NH_2 (25 mg) in 20% EtOH/PBS (1 mL) was added dropwise under stirring. The mixture was stirred at room temperature overnight and then centrifuged for 15 min at 13200 rpm. The supernatant was washed with 20% EtOH/water for 6 times. The precipitate was collected, dispersed in water and lyophilized, giving the control sample MoS_2 **3-CTR**.

Preparation of MoS_2 nanosheets *via* benzoquinone-assisted liquid phase exfoliation

To isolate MoS_2 nanosheets *via* benzoquinone-assisted liquid phase exfoliation, 500 mg of bulk MoS_2 powder was mixed with 500 mg benzoquinone and milled for 3 h at 100 rmp with a Rescht Planetary Ball Mill PM 100. The mixture was then transferred to 500 mL Milli-Q water and sonicated at 37 MHz for 2 hours in ice bath to control the temperature under 26 ℃. The obtained black suspension was centrifuged at 1500 rpm for 90 minutes and the supernatant was collected. The MoS_2 suspension was filtered over PTFE membrane with 0.1 μm pore size and the precipitate was washed with Milli-Q water and ethanol for 3 times each to remove the excess of benzoquinone. The precipitate was collected, redispersed in Milli-Q water and lyophilized, giving the MoS_2-Q nanosheets isolated though benzoquinone-assisted exfoliation in water.

4.6 References

1. X. Zhang, Z. Lai, C. Tan and H. Zhang, "Solution-Processed Two-Dimensional MoS_2 Nanosheets: Preparation, Hybridization, and Applications", *Angew. Chem. Int. Ed.*, 2016, **55**, 8816-8838.

2. J. N. Coleman, M. Lotya, A. O'Neill, S. D. Bergin, P. J. King, U. Khan, K. Young, A. Gaucher, S. De, R. J. Smith, I. V. Shvets, S. K. Arora, G. Stanton, H. Y. Kim, K. Lee, G. T. Kim, G. S. Duesberg, T. Hallam, J. J. Boland, J. J. Wang, J. F. Donegan, J. C. Grunlan, G. Moriarty, A. Shmeliov, R. J. Nicholls, J. M. Perkins, E. M. Grieveson, K. Theuwissen, D. W. McComb, P. D. Nellist and V. Nicolosi, "Two-dimensional nanosheets produced by liquid exfoliation of layered materials", *Science*, 2011, **331**, 568-571.

3. C. Backes, T. M. Higgins, A. Kelly, C. Boland, A. Harvey, D. Hanlon and J. N. Coleman, "Guidelines for Exfoliation, Characterization and Processing of Layered Materials Produced by Liquid Exfoliation", *Chem. Mater.*, 2016, **29**, 243-255.

4. Y. Yang, H. Hou, G. Zou, W. Shi, H. Shuai, J. Li and X. Ji, "Electrochemical exfoliation of graphene-like two-dimensional nanomaterials", *Nanoscale*, 2019, **11**, 16-33.

5. T. Liu, S. Shen, Y. Huang, X. Zhang, Z. Lai, T. H. Tran, Z. Liu and L. Cheng, "Controllable Growth of Au Nanostructures onto MoS_2 Nanosheets for Dual-modal Imaging and Photothermal-radiation Combined Therapy", *Nanoscale*, 2019, **11**, 22788-22795.

6. A. Hirsch and F. Hauke, "Post-Graphene 2D Chemistry: The Emerging Field of Molybdenum Disulfide and Black Phosphorus Functionalization", *Angew. Chem. Int. Ed.* , 2018, **57**, 4338-4354.

7. E. Er, H.-L. Hou, A. Criado, J. Langer, M. Möller, N. Erk, L. M. Liz-Marzán and M. Prato, "High-Yield Preparation of Exfoliated 1T-MoS_2 with SERS Activity", *Chem. Mater.*, 2019, **31**, 5725-5734.

8. G. Yilmaz, T. Yang, Y. Du, X. Yu, Y. P. Feng, L. Shen and G. W. Ho, "Stimulated Electrocatalytic Hydrogen Evolution Activity of MOF-Derived MoS_2 Basal Domains via Charge Injection through Surface Functionalization and Heteroatom Doping", *Adv. Sci.*, 2019, **6**, 1900140-1900149.

9. C. Backes, N. C. Berner, X. Chen, P. Lafargue, P. LaPlace, M. Freeley, G. S. Duesberg, J. N. Coleman and A. R. McDonald, Functionalization of liquid-exfoliated two-dimensional 2H-MoS_2 *Angew. Chem. Int. Ed.*, 2015, **54**, 2638-2642.

10. M. Vera-Hidalgo, E. Giovanelli, C. Navio and E. M. Perez, Mild Covalent Functionalization of Transition Metal Dichalcogenides with Maleimides: A "Click" Reaction for 2H-MoS_2 and WS_2 *J. Am. Chem. Soc.*, 2019, **141**, 3767-3771.

11. G. Greczynski and L. Hultman, "X-ray photoelectron spectroscopy: Towards reliable binding energy referencing", *Prog. Mater. Sci.*, 2020, **107**, 100591-100636.

12. W. Ren, H. Zhang, C. Guan and C. Cheng, "Ultrathin MoS_2Nanosheets@Metal Organic Framework-Derived N-Doped Carbon Nanowall Arrays as Sodium Ion Battery Anode with Superior Cycling Life and Rate Capability", *Adv. Funct. Mater.*, 2017, **27**, 1702116-1702125.

13. J. Makuraza, "Vibrational and Electronic Spectra of Natural Dyes Constituents for Solar Cell Application: DFT and TDDFT Study", *Int. J. Mater. Sci. Appl.*, 2015, **4**, 314-324.

14. R. Quiros-Ovies, M. Vazquez Sulleiro, M. Vera-Hidalgo, J. Prieto, I. J. Gomez, V. Sebastian, J. Santamaria and E. M. Perez, "Controlled Covalent Functionalization of 2H-MoS2 with Molecular or Polymeric Adlayers", *Chem. Eur. J.*, 2020, **26**, 6629 –6634.

Chapter 4
Benzoquinone-assisted covalent functionalization and liquid phase exfoliation of MoS_2

Chapter 5 Conclusions and perspectives

5.1 Conclusions

In this Thesis, I explored the covalent multi-functionalization on 2D nanomaterials including graphene oxide and transition metal dichalcogenides (e.g. MoS_2). The prepared folic acid and chlorine 6 (FA/Ce6) double functional GO was then developed for the photothermal and photodynamic therapy on cancer and rheumatoid arthritis.

I firstly investigated different protocols for the covalently multi-functionalization of GO by targeting different oxygenated functional groups present onto GO surface. Epoxide rings and hydroxyl groups were chosen for derivatization due to the abundant amount on GO basal plane. A nucleophilic addition with amines or thiols was used to open the epoxide rings, thus binding functional molecules. To achieve better reactivity of hydroxyl groups, the OH moieties on GO were carboxylated by chloroacetic acid to introduce more carboxyl groups or derivatized by benzoquinone through Michael addition. By combining the epoxide ring opening and carboxylation, the GO was successfully double functionalized using Boc-PEG_{10}-NH_2 in a stepwise procedure. However, the introduction of carboxyl groups only occurred with the high amount of sodium hydroxide, which would in turn, induce a severe deoxygenation and reduce the total efficiency of functionalization. The reduction of GO induced by the strong alkaline condition during the carboxylation was not well-addressed in the literature, when this method was used for GO functionalization. It was very important to consider side reactions that may not be mentioned in the previous articles. Indeed, the surface modification such as carboxylation under strong alkalic condition or other chemical derivation would tune the intrinsic properties of GO, affecting the loading efficiency and other factors including dispersibility and cytotoxicity, which are important for its application in biosensing and disease treatment as drug nanocarriers.

Then, I explored protocol strategy that combines the opening of epoxides and Michael addition of benzoquinone. This method was easy to perform and the reactions were running in mild conditions. The GO was successfully double functionalized using different molecules as confirmed by XPS, TGA, FT-IR and CV. This method is suitable for the grafting of functionalities, which are sensitive to temperature or pH on GO to form a robust complex, which could greatly extend the application of GO.

While exploring the covalent double functionalization targeting different groups on GO, a FA/Ce6 double-functionalized GO was successfully prepared by derivatizing the epoxides with two PEG chains. The obtained GO-FA/Ce6 showed good photothermal converting efficiency and high ROS generation ability. This nanomaterial was then developed for *in vitro* PTT/PDT synergistic cancer therapy. Due to the FA groups on GO, the GO-FA/Ce6 was quickly internalized into cancer cells through the FR-mediated endocytosis. The Live/Dead assay was applied to evaluate the cell viability after different treatments. The GO-FA/Ce6 exhibited high killing efficiency on breast cancer cells, MCF-7, after PTT or PDT alone. By combining the photothermal and photodynamic treatment, a

higher therapeutic effect was achieved, leading to satisfactory antitumor efficacy. Furthermore, the GO-FA/Ce6 was explored in the phototherapy against RA. Some preliminary experiments were performed on murine macrophage RAW 264.7 cells. RAW 264.7 cells showed a higher sensitivity to PTT leading to a high killing efficiency after irradiation, but a certain resistance against ROS was observed with less cells affected by photodynamic treatment.

Finally, in addition to GO, I also studied the chemical modification and the liquid phase exfoliation of MoS_2 assisted by benzoquinone. A benzoquinone-mediated method for the covalent functionalization of MoS_2 in mild conditions was developed. The functionalization was performed on 2D MoS_2 nanosheets prepared *via* liquid phase exfoliation in the presence of sodium cholate. MoS_2 was derivatized by benzoquinone through Michael addition and the quinone-modified MoS_2 nanosheets were subsequently functionalized with 3-(pentafluorothio)-DL-phenylalanine e increased the water dispersibility of MoS_2 nanosheets, the benzoquinone-assisted liquid phase exfoliation was then investigated. The prepared 2D MoS_2 was well-dispersed in water at high concentration and some preliminary characterization methods were performed including XPS, TEM and TGA. Apart from partial physisorbtion onto MoS_2 surface, benzoquinone molecule was covalently grafted onto MoS_2 surface with the formation of C-S bond.

5.2 Perspectives

This project has allowed me to explore the chemistry of 2D materials aimed to develop multi-functional systems for biomedical applications. Many chemical aspects still need to be explored more in details. For the covalent multi-functionalization onto GO targeting different oxygenated groups, the benzoquinone method is easy to perform in mild condition, which is especially appropriate for the conjugation of biomolecules. Carboxylic acid on phenylalanine derivative and the free amine on PEG after deprotection can be further modified for example with various functional molecules such as drugs, peptides, proteins, or aptamers, to obtain multi-functional GO for applications in therapy, biosensing, and bioimaging. Compared with other covalent multi-functionalization protocols, the benzoquinone-based method is performed in mild conditions without heating or without adding metal catalysts. In addition to amine-containing functional groups, benzoquinone can also react with azides *via* a cycloaddition reaction, thiol groups through Michael addition and with cyclopentadienes via Diels-Alder reaction, further expanding the versatility and the flexibility of our approach. The morphology of the sheets is preserved and the functionalization does not cause reduction of GO. Temperature- and pH-sensitive functional groups could be covalently grafted, thus extending the use of GO for further research not only in biomedicine, but also in other fields.

The FA/Ce6 double functionalized GO has proved its great potential in the application for phototherapy in the anticancer treatment. In addition to *in vitro* tests, it would be interesting to apply this nanomaterial to *in vivo* experiments to evaluate the PTT and PDT efficiency as well as the synergistic efficiency since the local hyperthermia would improve tissue hypoxia and benefit the

accumulation of the nanomaterial into the tumor. For the application of GO-FA/Ce6 in RA treatment, the synergistic effect of combining PTT and PDT on RAW 264.7 still needs to be proved by further experiments. However, experiments, not reported in this Thesis, showed us that the activation of RAW 264.7 macrophages with lipopolysaccharide (LPS) did not enhance the overexpression of folate receptors. Although this method was commonly used in literature studying anti-RA property of nanomaterials, we did not obtain a convincing proof showing that the LPS stimulation would induce the overexpression of FR on RAW 264.7 cells. For further study, we would apply this nanomaterial on activated primary murine macrophages.

Besides the functionalization onto GO nanomaterial, the strategy we developed for the covalent modification on MoS_2 is also worth further studying. This method is simple to perform and MoS_2 can be efficiently functionalized with different functional groups in mild condition resulting in a higher loading efficiency than simple physisorbtion. The phenylalanine and PEG derivatized nanomaterial can be modified with diverse functional molecules through reactions such as amidation for different applications. MoS_2 nanosheets obtained by benzoquinone-assisted liquid phase exfoliation still need further characterization. The benzoquinone derivatives on MoS_2 are supposed to hold the potential for covalent functionalization *via* Michael addition and further experiments need to be performed. The protocol of bulk MoS_2 exfoliation directly using benzoquinone can provide an alternative solution for the preparation of MoS_2 nanosheets with good water dispersion and high reactivity for chemical modification.

List of publications and communications

Publications

1. S. Guo, Y. Nishina, A. Bianco and C. Ménard-Moyon. A Flexible Method for Covalent Double Functionalization of Graphene Oxide, *Angew. Chem. Int Ed.*, 2020, **59**, 1542-1547.
2. I. A. Vacchi, S. Guo, J. Raya, A. Bianco and C. Menard-Moyon. Strategies for the Controlled Covalent Double Functionalization of Graphene Oxide, *Chem. Eur. J.*, 2020, **26**, 6591-6598.
3. R. Soltani,[#] S. Guo,[#] A. Bianco, C. Ménard-Moyon. Carbon Nanomaterials Applied for the Treatment of Inflammatory Diseases: Preclinical Evidence, *Adv. Therap.*, 2020, **3**, 2000051. [#]These authors contributed equally to this work.
4. D.-K. Ji, G. Reina, S. Guo, M. Eredia, P. Samorì, C. Ménard-Moyon and A. Bianco. Controlled functionalization of carbon nanodots for targeted intracellular production of reactive oxygen species, *Nanoscale Horiz.*, 2020, **5**, 1240-1249.
5. S. Guo, J. Raya, D.-K. Ji, Y. Nishina, C. Ménard-Moyon and A. Bianco. Is carboxylation an efficient method for graphene oxide functionalization? *Nanoscale Adv.*, **2**, 4085-4092.
6. D.-K. Ji, G. Reina, H. Liang, D. Zhang, S. Guo, B. Ballesteros, C. Ménard-Moyon, J. li and A. Bianco. Functional carbon nanodots for T_1-weighted magnetic resonance imaging, *Angew. Chem. Int Ed.*, under revision.
7. B. Ma, S. Guo, Y. Nishina and A. Bianco. Intracellular Reaction between Graphene Oxide and Glutathione as One Cause of its Cytotoxicity, *Adv. Healthc. Mater.*, submitted.

Book chapter

1. S. Guo,[#] R. Soltani,[#] A. Bianco, C. Ménard-Moyon. Carbon nanomaterials as carriers of anti-inflammatory drugs in Carbon Nanostructures for Bio-Medical Applications, Da Ros T., Nierengarten J.-F. and Martín N. Eds., the Royal Society of Chemistry, Cambridge, UK, **2020**, in press. [#]These authors contributed equally to this work.

Communications

1. Covalent Multi-Functionalization of Graphene Oxide, Shi Guo, Cécilia Ménard-Moyon, Alberto Bianco, Chem2Dmat, Dresden, Germany. September, 2019. Poster
2. Covalent multi-functionalization of Graphene Oxide, Shi Guo, Cécilia Ménard-Moyon, Alberto Bianco, "Journée des Doctorants de l'Ecole Doctorale des Sciences Chimiques", Strasbourg, France. December, 2019. Oral presentation

Shi GUO

Photothérapies combinées à base de matériaux 2D multifonctionnels pour le traitement du cancer et de maladies auto-immunes

Résumé

Les matériaux 2D, y compris l'oxyde de graphène et le MoS_2, sont des plates-formes idéales pour l'administration de médicaments et la photothérapie. Cette thèse vise à étudier l'application de ces matériaux dans le traitement du cancer et de la polyarthrite rhumatoïde combinant thérapie photothermique et photodynamique.

Nous avons d'abord exploré la modification covalente du GO ciblant différents groupements fonctionnels. Les époxydes ont été modifiés par addition nucléophile avec des fonctionnalités contenant des amines ou des thiols. Les groupes hydroxyles ont ensuite été modifiés par carboxylation ou par addition de Michael médiée par la benzoquinone. Cet approche a été suivie par la fixation d'un second groupement fonctionnel par amidation de l'acide carboxylique ou par addition de Michael sur la benzoquinone.

Pendant ce temps, nous avons préparé l'oxyde de graphène doublement fonctionnalisé avec un dérivé d'acide folique et le photosensibilisateur chlorine e6 en vue de cibler les cellules cancéreuses du sein MCF-7 et les macrophages RAW 264.7 par photothérapie. Ce conjugué a montré une capacité cytotoxique efficace contre les MCF-7. La combinaison de la therapié photothermique et photodynamique a montré un effet synergique. Par contre, les cellules RAW 264.7 n'étaient sensible qu'à la thérapie photothermique.

Enfin, nous avons développé la méthode de fonctionnalisation covalente de MoS2 avec une addition de Michael médiée par la benzoquinone. Ensuite, nous avons préparé des nanofeuillets MoS2 directement en utilisant une exfoliation en phase liquide assistée par benzoquinone.

Mots-Clés: Oxyde de graphène, MoS_2, multifonctionnalisation, photothérapie, cancer, polyarthrite rhumatoïde

Résumé en anglais

2D materials including graphene oxide and MoS_2 are ideal platforms for drug delivery and phototherapy. This Thesis is aiming to investigate the application of these materials in the treatment of cancer and rheumatoid arthritis combining photothermal and photodynamic therapy.

We first explored the covalent modification onto GO targeting different functional groups. The epoxide rings were derivatized through nucleophilic addition with functionalities containing amines or thiols. The hydroxyl groups were then modified *via* carboxylation or benzoquinone-mediated Michael addition followed by the attachment of a second functional group through amidation to carboxylic acid or through Michael addition to benzoquinone.

Meanwhile, we prepared the folic acid and chlorin e6 double functional graphene oxide for the phototherapy targeting MCF-7 breast cancer cells and RAW 264.7 macrophages. The double functional graphene oxide showed high killing efficiency against MCF-7. Following a combination of photothermal and photodynamic strategies a synergistic effect was observed. RAW 264.7 cells were instead more sensitive only to the photothermal treatment.

Finally, we developed the method to covalent functionalize MoS_2 with benzoquinone-mediated Michael addition. In addition, we prepared MoS_2 nanosheets directly using a benzoquinone-assisted liquid phase exfoliation

Keywords: Graphene oxide, MoS_2, multi-functionalization, phototherapy, cancer, rheumatoid arthritis